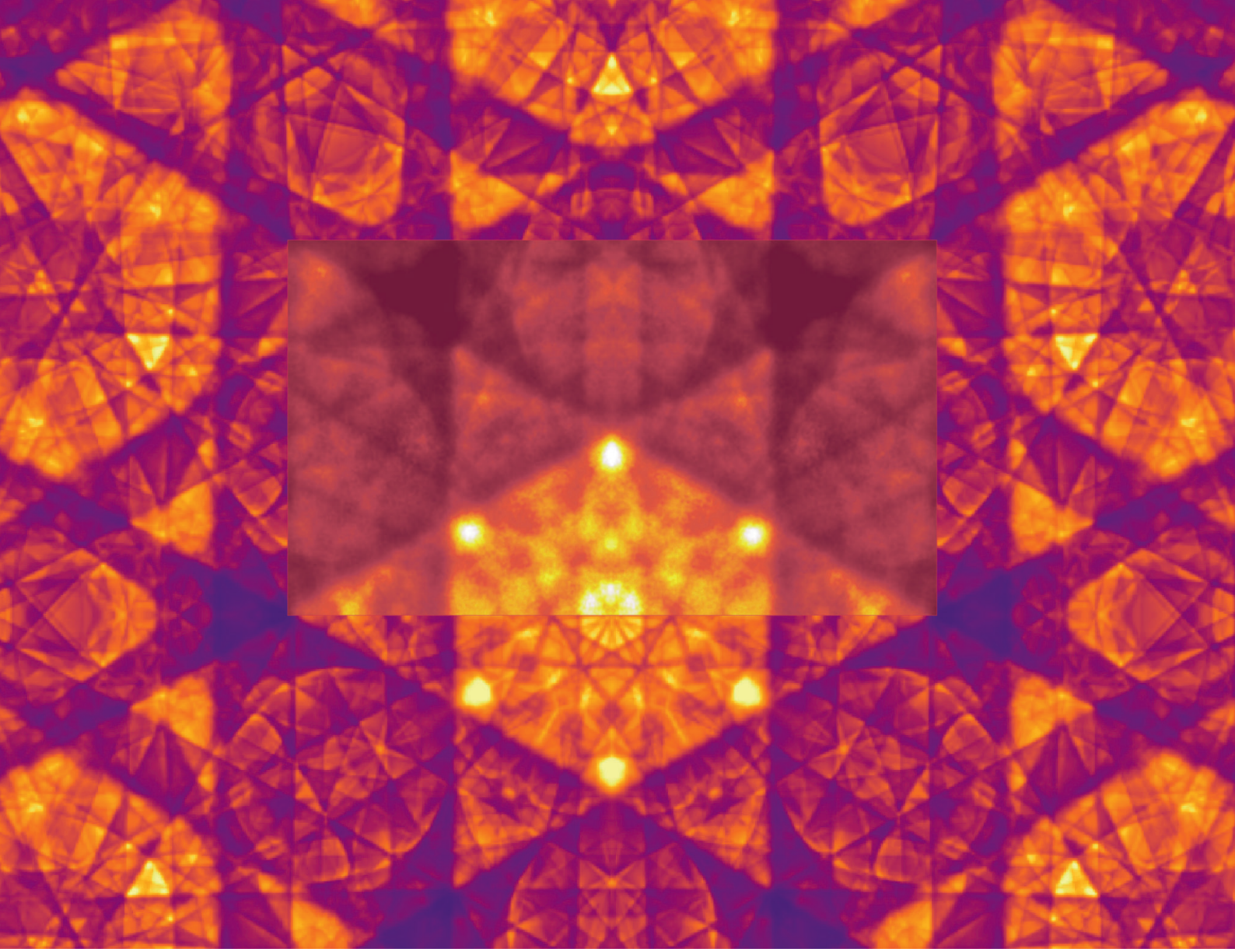

PHOTON SCIENCE 2019.

Highlights and Annual Report

Deutsches Elektronen-Synchrotron DESY
A Research Centre of the Helmholtz Association

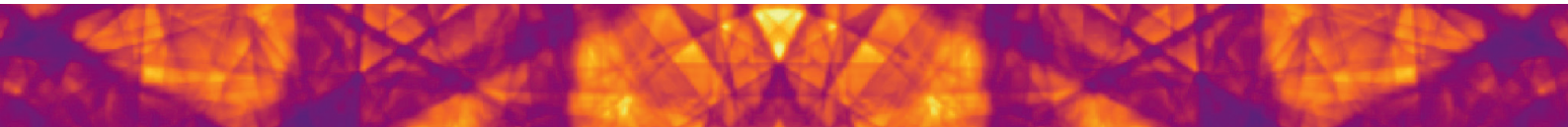

Cover

Angle-resolved photoemission spectroscopy (ARPES) is a very powerful method to analyse electronic properties of novel materials. However, contributions from photoelectron diffraction complicate data analysis. Scientists from Johannes Gutenberg University Mainz and beamline P22 at PETRA III chose graphite, a low-Z material, as a model case. They compared the measured photoelectron diffraction pattern with corresponding theoretical calculations.

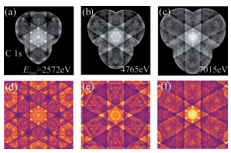

The cover picture shows a near perfect agreement of these calculated (whole picture) and measured diffraction pattern (rectangular picture detail in the middle of the cover picture) of graphite at a photon energy of 2575 eV (details see p. 34/35).

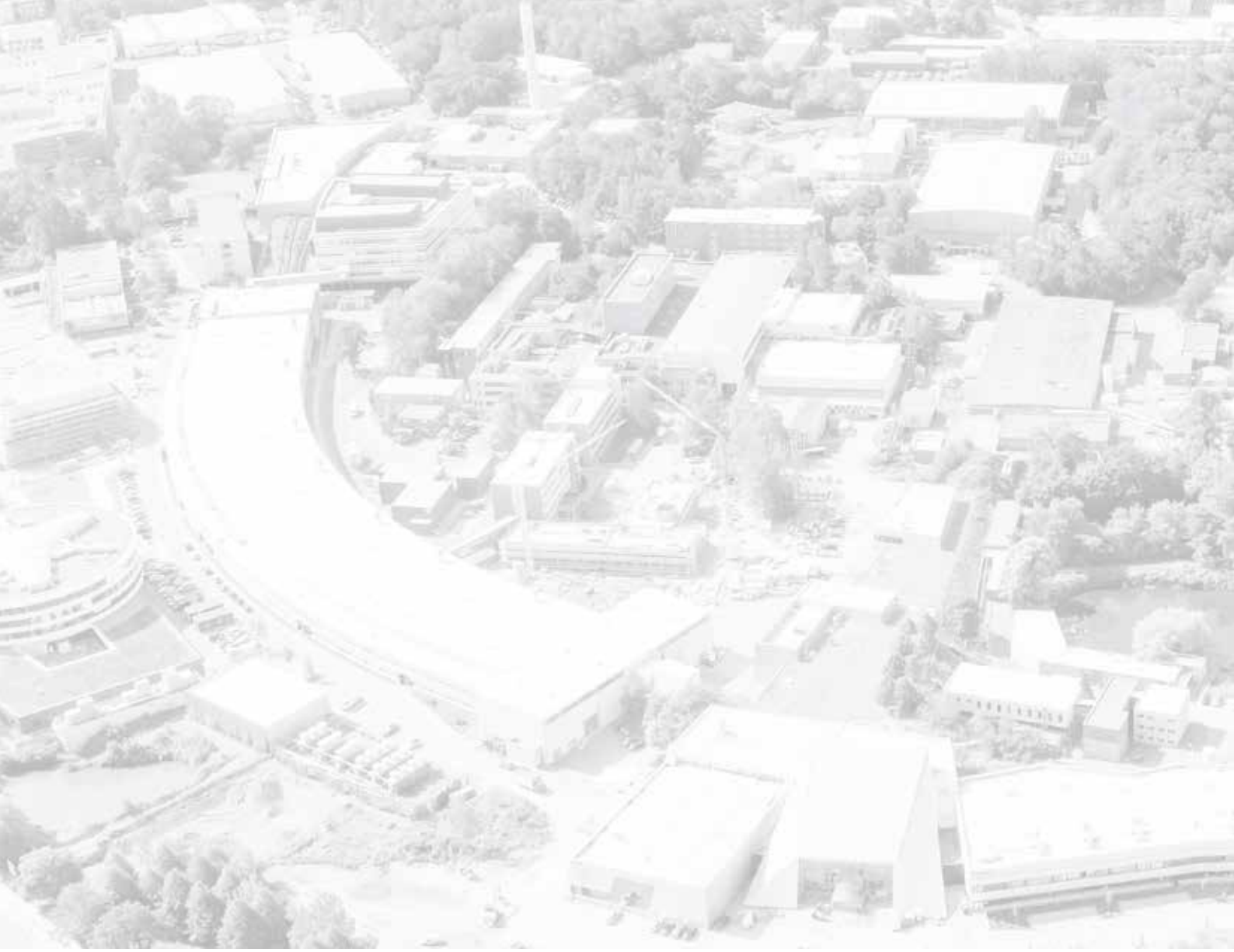

PHOTON SCIENCE 2019.

Highlights and Annual Report

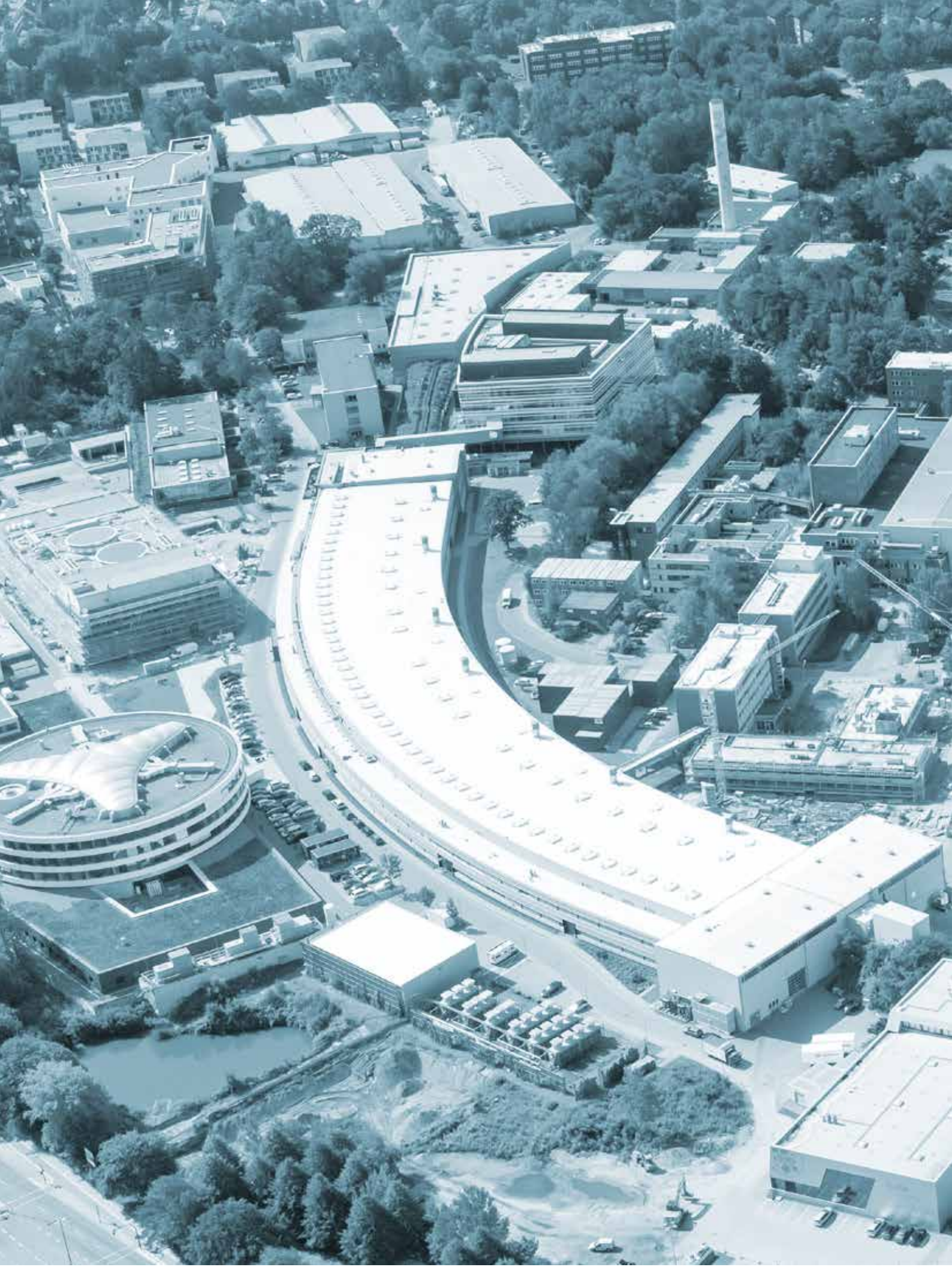

Contents

Publications

The list of publications based on work done at DESY Photon Science is accessible online:
http://photon-science.desy.de/research/publications/list_of_publications/index_eng.html

DESY tries to keep this list as complete and as updated as possible, and relies on the support by all users, who are kindly requested to register their publications via DOOR (door.desy.de).

DESY on the research campus in Hamburg-Bahrenfeld in the foreground and the river Elbe in the background (July 2019).

The year 2019 at DESY

Chairman's foreword

DESY Photon Science continues to develop with great momentum and high ambitions for the future.

The user operation of PETRA III was very successful. We were able to further increase the availability of beamtime for our users. The reward is outstanding results that have led to impressive publications. I was particularly pleased with the report on our cooperation with KTH Stockholm which was covered in detail by the TV broadcaster ZDF 'Heute Journal' at prime time.

In research with free-electron lasers, remarkable new results were achieved this year. I would like to mention the results of Max Rose's doctoral thesis which was awarded the PhD prize of the 'Verein der Freunde und Förderer des DESY (VFFD)' this year: His thesis dealt with ultrafast imaging of biological samples, a new technique that enables the imaging of opaque, biological materials in 3D at nanometer resolution.

DESY offers ideal conditions for such investigations, as X-ray sources with a high coherence component are available for new experimental techniques, such as PETRA III and in future PETRA IV, FLASH and the European XFEL. The potential of these new techniques, which will also increasingly use machine learning techniques, is enormous for future biomedical applications.

Currently DESY is concentrating strongly on the preparations for the upgrade of PETRA III. The CDR for PETRA IV has now been completed and approved by our advisory bodies. In the next two years we will have to work on the TDR. The necessary resources will be made available for this purpose. In the meantime, there also is a first position paper on the National Photon Science Strategy, which was developed jointly by DESY, the HZB and the HZDR under the leadership of the Helmholtz office. For the upgrade of FLASH – 'FLASH2020+' – DESY now has the necessary financial means as well so that this project can be started next year.

This year DESY had to cope with the sudden death of Wilfried Wurth, who died unexpectedly in May during a business trip in Sweden. With him we lost one of our pioneers in FEL research and our charismatic leading scientist of the FLASH facility. During a touching international commemorative colloquium, in which scientists from universities and other light sources all over Europe participated, it once again became clear to everyone what esteem Wilfried enjoyed in the worldwide scientific community. We owe a great deal to Wilfried Wurth and will never forget him.

Finally, I would like to thank the DESY staff and all our national and international partners, who have lead the way to developing a vibrant Bahrenfeld research campus in Hamburg.

Helmut Dosch
Chairman of the DESY Board of Directors

Photon Science at DESY

Introduction

The joint DESY Photon Science and European XFEL users' meeting 2019 attracted about 1200 participants. Over 350 posters were presented during the poster session.

Dear Colleagues and Friends,

During the last few years the developments in our field have gained additional momentum. Not only do new ideas emerge to further improve synchrotron and free-electron laser (FEL) radiation sources but this also holds for the experimental techniques including new types of highly performing detectors. The entire field is extremely competitive and it requires considerable effort to stay at the forefront. DESY is intending to meet this challenge with a very ambitious plan for the upgrade of its photon science facilities as well as the associated infrastructure.

The DESY workhorse for synchrotron radiation science – PETRA III – is still among the high energy sources with the lowest emittance worldwide. But this will change as soon as new upgraded sources will start user operation like ESRF-EBS. The planned upgrade to PETRA IV installing a multi-bend achromat lattice into the present PETRA ring tunnel is expected to achieve an emittance in the 10 – 20 pmrad range. This measure will bring PETRA IV to the forefront of synchrotron radiation science with a 50 to > 100 times increase of brightness and coherent flux depending on the photon energy range. From our present point of view, such a source will enable almost all present synchrotron radiation techniques to be applied in a spatially resolved manner for the investigation of heterogenous samples. Thus supporting e.g. the design of totally new materials artificially structured on the micro to nanoscale with tailored physical, chemical, or mechanical properties.

The conceptual design report (CDR) for PETRA IV has been finalised by the end of 2019 and the work for a detailed technical design report (TDR) has started. Here I explicitly would like to thank all users and DESY staff members who have contributed to the PETRA IV CDR. More information on the plans for PETRA IV are given in the PETRA part of this report. The year 2019 has also been a successful one for the PETRA III user operation with a record number of proposals, users, and user visits that is approaching 6400. These numbers are likely to increase as soon as the last PETRA III beamlines will become operational. PETRA III is slowly approaching the target number of 5000 h/a for synchrotron radiation delivery since less time for shutdowns is needed to install the remaining components for the last PETRA III extension beamlines into the ring tunnel.

Also at FLASH a record amount of beamtime has been served. The partial parallel operation of the FLASH1 and FLASH2 FELs enabled an increase of about 40% of the available user time as compared to a single FEL. Many ground-breaking experiments have been carried out with some examples shown in this brochure. DESY's medium term goal is to significantly enhance the capabilities at FLASH within the FLASH2020+ project. Among other improvements, this project will include some refurbishments of the linear accelerator with a slight increase of the electron energy, a fully polarisation tuneable afterburner undulator at FLASH2, variable gap undulators for FLASH1 for easier wavelength changes and in order to further decouple FLASH1 and FLASH2 photon beam parameters for parallel operation, external

seeding of FLASH1 for almost transforming limited photon pulses, improvements in the infrastructure, partial refurbishment of FLASH1 beamlines and a considerable expansion of pump-probe laser capabilities. The CDR for the FLASH2020+ project has also been finished during the year 2019 and a TDR is now in preparation. Let me also thank cordially all, who have contributed to the FLASH2020+ CDR. More information on the FLASH2020+ project is given later in this report.

Technical developments for synchrotron and FEL-radiation experiments are getting increasingly elaborated, especially in the field of detectors or X-ray optics but also if it comes to sample environment and nano-positioning. Within the 'League of European Accelerator driven Photon Sources' (LEAPS) all sources within Europe will coordinate their stra-tegy and carry out technical development in joint efforts to make the most efficent use of the available resources to the benefit of the entire user community. It is hoped that this activity will also result in additional funding by the European Commission.

Sample preparation and complementary analysis tools are becoming increasingly important for experiments at photon sources. This is in particular the case for nano scale samples. DESY is addressing this issue by the establishment of the NanoLab providing basic tools for this purpose. Meanwhile, its services are requested by about 5% of all proposals at PETRA III and FLASH. The DESY NanoLab will finally be housed in a new building close to our photon sources, the Centre of X-ray and Nano Science (CXNS) that is realised in collaboration with Helmholtz-Zentrum Geesthacht (HZG) and the Christians-Albrechts-Universität zu Kiel (CAU). The topping out procedure for this building was celebrated on 10 December and we hope that we are able to move in by the end of 2020.

During the last two years DESY started a new initiative to establish a Centre for Molecular Water Science (CMWS). Research in this centre is targeted towards unravelling the secrets of water on the molecular and atomic level from the very fundamental point of view but also in various environments and applications. DESY has received more than 35 letters of support for this initiative mostly from European universities and research institutions. A White Paper on this activity is about to be concluded and an Early Science Programme has been started in order to foster the collaboration with the participating institutions. The concept of the CMWS will be further developed during the year 2020, e.g. by a 'Water Week' in spring, where not only water science but also aspects of funding and governance will be discussed.

The Centre for Structural Systems Biology (CSSB) is meanwhile fully operational including the core facilities and five cryogenic electron microscopes (cryoEMs), two of them being top class instruments. DESY is not only hosting this centre but will also deploy one research group in collaboration with the CAU in order to better connect CSSB activities in structural biology to other research activities on campus and the DESY photon sources.

Better source parameters, improved X-ray optics and experimental techniques and last but not least dramatic development in the performance of detectors provide excellent means to characterise samples in unprecedented resolution in space (real or reciprocal) and time. However, this information does not come for free since the amount of data collected is huge already now and often beyond the capabilities of individual user groups to be handled by themselves. The challenges in this field are manifold. We need better means for a fast feedback already during the experiment to adjust para-meters in time. In addition, we need new soft- and hardware capable of handling these huge amounts of data. And for those cases where data cannot be transferred to the users' home institutions, data evaluation as a facility service will be mandatory to speed up the evaluation and publication process. A large part of experiments at photon sources require imaging or inverse problem evaluations. For this reason, DESY in collaboration with other Helmholtz centres proposed the Helmholtz Imaging Platform (HIP) which was approved by the Helmholtz Senate. From these funds DESY will be able to establish a research group on imaging and reverse problems algorithms and a service as well as an administrative team for coordinating and supporting development of new imaging algorithms across Helmholtz.

At present it is challenging to find scientists trained for these data intensive computing task. For this reason, DESY in collaboration with Universität Hamburg and Hamburg University of Technology proposed a new graduate school to the Helmholtz Association. This school called 'Data Science in Hamburg Helmholtz Graduate School for the Structure of Matter' (DASHH) was granted in 2018 and could welcome already first PhD students. As mentioned above, experiments at photon sources get increasingly elaborated and often require knowledge of modern instrumentation, detection and evaluation tools. In order to educate PhD students for this task, DESY in collaboration with University Hamburg and Lund University was able to acquire another graduate school – the Helmholtz-Lund International School (HELIOS) – to exactly address these issues.

Last but not least, many exciting science highlights have been obtained at our photon science facilities but also within our research groups. Please enjoy reading the examples in this report.

I am very grateful to all DESY staff, our advisory and review bodies, as well as to our users and collaboration partners for the continued support which is the key for our success.

Edgar Weckert
Director Photon Science

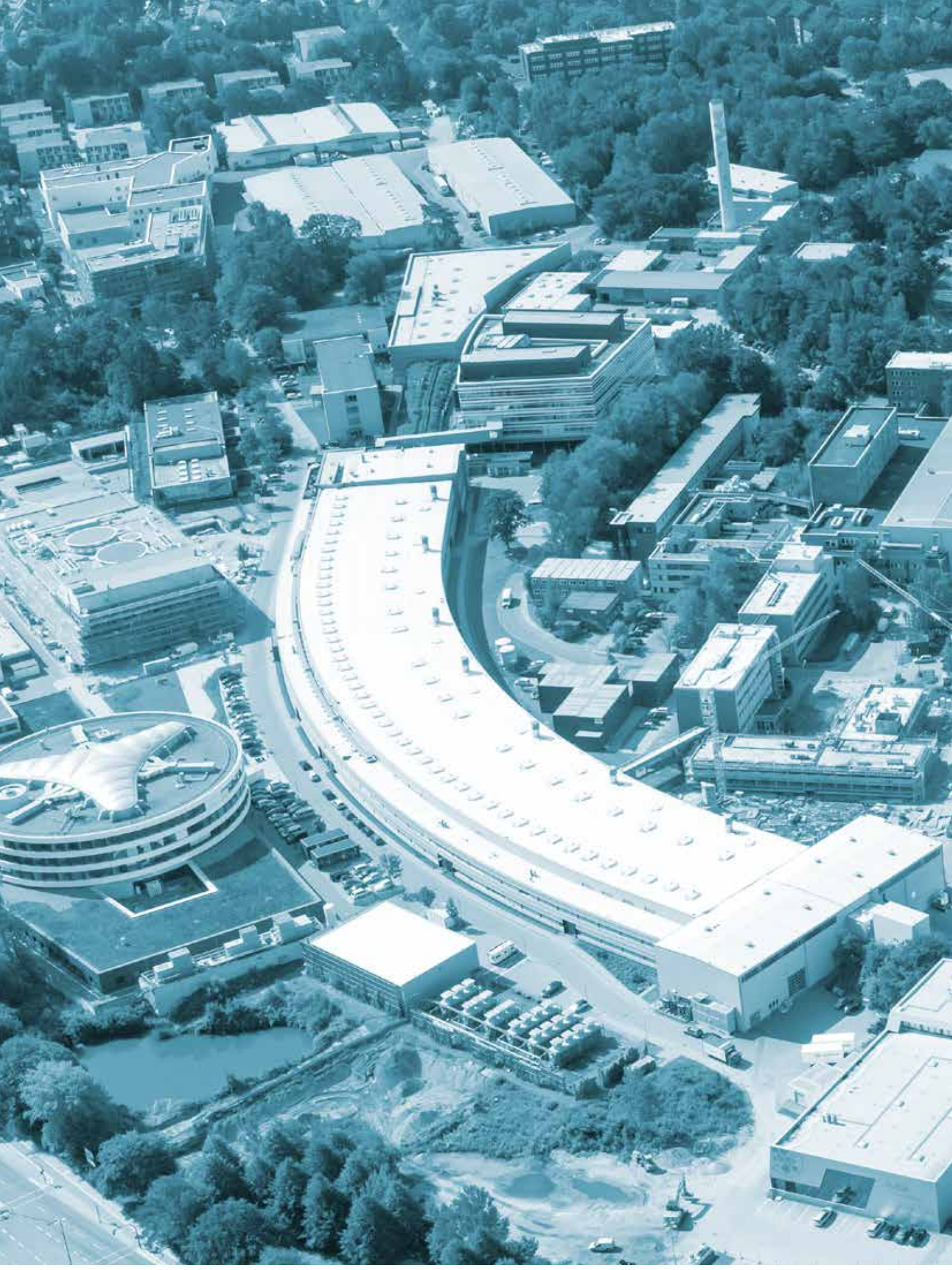

News and Events

News and Events

A busy year 2019

January

23 – 25 January:
The annual joint users' meeting of DESY Photon Science and European XFEL

The joint DESY Photon Science/European XFEL annual users' meeting again attracted more than 1100 participants from 30 nations worldwide, making this annual meeting of photon science facility users the largest gathering of its kind in the world. The attendees represented a community of more than 3000 guest researchers who each year visit the photon science facilities at DESY and European XFEL. For this steadily growing and diversifying community the users' meeting is a very popular and extremely attractive forum for exchange and discussion related to the broad inter-disciplinary use of the research infrastructure.

The first day of the three-day event was devoted to the activities and achievements at European XFEL. The facility could look back to its first year of user operation which started in September 2017. Since then more than 500 researchers have performed experiments at the first two instruments (FXE and SPB/SFX at undulator SASE1). Two more instruments (SCS and SQS at SASE3) became available for users at the end of 2018, and the final two instruments located at SASE2 were going to start user operation during early 2019, thus completing the facility's initial configuration. The first published results show the potential of the unique ultrafast pulses of European XFEL for the investigation of atomic structures and biomolecular dynamics.

At the users' meeting no empty seats were left in the DESY Auditorium.

The morning of the second day was focused on the use of FLASH with reports on technical developments at the facility and presentations of scientific highlights. The afternoon was reserved for 18 satellite meetings and workshops on specific scientific or technical topics.

At the poster session of the joint DESY Photon Science/European XFEL users' meeting.

The last day of the meeting provided an overview across all DESY Photon Science activities in general with special focus on PETRA III and the planned upgrade to a diffraction limited high-resolution X-ray microscope PETRA IV. Furthermore, various presentations featured scientific highlights achieved at the existing PETRA III facility.

The users' meeting ended with a poster session including more than 350 contributions. It was combined with a vendor exhibition that attracted about 80 companies presenting their highly specialised products for cutting-edge research.

February

27 February – 1 March:
18th DESY Research Course: Trends in Modern Photon Science

More than 100 participants attended the 18th DESY Research Course. This annual event has taken place since 2001 and addresses master and PhD students, young research fellows, as well as interested scientists. This year the course was not devoted to a special topic but generally entitled 'Trends in Modern Photon Science'. The ten lectures of the course were given by speakers from DESY, Universität Hamburg, and European XFEL and covered a wide range of topics from FEL and attosecond science via quantum gas science and lasing schemes to exciting new developments in X-ray optics.

The attendants could contribute to the course by presenting their own research work in a poster session, an opportunity that was taken by 35 participants. The three most excellent poster contributions were awarded with a prize and the course was completed with a dinner featuring a dinner talk given by Arwen Pearson from The Hamburg Centre for Ultrafast Imaging at CFEL.

The three winners of the poster prize at the 18th DESY Research Course. From left: Research course organiser Felix Lehmkühler (DESY), the awardees Markus Batzer (MPI Mainz), Philipp Kagerer (Univ. Würzburg), and Kaja Schubert (DESY), and the head of the poster prize committee Martin A. Schroer (EMBL Hamburg).

March

18 – 21 March:
Young scientists from Israel and Germany meet at DESY

DESY hosted a meeting of young scientists from Israel and Germany. This 'GIF Young Scientists' Meeting', organised by the German-Israeli Foundation (GIF), particularly aimed at fostering the exchange and networking of young researchers and to initiate joint, transnational research projects in the field of photon science. The 35 participants were divided equally among the two countries. They presented the current state of their research activities in various disciplines and had time to exchange and discuss ideas among each other and with senior scientists.

Participants of the 'GIF Young Scientists' Meeting' at DESY.

The 'GIF Young Scientists' Meetings' were established in 2017 and complement project funding in the GIF Young Scientists' Program. GIF organises about three such workshops each year, alternating between Israel and Germany.

April

8 - 12 April:
A group of Hercules School students visits DESY and European XFEL

Participants of the HERCULES European School 2019 visited Hamburg to perform tutorials and practical exercises at DESY and European XFEL. Every year the four-week school is organised at the European Synchrotron Radiation Facility ESRF in Grenoble, France and this year it included two one-week excursions to ESRF partner institutions. One group of 20 students went to Sincrotrone Trieste and DESY/European XFEL. The scientific interest of 16 members were related to condensed matter research and they were offered practical exercises at three PETRA III beamlines covering inelastic X-ray scattering (P01), small angle X-ray scattering (P07), and X-ray scattering on thin films and surfaces (P08). At European XFEL each of these students joined a practical exercise at one instrument covering various aspects of X-ray spectroscopy with free-electron lasers. The remaining four students were interested in biological research and were offered a different agenda, which was organised by colleagues from EMBL. This work comprised small angle X-ray scattering and macromolecular crystallography at the PETRA III beamlines P12 and P13 and at European XFEL exercises in the bio labs in the field of crystallisation and nano-crystal injection experiment and with small angle scattering using coherent beams at the SPB/SFX beamline.

Participant of the HERCULES European School on their visit to Hamburg.

May

5 – 9 May:
10th International Workshop on Warm-Dense-Matter 2019

The first 'International Workshop on Warm-Dense-Matter' took place 2000 in Vancouver and two years later it was held at DESY for the first time. Now this renowned workshop series came back to DESY and was jointly organised by DESY and European XFEL. The event took place in a conference location in Kiel-Travemünde and attracted 90 participants from all over the world. The workshop was addressed at the entire community working in the field of plasma and warm dense matter, both experimental and theoretical. The topics of the workshop comprised ultrafast phenomena and non-equilibrium kinetics, transport properties, planetary science with special attention on geoscience and giant planets, material sciences and its applications, and XFEL applications in the field of warm-dense-matter. This wide variety of topics was complemented by reports on technological advances at various facilities, e.g. in the field of diagnostics. Lively discussions after each of the more than 40 talks and in the poster session outlined the potential future developments based on the recent research highlights in this field.

June

17 – 21 June:
13th Ultrafast X-ray Summer School

Participants of the UXSS 2019.

The Center for Free-Electron Laser Science (CFEL) hosted the Ultrafast X-ray Summer School, UXSS 2019, which was jointly organised by CFEL and the PULSE institute at SLAC National Accelerator Laboratory, United States. It was the 13th UXSS summer school since 2007 and this year it was organised by the Max Planck Institute for the Structure and Dynamics of Matter (MPSD) which is one of the three partners forming CFEL. For the first time the school was extended to five full days. The school offered the opportunity to get familiar with the latest developments and opportunities in ultrafast X-ray science to more than 70 doctoral students and postdoctoral researchers. The program was highly interdisciplinary, with nine lectures covering topics from light

sources to molecular biology and matter in extreme conditions. The school also included visits to instruments at DESY and European XFEL, as well as a final project presentation and prize ceremony honouring the best contributions.

The UXSS 2019 poster.

19 – 23 June:
DESY participates in the 'Summer of Knowledge' on the occasion of the 100th anniversary of Universität Hamburg

For four days in summer the large square in front of the Hamburg town hall was transformed into a science campus celebrating the occasion of the 100th anniversary of Universität Hamburg.

In the framework of the festival 'Summer of Knowledge' about 40 research institutions of the Hamburg area offered insight into their activities. Together with Universität Hamburg, DESY, and its partners MPSD, European XFEL, CSSB, and EMBL provided major contributions to the program in a large tent devoted to the theme 'HiTech Laboratory'. The interested public was informed about research with the powerful light sources available at DESY and European XFEL and could experience presentations, demonstrations, and hands-on experiments related to various topics like research with light, application of superconductivity, or a virtual reality tour along European XFEL. The exhibition was complemented by a couple of 45-minutes talks addressing specific topics. During the four days the whole event welcomed about 50 000 visitors.

Demonstration of superconductivity in action: A floating train.
(Image: Alena Zielinski; license CC-BY-2.0)

Summer of Knowledge 2019: View from the Hamburg town hall balcony.

July

1 July:
Cooperation agreements signed for Early Science Programme (ESP) of the Centre for Molecular Water Science

The Centre for Molecular Water Science (CMWS) is an initiative by DESY Photon Science, and is driven by the research expertise and X-ray infrastructure on the campus. Its aim is to combine local expertise and infrastructure with the expertise of regional, national, European and international partners to address the relevant fundamental questions in water-related sciences. Over 30 national and international institutions have sent 'Letters of Intent' to join the CMWS. Part of the initiative is the Early Science Program (ESP) that funds young researchers carrying out projects within the centre. The ESP is co-funded by DESY and its partners and the first six cooperation agreements were signed in summer 2019.

CMWS research is based on five pillars: Fundamental properties, Geo-and astrophysical processes, Water in nanoscience and technology, Real time chemical dynamics, and Water in biochemistry and biology. The first pilot projects of this ambitious science program have already been started.

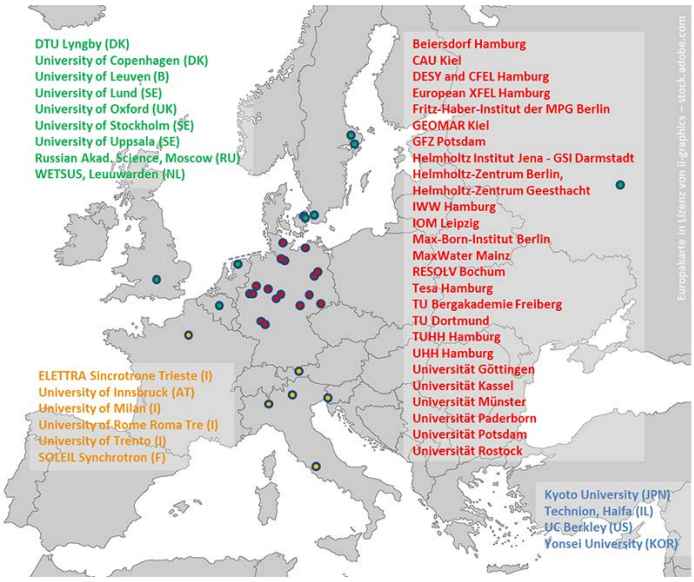

The research institutions on the maps have declared their interest to join the CMWS by sending Letters of Intent to DESY.

16 July:
DESY Summer Student Programme 2019

91 students attended the summer student programme 2019 in Hamburg.

As every year, starting from the mid of July until beginning of September about 100 selected students had the opportunity to take part in the all-day work of a DESY or European XFEL research group. Each student could work on an own small project, and in a series of lectures the students learned about the DESY activities in general and about special topics related to high energy physics or the forefront of photon science. The programme addresses students of physics and related natural sciences who have completed at least three years of studies but are not going to finish a master's degree in the corresponding year. The application deadline is always at the end of January, and this year again more than 1100 students from all over the world applied, about 400 of them for the field of photon science. Finally, about 90 students were accepted for the whole programme in Hamburg, and from these 19 female and 12 male students from eleven nations were distributed among the Photon Science research groups. Thus, the DESY Summer Student programme is not only popular because of the practical experience it offers in real research projects, but also because of its internationality. The exchange between students is an important factor and the mix of cultures and nationalities creates the inspiring atmosphere that is also typical for many of DESY's research collaborations.

Group photo of the summer students in the photon science part of the programme.

August

26 – 30 August:
The largest conference on free-electron lasers, FEL2019

The audience listening to the opening talks of the FEL2019 Conference. First row with Hamburg's Second Mayor and Senator for Science, Research and Equality, Katharina Fegebank (left), Managing Director of European XFEL, Robert Feidenhans'l (middle) and DESY's Director of the Accelerator Division, Wim Leemans (right).

Hamburg's Second Mayor and Senator of Science Katharina Fegebank opened the world's largest conference devoted to free-electron lasers. At the 39th International Free-Electron Laser Conference (FEL2019), which was co-hosted by DESY and European XFEL, around 400 participants from 25 countries worldwide gathered in Hamburg for a whole week to discuss the latest progress in development and application of these unique research tools. The scientific programme comprised more than 50 talks and tutorials, three poster sessions, a prize ceremony, and laboratory visits to European XFEL and FLASH. The talks were focused on status reports of facilities and projects, recent advances in free-electron laser theory and experiments, electron beam, photon beam and undulator technologies, and applications of free-electron lasers. The FEL conference is held every two years at different locations.

Two FEL-related prizes were awarded at the FEL2019: The 2019 Young Scientist FEL Award was given to Joe Duris (SLAC) and Chao Feng (SARI). Enrico Allaria (Sincrotrone Trieste), Alex Lumpkin (Argonne/Fermilab), and Gennady Stupakov (SLAC) received the 2019 FEL Prize.

DESY last hosted the conference in 1999 when X-ray free-electron lasers only existed on paper. Since then, the field of free-electron laser science, as well as the construction of free-electron lasers at the DESY research campus, has evolved dramatically. This includes the first observation of short wavelength FEL light at DESY's FEL FLASH in 2000 and the opening of European XFEL in 2017, developed and built by a cooperation of DESY and international partners. In the meantime several XFEL user facilities are in operation all over the world, with FLASH being the prototype.

September

3 September:
Freigeist Fellowship for Daria Gorelova

Daria Gorelova. (Credit: Universität Hamburg, Ohme)

The Volkswagen Foundation awarded Daria Gorelova from the DESY Photon Science division a Freigeist Fellowship. Daria Gorelova is currently working at the Center for Free-Electron Laser Science (CFEL at DESY) on ultrafast processes in solids and molecules. In particular, she uses quantum mechanical methods to investigate possibilities to characterize these processes with X-ray radiation generated by free-electron lasers like European XFEL. In her research, Gorelova intends to investigate microscopic phenomena that could be important in the field of renewable energies. Funding from the Volkswagen Foundation will enable her to set up a junior research group at the Universität Hamburg.
The Volkswagen Foundation's Freigeist Fellowships aim at exceptional research personalities who are acting between established research fields and wish to pursue high-risk science. Since 2014, each year ten to fifteen Freigeist Fellows have been selected. Over a maximum of eight years, they receive a total funding of up to 2.2 million Euro to set up their own junior research group.

16 – 20 September:
Course on synchrotron-based XAFS techniques

This course aiming at *in situ*/*operando* X-ray absorption fine structure (XAFS) was organised by DESY scientists responsible for the PETRA III XAFS instruments together with XAFS experts from Karlsruhe Institute of Technology (KIT). The organisers from KIT are also coordinating a priority program of the German Research Foundation (DFG) entitled 'catalysts and reactors under dynamic conditions for energy storage and conversion, SPP 2080'. The workshop was supported by this program and about half of the participants were PhD students working in this program. Due to the planned hands-on experiments the total number of participants was limited to 32 students. In the workshop the basics of XAFS spectroscopy were presented in lectures and during practical exercises at PETRA III beamlines P64 and P65 including data evaluation. The second part focused on *in situ* experiments at the beamlines. The workshop was complemented by lectures about other synchrotron-based analytical methods useful in catalysis research, like X-ray diffraction, inelastic scattering, and pair distribution function.

20 September:
Memorial symposium for Wilfried Wurth

Wilfried Wurth.

On 8 May, Wilfried Wurth, lead scientist at DESY and one of the pioneers in research with free-electron lasers at DESY died unexpectedly at the age of 62. Wilfried Wurth, who was also professor for experimental physics at the Universität Hamburg since 2000, has been a recognised expert in X-ray spectroscopy and for the investigation of ultrafast processes like the real-time observation of dynamics of atoms on surfaces. Already before he joined DESY in 2014, he was one of the major researchers at FLASH. He played an important role in the construction and development of the Center for Free-Electron Laser Science. Wilfried Wurth was the founder and leader of the Advanced Study Group of Universität Hamburg at CFEL and in this function he shaped the cooperation of the university with the other partners, including his strong influence on the excellence strategy in Hamburg. From 2007 to 2013, Wilfried Wurth was spokesman of the BMBF research priority programme 'FLASH' which was the first priority programme in the condensed matter field. During Wurth's time as scientific director of FLASH a second undulator line for light generation and a second experimental hall for experiments at this line were built in the framework of the FLASH II expansion project. During DESY's strategy process, completed in 2018, Wilfried Wurth took a leading role in developing visions for the future of the pioneering facility. Most recently, he was leading the creation of the FLASH2020+ CDR.

On 20 September friends and colleagues gathered at DESY to commemorate Wilfried Wurth in a scientific memorial symposium. After some introductory words of reminiscence and recollection his work was honoured by talks related to his scientific activities and achievements.

25 – 26 September:
Workshop on Soft X-ray Science at PETRA

At DESY most research with soft X-rays is currently performed at PETRA III beamline P04. The workshop entitled 'Soft X-ray Science at PETRA' attracted 80 members of the soft X-ray science community. The main objectives of the workshop were to identify emergent science themes as well as synergies and potential collaborations in the field of research with soft X-rays, and to review the existing instrumentation for these experiments. Furthermore, the workshop was intended to start a detailed discussion about the science case for the upcoming technical design report of PETRA IV. The workshop was organised in eight sessions with 26 talks and a poster session with 22 contributions. The scientific fields covered development of XUV sources and instrumentation, fundamentals of interaction of radiation with matter, microscopy of magnetic structures, minerals and biological samples, electronic structure of quantum materials and of molecules in liquid environment, and ion absorption spectroscopy in relation to astronomical observations. A keynote talk was given by Jan Lüning (HZB).

Participants of the workshop on Soft X-ray Science at PETRA.

October

16 October:
PhD thesis prize for Max Rose for his photon science related work

Each year DESY's Science Day is an internal event to celebrate the achievement of the past year, to honour deserving DESY employees and to welcome new leading scientists. Further topics of this event are the 'Jentschke Lecture' given by an invited renowned scientific person and the presentation of the PhD thesis prize of the Association of the Friends and Sponsors of DESY for outstanding PhD theses resulting from work at DESY. This year the prize was equally shared between Max Rose and Marcel Usner. Max Rose studied physics in Göttingen before he started his PhD work at DESY and Universität Hamburg with support from a Joachim Herz Foundation scholarship. His thesis entitled 'Coherent X-ray diffractive imaging of biological samples in 2D and 3D with synchrotron and XFEL radiation' addresses imaging of samples with nanometre special resolution. The used technique requires highly coherent X-ray radiation as provided by PETRA III, FLASH, and European XFEL.
Max Rose developed important and innovative improvements for the experimental technique in order to get high resolution images of biological cells. He then could apply the achieved knowledge to single particle imaging (SPI) experiments at free-electron lasers which were performed by the SPI consortium on virus particles at LCLS in Stanford (US). The achieved resolution of ten nanometres is currently the best that has ever been reached with an SPI experiment and the given type of samples.

At the prize ceremony for the DESY PhD thesis award. From left: Prize winners Marcel Usner and Max Rose, together with Wilfried Buchmüller, Chairman of the Association of the Friends and Sponsors of DESY and DESY Director Helmut Dosch.

Marcel Usner (DESY and Humboldt University Berlin) worked in the field of astroparticle physics. He improved the reconstruction of data from the IceCube Detector significantly, making it possible to detect cosmic tau-neutrinos. These are of special interest because the probability of their being produced within the atmosphere of the earth is extremely low, pointing at an origin from cosmic events.

November

5 November:
Francesca Calegari was elected 2020 Fellow of the Optical Society

Francesca Calegari, DESY Lead Scientist and Professor at Universität Hamburg, was elected a Fellow of the Optical Society (OSA) in recognition of her major contributions to attosecond science. With 21 000 members in more than 100 countries, the Optical Society is the leading scientific society in the field of optics and photonics. Francesca Calegari, who leads the attosecond science group at DESY, is developing advanced laser sources providing extremely short light pulses with pulse duration in the order of 10^{-18} seconds (attoseconds). Her work has a major impact in the field of research on ultrafast processes, since it pioneered the possibility to image and to control the electron dynamics in complex molecules. This is an important ingredient for a future 'attochemistry', a concept going back to an idea that has been pursued by scientists ever since the development of the first sources of attosecond light pulses.

DESY Lead Scientist Francesca Calegari.

6 November:
Helmholtz Doctoral Award for Yi-Jen Chen

Yi-Jen Chen from DESY Photon Science was awarded the Helmholtz Association's Doctoral Prize in the research area 'Matter' for her outstanding doctoral thesis in the field of ultrafast physics. In her dissertation Chen could successfully explain experimental findings on the behaviour of electron clouds in strong laser light within the temporal regime of attoseconds. The award was presented to her by Helmholtz President Otmar Wiestler at the Helmholtz Horizons event in Berlin. Together with Chen, five other students were honoured for the best doctoral thesis in one of the six Helmholtz research areas. Five of these six young researchers are women. The Helmholtz Doctoral Prize is awarded annually and includes prize money of as well as support for an up to six month stay at an international research institution. The Helmholtz Association is currently supervising more than 8 000 doctoral candidates.

The Helmholtz Doctoral Award was presented to Yi-Jen Chen by Otmar Wiestler, President of the Helmholtz Association.

20 – 22 November:
International Workshop on Grazing Incidence Small Angle Scattering, GISAXS2019

The GISAXS workshop 2019 attracted 90 participants. This series of workshops started in 2005 intending to join the various communities working in the field of thin films, nanostructures, surfaces and interfaces, to gain insights to the powerful method of grazing incidence small angle X-ray scattering and related techniques including small angle neutron scattering. Since then ten GISAXS workshops have been organised either at DESY or as satellite events along with the International Small Angle Scattering (SAS) Conferences. The workshop aims at experienced as well as new users of this experimental technique. Therefore, it offers a basic introduction to small angle scattering and in four keynote and ten invited talks scientific possibilities and new trends in GISAXS and GISANS were highlighted with special emphasis on real-time investigations and data analysis. The second part of the workshop was devoted to practical hands-on training focusing on on-line data treatment and simulation of GISAXS data. The participants could also visit the state-of-the-art instrumentation for small angle X-ray scattering under grazing incidence with micro- or nanometre-sized beams at PETRA III beamline P03.

December

5 December:
Innovation Award on Synchrotron Radiation for cutting edge detector development

At the Innovation Award 2019 ceremony in Berlin (from left): The laudator Edgar Weckert (DESY) with the awardees Aldo Mozzanica, Bernd Schmitt (both from PSI, Villigen, Switzerland), Heinz Graafsma (DESY) and the chair of the 'Freundeskreis des Helmholtz-Zentrums Berlin (HZB)' Mathias Richter (PTB).
(Photo: M. Setzpfand/HZB)

Each year the Friends of the Helmholtz-Zentrum Berlin present the Innovation Award on Synchrotron Radiation. The prize is to be granted for an excellent achievement which has significantly contributed to the further development of techniques, methods or use of synchrotron radiation. It addresses scientist and engineers from research institutions and industry in Europe. The 2019 award was presented to Heinz Graafsma from the DESY Photon Science Detector group and Aldo Mozzanica and Bernd Schmitt from the Detectors Group of the Paul Scherrer Institut (PSI) for the development of the automatic gain-switch in the individual pixels of X-ray pixel detectors. This technique is used in the 'Jungfrau Detector' of PSI and in the 'Adaptive Gain Integrating Pixel Detector AGIPD' of DESY. The high dynamic range of this X-ray detector, achieved by the new technology, and its capability to locally store up to 350 images that arrive at the detector at 4.5 MHz rate provide the essential prerequisites for performing X-ray scattering experiments at free-electron lasers like the European XFEL.

10 December:
Topping-out ceremony for the new Center for X-ray and Nanoscience

The new building for the Center for X-ray and Nanoscience (CXNS) currently under construction celebrated its topping-out ceremony. CXNS is a cooperation of DESY with the Helmholtz-Zentrum Geesthacht (HZG) and the Christians-Albrechts-Universität zu Kiel (CAU). The building will be the home of DESY NanoLab, the German Engineering Materials Science Centre (GEMS) of HZG, the 'Ruprecht-Haensel-Labor', which is a long-standing cooperation between CAU and DESY, and a few other groups working in the field of photon science at DESY. CXNS will thus integrate some already existing activities which are currently spread all over the DESY campus with the aim to offer excellent conditions for research in nanoscience. The five-storeyed building provides 5000 square metres of floor space of which 700 square metres are reserved for laboratories which will host mutually complementary preparation and analysis facilities. Office space is foreseen for about 250 researchers.

At the CXNS topping-out ceremony. From left: Matthias Rehahn and Martin Müller (HZG), Helmut Dosch (DESY), Volkmar Dietz (German Federal Ministry of Education and Research), Eva Gümbel (BWFG), Lutz Kipp (CAU), Edgar Weckert (DESY), Frank Duddeck (SBI Siemke & Co), Andreas Stierle (DESY).

Construction started in autumn 2019 and is planned to be finished by the end of 2020. The 18 million Euro for the building derive from funding by the German national government, by the regional governments of Hamburg and Schleswig-Holstein, and from the budgets of the three involved research institutions.

18 December:
60 Years of DESY in Hamburg

The story of DESY began on 18 December 1959 with the signing of a contract in Hamburg's town hall. It is a story of successful global research and for Germany as a science hub. For the past 60 years, fundamental research has been carried out at DESY in Hamburg-Bahrenfeld – which was joined in 1991 by a second DESY site in Zeuthen. In those 60 years, DESY has become a world leader in accelerator technology, photon science, particle physics and astroparticle physics. DESY has developed pioneering technologies, which have been used by scientists from all over the world to make outstanding advances in research. Amongst others, the gluon was discovered and the structure of ribosomes was determined at DESY. Some special events are planned for 2020 to celebrate DESY's 60th birthday.

Aerial view of the DESY campus in Hamburg-Bahrenfeld in 1963: The construction of the accelerator ring (centre) is finished, other buildings are still under construction.

Science Highlights

Hot aluminium nanodroplets etch faceted holes in semiconductors

Promising technique for quantum dot fabrication finds surprisingly smooth etch pit morphologies

Controlling material structures and properties at the nanoscale remains a key challenge for contemporary science. In the case of optoelectronic semi-conductor nanostructures, applications like quantum computing and communication are just around the corner. These rely on robust and reproducible nano-fabrication techniques. The physics behind such applications is electron confinement. It occurs within nanoscale structures and opens up a whole new bunch of properties by the fact that quantum mechanical laws start to apply. We report on the morphology and crystallographic shape of nano-scaled etch pits, which are created by aluminium droplets deposited at elevated temperatures. The fabrication of these structures is very promising in the light of single photon source applications.

Semiconductor nanostructures hold promise for use in quantum information technology and nanoscale optoelectronics. In particular, semiconductor quantum dots represent building blocks as qubits for quantum computing or as sources for entangled photons for quantum communication [1].

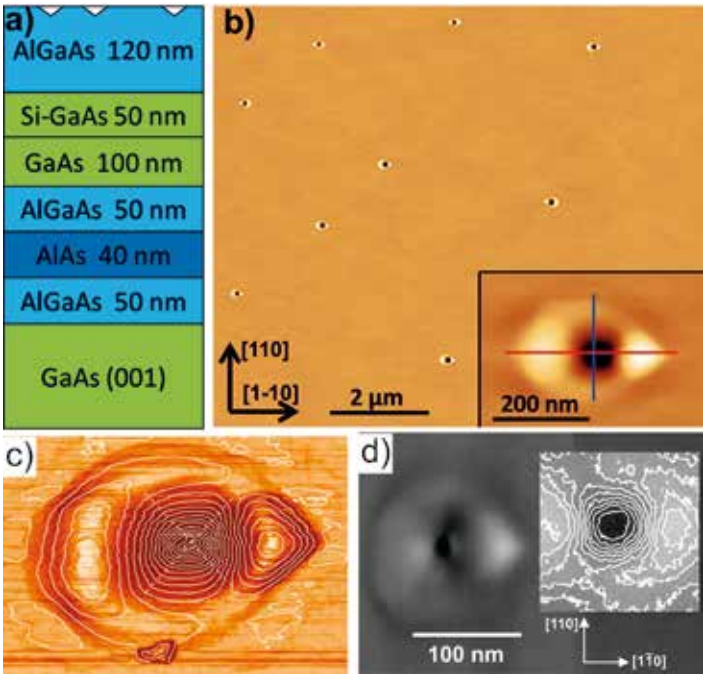

Figure 1

a) Schematic view of the layered structure of the sample. Local droplet etching takes place in the topmost AlGaAs layer. b) Atomic force micrograph (AFM) showing the relatively low density of nanoholes. The inset shows a magnified part of the image, revealing the anisotropic shape of the hole and surrounding ring. c) AFM image of a single hole with height contour lines. d) High resolution scanning electron micrograph of a single hole. The inset shows the contrast contour lines. c) and d) highlight the rectangular shape of the inner walls.

There are basically two approaches to the production of nanostructures. In a so-called top-down approach, a crystal surface produced from several layers of different materials can be subsequently structured. However, this method established in the semiconductor industry has not yet led to success in the manufacturing of optical quantum dots. In an alternative bottom-up approach, physical mechanisms are exploited that lead to the spontaneous self-formation of nanostructures during crystal growth. The strain-induced quantum dot formation in InAs structures on GaAs substrates during an epitaxial Stranski-Krastanow growth process is the most well-known. Another method applies local etching. First, metallic nanodroplets are spontaneously formed on a crystal surface of GaAs. During a thermal annealing step after growth the droplets transform into nanoholes surrounded by a crystalline AlAs wall. Details of the process and discussions of the mechanisms behind droplet etching are given in previous publications [2]. Although etching is an important technology in semiconductor industry, the microscopic mechanisms underlying such a process on the nanoscale are not very well understood yet.

The samples were grown at the Centre for Hybrid Nanostructres (CHyN) in a molecular beam epitaxy system on epiready GaAs(001) wafers. The layer sequence of the investigated sample that is extensively studied here is grown at T = 625 °C using Al droplets and sketched in Fig. 1a. This multilayer structure allows for investigating local droplet etching on more complicated heterostructures, which are needed for real applications. Nanoholes formed in the topmost AlGaAs layer by local droplet-etching have been characterized using atomic force microscopy and scanning electron microscopy (see Figs. 1b-d). X-ray diffraction on hole ensembles and single holes performed at the ESRF are shown in Figs. 2 and 3,

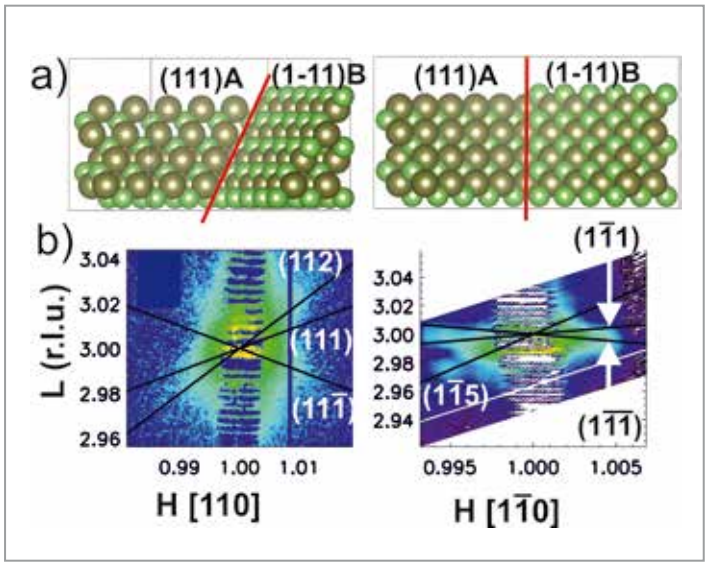

Figure 3

a) 3D representation of the {111}-type etch pit walls. Shown are a side view (left) and top view (right) of (111)A and (11-1)B facets that meet at a common edge, which is indicated by the red line. For the (111)A facet, the Ga atoms (dark green) are at the terminating layer, for the (1-11)B facet the As atoms are terminating (light green). b) Difference intensity reciprocal space maps taken at the 113 GaAs Bragg peak using a 300-nm X-ray beam. Left and right panels show data for two different crystallographic planes. The difference is obtained from data when illuminating a single nanohole and in between the holes. Clearly, there is a significant intensity difference, which arises due to scattering from facets, which are absent in between the holes. The indices of the facets giving rise to particular streaks are indicated.

respectively. The combination of real and reciprocal space techniques allows for circumventing particular data interpretation problems that would arise when only one of them would have been used. The picture of the nanohole's shape formation implied from our results is that of etch-pit wall faceting, most notably forming {111}A, {1-11}B, and {112} facets (Figs. 2 and 3b). The redeposited ring material consists of much flatter surfaces, i.e., facets with higher indices, which are clearly seen in the X-ray diffraction (Figs. 2 and 3b) and atomic force microscopy (Fig. 1).

The strictly Ga or As terminations of the facets in both perpendicular directions (Fig. 3a) probably play an important role. It is known that the two different terminations can lead to different etch rates. The stepped {112} and {113} surfaces contain {111}A terraces and are therefore considered to be almost equally stable as the slowest etching planar {111}A surface. Below an etching temperature of T ~ 665 °C, the average steepness of the walls diminishes, indicating that flatter facets become more pronounced. Below approximately 620 °C, {111}-type facets seem not to form at all. These results imply that to a large extent the local droplet-etching process can be described by considering thermodynamics and etch rates in different crystallographic directions taking into account the specific atomic terminations. Moreover, the results presented here are very important if the holes will be used as templates for quantum-dot growth. They will help understanding and controlling the symmetry of the holes, which is essential, for instance, in applications in which the dots are sources of entangled photons [1].

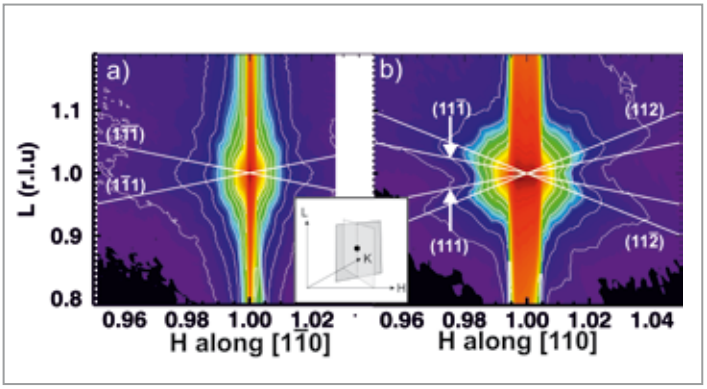

Figure 2

Reciprocal space maps around the AlGaAs 111 Bragg reflection, obtained by X-ray illumination of approximately 10^5 nanoholes. a) Map in the h-hl-plane. b) Map in the hhl-plane. The inset shows schematically the two perpendicular planes that were measured. Intensity streaks along different directions have been indexed according to the corresponding facets.

Author contact: Vedran Vonk, vedran.vonk@desy.de

References

1. M. Gurioli, Z. Wang, A. Rastelli, T. Kuroda and S. Sanguinetti, 'Droplet epitaxy of semiconductor nanostructures for quantum photonic devices', Nature Mater. 18, 799–819 (2018).
2. C. Heyn, A. Stemmann and W. Hansen, 'Dynamics of self-assembled droplet etching', Appl. Phys. Lett. 95, 173110 (2009).

Original publication

'Faceting of local droplet-etched nanoholes in AlGaAs', Phys. Rev. Mat. 2, 106001 (2018).
DOI: 10.1103/PhysRevMaterials.2.106001

Vedran Vonk[1], Taras Slobodskyy[2], Thomas F. Keller[1,3], Marie-Ingrid Richard[4], Sara Fernández[4], Tobias Schülli[4], Christian Heyn[2], Wolfgang Hansen[2] and Andreas Stierle[1,3]

1. Deutsches Elektronen-Synchrotron DESY, Hamburg, Germany
2. Center for Hybrid Nanostructures (CHyN), Universität Hamburg, Germany
3. Fachbereich Physik, Universität Hamburg, Germany
4. European Synchrotron Radiation Facility, Grenoble, France

Controllable growth of few-layer graphene

Using synchrotron radiation facilities the mechanism of epitaxial layer-by-layer graphene growth on cubic SiC(001) is uncovered

The unique properties of graphene make it a competitive alternative to silicon in electronic applications. Synthesis on low-cost cubic SiC/Si(001) wafers is a viable method for graphene mass-production on semiconducting substrates, compatible with existing technologies. Moreover, utilising vicinal SiC/Si(001) wafers, one can synthesise self-aligned graphene nanoribbons that exhibit charge transport gaps on the order of 1 eV, large positive in-plane magnetoresistance and the potential to work as a spin filter, opening opportunities for electronic and spintronic applications. This work demonstrates the capabilities to control the lattice and boundary orientations and the layer thickness *in situ* during the few-layer graphene synthesis in ultra-high vacuum.

Graphitisation of cubic SiC/Si(001) wafers [1-3] permits the fabrication of a few-layer graphene supported on a cheap and commercially available wide-gap semiconductor substrate. Vicinal substrates with small miscuts from the (001) crystallographic plane allow the synthesis of nanostructured graphene with domain boundaries preferentially aligned along the step direction. This leads to anisotropy of transport properties of the graphene layer, namely, the emergence of a charge transport gap when electrical current is applied across the nanodomain boundaries [4, 5].

The thickness of the graphene overlayer grown on silicon carbide substrates depends critically on the vacuum conditions, the temperature during synthesis and its duration.

Therefore, it is feasible to control the number of the synthesised graphene layers *in situ*, during the few-layer graphene growth. We demonstrate the possibility to obtain mono-, bi-, and trilayer graphene on cubic SiC(001) substrates with *in situ* control under ultra-high vacuum (UHV) conditions.

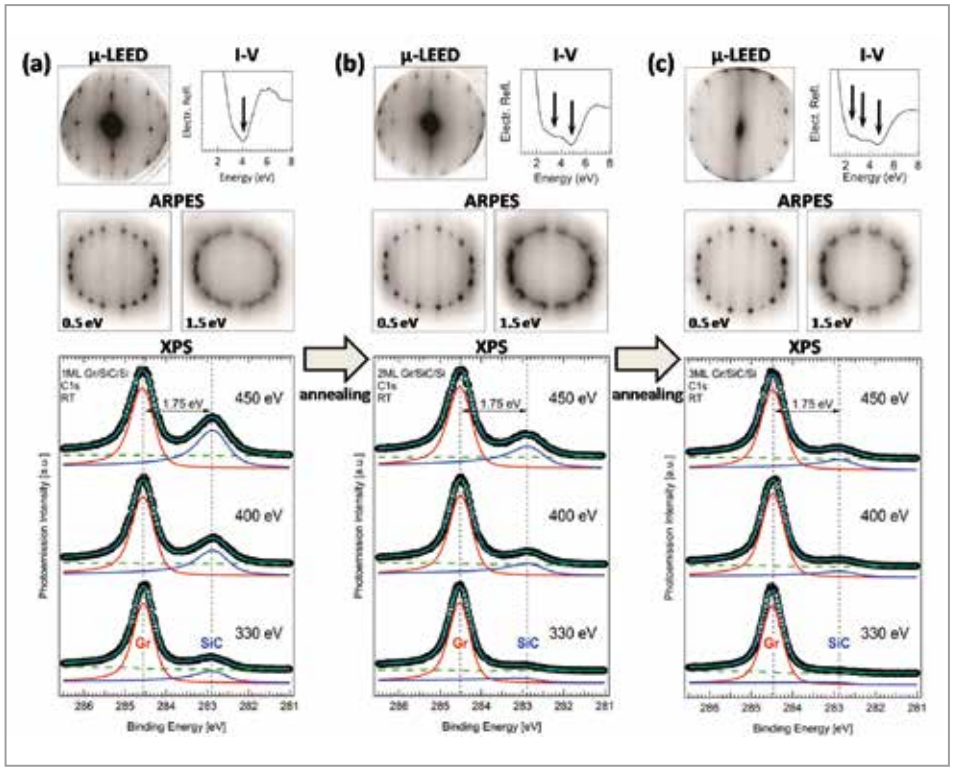

Figure 1

In situ LEEM, μ-LEED, ARPES and XPS showing control over the SiC(001) surface graphitization during heating in UHV. (a-c) μ-LEED, reflectivity spectra, ARPES constant-energy maps and μ-XPS data obtained from one of the micrometre-sized domains of the graphene/SiC(001) system at approximately 1 ML (a), 2 ML (b), and 3 ML (c) coverage.

Top row: μ-LEED taken from a circular sample area (d = 0.5 μm) using a 44 eV electron beam (left) and LEEM I–V curves demonstrating one (a), two (b) and three (c) minima (indicated by arrows) corresponding to the number of synthesised graphene layers (right). Middle row: Photoemission angular-distribution maps taken at 0.5 eV (left) and 1.5 eV (right) binding energies, measured using at 47 eV photon energy.

Bottom row: Experimental XPS C 1*s* spectra (black circles) obtained with 330, 400 and 450 eV photon beams for 1, 2 and 3 layers from selected circular sample area (d = 2 μm) and results of the spectra deconvolution (red, blue, green and cyan lines).

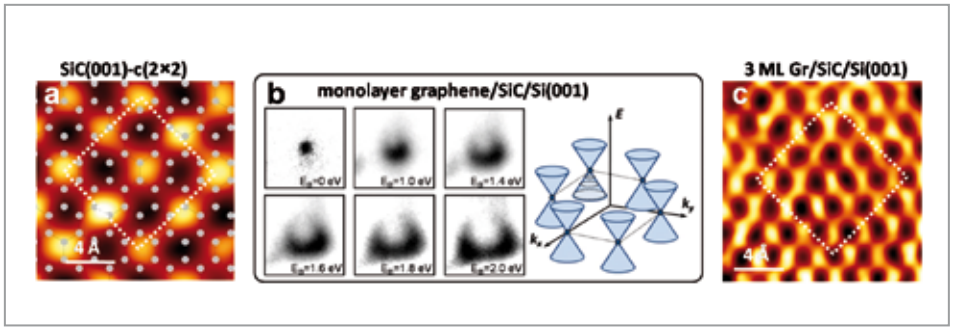

Figure 2

(a) 2 × 2 nm² STM image of the SiC(001)-c(2×2) reconstruction with the model of the non-rotated graphene lattice overlaid. (b) Constant energy ARPES intensity maps taken near one of the K points at binding energies (E_B) from 0 to 2.0 eV, showing the electronic structure in the k_x–k_y plane ($h\nu$ = 47 eV). (c) 2 × 2 nm² STM image of trilayer graphene synthesized on cubic-SiC(001) measured from a nanodomain with non-rotated graphene lattice.

This study builds on core-level X-ray photoelectron spectroscopy (XPS) results from beamline P04 at PETRA III using a dynamic-XPS end station with the electron spectrometer ARGUS and by high-resolution angle-resolved photoelectron spectroscopy (ARPES) results measured at the Nanospectroscopy Beamline (ELETTRA, Trieste).

At each stage of the graphene synthesis, the sample was characterised by a set of complimentary high-resolution micro-spectroscopic methods (Fig. 1). In particular, ARPES data reveal the Dirac cones typical for graphene, crossing at the Fermi level in the vicinity of the K points. The measured ARPES dispersions prove, that mono-, bi- and trilayer graphene grown on cubic SiC(001) exhibits quasi-freestanding electronic properties (e.g., Fig. 2b shows the constant-energy ARPES intensity maps in the k_x–k_y plane for one of the Dirac cones measured from monolayer graphene). At the same time, homogeneity and thickness of the graphene overlayer is controlled by low-energy electron microscopy (LEEM). In the measured electron reflectivity (*I*-*V*) curves the number of synthesised graphene layers is equal to the number of minima in the low energy part of the curve. Low energy electron diffraction (LEED) and scanning tunnelling microscopy (STM) revealed three preferential graphene lattice orientations in the nanostructured graphene (non-rotated and ±13.5°-rotated relative to the [110] direction).

The signal from domains with non-rotated graphene lattices is systematically suppressed in LEED and ARPES when graphene coverage exceeds one monolayer. Detailed analysis of the experimental data suggests a mechanism of the graphene growth on cubic SiC(001) that considers the well-known carbon-terminated c(2×2) reconstruction as a necessary predecessor of graphene. The double unit cell of this reconstruction has a very small (< 2%) mismatch with the non-rotated graphene lattice (Fig. 2a,c). Suppression of the signal from domains with non-rotated lattices at graphene coverages above one monolayer can be explained by the growth of the second and third monolayer starting from the linear defects (atomic chains on the c(2×2) reconstruction) which are predominantly aligned along the [110] direction. That leads to the emergence of 2 types of domains with graphene lattices rotated by ±13.5° relative to the [110] direction, which prevails on the nanostructured trilayer graphene.

The XPS spectra of mono-, bi- and trilayer graphene recorded in normal emission geometry at several photon energies can serve as a reference for quick identification of the different graphene coverages grown on cubic SiC(001) substrates. This is particularly interesting since XPS is routinely available in nearly all surface science laboratories and synchrotron radiation centres. For example, the dynamic-XPS station with real-time control of the C 1*s* core-level spectra shape during the sample heating, developed for beamline P04 at PETRA III [6], can be used for controllable growth of mono-, bi- and trilayer graphene.

Author contact: Victor Aristov, victor.aristov@desy.de
Olga Molodtsova, olga.molodtsova@desy.de
Alexander Chaika, chaika@issp.ac.ru

References

1. V. Y. Aristov et al., 'Graphene synthesis on cubic SiC/Si wafers. perspectives for mass production of graphene-based electronic devices', Nano Lett. 10 (3), 992-995 (2010).
2. A. N. Chaika et al., 'Continuous wafer-scale graphene on cubic-SiC(001)', Nano Res. 6, 562-370 (2013).
3. A. N. Chaika et al., 'Rotated domain network in graphene on cubic-SiC(001)', Nanotechnology 25, 135605 (2014).
4. H.-C. Wu et al., 'Transport gap opening and high on-off current ratio in trilayer graphene with self-aligned nanodomain boundaries', ACS Nano 9, 8967-8975 (2015).
5. H.-C. Wu et al.,'Large positive in-plane magnetoresistance induced by localized states at nanodomain boundaries in graphene', Nat. Commun. 8, 14453 (2017).
6. S.V. Babenkov et al., 'A new dynamic-XPS end-station for beamline P04 at PETRA III/DESY', Nucl. Instrum. Methods Phys. Res., Sect. A 777, 189-193 (2015).

Original publication

'Layer-by-layer graphene growth on βSiC/ Si(001)', ACS Nano 13, 526-535 (2019).
DOI:10.1021/acsnano.8b07237

Victor Yu. Aristov[1,2], Alexander N. Chaika[2,3], Olga V. Molodtsova[1,4], Sergey V. Babenkov[1,5], Andrea Locatelli[6], Tevfik Onur Menteş[6], Alessandro Sala[6], Dmitrii Potorochin[1,4,7], Dmitry Marchenko[8], Barry Murphy[3], Brian Walls[3], Kuanysh Zhussupbekov[3] and Igor V. Shvets[3]

1. Deutsches Elektronen-Synchrotron DESY, Hamburg, Germany
2. ISSP RAS, Chernogolovka, Russian Federation
3. CRANN, School of Physics, Trinity College Dublin, Ireland
4. ITMO University, Saint Petersburg, Russian Federation
5. Johannes Gutenberg-Universität, Mainz, Germany
6. Elettra Sincrotrone, Trieste, Italy
7. TU Bergakademie, Freiberg, Germany
8. Helmholtz-Zentrum Berlin/BESSY, Germany

Watching nanocrystal assembly in real time

Self-organisation of colloidal nanocrystals revealed by SAXS

Colloidal nanocrystals are nanometre-sized inorganic particles grown in a solution and covered by organic ligands. Depending on the composition, size and shape of the inorganic core, as well as properties of the stabilising coating, nanocrystals exhibit different physical properties. The combination of size and shape-dependent properties as well as ease of processing from a colloidal suspension makes nanocrystals promising building blocks for functional materials. Under certain conditions, e.g., upon solvent evaporation, colloidal nanocrystals can self-assemble into highly ordered supercrystals or superlattices. Such assemblies possess novel collective properties resulting from interactions of individual nanocrystals, which are important for potential technological applications.

Monodisperse colloidal nanocrystals (NCs) are able to self-assemble into ordered arrays, a process representing an attractive way to produce functional devices. One of the experimental approaches for the self-assembly of colloidal NCs is solvent evaporation. Despite numerous studies in the field of evaporative assembly, it is still difficult to understand and predict the obtained superstructure phase. This depends on multiple parameters, such as interactions between inorganic core, soft organic surface-coating ligands and surrounding solvent molecules. Additionally, the assembly geometry, the evaporation rate and the nature of the solvent are reported to influence the resulting superlattice structure. In that regard, a thorough understanding of the solvent-mediated assembly process is required to produce NC superlattices with tailored properties.

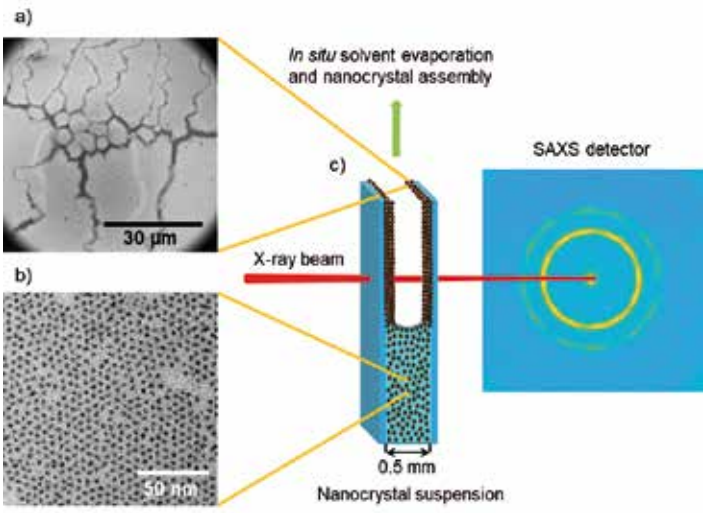

Figure 1

Schematic representation of the *in situ* self-assembly of colloidal PbS NCs upon controlled solvent evaporation using SAXS. a) Scanning electron microscopy (SEM) image of the superlattice film assembled along the cell windows. b) Transmission electron microscopy (TEM) image of PbS NCs prior to the assembly experiment. c) Sample cell for monitoring of the real-time NC assembly by means of SAXS. Colloidal NCs self-organise into highly ordered superlattices along the X-ray transparent Si_3N_4 windows.

We chose lead sulphide (PbS) NCs as model system for studying the assembly process due to the possibility to produce monodisperse particles with a chosen size in a colloidal suspension. Furthermore, PbS NCs exhibit unique optical and electronic properties, which makes them appealing for different applications including solar cells, light-emitting diodes, transistors, photodetectors etc.

Recently, time-resolved X-ray scattering techniques have emerged as powerful tools for investigating NC assembly in real time under controlled conditions. For our *in situ* small-angle X-ray scattering (SAXS) experiment at ESRF (Grenoble, France), beamline ID02, we designed a dedicated sample environment [1]. The real-time NC assembly was monitored by SAXS in transmission geometry upon controlled solvent evaporation from a bulk colloidal suspension at a very low evaporation rate (Fig. 1). The superlattices were formed along the X-ray-transparent cell windows.

For the experiment, we used quasi-spherical oleic-acid-capped PbS NCs with a diameter of 3.9 nm and 8% dispersity dissolved in heptane or toluene. The oleic-acid-stabilised PbS NCs exhibited a softness parameter, i.e., ratio of the fully extended ligand length to the core radius, of 1.17 and a ligand grafting density of 4.6 nm^{-2}. A small amount of the colloidal suspension (< 25 µl) was evaporated within approximately 1.5–2.5 hours, which allows one to capture the smallest transitions in superlattice growth and rearrangement

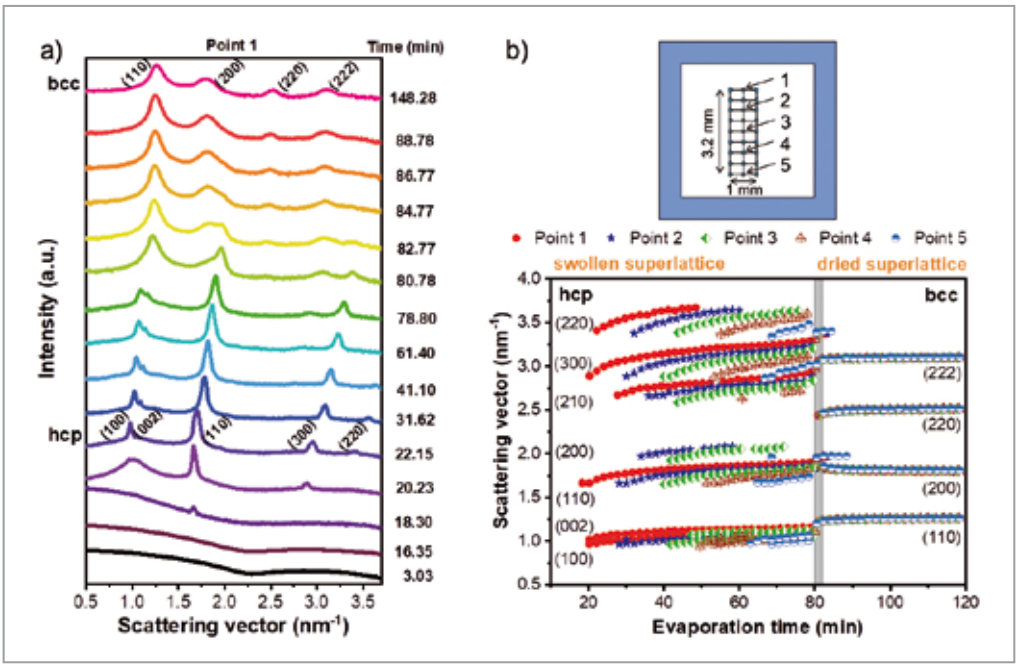

Figure 2

Time and space-resolved assembly of colloidal nanocrystals into highly ordered superlattices upon slow solvent evaporation.

a) Time-resolved scattering curves during the *in situ* nanocrystal assembly reveal formation of an intermediate hcp phase, followed by a transition to the final bcc superlattice.

b) Comparison of scattering-vector values of the superlattice Bragg peaks for different vertical points on the cell windows in the evaporative assembly. Evidently, the transition of the hcp into the bcc phase occurs at all points simultaneously, indicating structure rearrangement upon complete solvent evaporation. The grey area shows the moment of drying of the swollen superstructure.

in a close-to-equilibrium state. The superlattice films exhibit large domain sizes and thicknesses in the micrometre range.

Using real-time SAXS measurements, we observed that during NC assembly the colloidal suspension crystallised first into a hexagonal closed-packed (hcp) phase which later, upon drying out, rearranged into a body-centred cubic (bcc) superlattice (Fig. 2a). Well-resolved Bragg peaks indicated high crystallinity of the superstructures. The design of our sample cell for transmission SAXS allows for monitoring the transitions in the superlattice structure in both, the solvated and dried states, because the self-organised superlattices in the upper part of the cell windows remain in the solvent-vapour-saturated atmosphere as long as solvent is still present in the cell.

Intriguingly, in our *in situ* experiment, we observed that the original hcp superlattice, formed at different vertical points of the cell windows upon movement of the evaporation front, rearranged into the final bcc phase at all vertical points simultaneously (Fig. 2b). Thus, we clearly revealed the role of solvent molecules in the process of NC assembly. Additionally, our subsequent results [2] using the same experimental approach on different particles suggest that the system, at these experimental conditions, reaches equilibrium states.

Moreover, we carried out X-ray cross-correlation analysis (XCCA) [3] of Bragg reflections in order to access information on precursor structures in the assembly process which is not evident from conventional SAXS analysis. Interestingly, the XCCA results revealed the formation of small amounts of bcc superstructures already in the solvent-vapour-saturated hcp superlattice. In total, we found a space-filling fraction of soft particles in the final bcc superlattice of 71%, which confirms previous observations that soft NCs can fill space more efficiently than hard ones with 68%.

In conclusion, we performed an *in situ* SAXS study during the evaporation-induced assembly of colloidal NCs into highly ordered superlattices. For the first time for the investigated system, we observed the hcp superstructure in a solvent-vapour-saturated atmosphere, rearranging into the bcc phase upon drying. The real-time evolution of the crystal structure provides insights into the assembly mechanism and uncovers the role of ligand–solvent interactions during the NC assembly.

Author contact: Irina Lokteva, irina.lokteva@desy.de

References

1. I. Lokteva, M. Walther, M. Koof, G. Grübel and F. Lehmkühler, '*In situ* small-angle X-ray scattering environment for studying nanocrystal self-assembly upon controlled solvent evaporation', Rev. Sci. Instrum. 90, 036103 (2019).
2. I. Lokteva, M. Koof, M. Walther, G. Grübel and F. Lehmkühler, 'Coexistence of hcp and bct phases during *in situ* superlattice assembly from faceted colloidal nanocrystals', J. Phys. Chem. Lett. 10, 6331–6338 (2019).
3. F. Lehmkühler, G. Grübel and C. Gutt, 'Detecting orientational order in model systems by X-ray cross-correlation methods', J. Appl. Crystallogr. 47, 1315–1323 (2014).

Original publication

'Monitoring nanocrystal self-assembly in real time using *in situ* small-angle X-ray scattering', Small 15, 1900438 (2019). DOI: 10.1002/smll.201900438

Irina Lokteva[1,2], Michael Koof[1,2], Michael Walther[1], Gerhard Grübel[1,2], and Felix Lehmkühler[1,2]

1. Deutsches Elektronen-Synchrotron DESY, Hamburg, Germany
2. The Hamburg Centre for Ultrafast Imaging (CUI), Hamburg, Germany

Polyanionic material boosts high-power density for sodium-ion batteries

A combined XRD and EXAFS study at beamlines P02.1 and P64

Sodium-ion batteries (SIBs) have been considered as promising candidates for large-scale energy storage systems (ESSs) because of the high abundance, wide availability and low cost of sodium resources. The use of the redox chemistry of earth abundant transition metals such as iron will particularly reduce manufacturing costs, which will boost the real applications of SIBs in the commercial ESS market. Combined with the robust and inflammable framework of polyanionic material, we developed a new Fe-based cathode material for SIBs with 3D ion diffusion pathways with all-climate performance.

The polyanionic or mixed-polyanion system is one of the most important candidates among the various types of electrode materials suitable for SIBs, and it has been the subject of extensive investigations in recent years. The 3D framework of such electrodes can provide strong and lasting structural support for repeated Na^+ ion de-/insertions with relatively high operating potentials [1]. Several vanadium-based compounds have been widely studied as an important group of promising electrodes, such as sodium superionic conductor (NASICON)-type $Na_3V_2(PO_4)_2$, $Na_3(VO_x)_2(PO_4)F_{3-2x}$ (x = 0 or 1) and $Na_7V_4(P_2O_7)_4PO_4$. These compounds exhibit satisfactory high energy densities that are comparable to those of lithium ion batteries (LIBs), based on multi-electron redox reactions (V^{3+}/V^{4+} and V^{4+}/V^{5+}) and high operating voltage, although the use of toxic and expensive vanadium remains a critical issue for real applications. Other electrodes based on costly 3*d* transition metal elements such as Ni-based or Co-based electrodes also face this problem. Therefore, the most abundant and non-toxic 3*d* element, iron, is the first choice as the redox centre in the polyanionic system [2]. The Fe-based polyanionic compounds have shown high structural stability with small volume change during cycling and sufficiently long cycling stability with high energy density, which will definitely reduce the overall electrode cost and promote the real application of SIBs in large-scale ESSs in the near future [3].

Another critical issue for both LIBs and SIBs is their performance and reliability at temperatures that might be encountered under all-climate conditions. SIBs face an even more severe low-temperature problem due to their intrinsically more sluggish solid-state diffusion compared with LIBs. Cathode Na^+-host materials operated at room temperature have been extensively investigated, but their all-climate performance has received little attention in recent years. For real applications of SIBs in the commercial market, all-climate performance is strongly required because the energy storage systems must work over a wide range of temperatures. Therefore, finding an environmentally friendly, low-cost and

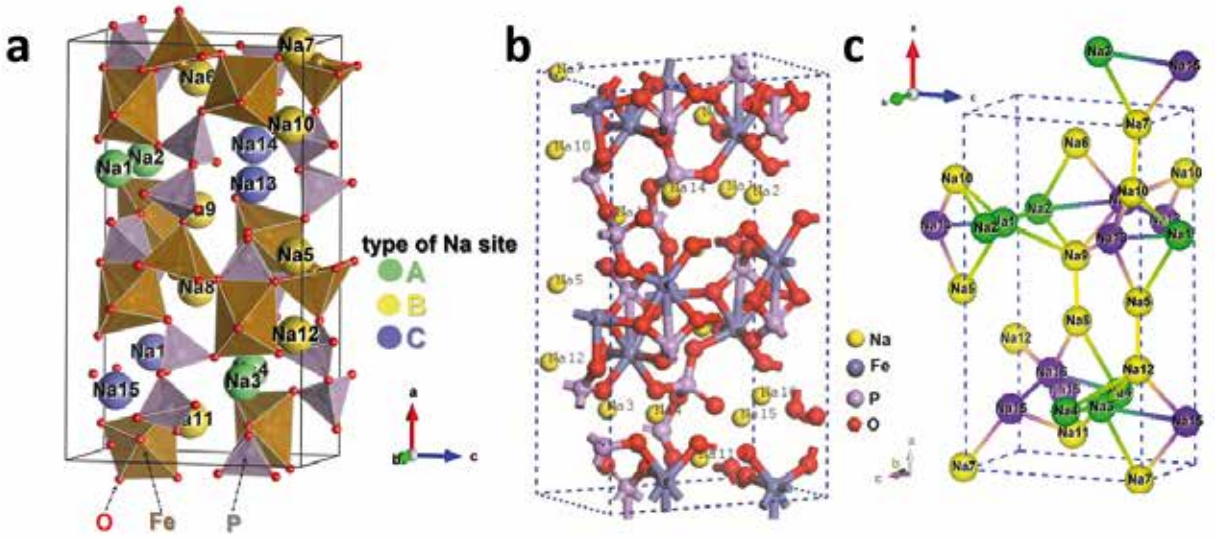

Figure 1
The crystal structure of $Na_4Fe_3(PO_4)_2(P_4O_7)$ cathode for sodium-ion batteries with three different sites for Na^+ ions. Copyright @ 2019 Nature Publishing Groups.

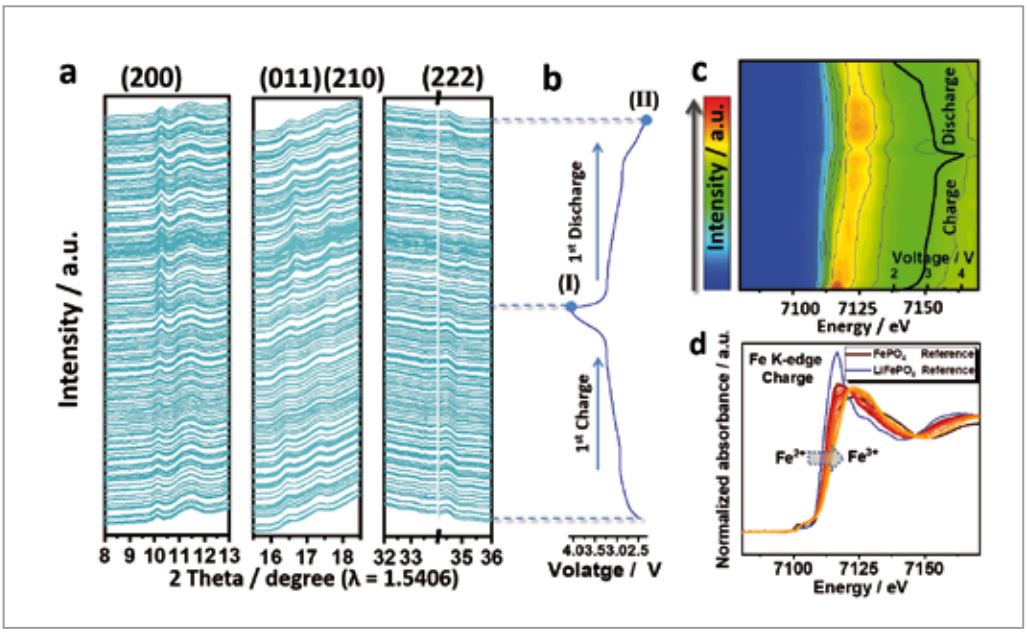

Figure 2

a) *In situ* synchrotron radiation diffraction patterns and b) the corresponding charge-discharge voltage profile of $Na_4Fe_3(PO_4)_2(P_4O_7)$ during the first cycle. c) *In situ* XANES spectra at the Fe K-edge of $Na_4Fe_3(PO_4)_2(P_4O_7)$ (2D contour plot) together with the charge-discharge curve. d) The changes in the Fe K-edge spectra observed during charging. Copyright @ 2019 Nature Publishing Groups.

all-climate cathode material is very important for the real application of SIBs [3]. Inspired by this, we have reported on a low-cost NASICON-type cathode material, $Na_4Fe_3(PO_4)_2(P_2O_7)$, with favorable Na storage properties under all-climate temperatures, combined with tunable carbon-coated nanoparticles to form a robust composite material without losing its crystallinity.

Nanosized $Na_4Fe_3(PO_4)_2(P_2O_7)$ material was successfully synthesised via a facile one-step sol-gel method. The sample was indexed to the orthorhombic $Pna2_1$ space group, with lattice parameters a = 17.6433(6) Å, b = 6.3616(4) Å, c = 10.2043(4) Å and V = 1145.342(3) Å^3. In the robust and open 3D framework, the $[Fe_3P_2O_{13}]$ units along the a-axis consist of three FeO_6 octahedra and three PO_4 groups, while the $[Fe_3P_2O_{13}]_\infty$ infinite layers are connected by $[P_2O_7]$ groups along the a direction, thus leading to the formation of large primary tunnels along the b direction (Fig. 1). In order to obtain a comprehensive understanding of the structural superiority of $Na_4Fe_3(PO_4)_2(P_2O_7)$, both *in situ* synchrotron radiation diffraction patterns and X-ray absorption spectra (XAS) were collected at beamlines P02.1 and P64 at PETRA III. Several reflections in the initial states were indexed and identified (Fig. 2 a,b). It can be seen that the positions of all reflections change reversibly during the charge/discharge process with the general patterns remaining unchanged, indicating that the robust crystal framework can be well maintained after electrochemical activation. Therefore, it can be deduced that a topotactic one-phase transition occurs in the $Na_4Fe_3(PO_4)_2(P_2O_7)$ electrode during cycling. The X-ray absorption near edge structure (XANES) spectrum is shifted to the right (higher binding energy) during charging, indicating oxidation of iron from Fe^{2+} to Fe^{3+}. The spectrum of the fully charged state is very close to that of the $FePO_4$ reference sample, indicating that most of the iron in the crystal structure had become Fe^{3+} (Fig. 2c-e). The pre-edge region of the Fe K-edge also shows discernible variation during charging (inset in Fig. 2d,e), with the peak shifting towards higher energy.

The results allow us to identify the phase variation during the charging/discharging process along with the changes of the crystal lattice. It is important to determine the phase transitions in order to further optimization these materials. The changes in the valence state determined from XANES are important for future modifications with respect to elemental composition, which can in turn lead to higher operating voltages.

Author contact: Shu-Lei Chou, shulei@uow.edu.au
Weihua Chen, chenweih@zzu.edu.cn

References

1. J.-Y. Hwang, S.-T. Myung and Y.-K. Sun, 'Sodium-ion batteries: present and future', Chem. Soc. Rev. 46, 3529–3614 (2017).
2. M. Chen, Q. Liu, S.-W. Wang, E. Wang, X. Guo and S.-L. Chou, 'High-abundance and low-cost metal-based cathode materials for sodium-ion batteries: problems, progress, and key technologies', Adv. Energy Mater. 9, 1803609 (2019).
3. Y. You, H.-R. Yao, S. Xin, Y.-X. Yin, T.-T. Zuo, C.-P. Yang, Y.-Y. Guo, Y. Cui, L.-J. Wan and J. B. Goodenough, 'Subzero-temperature cathode for a sodium-ion battery', Adv. Mater. 28, 7243–7248 (2016).

Original publication

'NASICON-type air-stable and all-climate cathode for sodium-ion batteries with low cost and high-power density', *Nat. Commun.* 10, 1480 (2019). doi: 10.1038/s41467-019-09170-5

Mingzhe Chen[1], Weibo Hua[2], Jin Xiao[3,4], David Cortie[1], Weihua Chen[5], Enhui Wang[1,6], Zhe Hu[1], Qinfen Gu[7], Xiaolin Wang[1], Sylvio Indris[2], Shu-Lei Chou[1] and Shi-Xue Dou[1]

1. University of Wollongong, North Wollongong, Australia
2. Institute of Technology (KIT), Eggenstein-Leopoldshafen, Germany
3. Hunan University of Technology, Zhuzhou, China
4. Chinese Academy of Sciences, Beijing, China
5. Zhengzhou University, Zhengzhou, China
6. Sichuan University, Chengdu, China
7. Australian Synchrotron, Clayton, Australia

Atomic-scale disorder in (ultra)thin films

Brilliant team play of surface high-energy X-ray diffraction and PDF analysis

Pair distribution function (PDF) analysis is a widely used and most effective tool to study the local structure of materials exhibiting some degree of disorder on the atomic scale. In particular, for nanomaterials that generally lack any long-range periodic order, the PDF technique has provided unrivalled insight into structure–property relationships. With the increasing availability of high-energy X-ray sources and suitable large, fast area detectors, *in situ* and *operando* PDF studies have emerged to follow processes, e.g., in chemical reactions, electrochemistry and mechanical testing. For thin films, however, the traditional PDF approach fails. We show how the best of two worlds, surface diffraction and total scattering, are joined to enable PDF analysis of films as thin as a few nanometres.

Complementary to X-ray diffraction patterns that visualise the crystal lattice in reciprocal space based on Bragg's law, the PDF describes the structure of a material as a histogram of interatomic distances r in real space. Hence, the PDF facilitates a rather intuitive understanding of the atomic order while the interpretation of reciprocal-space data requires more abstract thinking. Yet, both data-interpretation methods originate in X-ray scattering techniques. The total scattering (TS) approach that enables PDF analysis requires that scattering data is collected over a wide range in reciprocal space up to a momentum transfer $Q = 4\pi \sin\theta / \lambda$ in the range of 20 Å^{-1}. Subsequently, the whole scattering pattern is Fourier transformed into real space to obtain the PDF. Most effectively, TS data is acquired using a large area detector and high-energy X-rays at a synchrotron beamline so that the entire scattering pattern up to high Q is collected in a single exposure. While this routine has become standard for bulk-type samples, the nature of thin films requires dedicated experimental procedures. Mainly, the unfavourable thickness ratio of the film (nanometre regime) and its substrate (micrometre regime) limits the detectability of the film's signal in the dominating substrate scattering. The exfoliation of the film from its support and transfer to a capillary for a powder-type measurement, as reported, e.g., in [1], potentially destroys the film characteristics. Jensen et al. [2] first described the feasibility of measurements under normal incidence with respect to the surface for layers of considerable thickness. For thin (< 100 nm) and ultrathin (< 10 nm) films, however, the established method of surface diffraction under grazing incidence is the unique tool to obtain structural information.

As the critical angles for total external reflection are very small at X-ray energies typically used in PDF experiments (< 0.1° at > 60 keV), the demands on beam size and sample alignment are only met by specialised synchrotron beamlines. Gustafson et al. [3] first proved that the second experimental hutch (EH2) at beamline P07 at PETRA III is ideally suited for time-resolved surface high-energy X-ray diffraction (SHEXRD) on single-crystal surfaces. By applying this technique to less ordered thin-film systems, we have now successfully combined SHEXRD with TS at P07 and thus pushed the capabilities for thin-film PDF analysis to unprecedented limits in

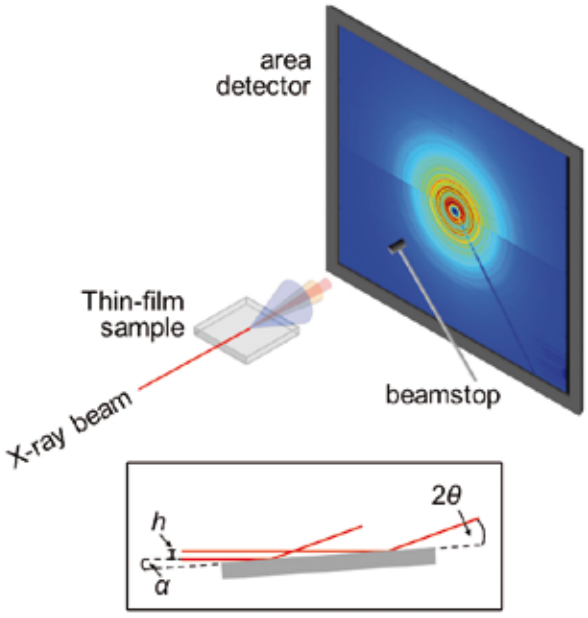

Figure 1

Schematic illustration of the grazing-incidence geometry. In the inset drawing, the beam height h (here approximately 3 µm), the fixed incidence angle α (< 0.1°) and the varying diffraction angle 2θ are defined. In the 2D diffraction pattern, the so-called sample horizon divides the image into an upper and a lower half. In the lower half, the intensities are less than in the upper part as the diffracted signal is partly absorbed by the substrate it passes on its way to the detector, whereas the upward scattering reaches the detector unattenuated.

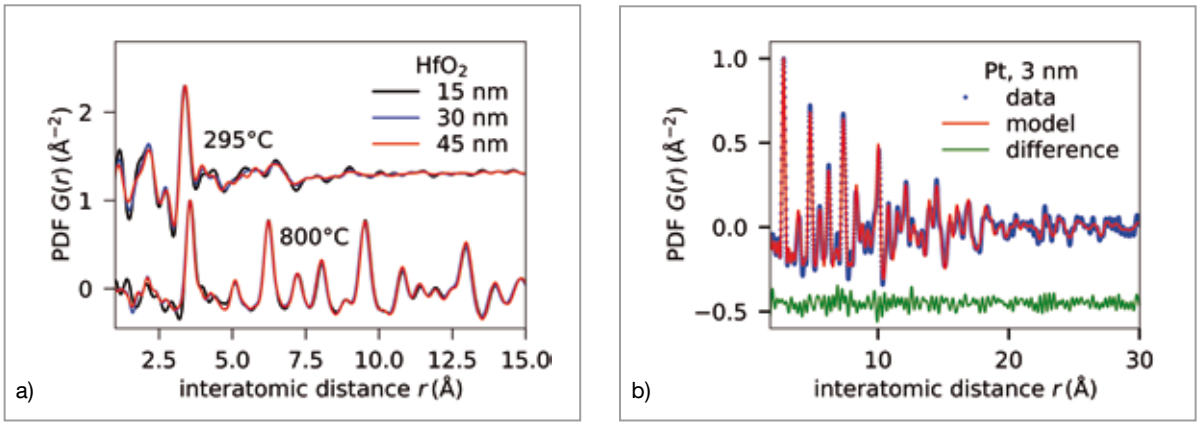

Figure 2

(a) Reduced pair distribution function $G(r)$ of HfO_2 thin films of different thicknesses on fused silica deposited by chemical solution deposition and heat-treated at the indicated temperatures (offset in $G(r)$ for clarity). The film thickness increases in steps owing to the preparation by stacking multiple coatings of 15 nm each, i.e., the samples correspond to 1, 2 and 3 coatings, respectively; (b) Normalized PDF data and refinement of a 3 nm sputter-deposited Pt layer on fused silica. The weighted residual of the least-squares fit R_w (in green) amounts to 24% for the r fitting range 1.75–60 Å (shown only to 30 Å for clarity).

terms of minimum film thickness and time resolution. Figure 1 schematically depicts the experimental setup.

We studied various material systems (metals, oxides) and different degrees of ordering (polycrystalline, amorphous, textured). All films were deposited on fused silica which provides a well-scalable background to subtract from the data in order to isolate the film's scattering signal. We found that the detection limit does not crucially depend on the presence of long-range ordering which gives rise to distinct Bragg peaks in the diffraction pattern. By careful data treatment, we successfully derived PDFs of comparable quality from two different kinds of HfO_2 films with thicknesses down to 15 nm, i.e., for polycrystalline layers as well as for films with only short-range order with correlation lengths down to only ~ 5 Å (Fig. 2a). As the scattering power of X-rays increases with the atomic number, the detection limit was even enhanced for Pt thin films. Figure 2b illustrates the PDF of a 3 nm thin Pt film and the fit of the data assuming an fcc lattice. In a follow-up publication [4], we described the growth of Pt thin films *in situ* during sputter deposition by applying the grazing incidence PDF technique. With a time resolution of 0.5 s, we continuously followed the evolution of strain and coherent domain size.

Based on our work, PDF analysis of thin films has advanced beyond previously existing boundaries and is going to conquer the thin-film community who, up to now, has only rarely made use of this technique. A thorough evaluation was carried out on how the PDF-data quality is optimized given the decreased Q resolution originating in the long footprint of the X-ray beam on the sample at the low incidence angle. Remaining open questions include the modelling of texture and preferred orientation which are not yet taken into account in the traditional PDF approach. In addition, expanding the *in situ* grazing incidence PDF method to variable-temperature processes requires novel technical solutions for stabilising the sample position within the tight geometrical constraints, i.e., the incidence angle in the order of millidegrees and the vertical position within 1 µm.

Author contact: Ann-Christin Dippel, ann-christin.dippel@desy.de

References

1. J. A. Kurzman, K. E. Dettelbach, A. J. Martinolich, C. P. Berlinguette and J. R. Neilson, 'Structural characteristics and eutaxy in the photo-deposited amorphous iron oxide oxygen evolution catalyst', Chem. Mater. 27, 3462–3470 (2015).
2. K. M. Ø. Jensen, A. B. Blichfeld, S. R. Bauers, S. R. Wood, E. Dooryhee, D. C. Johnson, B. B. Iversen and S. J. L. Billinge, 'Demonstration of thin film pair distribution function analysis (tfPDF) for the study of local structure in amorphous and crystalline thin films', IUCrJ 2, 481–489 (2015).
3. J. Gustafson, M. Shipilin, C. Zhang, A. Stierle, U. Hejral, U. Ruett, O. Gutowski, P.-A. Carlsson, M. Skoglundh and E. Lundgren, 'High-energy surface X-ray diffraction for fast surface structure determination', Science 343, 758–761 (2014).
4. M. Roelsgaard, A.-C. Dippel, K. A. Borup, I. G. Nielsen, N. L. N. Broge, J. T. Röh, O. Gutowski and B. B. Iversen, 'Time-resolved grazing-incidence pair distribution functions during deposition by radio-frequency magnetron sputtering', IUCrJ 6, 299–304 (2019).

Original publication

'Local atomic structure of thin and ultrathin films via rapid high-energy X-ray total scattering at grazing incidence', IUCrJ 6, 290–298 (2019). DOI: 10.1107/S2052252519000514

Ann-Christin Dippel[1], Martin Roelsgaard[2], Ulrich Böttger[3], Theodor Schneller[3], Olof Gutowski[1] and Uta Rütt[4]

1. Deutsches Elektronen-Synchrotron DESY, Hamburg, Germany
2. Center for Materials Crystallography, Department of Chemistry, Aarhus University, Aarhus, Denmark
3. Institute for Materials in Electrical Engineering (IWE-2), RWTH Aachen University, Aachen, Germany
4. Advanced Photon Source, Argonne National Laboratory, Argonne, Illinois, USA

Spin waves from microcrystals

Tender X-ray spectroscopy reveals elementary excitations in *4d* transition metal compounds

The newly developed Intermediate-energy Resonant Inelastic X-ray Scattering (IRIXS) spectrometer at the Dynamics Beamline P01 of PETRA III allows the determination of the spectrum of collective magnetic excitations ('spin waves') in transition metal compounds with *4d* valence electrons. Such measurements are important because they yield insight into the magnetic interactions between spins inside the material, but these measurements usually require large single crystals that are difficult to synthesise. Aided by the IRIXS spectrometer, it is now possible to perform a complete set of measurements on a microcrystal invisible to the naked eye, ushering in a new era of magnetism research in *4d* quantum materials.

Ruthenium oxides and other transition metal compounds with *4d* valence electrons play prominent roles in many areas of materials research ranging from oxide electronics to catalysis [1]. Furthermore, they serve as a platform for fundamental concepts in condensed matter physics, such as unconventional superconductivity, spin liquids, and solid-state analogues of the Higgs mode in particle physics [2]. These collective quantum phenomena emerge as a result of a delicate interplay among the Coulomb interaction between the electrons, their interaction with the crystal lattice, and the intra-atomic spin-orbit coupling. However, basic questions about the mechanisms underlying these phenomena remain unanswered, because these key parameters are comparable in magnitude and not accurately known, and because sizable single crystals required for spectroscopic experiments are often difficult to synthesise.

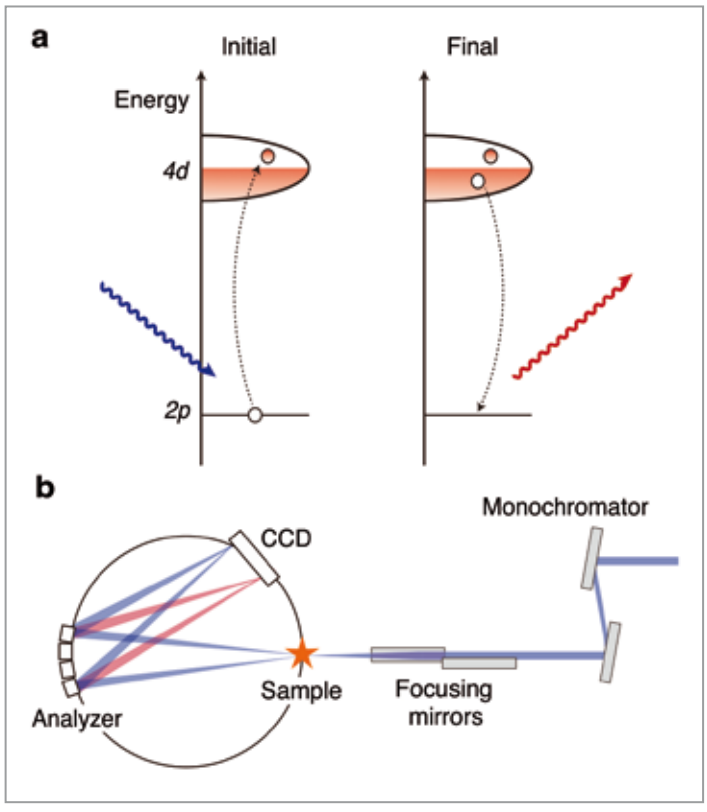

An experimental scheme called resonant inelastic X-ray scattering (RIXS) allows one to cope with these obstacles [3]. In the RIXS process, X-ray photons tuned to the absorption edge of a chemical element impinge on the sample and excite the system, which then undergoes radiative decay to the final state (Fig. 1a). The energy of the photons emitted into a given direction is accurately measured, and the scattering intensity as a function of transferred energy and momentum is directly associated with the dispersion relations of elementary excitations of the system. This is of crucial importance since the elementary excitations can be regarded as 'elementary particles' living in the ground state of a material, which often behave rather differently from the individual constituents of the material. Thanks to the energy and momentum carried by X-ray photons, RIXS is capable of detecting charge, spin, and orbital excitations in a momen-

Figure 1

(a) Schematic of the RIXS process. X-ray photons tuned to a chemical absorption edge (the *2p*-*4d* transition for the Ru L_3 edge) excite core electrons to the valence state. The excited system then undergoes radiative decay, thereby filling the core holes and emitting X-ray photons. As a result, the energy and momentum difference between the incoming and outgoing photons is transferred to the valence state, which generates various elementary excitations. (b) Schematic of the IRIXS spectrometer. The incident X-ray photons from the synchrotron are monochromatised by an asymmetrical Si(111) channel-cut crystal and focused on the sample. The energy of the scattered X-rays is analysed with a SiO_2 diced spherical analyser and collected with a charge-coupled device camera.

Figure 2

(a) Inelastic scattering of X-rays from the antiferromagnetic ruthenate $SrRu_2O_6$. The incident X-ray photons are tuned to the Ru L_3 absorption edge (2837.5 eV) and focused on the sample. They interact with the Ru spins arranged on a two-dimensional honeycomb lattice. The loss of X-ray energy (namely, the change in 'colour') is transferred to the system, which in turn excites the collective magnetic excitations. (b) Experimentally determined dispersion of spin waves (blue circles). The experimental dispersion is well reproduced by a theoretical model calculation (dotted line).

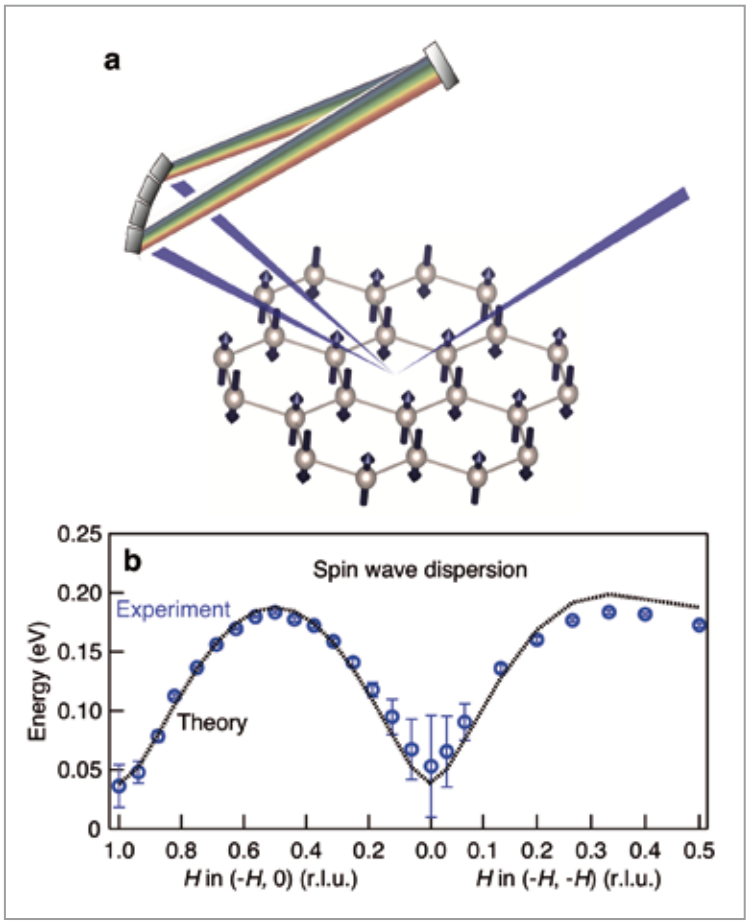

tum-resolved and chemically selective manner. Crucially, the resonant condition greatly enhances the cross section of the RIXS process, enabling experiments on microcrystals and thin-film structures, which are not accessible to other spectroscopic probes such as inelastic neutron scattering.

Recent remarkable progress in the development of RIXS instrumentation in the soft and hard X-ray regimes has enabled comprehensive studies of magnetic compounds with *3d* and *5d* valence electrons, respectively. However, a RIXS instrument with coverage of the L-absorption edges of *4d* transition metal compounds had not been available, since the relevant absorption edges lie in the intermediate ('tender') X-ray regime, where suitable X-ray optics had not grown to maturity. A large and important class of *4d* magnetic materials had therefore been inaccessible to X-ray experimentation. This situation has now changed following the construction of the IRIXS spectrometer at the Dynamics Beamline P01 at PETRA III, which is equipped with a specifically designed high-resolution X-ray monochromator and an X-ray energy analyser (Fig. 1b). The complementary capability to determine magnetic structures at Beamline P09 was also important for the success of this project.

The research team investigated the antiferromagnet $SrRu_2O_6$ [4], where Ru spins are arranged on a two-dimensional honeycomb lattice, to demonstrate the capabilities of the new instrument (Fig. 2a). The exceptionally high Néel temperature of this compound has attracted considerable recent attention, but spectroscopic experiments have thus far not been reported because only small single crystals (50 microns in diameter) could be synthesised. The IRIXS spectrometer enabled measurements of the complete dispersion relation of spin waves (Fig. 2b), which allowed the researchers to determine the interactions between the spins and their coupling to the crystal lattice. The results yield a complete explanation of the high magnetic ordering temperature, and they highlight the critical role of the intra-atomic spin-orbit coupling for the unconventional high-temperature antiferromagnetism of $SrRu_2O_6$. This work firmly establishes IRIXS as a versatile probe of the low-energy electronic and magnetic structure of a large variety of ruthenates and other *4d* metal compounds.

Author contact: Hakuto Suzuki, h.suzuki@fkf.mpg.de
Hlynur Gretarsson, hlynur.gretarsson@desy.de
Bernhard Keimer, b.keimer@fkf.mpg.de

References

1. H. Over, 'Surface chemistry of ruthenium dioxide in heterogeneous catalysis and electrocatalysis: from fundamental to applied research', Chem. Rev. 112, 3356–3426 (2012).
2. W. Witczak-Krempa, G. Chen, Y. B. Kim and L. Balents, 'Correlated quantum phenomena in the strong spin-orbit regime', Annu. Rev. Condens. Matter Phys. 5, 57–82 (2014).
3. L. J. P. Ament, M. van Veenendaal, T. P. Devereaux, J. P. Hill and J. van den Brink, 'Resonant inelastic x-ray scattering studies of elementary excitations', Rev. Mod. Phys. 83, 705–767 (2011).
4. C. I. Hiley, D. O. Scanlon, A. A. Sokol, S. M. Woodley, A. M. Ganose, S. Sangiao, J. M. De Teresa, P. Manuel, D. D. Khalyavin, M. Walker, M. R. Lees and R. I. Walton, 'Antiferromagnetism at $T > 500$ K in the layered hexagonal ruthenate $SrRu_2O_6$', Phys. Rev. B 92, 104413 (2015).

Original publication

'Spin waves and spin-state transitions in a ruthenate high-temperature antiferromagnet', Nature Materials 18, 563–567 (2019). DOI:10.1038/s41563-019-0327-2

H. Suzuki[1], H. Gretarsson[1,2], H. Ishikawa[1,3], K. Ueda[1], Z. Yang[1], H. Liu[1], H. Kim[1,4,5], D. Kukusta[1], A. Yaresko[1], M. Minola[1], J. A. Sears[2], S. Francoual[2], H.-C. Wille[2], J. Nuss[1], H. Takagi[1,3,6], B. J. Kim[1,4,5], G. Khaliullin[1], H. Yavaş[2] and B. Keimer[1]

1. Max-Planck-Institut für Festkörperforschung, Stuttgart, Germany
2. Deutsches Elektronen-Synchrotron DESY, Hamburg, Germany
3. Institut für Funktionelle Materie und Quantentechnologien, Universität Stuttgart, Stuttgart, Germany
4. Pohang University of Science and Technology, Pohang, South Korea
5. Institute for Basic Science, Pohang, South Korea
6. Department of Physics, University of Tokyo, Tokyo, Japan

Breakthrough in HAXPES performance by 3D-recording

Full-field momentum imaging with time-of-flight energy recording sets new benchmarks in bulk photoemission using hard X-rays at P22

Angle-resolved photoemission spectroscopy (ARPES) is a very powerful method to analyse electronic properties of novel materials. With probing depths of up to 20 nm, hard X-ray ARPES gives access to the bulk electronic structure of materials with reactive surfaces, device-like heterostructures, bulk impurities and buried interfaces. However, severe intrinsic effects (low cross sections, phonon scattering and photoelectron diffraction) and extrinsic effects (electron-optical constraints, strong energy retardation and the need for high angular resolution) render hard X-ray ARPES a challenging task. At the high-brilliance beamline P22 an innovative new technique is established, combining 3D parallel detection with excellent energy resolution (resolving power > 10^5). The approach opens a new avenue towards hard X-ray ARPES.

Due to experimental obstacles, only a few hard X-ray ARPES experiments have been performed up to now [1]. Following recent success with the development of a highly efficient soft X-ray photoemission *k*-microscope [2], we developed a hard X-ray version of this microscope. It utilises the concept of simultaneous acquisition of the spectral density function $\rho(E_B;\boldsymbol{k})$, where E_B is the binding energy and $\boldsymbol{k}$ is the coordinate in 3D *k*-space. The coordinates (k_x,k_y) are resolved by full-field momentum imaging and k_z is varied by changing the photon energy. Energy resolution is achieved by recording the electron time-of-flight (ToF). The increase in dimensionality in combination with the high brilliance of beamline P22 at PETRA III has proven superior to conventional ARPES instrumentation [3].

There are several effects which hamper such experiments. First of all, the approximated wavelength of the final-state wavefunction $\lambda_e=2\pi/k_f$ varies from 61 to 15.8 pm in the region between 400 eV and 6 keV. Consequently, photoionisation cross sections drop by several orders of magnitude due to cancellations in the overlap integral of the transition matrix elements. In addition, λ_e shorter than interatomic distances give rise to core-like X-ray photoelectron diffraction (XPD), leading to pronounced intensity modulations in angle or momentum.

The strong modulation of XPD can be seen in the C 1*s* core level in the prototypical low-Z material graphite in Fig. 1. Sharp Kikuchi bands (bright and dark lines) are clearly visible and shift with electron kinetic energy. Particularly, the regions of Kikuchi band crossings near a zone axis exhibit a filigree structure which also varies rapidly with energy. In our publication we show calculations based on the Bloch-wave approach to electron diffraction from lattice planes (examples in bottom row of Fig. 1). The calculations are in excellent agreement with the experimental results throughout the entire energy range. The main Kikuchi bands in the [001] zone axis appear fixed on the momentum scale with a width of the corresponding reciprocal lattice vector, allowing to reconstruct the size of the projected Brillouin zone.

Furthermore, we developed an approach, which eliminates the strong inherent distortions in the measured hard X-ray

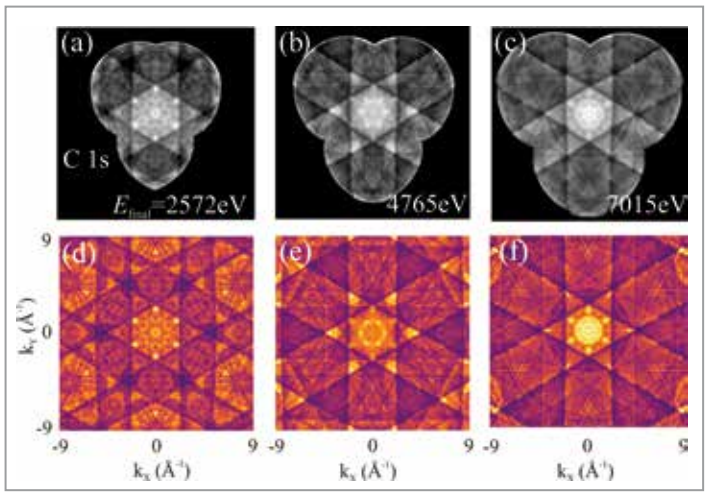

Figure 1

Comparison of measured (a-c) and computed (d-f) carbon 1*s* XPD patterns of graphite. Close inspection reveals the perfect one-to-one correspondence except for differences in brightness of some details and a larger blur in the experimental patterns. The full sequence is available as movie in the supplemental material of the original publication in New Journal of Physics 21.

Figure 2

Momentum-resolved hard X-ray photoemission from Mo (001) at 4.2 and 6 keV, corresponding to the final states given on top. a, b) As-measured large-area momentum maps of valence bands (VB) (section at the Fermi level). c, d) High-resolution 4*p* core-level diffraction patterns taken at identical final-state energies as a and b. e, f) Same distributions as top row after pixel-by-pixel division by the core-level patterns from the second row. g, h) E_B-vs-*k* sections through the arrays of the fourth row along the dashed lines.

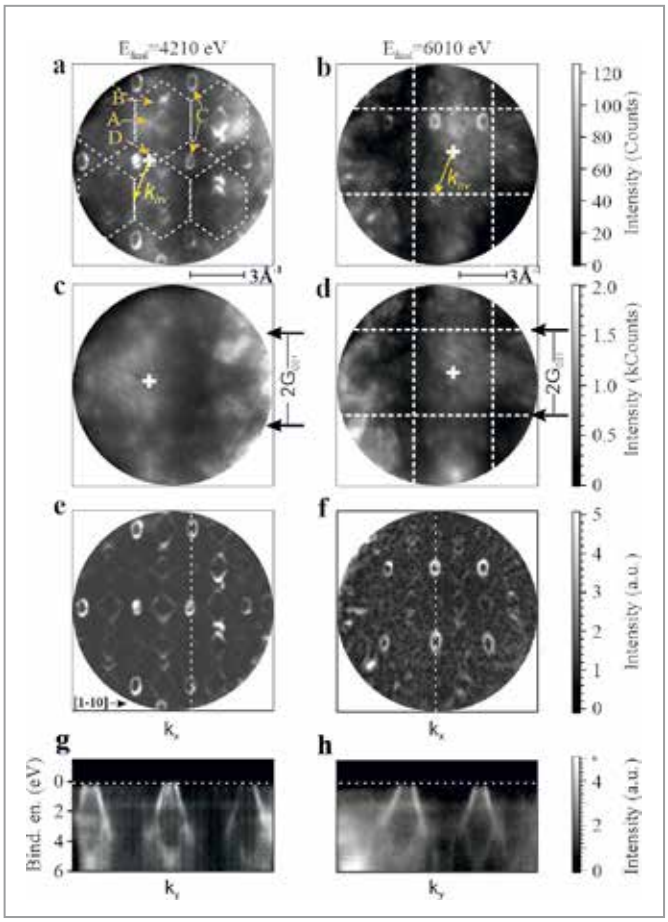

ARPES band maps. As samples we have chosen the medium-Z metal Mo (Z = 42) and the reference transition-metal dichalcogenide $TiTe_2$. The key to this approach is simultaneous measurement of valence-band momentum maps and core-level photoelectron diffraction patterns, taken at identical settings of the microscope (kinetic energy and *k*-field of view).

The top row of Fig. 2 (a,b) shows the as-measured *k*-distributions (sections at E_F) from a Mo (110) crystal at two selected final-state energies 4210 and 6010 eV. Various sharp band features (A, B, C and D) can be identified in the imaged *k*-region of ~ 12 Å^{-1} diameter. However, intense background patterns with characteristic shapes are superimposed on the *k*-distributions in the top row. Assuming that the structured background patterns in Fig. 2 (a,b) are the fingerprint of XPD, we took high-resolution diffraction patterns of the shallow Mo 4*p* core level at the same kinetic energies and using identical settings of the microscope (Fig. 2 c,d). In order to remove XPD background we employ a multiplicative correction in the form of a pixel-by-pixel division of the raw data by the XPD patterns. The result is shown in the third row (Fig. 2 e,f). Clearly, the XPD signature of the background is better removed, suggesting that the background intensity has been divided by itself yielding just a constant intensity offset. Fig. 2 (g,h) shows E_B-vs-*k* sections through the corrected arrays of Fig. 2 (e,f) cut along the dashed lines. These cuts clearly reveal the band dispersions which in the uncorrected arrays would be partly masked by the imprinted XPD modulation.

In conclusion, the high-energy *k*-microscope allows full-field imaging of (k_x,k_y)-distributions in large *k*-fields (up to > 22 Å^{-1} diameter) and time-of-flight energy recording. Using two medium-weight element materials as examples, Mo and $TiTe_2$, we have presented a powerful method for high-accuracy bulk electronic-structure mapping using momentum-resolved hard X-ray photoelectron spectroscopy. The key ingredients are high-resolution valence-band maps and core-level diffractograms taken at exactly the same kinetic energy and *k*-range. This allows for voxel-by-voxel processing of the 3D data arrays and disentangling of the different distortion effects due to quasi-elastic phonon scattering and photoelectron diffraction.

Author contact: Sergey Babenkov, sbabenko@uni-mainz.de; Christoph Schlueter, christoph.schlueter@desy.de; Gerd Schönhense, schoenhe@uni-mainz.de

References

1. A. Gray, C. Papp, S. Ueda, B. Balke, Y. Yamashita, L. Plucinski, J. Minár, J. Braun, E. R. Ylvisaker, C. M. Schneider, W. E. Pickett, H. Ebert, K. Kobayashi and C. S. Fadley, 'Probing bulk electronic structure with hard X-ray angle-resolved photoemission', Nature Materials 10, 759–764 (2011).
2. K. Medjanik, O. Fedchenko, S. Chernov, D. Kutnyakhov, M. Ellguth, A. Oelsner, B. Schönhense, T. R. F. Peixoto, P. Lutz, C.-H. Min, F. Reinert, S. Däster, Y. Acremann, J. Viefhaus, W. Wurth, H. J. Elmers and G. Schönhense, 'Direct 3D mapping of the Fermi surface and Fermi velocity', Nature Materials 16, 615–621 (2017).
3. K. Medjanik, S. V. Babenkov, S. Chernov, D. Vasilyev, B. Schönhense, C. Schlueter, A. Gloskowskii, Yu. Matveyev, W. Drube, H. J. Elmers and G. Schönhense, 'Progress in HAXPES performance combining full-field *k*-imaging with time-of-flight recording', J. Sync. Rad., 26, 1996–2012 (2019).

Original publications

'High-accuracy bulk electronic bandmapping with eliminated diffraction effects using hard X-ray photoelectron momentum microscopy', Communications Physics 2, 107 (2019). DOI: 10.1038/s42005-019-0208-7

S. Babenkov[1], K. Medjanik[1], D. Vasilyev[1], S. Chernov[1], C. Schlueter[2], A. Gloskovskii[2], Yu. Matveyev[2], W. Drube[2], B. Schönhense[3], K. Rossnagel[2,4], H.-J. Elmers[1] and G. Schönhense[1]

'High-resolution hard-X-ray photoelectron diffraction in a momentum microscope – the model case of graphite', New Journal of Physics 21, 113031 (2019). DOI: 10.1088/1367-2630/ab51fe

O. Fedchenko[1], A. Winkelmann[5], K. Medjanik[1], S. Babenkov[1], D. Vasilyev[1], S. Chernov[1], C. Schlueter[2], A. Gloskovskii[2], Yu. Matveyev[2], W. Drube[2], B. Schönhense[3], H. J. Elmers[1] and G. Schönhense[1]

1. Johannes Gutenberg-Universität, Mainz, Germany
2. Deutsches Elektronen-Synchrotron DESY, Hamburg, Germany
3. Imperial College London, United Kingdom
4. Christian-Albrechts-Universität zu Kiel, Kiel, Germany
5. Laser Zentrum Hannover e.V, Hannover, Germany

Imaging orbitals of quantum materials

Taking a photograph of a quantum mechanical object

The search for new quantum materials with novel properties is often focused on materials containing transition-metal or rare-earth elements. The presence of the *d* or *f* orbitals provides a fruitful playground to generate novel phenomena. In order to efficiently design and tune the materials, it is essential to identify the *d* or *f* orbitals that actively participate in the formation of the ground state. So far, this has been done using optical, X-ray or neutron spectroscopies in which spectra must be analysed using theory. This, however, is also a challenge in itself, since calculations hit their limits due to the many-body nature of the problem. Here we developed a new experimental method that circumvents the need for theory and instead provides the information as measured.

Our objective is to develop a measurement method by which we can make a direct image of the active *d* or *f* electron orbital in a material and thus determine how the quantum-mechanical object looks like in a real solid. Such a method has now been tested at the PETRA III beamline P01 which has been recently upgraded with contributions from the Max Planck Society.

In X-ray absorption spectroscopy, the spectral intensity of an absorption process involving the dipole-allowed *s*→*p* transition depends on the orientation of the electric field polarisation vector $\vec{E}$ of the photon relative to the orientation of the *p* orbital. Because the *s* orbital is spherically symmetric, sweeping the polarisation vector over all angles would yield an angular intensity distribution of the absorption that directly reflects the shape and orientation of the *p*-orbital hole. We now would like to do the same for *d* or *f* orbitals. However, *s*→*d* or *s*→*f* transitions are dipole-forbidden so we cannot resort to conventional techniques such as X-ray absorption spectroscopy. Here is where non-resonant inelastic X-ray scattering (NIXS), also called X-ray Raman, and the P01 beamline come into play.

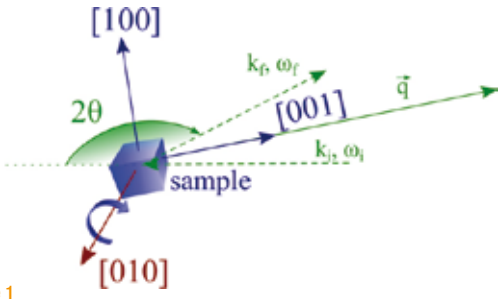

Figure 1

Scattering geometry of the non-resonant inelastic X-ray scattering experiment at P01. The scattering triangle, defined by the scattering vectors $\vec{k}_i$ and $\vec{k}_f$, remains unchanged throughout the energy scan (see text).

In NIXS, we have the ability to select not only the energy but also the size $|\vec{q}|$ and direction $\vec{q}$ of the momentum transfer [1]. This can be done by appropriately choosing the scattering geometry and energy of the incoming X-rays. For small $|\vec{q}|$, the transitions are determined by the dipole selection rules and we obtain very much the same information as in X-ray absorption spectroscopy (XAS). The difference is that in NIXS the directional dependence of the momentum transfer $\vec{q}$ with respect to the crystal lattice takes over the role of the polarisation dependence of the electric field vector in XAS [1-4]. For large momentum transfers of $|\vec{q}| \approx 10$ Å^{-1}, however, transitions that are governed by *beyond-dipole* or *multipole* terms gain intensity [2-5]. For example, dipole forbidden 3*s*→3*d* (M_1) transitions of the 3*d* transition metal atoms become visible with intensities which are more than sufficient for quantitative experiments. Since we focus on transitions involving an *s* core level, we call our method *s*-NIXS.

We tested the feasibility and power of the *s*-NIXS method on NiO, a text book example for a strongly correlated antiferromagnetic insulator. Figure 1 shows how the cubic NiO single crystal is turned through the scattering triangle which is defined by the incoming and outgoing scattering vectors $\vec{k}_i$ and $\vec{k}_f$. Both vectors are next to constant when exciting the M_1 edge at 110 eV energy transfer in a scan from 100 to 120 eV since the energy transfer is negligible with respect to the incoming and outgoing energies of about 10 keV so that $|\vec{q}|$ does not vary across the scan. Turning the crystal around an axis perpendicular to the scattering plane changes the direction of the momentum transfer $\vec{q}$ with respect to the crystal lattice and the directional dependence of the hole distribution in the NiO *3d*-shell can be mapped when taking energy scans for many different crystal angles.

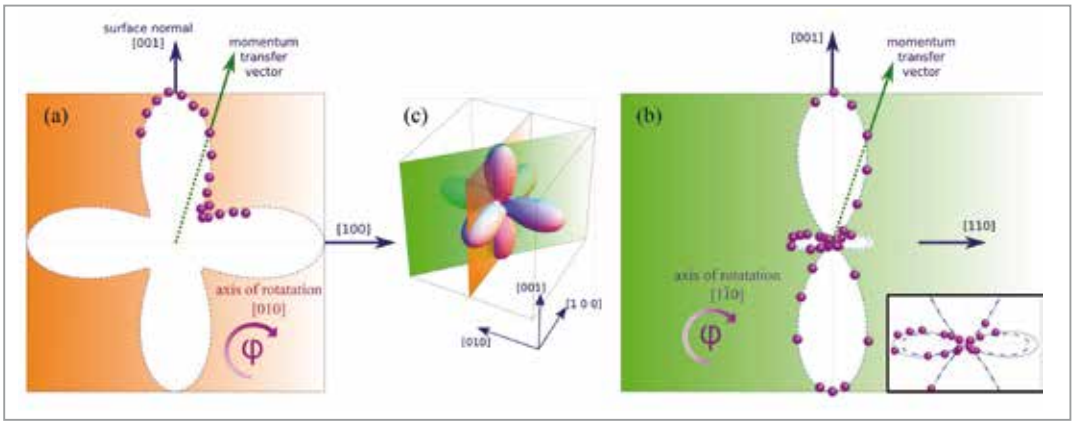

Figure 3

(a) and (b) projections of the 3D orbital shape on two planes defined by [001] and [100] (a) and [001] and [110] (b). The data points on polar plots (a) and (b) are integrated intensities for Ni M_1 ($3s \rightarrow 3d$) in Fig. 2 for corresponding ϕ. For (a) the sample is rotated such that q sweeps between [001] and [100]; for (b), q sweeps between [001] and [110]. The inset in (b) demonstrates the theoretical orbital function (blue dashed line) and the corrected function as a result of an angular convolution with the 3 × 4 analyser array. For (a), the correction was insignificant. (c) 3D hole density distribution of the Ni high-spin $3d^8$ configuration.

Figure 2 shows such scans for several crystal-orientations of NiO, from 001 to 101 (a), from 00-1 to -1-10 (b) and also from 001 to 00-1 (c). When plotting the integrated intensities in a polar plot we obtain directly an image of the orbital shape (see Fig. 3 a,b), as the comparison with the calculated Ni^{2+} hole density distribution $^3A_2$ $3d(x^2\text{-}y^2/3z^2\text{-}r^2)$ in Fig. 3c) shows. No fancy analysis routines are required, just plotting intensities yields the result. Hence, each scan in Fig. 2 may be viewed as a pixel in a slow motion photograph.

In summary, a particular atomic process (here the *3s* to *3d* excitation) is measured in NIXS as function of the orientation of the sample with respect to the momentum transfer. Displaying the intensities in a polar plot, yields directly the image of the *3d* orbital in the material under investigation. The new method presents a tangible and efficient alternative to current methods for studying orbitals in quantum materials which could ultimately enhance research in both physics and chemistry.

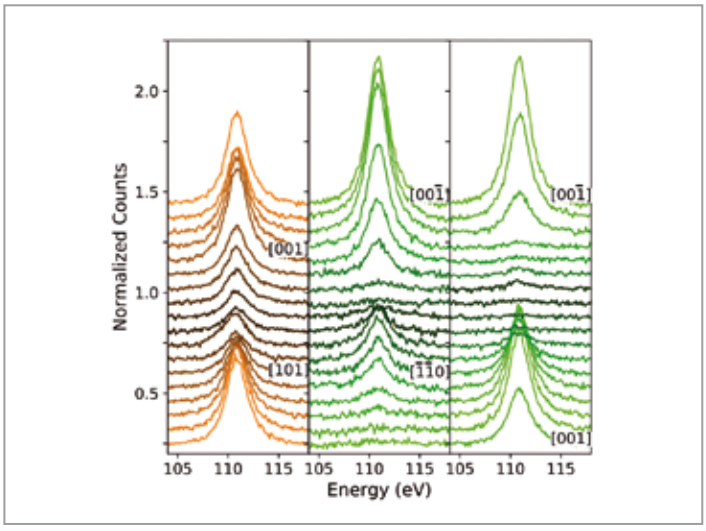

Figure 2

Spectra of energy scans across the Ni M_1 ($3s \rightarrow 3d$) edge for different sample rotations and orientations. The spectra are background corrected (linear background subtracted) and normalised in intensity to the Compton scattering. The respective energy scans are vertically off-set for graphical clarity.

Author contact: Liu Hao Tjeng, hao.tjeng@cpfs.mpg.de
Hasan Yavas, yavas@slac.stanford.edu
Andrea Severing, severing@ph2.uni-koeln.de

References

1. W. Schülke in Electron Dynamics by Inelastic X-ray Scattering (Oxford Univ. Press, 2008).
2. M. W. Haverkort et al., 'Nonresonant inelastic X-ray scattering involving excitonic excitations: the examples of NiO and CoO', Phys. Rev. Lett. 99, 257401 (2007).
3. R. A. Gordon et al., 'Orientation-dependent X-ray Raman scattering from cubic crystals: natural linear dichroism in MnO and CeO_2', J. Phys. Conf. Ser. 190, 012047 (2009).
4. T. Willers et al., 'Determining the in-plane orientation of the ground-state orbital of $CeCu_2Si_2$', Phys. Rev. Lett. 109, 046401 (2012).
5. R. A. Gordon et al., 'High multipole transitions in NIXS: valence and hybridization in 4f systems', Europhys. Lett. 81, 26004 (2008).

Original publication

'Direct imaging of orbitals in quantum materials', Nature Physics 15, 559 (2019), DOI: 10.1038/s41567-019-0471-2

Hasan Yavas[1,2,5], Martin Sundermann[1,3], Kai Chen[3,6], Andrea Amorese[1,3], Andrea Severing[1,3], Hlynur Gretarsson[1,2], Maurits W. Haverort[4] and Liu Hao Tjeng[1]

1. Max Planck Institute for Chemical Physics of Solids, Dresden, Germany
2. Deutsches Elektronen-Synchrotron DESY, Hamburg, Germany
3. Institute of Physics II, University of Cologne, Cologne, Germany
4. Institute for Theoretical Physics, Heidelberg University, Heidelberg, Germany
5. Present address: SLAC National Accelerator Lab, Menlo Park, CA, USA
6. Present address: Helmholtz-Zentrum Berlin, BESSY II, Berlin, Germany

Viscosity of polymer nanocomposites

A tale of two interfaces

Polymers constitute a huge part of our day-to-day life from protective thin film coatings to flexible electronics. Nanoparticles are added to polymers to obtain novel materials – polymer nanocomposites (PNC) – with significantly modified properties. To enhance compatibility, soft nanoparticles having surface grafted polymers are used, which leads to the presence of a micro interfacial layer at the nanoparticle host polymer interface. For many practical applications, polymers need to be used as thin film coatings where the film substrate interface can significantly alter polymer properties. Here we demonstrate how these two interfaces tune the viscosity of a polymer or PNC thin films.

Interfaces are ubiquitous in condensed matter and biological systems and play a crucial role in determining various physical properties of the respective systems. More recently soft colloidal nanoparticles with grafted polymers (PGNPs) are widely used to create novel polymer-based nanocomposites (PNC) having high loading and stable dispersions of these PGNPs. Most of the properties of these hybrid materials, are determined by the nature of the interfacial layer (IL) between the soft corona (the grafted chains) of the PGNPs and the matrix chains, both being chemically identical [1]. In several applications of the PNCs, it is desirable that these hybrid materials can be used as coatings or thin films on substrates. In such a configuration, reducing the thickness of the films introduces another important parameter: film–substrate interactions and the possibility of the presence of an interfacial adsorbed layer (h_{int}) dictated by the nature of these interactions. Here we investigate the contribution of these two interfaces on the dynamics of PNCs.

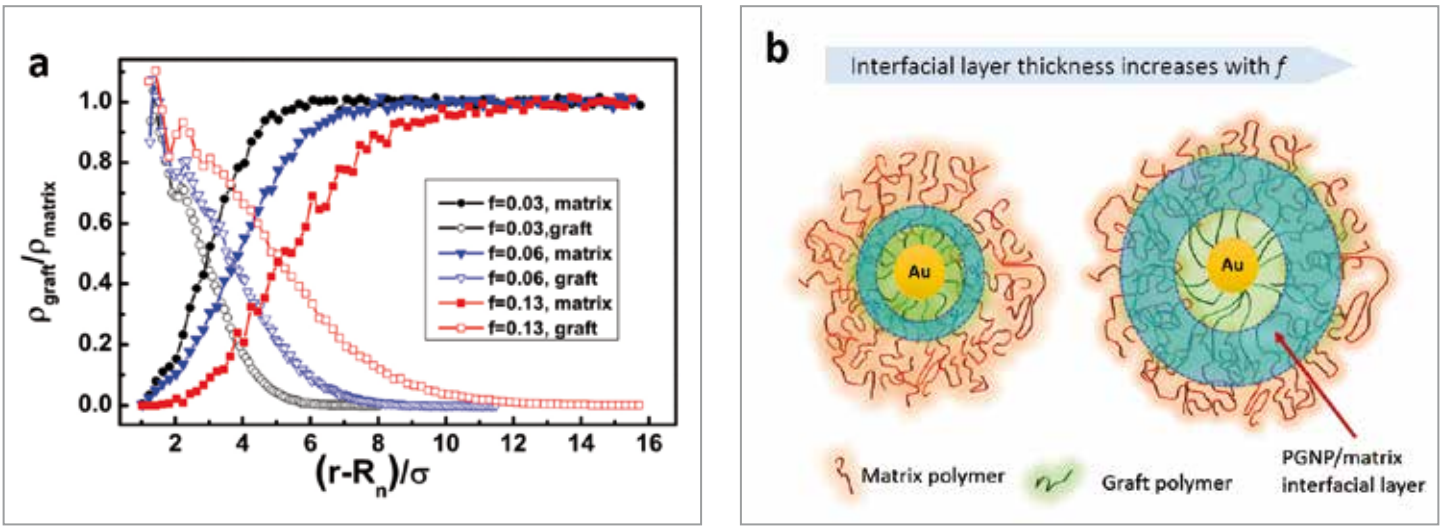

Figure 1

(a) Radial density profiles for graft and matrix monomers from the centre of nanoparticle for different *f* values (ratio of grafted to matrix chain length), calculated from MD simulation, where *r*, R_n and σ are the radial distance, radius of nanoparticles and size of a monomer respectively [2]. (b) Schematic of interfacial layer surrounding PGNP. The annular region represents the interfacial layer where matrix polymers penetrated into the graft polymer brushes.

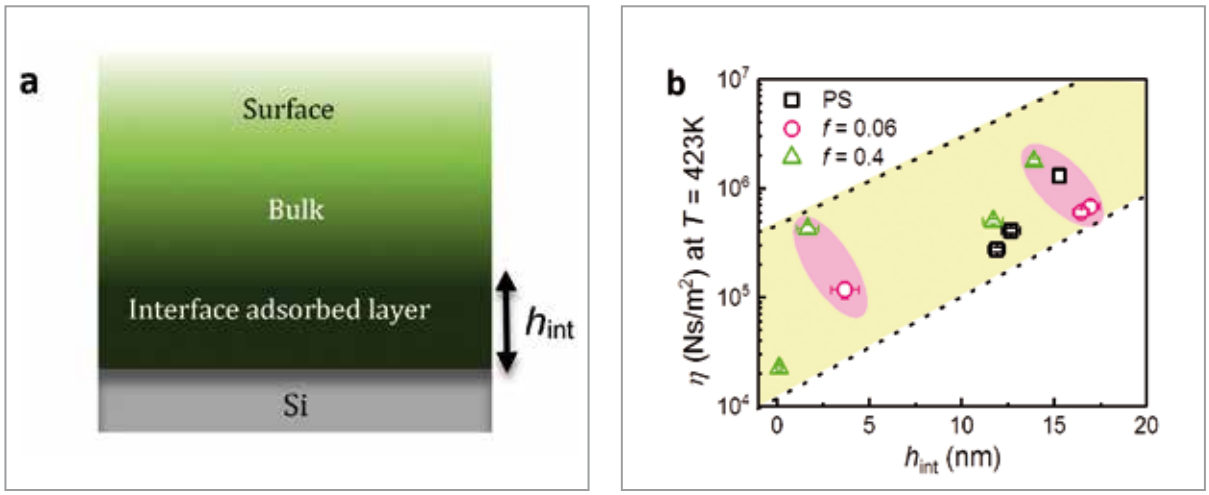

Figure 2

(a) The schematic showing different regions in thin film along the thickness. (b) Viscosity, η, at T = 423 K as a function of h_{int} for all the PS and PNC films of various thickness, h. The pink shaded regions indicate the scaling of η with IL thickness for approximately similar values of h_{int}.

PNCs with homogeneous distribution of PGNPs are desirable for many applications. One way to achieve this configuration is by increasing interface wettability between PGNP and matrix chains. It has been shown that interface wettability can be tuned by varying the ratio of grafted to matrix chain length, termed as *f* parameter [1, 2]. Molecular dynamics simulations performed on PNCs with different *f* values show that the penetration of matrix chains into graft brush layers increases by increasing *f* parameter (Fig. 1a), which means IL thickness increases with increasing the *f* value. The schematic illustrating the change in IL thickness with *f* is shown in Fig. 1b. In bulk PNCs, the key dynamical parameter viscosity is shown to scale with this *f* parameter [1]. The higher the value of *f*, the more viscous the PNC is. However, when PNCs are confined to thin films, the presence of h_{int} would play a crucial role in deciding the viscosity of these hybrid materials.

To understand such cases, we utilise X-ray photon correlation spectroscopy (XPCS) at the P10 beamline of PETRA III and probe the contribution of the IL and h_{int} on the thin film dynamics of PNCs. For this purpose, PNCs were prepared by embedding polystyrene-grafted gold nanoparticles in a linear polystyrene (PS) matrix. Thin films of PNCs of different *f* values and different thickness (65 nm, 40 nm and 30 nm) were prepared by spin-coating. In order to estimate the thickness of the adsorbed layer at the film–substrate interface (h_{int}) (Fig. 2a), we have washed off the top surface and bulk layer by thoroughly rinsing the films with a solvent of PS and X-ray reflectivity measurements revealed the thickness of this layer. The viscosity, η, of pure PS and PNC films extracted from XPCS measurements show the evidence of the positive correlation between viscosity and h_{int} (Fig. 2b). Interestingly, when h_{int} is of similar magnitude, viscosity of PNCs is controlled by IL thickness. It is noted that when the contribution of h_{int} to the dynamics is similar, the final viscosity depends on the *f* parameter (pink ellipses in Fig. 2b).

Our results suggest a novel method to control thermo-mechanical properties and stability of PNC coatings by independently controlling the two interfacial effects in athermal glassy PNCs.

Author contact: Jaydeep K. Basu, basu@iisc.ac.in

References

1. N. Begam et al., 'Nanoparticle–polymer interfacial layer properties tune fragility and dynamic heterogeneity of athermal polymer nanocomposite films', Soft Matter 14, 8853-8859 (2018).
2. M. Ibrahim et al., 'Correlation between grafted nanoparticle–matrix polymer interface wettability and slip in polymer nanocomposites', Soft matter 14, 6076-6082 (2018).

Original publication

'Viscosity and fragility of confined polymer nanocomposites: a tale of two interfaces', Nanoscale 11, 8546-8553 (2019). DOI: 10.1039/C8NR10362C.

Nimmi A. Das[1], Nafisa Begam[2], Mohd Ibrahim[1], Sivasurender Chandran[3], Venkat Padmanabhan[4], Michael Sprung[5], Jaydeep K. Basu[1]

1. Department of Physics, Indian Institute of Science, Bangalore, India
2. University of Tübingen,Tübingen, Germany
3. Institute of Physics, University of Freiburg, Freiburg, Germany
4. Department of Chemical Engineering, Tennessee Technological University, Cookeville,Tennessee, United States
5. Deutsches Elektronen-Synchrotron DESY, Hamburg, Germany

Superhard conductor synthesised at high pressure

New rhenium nitride pernitride is an ultra-incompressible and hard material

The traditional superhard materials diamond, cubic boron nitride and silicon nitride consist entirely of main-group elements that are bound with each other via directional covalent bonds. Due to the localised electron density, these materials are wide band gap insulators. However, some technological applications may require superhard conductive materials, which are much less common. Here we combined at high pressure a heavy transition metal rhenium, which itself is quite incompressible but not hard with nitrogen that forms directional covalent bonds. The resulting compound with the empirical formula ReN_2 is a very hard and incompressible but conductive material.

Hardness is a measure of a material's resistance to deformation. A superhard material has high shear modulus (resistance to shear deformation), high bulk modulus (resistance to compression) and does not deform plastically. Diamond is a well-known naturally occurring superhard material, and the standard approach to new superhard materials is mimicking the crystal structure and bonding of diamond. For example, the isostructural boron nitride compound, in which each carbon-carbon bond is replaced by a boron-nitrogen bond is also a superhard material. All these covalent compounds are usually wide-gap insulators or semiconductors.

Another approach to create superhard materials is based on the modification of ultra-incompressible, but not hard compounds. For instance, heavy transition metals like Os and Re which have high electron density have large bulk moduli (K_0(Os) ~400 GPa, K_0(Re) ~360 GPa) [1]. However, being incompressible these metals have low shear moduli. Metallic bonds are much easier to break than covalent bonds and close-packed atomic layers may easily slip. Light element atoms that fit into the interstitial sites of the close-packed metals may significantly strengthen the material. Indeed, hard transition metal nitrides like NbN, CrN, MoN are known [2]. All these nitrides contain interstitial nitrogen atoms. Even stronger reinforcement of the material can be achieved if the transition metal is combined with light elements that form short covalent bonds preventing the formation of slip planes. In this work we synthesised a novel material, rhenium nitride pernitride ReN_2, which unlike standard interstitial nitrides contains covalently bound dinitrogen units N-N.

To synthesise ReN_2, rhenium metal was loaded into a diamond anvil cell with nitrogen and compressed up to 42 GPa. The sample was then heated with a near infrared laser at the Extreme Conditions Beamline P02.2 at PETRA III and the structural changes were monitored *in situ* by single-crystal X-ray diffraction. Drastic changes of the diffraction pattern clearly indicated that rhenium reacted with nitrogen and we were able to identify the crystal structure of the reaction product. Unlike nitrides and pernitrides, this compound exhibits a very peculiar crystal structure, because it contains isolated nitrogen atoms like 'standard' interstitial nitrides as well as covalently bound dinitrogen units (Fig. 1a). Therefore, this compound is a nitride pernitride – the first of a kind. Compressibility measurements have shown that ReN_2 is an ultra-incompressible compound with a bulk modulus of 428 GPa (Fig. 1b) – almost as incompressible as diamond.

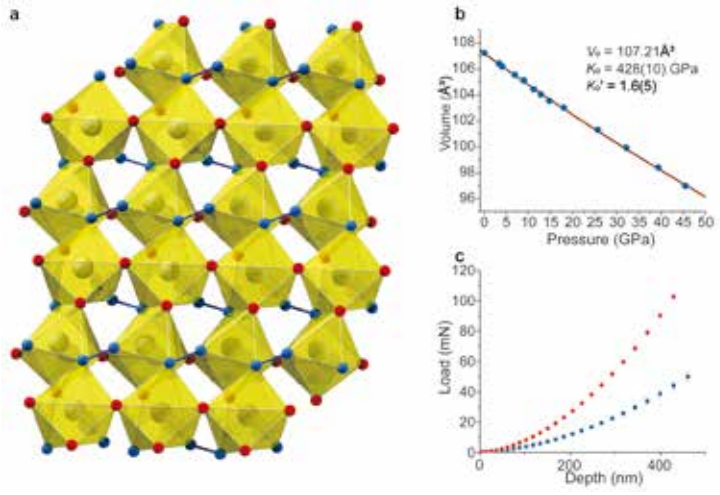

Figure 1

a) Crystal structure of ReN_2 at ambient conditions. Blue spheres show nitrogen atoms that form covalently bound N-N units. Red spheres show discrete N atoms. ReN_7 polyhedra are shown in yellow. b) Pressure-dependence of the unit-cell volume of ReN_2. The solid line shows the fit of the third order Birch–Murnaghan equation of state to the experimental data. c) Averaged indentation load-displacement data for Re (blue squares) and for ReN_2 (red circles).

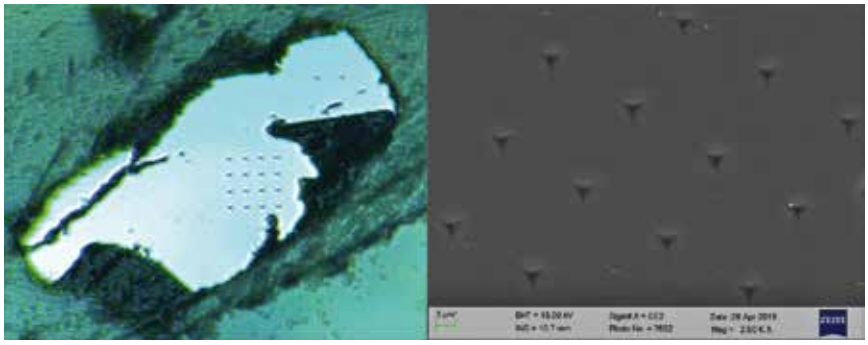

Figure 2

Sample of ReN_2 synthesised in the large volume press that was used for the nano-indentation experiment. SEM image of the indented region is shown in the right part of the figure.

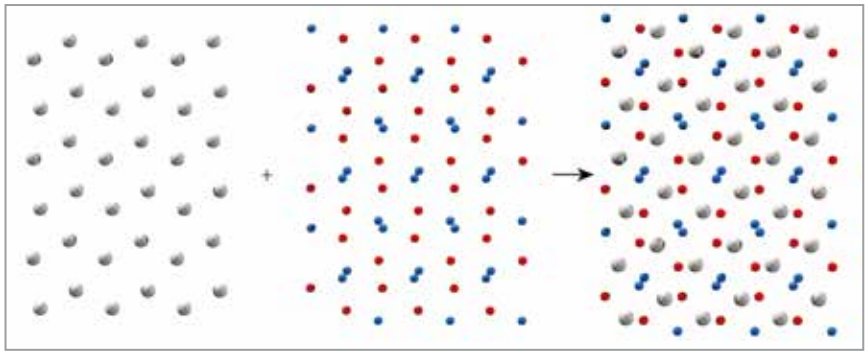

Figure 3

ReN_2 can be thought of as nitrogen atoms (red) and molecules (blue) being inserted into the matrix of Re metal (grey).

A key challenge is the scalability of the high-pressure synthesis of hard or superhard materials. The size of a pressure chamber in a diamond anvil cell is usually limited to a few tens of microns not allowing the synthesis of bulk samples. Modern autoclaves do not allow reaching pressures high enough for the synthesis of ReN_2, while the reaction between rhenium and nitrogen in a large volume press apparatus cannot be realised because it is not possible to seal enough nitrogen in a capsule. We solved the problem of scaling up the synthesis by using a solid nitrogen precursor ammonium azide NH_4N_3 that was sealed with Re metal in a capsule of a large volume press apparatus. The synthesis carried out at 33 GPa resulted in bulk phase-pure polycrystalline ReN_2 of the size sufficient for hardness and electrical resistance measurements (Fig. 2).

Nano-indentation measurements allow to determine the hardness and Young's modulus of the material from the dependence of the indenter displacement on the applied load. The average hardness and Young's modulus fitted for 200 and 400 nm depths are 36.7(8) GPa and 493(14) GPa, respectively (Fig. 1c). The hardness approaching 40 GPa – a threshold for superhard materials and extreme stiffness comparable with diamond – makes the mechanical properties of ReN_2 exceptional in the row of metal nitrides. ReN_2 can be thought as a composite material on an atomic level (Fig. 3), where nitrogen atoms and molecules are inserted into the metallic Re matrix. It is this combination with interstitial nitride anions and covalently bound pernitride units that makes this compound ultra-incompressible and extremely hard at the same time. Electrical conductivity measurements have demonstrated that ReN_2 is conductive – an extremely rare property for superhard compounds. The developed method for scaling up the synthesis of ReN_2 in a large volume press using ammonium azide as a nitrogen precursor may be applied for producing nitrides of other transition metals. We demonstrated the complete route for materials development from screening experiments in diamond anvil cells to the synthesis of samples large enough for physical property measurements.

Author contact: Maxim Bykov, maks.byk@gmail.com

References

1. L. Dubrovinsky, N. Dubrovinskaia, E. Bykova, M. Bykov, V. Prakapenka, C. Prescher, K. Glazyrin, H.-P. Liermann, M. Hanfland, M. Ekholm, Q. Feng, L. V. Pourovskii, M. I. Katsnelson, J. M. Wills and I. A. Abrikosov, 'The most incompressible metal osmium at static pressures above 750 gigapascals', Nature 525, 226-229 (2015).
2. M. T. Yeung, R. Mohammadi and R. B. Kaner, 'Ultraincompressible, superhard Materials', Annu. Rev. Mater. Res. 46, 465-485 (2016).

Original publication

'High-pressure synthesis of ultraincompressible hard rhenium nitride pernitride $Re_2(N_2)(N)_2$ stable at ambient conditions', Nature Communications 10, 2994 (2019).
DOI: 10.1038/s41467-019-10995-3

Maxim Bykov[1], Stella Chariton[1], Hongzhan Fei[1], Timofey Fedotenko[2], Georgios Aprilis[2], Alena V. Ponomareva[3], Ferenc Tasnádi[4], Igor A. Abrikosov[4], Benoit Merle[5], Patrick Feldner[5], Sebastian Vogel[6], Wolfgang Schnick[6], Vitali B. Prakapenka[7], Eran Greenberg[7], Michael Hanfland[8], Anna Pakhomova[9], Hanns-Peter Liermann[9], Tomoo Katsura[1], Natalia Dubrovinskaia[2] and Leonid Dubrovinsky[1]

1. Bayerisches Geoinstitut, University of Bayreuth, Bayreuth, Germany
2. Material Physics and Technology at Extreme Conditions, Laboratory of Crystallography, University of Bayreuth, Bayreuth, Germany
3. Materials Modelling and Development Laboratory, National University of Science and Technology 'MISIS', Moscow, Russia
4. Department of Physics, Chemistry and Biology (IFM), Linköping University, Linköping, Sweden
5. Materials Science and Engineering, Institute I, Friedrich-Alexander-Universität Erlangen-Nürnberg (FAU), Erlangen, Germany
6. Inorganic Solid-State Chemistry, Department of Chemistry, University of Munich (LMU), Munich, Germany
7. Center for Advanced Radiation Sources, University of Chicago, Chicago, USA
8. European Synchrotron Radiation Facility, Grenoble, France
9. Deutsches Elektronen-Synchrotron DESY, Hamburg, Germany

Standing waves with ultrashort pulses

Sub-Ångström spatial resolution achieved at an FEL

With the advent of X-ray free-electron lasers (FELs) new techniques for the investigation of structure and dynamics of matter emerged. Femtosecond X-ray diffraction enabled investigating the structural dynamics of bulk atoms in solid crystals. To obtain surface sensitive time-resolved structural data, electron or X-ray diffraction could be employed. However, these techniques require long range order of the structure to be resolved. In the field of heterogeneous catalysis, typical atoms and molecules involved in chemical reactions at surfaces are lacking lateral long range order. In order to obtain direct structural information of atoms and molecules at surfaces the X-ray standing wave technique (XSW) can be employed.

In this pioneering experiment, we provide for the first time experimental evidence of the structural sensitivity and accuracy of the standing wave technique at the high repetition rate free-electron laser FLASH by measuring the photoelectron yield from the surface of SiO_2 on top of Mo/Si multilayers. The combination of the high chemical specificity and surface sensitivity of photoemission spectroscopy, together with the XSW structural sensitivity and the femtosecond duration of FEL pulses opens up the possibility of obtaining atomic positions with unprecedented picometre spatial accuracy and femtosecond temporal resolution. This technique provides structural data as well as data on the electronic system. Furthermore, it offers invaluable benchmarks to improve the predictive quality of density function theory calculations.

The XSW is formed in the region of spatial overlap between two coherently coupled incoming and Bragg-diffracted X-ray plane waves [1-4]. This results in a periodic modulation of the X-ray intensity along the direction perpendicular to the reflecting planes with the period of the standing wave d_{SW} (Fig. 1a). The main interest of this technique lies in the inelastic scattering of the XSW from atoms that are probed, leading to photoelectron or X-ray fluorescence yield. The strength of this scattering signal is proportional to the intensity of the XSW at the position of the emitting atoms. In fact, since the angle of incidence θ of the incoming X-ray wave varies through the Bragg condition, the phase of incident and Bragg-reflected waves changes by π, thus the standing wave shifts along the z-direction by $d_{SW}/2$. Typically the position of light atoms, predominantly present in the reactants, is monitored by the photoelectron signal due to the larger cross-section as compared to fluorescence [2]. Therefore, performing XSW experiments combined with photoelectron spectroscopy at an FEL on chemical reactions at single crystal catalysts with

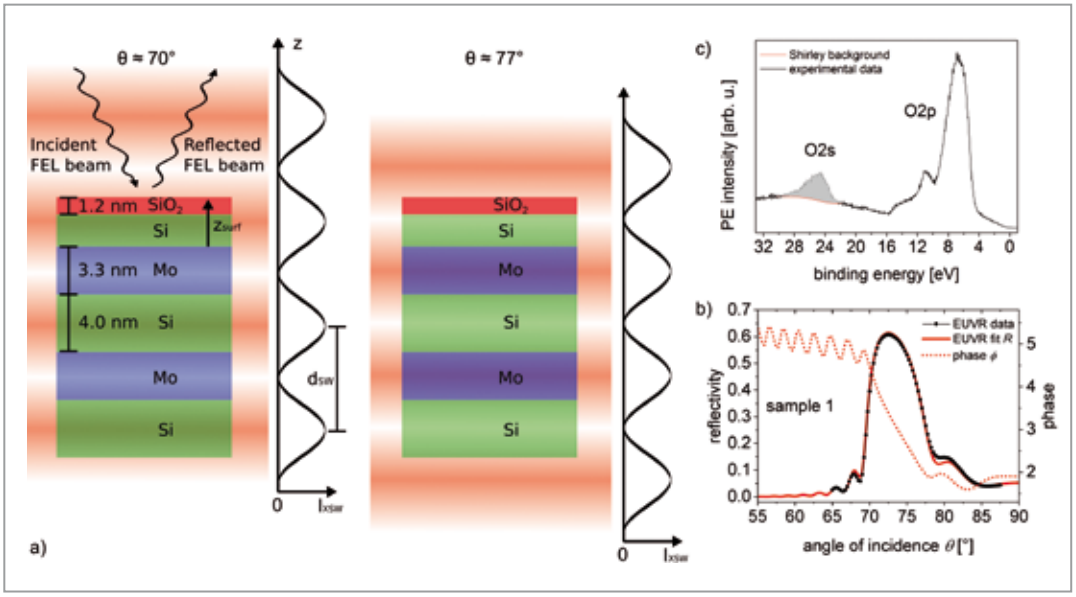

Figure 1

a) Sketch of Mo, Si and the SiO_2 top layer of the ML samples including the thicknesses of Mo and Si sublayers. The XSW field is shown for two different incident angles corresponding to the onset of the reflectivity ($\theta \approx 70°$) and after the phase has shifted by π ($\theta \approx 77°$). (b) Extreme ultraviolet reflectivity data of the ML sample with the shortest top Si sublayer, together with the corresponding reflectivity fit and calculated phase of the complex electric field ratio between Bragg-reflected and incident waves. (c) Photoelectron spectrum of O2s and O2p lines measured on a Mo/Si ML sample at $\theta = 90°$. The oxygen electron yield is marked by the gray area. [7]

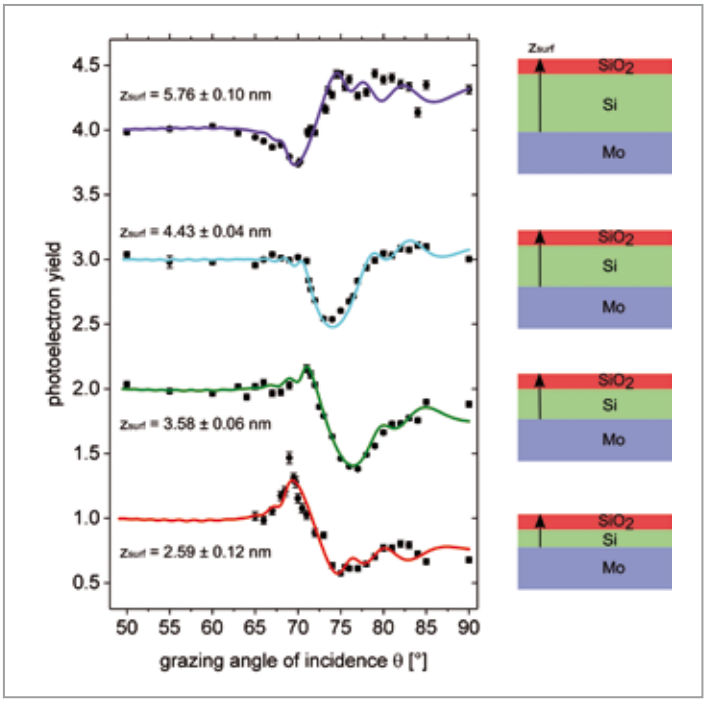

Figure 2

O2s photoelectron yield data (black dots) and fit model (solid lines) for ML samples with different thickness of the top Si layer as sketched on the right hand side. The resulting fit parameter z_{surf} is reported next to each curve. [7]

resolution of about few Ångströms (using a photon energy of few keV) may deliver structural information of the reactants with an unprecedented high spatial accuracy much below 1 Å [5] and femtosecond temporal resolution.

The XSW experiment was performed at the free-electron laser FLASH at the PG2 beamline delivering trains of 400 pulses with a repetition rate of 10 Hz. Our samples were Mo/Si multilayers (ML) consisting of 50 Mo/Si bilayers with a period of 7.3 nm and terminated with the top Si layer of 4 different nominal thicknesses. To match the first order Bragg condition, FLASH was tuned to the wavelength λ = 13.3 nm with an angle of incidence at maximum reflectivity of 72.5° (Fig. 1b). As the Si-terminated ML samples were exposed to air, a native SiO_2 layer of d_{SiO_2} = 1.2 nm was formed at the surface. This led to 4 different distances of the surface oxide from the underlying identical periodic structure. In our XSW experiments we measured the photoelectron yield of the O2s core level originating from the O atoms located at the surface of the SiO_2 layer (see Fig. 1c) as a function of the incident angle θ.

Notably, the photoelectron yield profiles in Fig. 2 are very different from each other and are strongly correlated with the thickness of the top Si layer. This indicates significantly different positions of the corresponding emitting oxygen atoms with respect to the standing wave modulation. The electron yield profiles were fitted with a model [6] based on grazing incidence X-ray reflectivity and extreme ultraviolet reflectivity data. As a result of the fits, the surface of SiO_2 in the 4 samples was found to be at z_{surf} = 2.59 ± 0.12 nm, 3.58 ± 0.06 nm, 4.43 ± 0.04 nm, and 5.76 ± 0.10 nm above the top Mo layer. In this way we demonstrate the structural sensitivity of the XSW technique using FEL pulses. In particular, the small error bars of z_{surf} (< 0.15 nm) indicate the high spatial accuracy of the measured SiO_2 surface positions.

In this study we have demonstrated the structural sensitivity and accuracy of the XSW technique at an FEL. In combination with the high chemical specificity and surface sensitivity of photoelectron spectroscopy and together with the femtosecond duration of FEL pulses, these experiments open up the possibility of obtaining direct ultrafast structural information of atoms at surfaces. Importantly, the wide applicability of time-resolved X-ray standing wave makes it an ideal tool to investigate structural dynamics of different class of materials, from single crystals to more exotic layered crystals as perovskites.

Author contact: Giuseppe Mercurio, giuseppe.mercurio@xfel.eu

References

1. J. Zegenhagen and A. Kazimirov (ed), 'The X-ray standing wave technique: Principles and applications' (Singapore: World Scientific) (2013).
2. J. Zegenhagen, 'Surface structure determination with X-ray standing waves', Surf. Sci. Rep. 18, 202–71 (1993).
3. I. A. Vartanyants and M. V. Kovalchuk, 'Theory and applications of X-ray standing waves in real crystals', Rep. Prog. Phys. 64, 1009 (2001).
4. D. P. Woodruff, 'Surface structure determination using X-ray standing waves', Rep. Prog. Phys. 68, 743–9 (2005).
5. G. Mercurio, O. Bauer, M. Willenbockel, N. Fairley, W. Reckien, C. H. Schmitz, B. Fiedler, S. Soubatch, T. Bredow, M. Sokolowski and F. S. Tautz, 'Adsorption height determination of nonequivalent C and O species of PTCDA on Ag(110) using X-ray standing waves', Phys. Rev. B 87, 045421 (2013).
6. S. Döring, F. Schönbohm, D. Weier, F. Lehmkühler, U. Berges, M. Tolan, C. S. Fadley and C. Westphal, 'Standing-wave excited photoemission experiments on Si/$MoSi_2$ multilayer mirrors in the soft X-ray regime: An analytical modeling approach', J. Appl. Phys. 106, 124906 (2009).
7. Figure published under CC-BY 3.0 in the original publication.

Original publication

'Surface structure determination by X-ray standing waves at a free-electron laser', New Journal of Physics 21, 033031 (2019). DOI: 10.1088/1367-2630/aafa47

Giuseppe Mercurio[1,2,6], Igor A. Makhotkin[3], Igor Milov[3], Young Yong Kim[4], Ivan A. Zaluzhnyy[4,5,7], Siarhei Dziarzhytski[4], Lukas Wenthaus[1,2], Ivan A. Vartanyants[4,5] and Wilfried Wurth[1,2,4]

1. Department Physik, Universität Hamburg, Hamburg, Germany
2. Center for Free-Electron Laser Science, Hamburg, Germany
3. Industrial Focus GroupXUVOptics, MESA+Institute for Nanotechnology, University of Twente, Enschede, The Netherlands
4. Deutsches Elektronen-Synchrotron DESY, Hamburg, Germany
5. National Research Nuclear University MEPhI (Moscow Engineering Physics Institute), Moscow, Russia
6. Present address: European XFEL GmbH, Schenefeld, Germany
7. Present address: Department of Physics, University of California San Diego, La Jolla, USA

Hierarchical nanostructures make spiders walk upside down

Fibre architecture in highly effective biological adhesive structures

Wandering spiders easily climb vertically and walk upside down on smooth and rough surfaces. They share this capability with many insects such as flies and beetles. However, the key mechanism underlying the strong adhesion between the animals' feet and a substrate is different in insects and spiders. Insect adhesion relies on capillary forces caused by fluid secretions between the attachment structures and a substrate. Spiders adhere residue-free, presumably because of intermolecular attractive van der Waals forces between their adhesive hairy structures on the feet and the surface. Using high-resolution scanning nanofocus X-ray diffraction and scattering allowed us for unprecedented detailed insights into the material composition and arrangement of the spider attachment hairs.

In our study we examined the attachment system of the large Central American wandering spider *Cupiennius salei,* which has been a model organism for sensor systems, neurobiology and its exoskeleton's function and mechanical properties [e.g. 1, 2]. The adhesion structures on the tips of all eight legs comprise approximately 2400 very densely arranged adhesive hairs (setae) per foot. These setae are 0.2–1.6 mm long and approximately 10 µm thick. Their surface is covered with thousands of cuticular protuberances, the so-called microtrichs, branching off the bulk hair. In the adhesive tip region of a seta, these microtrichs are highly ordered in up to 20 parallel rows (Fig. 1 a, b) and consist of narrowing stalks that emerge from the hair backbone and terminate in approximately 1 µm wide and 20 nm thin spatula-shaped platelets (Fig. 1 c). These are responsible for the formation of intimate contact and the enhancement of adhesion [3, 4] by their alignment in parallel with the surface of a substrate.

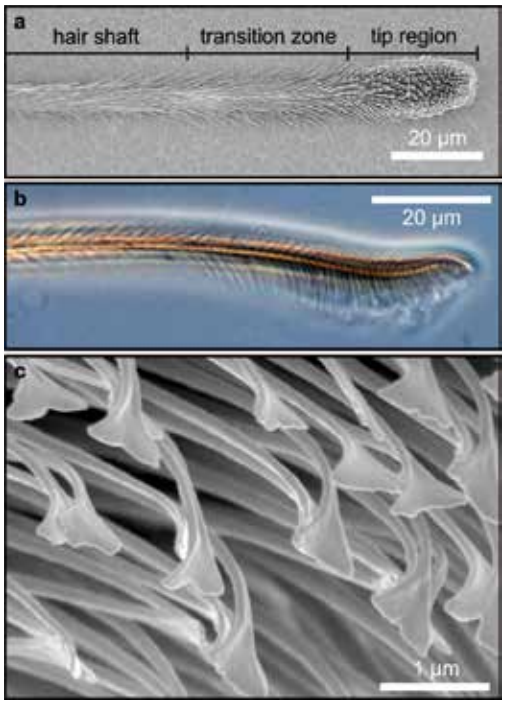

Figure 1

Morphology of the distal part of a spider attachment hair. a) Scanning electron micrograph, ventral view. The different sections are named corresponding to the presence of differently shaped microtrichs branching off the main hair. b) Phase-contrast transmitted light micrograph, side view. In the tip region, the elongated microtrichs form a brush-like structure. c) Scanning electron micrograph in the tip region. The spatula-shaped terminal structures of the microtrichs are the contact elements responsible for the spider's adhesion.

As part of the exoskeleton the setae are made of cuticle, a composite material that consists mainly of proteins and reinforcing polymeric chitin fibres. The crystalline chitin molecule chains are arranged in approximately 2–5 nm thick and 300 nm long nanofibrils embedded in a matrix of structural proteins.

Scanning wide-angle X-ray diffraction (XRD) at the Nanofocus end station of the MiNaXS beamline P03 at PETRA III and at beamline ID13 at ESRF (Grenoble, France) was used for two-dimensional mapping of the distribution and orientation of the crystalline chitin fibres in the different sections of the adhesive hairs with a resolution of 200 nm. Furthermore, the mapping of small-angle X-ray scattering (SAXS) signals gave insights into the distribution and orientation of mesoscopic structures approximately sized 100 nm.

Using SAXS the microscopic structures of the attachment hairs were well resolved (Fig. 2 a). In the hair shaft and the transition zone, single microtrichs were clearly visible. In the

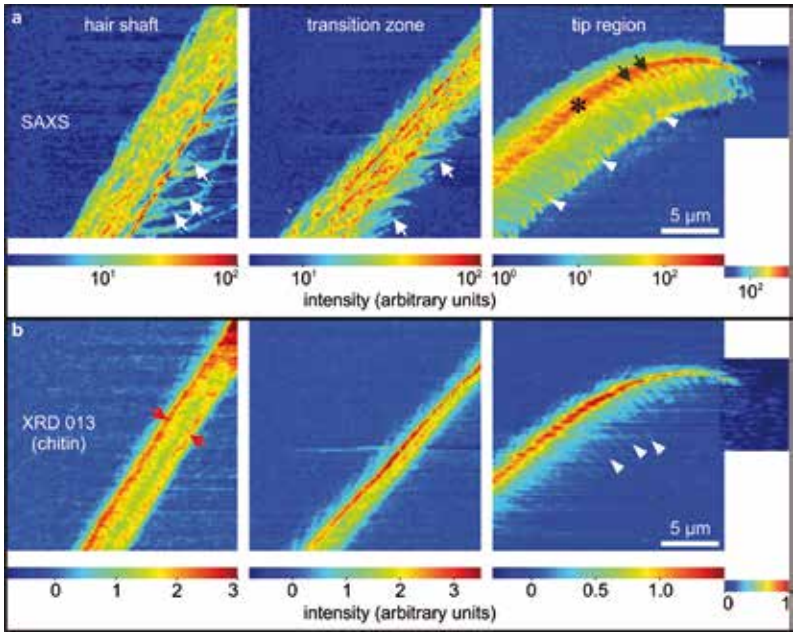

Figure 2

SAXS and XRD signal intensity maps of the different sections of an attachment hair in side view. A surface to attach to would be oriented vertically on the right side of the images. a) SAXS. In the hair shaft region and transition zone the white arrows point to single microtrichs. In the tip region the most intense signal was measured in a backbone-like structure (asterisk), from which the rows of microtrichs branch off (black arrows). The white arrowheads point to intense scattering in the spatula region. b) Intensity maps of the 013 wide-angle XRD peak of α-chitin in the same sections as in a). In the hair shaft region, the red arrows indicate the walls of the hollow hair shaft. The white arrowheads in the tip region mark the outreach of the 013 diffraction signal following the microtrichs.

tip region, the maximum SAXS intensities were found in a backbone-like stripe in the centre of the hair, pointing to a densification of more complex structures such as the microtrich branching sites. Interestingly, the SAXS intensity was also increased in the region of the adhesive spatulae, indicating strong scattering of the X-ray beam by their thin and flat structure.

Of the wide-angle XRD signals, the 013 reflections of α-chitin were selected to map the distribution and orientation of the chitin chains. The increased intensity at the edges of the bulk hair shaft region point to a tube-shape of this section (Fig. 2 b). The diffraction intensity was higher on the side to which bending would occur in the loaded hair. In the transition zone, there was an approximately 500 nm thick line with the highest intensity on the side of maximum strain, too. In the tip region, the most intense chitin signal was measured in the core backbone structure narrowing towards the very tip. The chitin signal could be detected up to the tips of the microtrichs indicating that they also are chitin-reinforced.

Orientation mapping from the azimuthal 013 reflection revealed that the chitin chains strictly followed the main orientation of the setae. This parallel orientation is remarkable and very different from other parts of the spider's exoskeleton, where reinforcement against bending is achieved by a rotating, plywood-manner orientation of the chitin fibril layers.

The parallel arrangement of the chitin fibres enhances the mechanical stability of the attachment hairs in the direction of the tensile forces. Latter act at every detachment of the setae from a surface and when the spider sits vertically or upside down, which is preferred by *C. salei*. High stiffness provided by the tube-shape of the hair shaft helps in proper positioning of the adhesive tip during locomotion. The flat structure of the backbone in the tip region is well suited to adapt to differently rough surfaces and increases the contact area of the spatulae with a surface.

Considering their high performance and resilience during attachment and, especially, detachment at every step of the walking spider, the setae are an excellent model for novel and biologically-inspired structured residue-free adhesives.

Author contact:
Clemens F. Schaber, cschaber@zoologie.uni-kiel.de

References

1. P. Fratzl and F. G. Barth, 'Biomaterial systems for mechanosensing and actuation', Nature 462, 442–448 (2009).
2. C. F. Schaber and F. G. Barth, 'Spider joint hair sensilla: adaptation to proprioreceptive stimulation', J. Comp. Physiol. A 201, 235–248 (2014).
3. S. Niederegger and S. N. Gorb, 'Friction and adhesion in the tarsal and metatarsal scopulae of spiders', J. Comp. Physiol. A 192, 1223–1232 (2006).
4. J. O. Wolff and S. N. Gorb, Surface roughness effects on attachment ability of the spider *Philodromus dispar* (Araneae, Philodromidae). J. Exp. Biol. 215, 179–184 (2012).

Original publication

'Hierarchical architecture of spider attachment setae reconstructed from scanning nano-focus X-ray diffraction data', Journal of the Royal Society Interface 16, 20180692 (2019). DOI: 10.1098/rsif.2018.0692

Clemens F. Schaber[1], Silja Flenner[2,3], Anja Glisovic[3], Igor Krasnov[3], Martin Rosenthal[4], Hergen Stieglitz[2,3], Christina Krywka[2], Manfred Burghammer[4], Martin Müller[2,3] and Stanislav N. Gorb[1]

1. Functional Morphology and Biomechanics, Zoological Institute, Kiel University, Kiel, Germany
2. Helmholtz-Zentrum Geesthacht, Geesthacht, Germany
3. Institute of Experimental and Applied Physics, Kiel University, Kiel, Germany
4. European Synchrotron Radiation Facility (ESRF), Grenoble, France

How manganese produces a parkinsonian syndrome

Synchrotron X-ray fluorescence imaging reveals manganese subcellular distribution

Parkinsonian syndrome is a set of diseases with symptoms similar to Parkinson's disease. Some are caused by accumulation of high quantities of manganese, a metal essential to the body at trace levels. This is especially so for a hereditary form of the disease caused by a mutation in the *Slc30a10* gene responsible for a toxic accumulation of manganese in cells. We have been able to locate manganese inside individual cells, using the fluorescent signature it produces under X-ray illumination. In the cell model of the disease, manganese concentrates essentially in the Golgi apparatus, a cellular compartment which acts as a dispatch centre for proteins. A corresponding accumulation of the metal is not observed in the Golgi apparatus of healthy cells.

Manganese is an essential element for humans. It is required for cell functions as a cofactor in a diversity of enzymes and proteins. Although essential at low concentration, manganese is neurotoxic at high dose, leading to parkinsonism, a clinical syndrome with symptoms of Parkinson's disease. We studied this toxicity in the case of a familial mutation affecting the manganese transporter protein SLC30A10, solute carrier family 30 member 10. This protein is normally responsible for the efflux of manganese and protects the cell against the toxicity of this metal.

Not much is known about manganese distribution in human cells because this element is present at low concentration in human cells, in the µg/g range, rendering its imaging very challenging. Very high spatial resolution and very sensitive imaging techniques are needed to detect µg/g traces of manganese in intracellular organelles. In other words, the challenge consists in detecting 10^{-6} g of manganese per gram of sample in structures of 1 µm^3 or less, resulting in the amount of manganese being around 10^{-18} g in intracellular structures. This is possible thanks to synchrotron radiation hard X-ray nanoprobes now available at several synchrotron facilities [1, 2].

However, another imaging method is required to identify in which cellular organelle(s) manganese is located. This is why we developed a correlative microscopy approach combining optical fluorescence and synchrotron X-ray fluorescence (SXRF) microscopy [3]. We first labelled the cellular organelles, here the nucleus and the Golgi apparatus, using organelle-specific dyes and performed optical fluorescence microscopy before employing the synchrotron-based techniques. The P06 hard X-ray microprobe at PETRA III at DESY enabled fast cell imaging at sub-micrometric (700 nm) resolution using the large solid-angle Maia detector array and allowed us to image many cells at different culture conditions (varying manganese concentration and protein expression). The ID16A X-ray nanoprobe at ESRF (Grenoble, France) enabled high-resolution imaging, allowing us to image some cells with 50 nm spatial resolution.

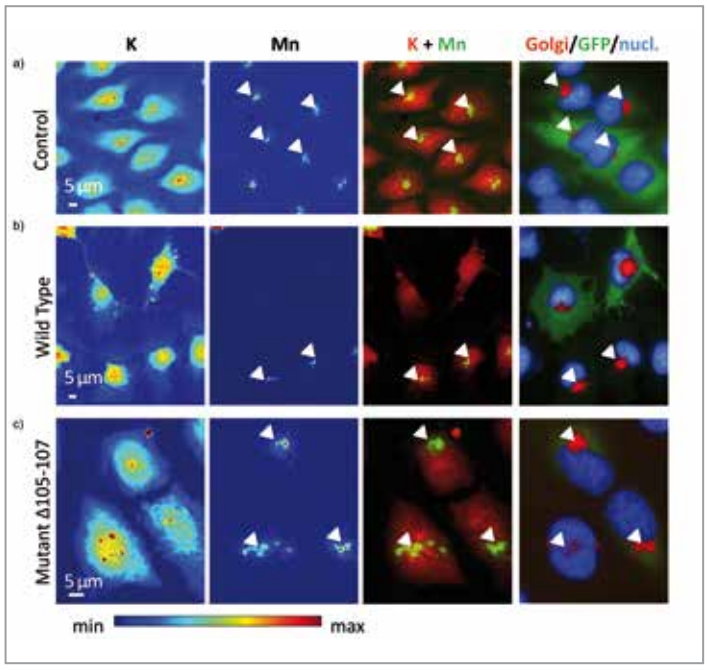

Figure 1

Representative examples of X-ray fluorescence imaging of cells exposed to 500 µM Mn. a) Control cells not expressing the wild-type or the mutated SLC30A10 protein. b) Cells transfected with the wild-type GFP-SLC30A10 construct, and c) cells transfected with GFP-SLC30A10-Δ105-107 construct. From left to right panels, K and Mn distributions in cells displayed with a colour scale from minimum (blue) to maximum (red) SXRF counts, overlay images of K (red) and Mn (green), fluorescence microscopy overlay images of nucleus staining (blue), Golgi apparatus labelling (red), and GFP-tagged proteins (green). Arrows indicate Mn and Golgi apparatus co-localization. Reprinted with permission. Copyright © American Chemical Society.

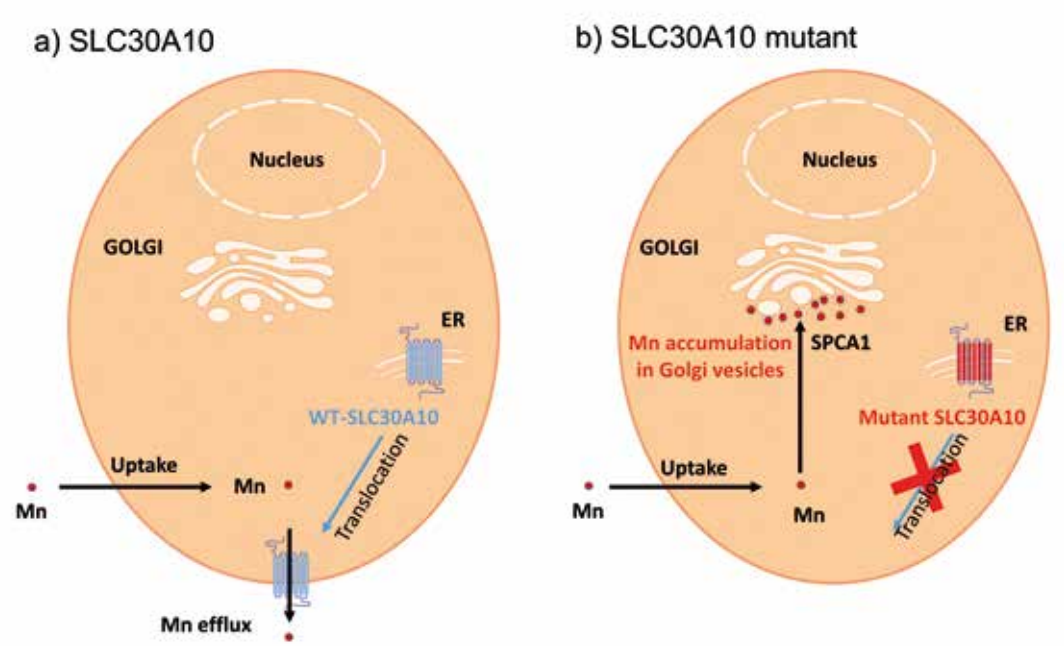

Figure 2

Schematic description of manganese excretion in healthy cells and accumulation in cells expressing the mutation involved in the disease. a) In healthy cells expressing SLC30A10 wild type, Mn is immediately excreted by the SLC30A10 protein expressed at the plasma membrane. b) In cells expressing the mutant, the SLC30A10-Δ105-107 protein is blocked in the endoplasmic reticulum (ER) and cannot be translocated to the plasma membrane resulting in Mn uptake in the cytoplasm. Mn is pumped from the cytoplasm into the Golgi vesicles by SPCA1 resulting in Mn accumulation in Golgi vesicles. Reprinted with permission. Copyright © American Chemical Society.

By comparing the images of organelle localisation and of manganese distribution in the same cells, we were able to clearly identify the sites of manganese accumulation (Fig. 1). We discovered that in control cells neither expressing the wild-type nor the mutated SLC30A10 protein (Fig. 1a), as well as in the cell model of the disease, i.e., cells expressing the pathological SLC30A10-Δ105-107 mutation (Fig. 1c), manganese accumulated in the Golgi apparatus. In contrast, manganese levels were very low in cells expressing the wild-type SLC30A10 protein (Fig. 1b). These results imply that the Golgi apparatus is the primary organelle that is impacted by manganese accumulation.

Our study illustrates the power of element imaging in single cells using X-ray fluorescence microscopy. We were for instance able to identify the cells that were correctly expressing the protein of interest fused with a green fluorescent protein (GFP), and compare the manganese distribution in cells either expressing or not expressing the protein within the same cellular population (Fig. 1b and c). This single-cell-analysis approach allows a clear understanding of the effect of a specific protein expression or mutation.

In conclusion, we propose the following mechanism for manganese toxicity in SLC30A10 mutants (Fig. 2). In cells expressing the functional SLC30A10 protein, manganese is efficiently expelled from the cell, probably immediately after uptake, since manganese is detected only in very small amounts even after high-exposure conditions. The pathological mutant proteins SLC30A10-Δ105-107 are blocked in the endoplasmic reticulum impeding the translocation to the plasma membrane and manganese efflux. Excess manganese is stored within Golgi vesicles by the SPCA1 transport protein (secretory pathway Ca^{2+}-ATPase isoform 1). At high concentrations manganese becomes toxic possibly because it disturbs the Golgi functions where it greatly accumulates in the absence of functional SLC30A10. Altered vesicular trafficking could be at the origin of the toxicity of the disease causing mutations of SLC30A10. Next it would be interesting to investigate whether manganese causes defects in Golgi vesicular trafficking and consequently on neurotransmitters or endocrine excretion. Our results also suggest that, if the mutated proteins retain transport activity, small molecules that would target the SLC30A10 mutant to the plasma membrane may be therapeutically effective.

Author contact: Richard Ortega, ortega@cenbg.in2p3.fr

References

1. A. Carmona, S. Roudeau, L. Perrin, G. Veronesi and R. Ortega, 'Environmental manganese compounds accumulate as Mn(II) within the Golgi apparatus of dopamine cells: relationship between speciation, subcellular distribution, and cytotoxicity', Metallomics 6, 822–832 (2014).
2. S. Das, K. Khatua, A. Rakshit, A. Carmona, A. Sarkar, S. Bakthavatsalam, R. Ortega and A. Datta, 'Emerging chemical tools and techniques for tracking biological manganese', Dalton Transact., 48, 7047–7061(2019).
3. S. Roudeau, A. Carmona, L. Perrin and R. Ortega, 'Correlative organelle fluorescence microscopy and synchrotron X-ray chemical element imaging in single cells', Anal. Bioanal. Chem., 406, 6979–6991 (2014).

Original publication

'SLC30A10 mutation involved in parkinsonism results in manganese accumulation within nano-vesicles of the Golgi apparatus', ACS Chemical Neuroscience 10, 599–609 (2019). DOI: 10.1021/acschemneuro.8b00451

Asuncion Carmona[1,2], Charles E. Zogzas[3], Stéphane Roudeau[1,2], Francesco Porcaro[1,2], Jan Garrevoet[4], Kathryn M. Spiers[4], Murielle Salomé[5], Peter Cloetens[5], Somshuvra Mukhopadhyay[3] and Richard Ortega[1,2]

1. Chemical Imaging and Speciation, CENBG, University of Bordeaux, Gradignan, France
2. CNRS, IN2P3, CENBG, Gradignan, France
3. Division of Pharmacology & Toxicology; Institute for Cellular & Molecular Biology and Institute for Neuroscience, University of Texas, Austin, USA
4. Deutsches Elektronen-Synchrotron DESY, Hamburg, Germany
5. European Synchrotron Radiation Facility, Grenoble, France

Structure of metabolic machine solves evolutionary riddle

ATP citrate lyase: a molecular gymnast as a target in atherosclerosis

Organisms across different kingdoms of life crucially rely on the high-energy metabolite acetyl-CoA in the cellular cytosol to fuel pivotal biochemical processes such as fatty acid and cholesterol synthesis and protein acetylation. Acting as a metabolic hub, ATP citrate lyase (ACLY) harnesses the hydrolysis of ATP and metabolically generated citrate and coenzyme A to catalyse a sequence of reactions that utilise high-energy adducts to yield acetyl-CoA. In humans, ACLY cleaves citrate exported from mitochondria and thereby links carbohydrate metabolism to *de novo* lipogenesis. Despite decades of research on the biochemical centrality of acetyl-CoA in many facets of physiology and disease, the enzymatic molecular machine responsible for its production had remained very poorly understood.

Consolidation of evolutionary and structure-function considerations of ACLY had remained elusive, in part due to the large molecular size and modular nature of ACLY holoenzymes. To facilitate structural studies on human ACLY (hACLY) by X-ray crystallography we employed an enzymatically-active variant that lacked a 60-residue disordered region. Following extensive crystal screening at European synchrotrons, including the EMBL beamlines P13 and P14 at PETRA III, we were able to determine the first ACLY crystal structures. These substrate-bound structures unraveled that in the ACLY holoenzyme four citryl-CoA synthetase (CCS) modules are connected to a tetrameric citryl-CoA lyase (CCL) core module (Fig. 1). In ACLY, the synthetase module initiates catalysis by the ATP-driven auto-phosphorylation of an active-site histidine, resulting in the formation of citryl-phosphate, which then reacts with CoA to generate the high-energy citryl-CoA intermediate. In the last step, citryl-CoA is cleaved into the reaction products oxaloacetate and acetyl-CoA by the central lyase module. The catalytic itinerary of ACLY is shown in Fig. 1.

To obtain insights into the possible divergence of ACLY assemblies across different domains of life we sought to determine crystal structures for prokaryotic ACLYs. Representative structures of ACLY from the autotrophic green sulphur bacteria *Chlorobium limicola* and the methanogenic archaeon *Methanosaeta concilii* revealed that prokaryotic and eukaryotic ACLY enzymes share a conserved modular architecture. Intriguingly, a comparison between the determined human and bacterial ACLY structures indicated that ACLY enzymes may undergo large-scale structural transitions by reorienting the synthetase modules with respect to the central lyase module (Fig. 2). To further study the structural plasticity of ACLY we conducted in solution small-angle X-ray scattering experiments at the PETRA III beamline P12. In collaboration with the EMBL BioSAXS group led by Dmitri Svergun we were able to show that ACLY in solution can undergo large-scale, substrate-induced structural transitions (Fig. 2). Parallel to our study, a research team led by Liang Tong at Columbia University was able to determine a high-resolution structure of hACLY by electron cryo-microscopy methods [1]. In complementary fashion to our work, this study had targeted hACLY in complex with an allosteric small-molecule inhibitor, and revealed that hACLY is able to adopt yet another conformational state. This provided further evidence that the CCS module pivots around the CCL module during catalysis.

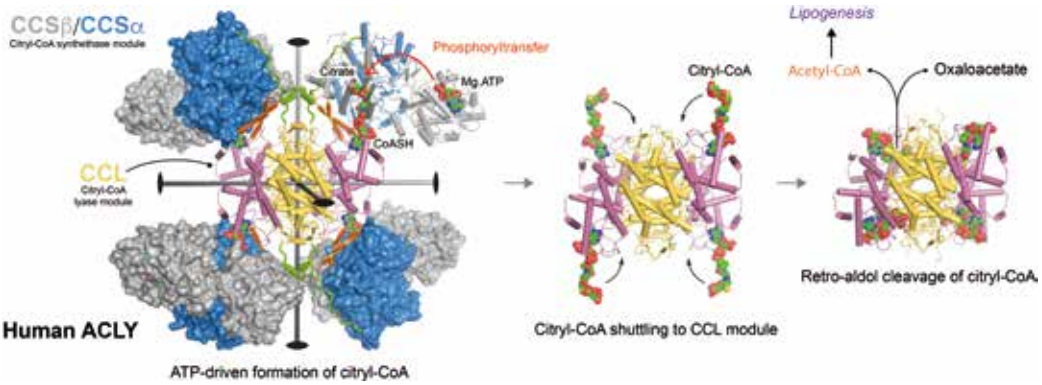

Figure 1

Stucture and catalytic itinerary of human ATP citrate lyase. Cartoons of crystal structures for hACLY (pdb 6hxh) and the CCL module of hACLY (pdb 6hxl) coloured according different functional regions. The three 2-fold axes of the D2 symmetric CCL module are shown. Citrate, CoASH, and ADP are shown as coloured spheres. The arrows indicate the itinerary of the reaction catalysed by ACLY.

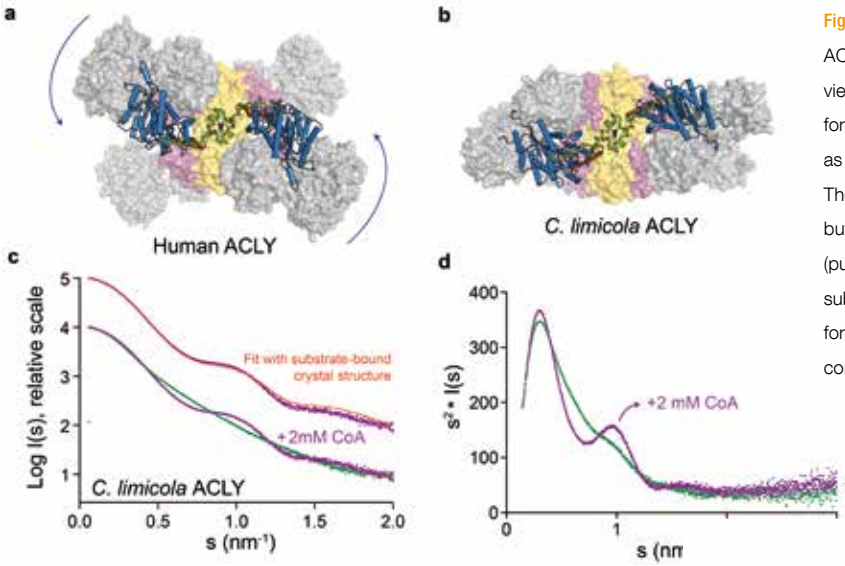

Figure 2

ACL enzymes undergo conformational switching during catalysis. (a-b) Top views of human and *C. limicola* ACLY crystal stuctures illustrating the conformational switching of ACLY. (c) SAXS profiles for *C. limicola* ACLY plotted as the scattered intensity in function of momentum transfer $s = 4\pi\sin\theta/\lambda$. The plots show a comparison of the experimental scattering profiles in HBS buffer (green) and in HBS buffer supplemented with both citrate and CoA (purple), and with the theoretical scattering profile calculated from the substrate-bound *C. limicola* ACLY crystal structure (red). (d) Kratky plots for the scattering data shown in panel c indicate a substrate-induced conformational transition.

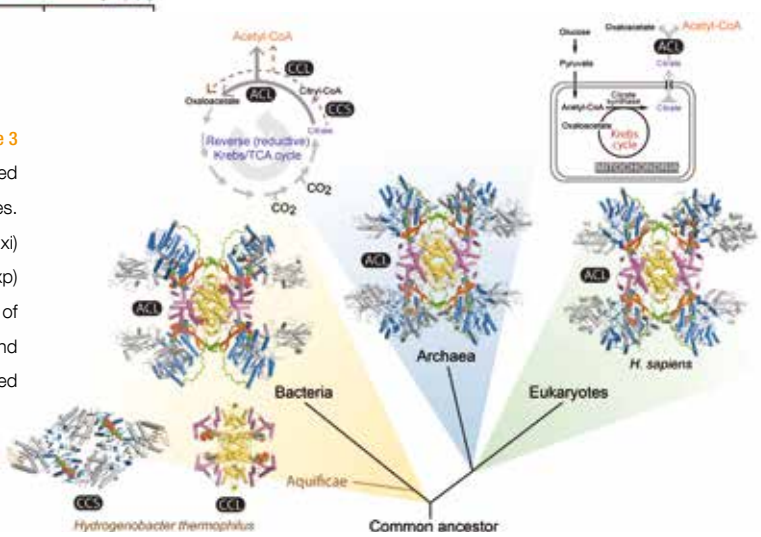

Figure 3

Evolutionary origin of ACLY and its distinct metabolic functions. Simplified evolutionary tree illustrating the distribution of ACLY, CCS and CCL enzymes. Determined crystal structures of *H. sapiens* (pdb 6hxh), *M. concilii* (pdb 6hxi) and *C. limicola* ACLY (pdb 6hxj), and *H. thermophilus* CCL (pdb 6hxp) and CCS (pdb 6hxq) are shown as cartoons. Distinct metabolic roles of ACL, CCS and CCL in the prokaryotic (two-step) rTCA cycle and eukaryotic citrate shuttle are indicated

Currently, the most advanced ACLY inhibitor is bempedoic acid, which is under clinical evaluation as possible treatment to lower low-density lipoprotein cholesterol [2]. Combined, the insights into the ACLY structure and dynamics now provide a molecular platform to unravel the molecular basis of allosteric regulation of hACLY activity, and for targeting ACLY in cancer and metabolic diseases [3].

In addition to our structural studies on the ACLY holoenzyme, we determined crystal structures of the CCS and CCL enzymes from the hyperthermophilic bacteria *Hydrogenobacter thermophiles* [4]. This deep-branching bacterium inhabits environments that resemble early earth and uses the reverse Krebs cycle for carbon assimilation but lacks an ATP citrate lyase. Instead, citrate-cleavage activity in *H. thermophilus* and other Aquificaceae is provided by the tandem action of CCS and CCL enzymes. Structural elucidation of stand-alone CCL shows that it adopts an intertwined tetrameric structure as seen in the ACLY CCL-core module, indicating that ACLY emerged from the fusion of CCS and CCL (Fig. 3). Further structural analysis also shows that dimeric citrate synthase (CS), the first enzyme of the oxidative Krebs cycle, actually evolved from tetrameric CCL. This crucial evolutionary relationship had hitherto remained undetected in sequence-based approaches, and is now poised to reshape our understanding of the evolutionary origins of the Krebs cycle for cellular respiration.

Author contact: Kenneth Verstraete, kenneth.verstraete@irc.vib-ugent.be

References

1. J. Wei, S. Leit, J. Kuai, E. Therrien, S. Rafi, H. J. Harwood, Jr., B. DeLaBarre and L. Tong, 'An allosteric mechanism for potent inhibition of human ATP-citrate lyase', Nature 568 (7753), 566–570 (2019).
2. K. K. Ray, H. E. Bays, A. L. Catapano, N. D. Lalwani, L. T. Bloedon, L. R. Sterling, P. L. Robinson, C. M. Ballantyne and Clear Harmony Trial, 'Safety and efficacy of bempedoic acid to reduce LDL cholesterol', N. Engl. J. Med. 380 (11), 1022–1032 (2019).
3. C. Granchi, 'ATP citrate lyase (ACLY) inhibitors: An anti-cancer strategy at the crossroads of glucose and lipid metabolism', Eur. J. Med. Chem. 157, 1276–1291 (2018).
4. M. Aoshima, M. Ishii and Y. Igarashi, 'A novel enzyme, citryl-CoA lyase, catalysing the second step of the citrate cleavage reaction in Hydrogenobacter thermophilus TK-6', Mol. Microbiol. 52 (3), 763–770 (2004).

Original publication

'Structure of ATP citrate lyase and the origin of citrate synthase in the Krebs cycle', Nature 568, 571–575 (2019). DOI: 10.1038/s41586-019-1095-5

Koen H. G. Verschueren[1,2], Clement Blanchet[3], Jan Felix[4], Ann Dansercoer[1,2], Dirk De Vos[5], Yehudi Bloch[1,2], Jozef Van Beeumen[2], Dmitri Svergun[3], Irina Gutsche[4], Savvas N. Savvides[1,2] and Kenneth Verstraete[1,2]

1. VIB Center for Inflammation Research, Belgium
2. Ghent University, Ghent, Belgium
3. European Molecular Biology Laboratory, Hamburg, Germany
4. University of Grenoble Alpes, Grenoble, France
5. University of Antwerp, Antwerp, Belgium

Time-resolved serial synchrotron crystallography

The whole picture of enzyme catalysis

All life is dynamic and so are its molecular building blocks. The motions and structural changes of biomolecules are fundamental to their functions. However, understanding these at a molecular level is a formidable challenge. How are proteins able to accelerate chemical reactions that – without help – could take years to proceed? One approach to answer such a question is time-resolved X-ray crystallography. By triggering the reaction performed by a biological molecule, one is able to take snapshots of the molecule's changing 3-dimensional structure as the reaction proceeds. When combined, these snapshots provide a high resolution series of the whole enzymatic turnover.

Nucleic acids, lipids, sugars and proteins constitute the four building blocks of life in all its different forms. However, life would not be possible if these building blocks remained static. Only when perturbed out of their equilibrium conformations are they able to maintain the free energy gradients which are the driving force of all cellular functions [1]. Moreover, any form of interaction relies on molecular recognition to permit the binding and release of the associated partners [2]. It also plays a crucial role in enzymatic catalysis, which allows chemical reactions to run at ambient temperatures under which the building blocks of life exist and function (Fig. 1). In light of this, proteins are not mere interaction surfaces, but are rather highly dynamic macromolecular machines which respond to and interact with both their environment and the compounds they transform.

The structures of proteins in their equilibrium conformations can be determined at high resolution by X-ray crystallography, NMR spectroscopy and electron cryo-microscopy. In recent decades, structural biology has been tremendously successful in resolving structures at ever increasing resolution; nearly 160,000 structures of biomolecules are now

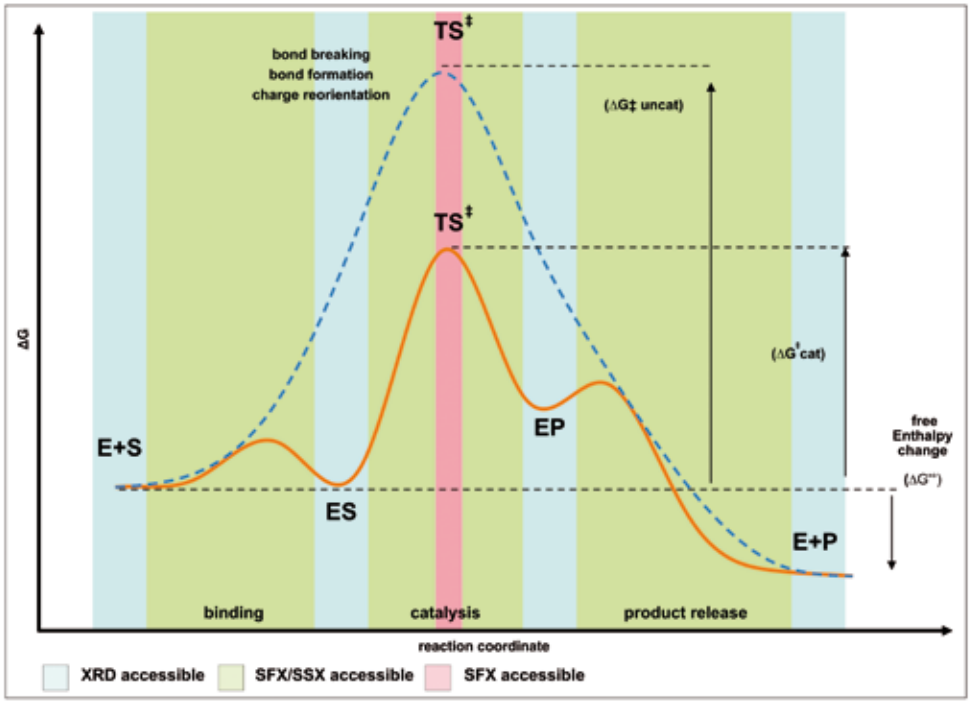

Figure 1

TR-SSX enables addressing most states of enzyme catalysis. Enzymes lower the energy barrier to enable biochemical reactions at ambient temperatures. While long-lived key intermediates can be addressed using canonical X-ray diffraction (XRD) techniques the short lived out-of-equilibrium states cannot be resolved using these canonical approaches. With time-resolved approaches (SFX/SSX) the binding, catalysis and product release can now be resolved at synchrotron and free-electron laser sources.

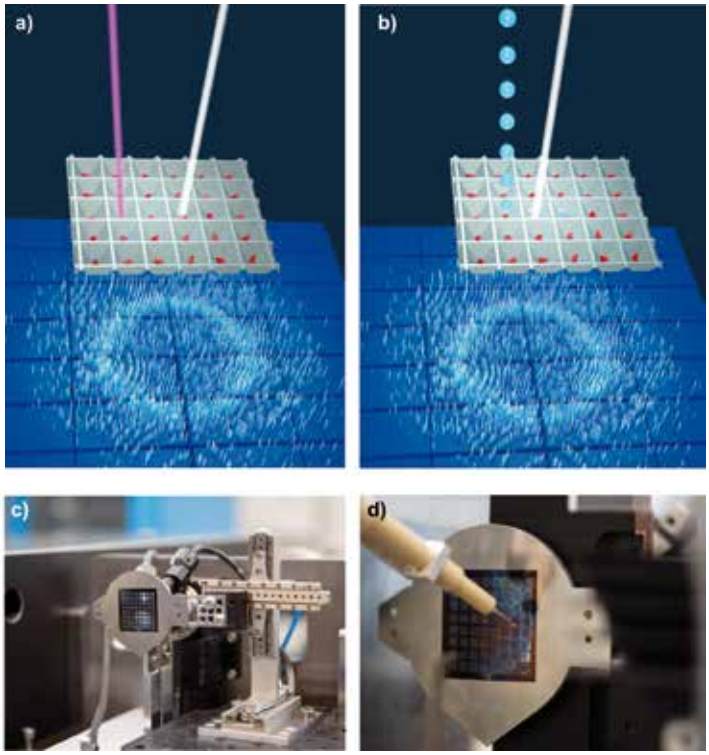

Figure 2

TR-SSX setup at beamline P14-2. a) Optical reaction initiation in the crystals (red) using a laser (pink), and recording a diffraction pattern (blue) with an X-ray pulse (white) after a delay time. b) *In situ* mixing for reaction initiation using the LAMA method (liquid droplet as blue spheres), and recording a diffraction pattern (blue) with an X-ray pulse (white) after a delay time. c) The setup of the translation stage holder with a mounted chip on EMBL beamline P14-2. The laser outlet can be seen in on the left hand side. d) A closeup of a chip with installed LAMA droplet injector.

available in the Protein Data Bank repository. The vast majority of these entries, however, represent static equilibrium states. To understand the dynamic motions of proteins during catalysis and molecular recognition, however, one has to study life's building blocks outside of their equilibrium states. Only those protein conformations will provide the comprehensive picture needed to understand the molecular foundations of life. Using cutting-edge technologies, snapshots of protein dynamics can be acquired in *time-resolved crystallographic experiments*, revealing details at the level of single atoms.

Traditionally, using single crystals, such time-resolved experiments were mostly restricted to reversible reactions and extremely time-consuming, with data collection taking up to several days at synchrotron beamlines. The advent of X-ray free-electron lasers has changed this picture. Experiments at these high brilliance sources entail data-collection in a serial fashion, where thousands of tiny protein crystals are streamed into the X-ray beam. Here they briefly give rise to a diffraction pattern before they are ultimately destroyed. This new approach to data collection and reduction also simplifies time-resolved experiments because only a single snapshot of a crystal needs to be recorded after a certain delay time once a reaction has been initiated. However, while XFELs aim to shed light on the ultrafast time-scales down to the femtosecond time-domain (10^{-15} s), most enzymatic reactions are comparably slow with median turnovers of ~100 milliseconds [3]. These biologically relevant timescales are well accessible to 3rd and 4th generation synchrotrons. With this prospect in mind, we developed new methods that simplify and accelerate time-resolved data collection at synchrotron sources. The new '*Hit-and-Return*' (HARE) method is tailored to the study of biologically relevant reaction timescales, which are on the order of milliseconds (10^{-3}) to seconds, sometimes even minutes. These timescales are of particular interest to biologists and researchers in pharmaceutical sciences as they often reveal the structural changes relevant to a particular biological function or the modification of a drug. In addition, the HARE method requires a lot less time to perform an entire experiment than traditional approaches based on the use of single crystals. While a time-resolved study from single crystals could previously only be obtained after several hours of data collection, the HARE method enables one to collect about one time-point per hour irrespective of the delay-time, facilitating the recording of the structural changes undergone during a biomolecule's complete reaction within a single 24-hour experiment. It is exciting to think about the great potential this new method provides for further time-resolved crystallography studies on existing and up-coming high-brilliance synchrotron radiation sources.

To exploit the full power of the HARE method, we turned to an enzyme that splits the strongest single-bond in organic chemistry: the carbon-fluorine bond. In terms of characterising the biochemistry of the cleaving of a C-F bond, there are only a few enzymes that can catalyse such a detoxification reaction and they are not very fast [4].

The enzyme most amenable to investigation – fluoroacetate dehalogenase – has a turnover rate in the tens of seconds of seconds. However, this is far too slow to be efficiently analyzed on XFEL sources e.g. by liquid jet injection methods due to the high velocity of the crystals in the liquid jet, which pass through the beam before reaction intermediates have built up. A fixed target approach is needed, and the time

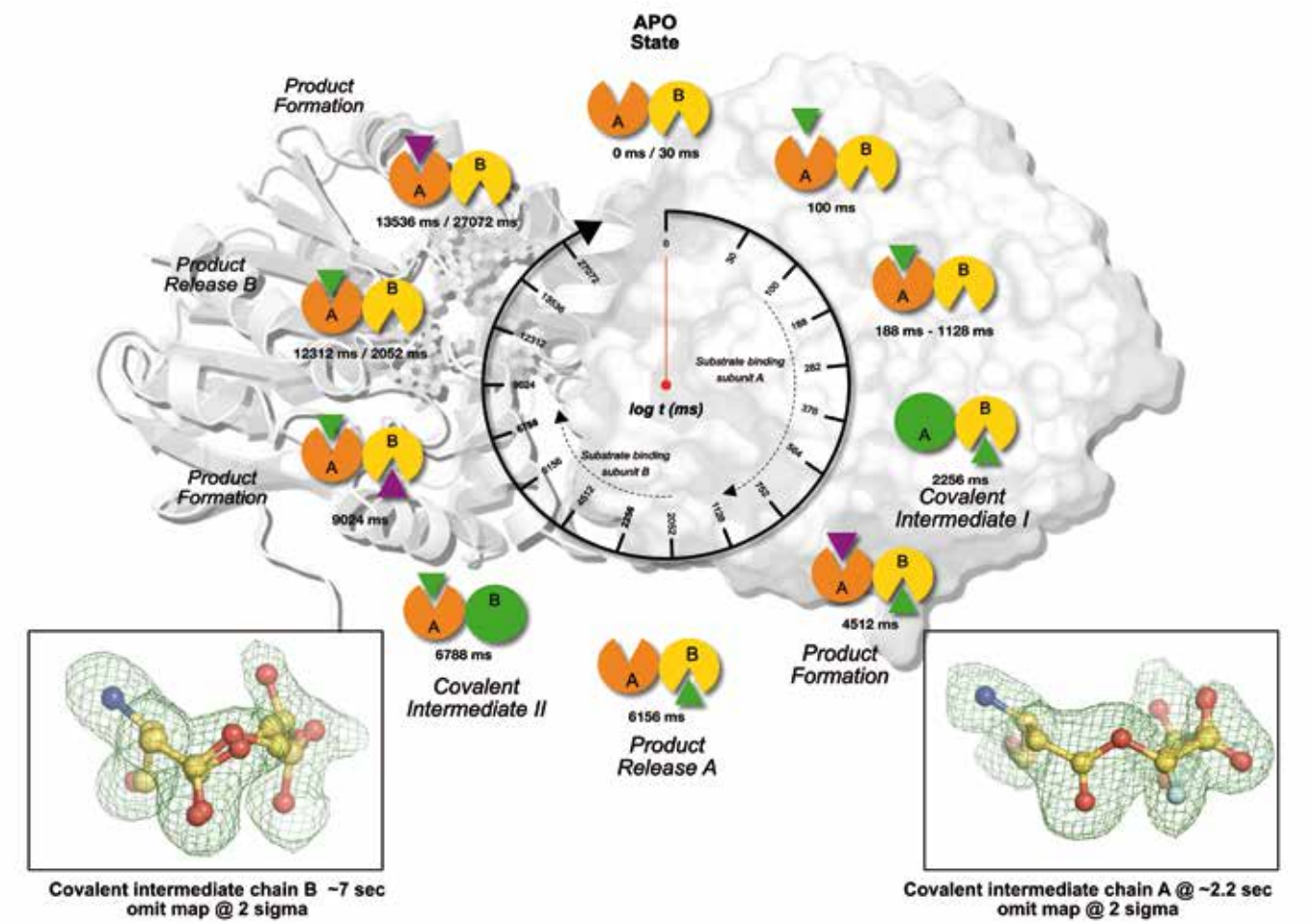

Figure 3

Reaction overview of fluoroacetate dehalogenase (FAcD).The full catalytic cycle of an enzyme (FAcD) could be resolved using the HARE approach, resolving substrate binding, Michaelis-Menten complex formation, covalent intermediate formation, product formation and release. The insets show the electron density at ~2.2 and ~7 seconds after reaction initiation representing the covalent substrate-enzyme intermediates. Green triangle – substrate, Purple triangle – product, Orange and Yellow 'pacmen' – subunits A and B, respectively, Green sphere – covalent intermediate, time after light activation is given in ms.

scale is well suited for the BMBF-funded end station T-REXX (time-resolved experiments with crystallography) at beamline P14 at PETRA III. Therefore, we used our fixed-target approach combined with the HARE method to take molecular snapshots during the turnover reaction of this unmodified enzyme at physiological temperatures. This time-lapse movie revealed eighteen time points from 30 milliseconds to 30 seconds, covering all catalytic states that lead to the breaking of the C-F bond (Fig. 2).

These key states include binding of the substrate, Michaelis-Menten complex formation, substrate reorientation in the active site, covalent intermediate formation, hydrolytic water positioning, product formation and product release. All these steps are repetitive and can be observed sequentially in both active sites of the dimeric enzyme at different time-points. This is possible because the enzyme adopts a half-of-the-sites reaction pattern whereby only ever one of its two active sites is catalytically active at any given time. The question arose of how is this possible; how does one active site communicate with the other? Internal communication in proteins is known under the term allostery, which has been in use since the mid-1960s to describe the cooperative behaviour of identical protein subunits. Although allostery has been the focus of much research, many questions remain unresolved.

Our time-lapse movie of fluoroacetate dehalogenase displays ample cooperative allosteric behaviour in the enzyme as it smoothly transitions from one catalytic state to the next. This includes fluctuations in water content and intermolecular contacts; they correlate with changes in single-point energies as determined by molecular dynamics simulations. The time-lapse movie also clearly shows that the enzyme 'breathes' during turnover, that is it expands and contracts, again aligned with the catalytic sub-steps.

Strikingly, the two halves of the enzyme communicate with each other via a string of water molecules that connects both halves; changes in the number of these water molecules are also aligned with the 'breathing' motion, the fluctuations in water content and the single-point energies. This water network allows the two halves to 'talk' to one another and share information about their catalytic state. This is crucial to the enzyme's function as only one half of the enzyme can ever be active at a given time, the other subunit is needed to provide entropic support of the reaction [5,6].

While photolytic cleavage of a light-sensitive precursor substrate worked well for fluoroacetate dehalogenase, triggering protein reactions in enzymes in general can be extremely challenging, usually involving lasers, modified substrates or photoactive proteins [7,8]. To circumvent this problem and thereby open up many more protein systems for time-resolved analyses as well as to make the method more user-friendly, we developed a new method that uses the simplest way to initiate a reaction: the *in situ* mixing of the protein crystals with their natural substrates.

The new '*Liquid Application Method for time-resolved Analyses (LAMA)*' overcomes the need for optical triggers (Fig. 3). Again, it is tailored to the study of biologically relevant reaction timescales in the order of milliseconds (10^{-3}) to seconds or even minutes. The *LAMA* method significantly simplifies the whole experiment when compared to previous approaches and the use of micron scale crystals to decrease the diffusion time of substate to the active site pushes the time resolution to the sub-ms timescale – perfectly suited to microfocus beamlines. To start a reaction, piezo-driven droplets of a few picolitres (10^{-12} litre) of the reactant are simply mixed with microcrystals of the target protein situated in the features of the chip. Reaction snapshots are then recorded as the enzyme proceeds with the turnover of the reactant.

We demonstrated applicability of this method with two different enzymes. First, we used lysozyme to demonstrate that large and flexible ligands like sugar-oligomers can be effectively mixed with the crystals. Further, we have demonstrated that snapshots of enzymatic reactions can be acquired using the LAMA method. Applying a combination of the HARE and the LAMA method to xylose isomerase, we obtained reaction snapshots demonstrating binding and ring-opening at 15 milliseconds and ~1 minute of the reaction, respectively. For the first time an open-ring intermediate of an enzymatic reaction was captured using an unmodified enzyme.

One of the driving question of structural biology is: How does the atomic structure of an enzyme change during catalysis? TR-SSX is able to provide high resolution insight into most steps of enzymatic catalysis including binding, turnover, and product release. Our experiments highlight that important reaction intermediates of enzymatic reactions like covalent intermediates, and even open ring structures can be observed with TR-SSX. These results hold the promise that many more important insights into biochemical processes will forthcoming from these cutting-edge technologies. Their use will contribute to answering some of the most pressing questions on key health and environmental issues.

Like the HARE method, the LAMA method is being implemented as a generally accessible option at the new time-resolved macromolecular crystallography end station T-REXX on the EMBL beamline P14 at PETRA III.

Author contact: Eike Schulz, eike.schulz@mpsd.mpg.de
Pedram Mehrabi, pedram.mehrabi@mpsd.mpg.de

References

1. K. Henzler-Wildman and D. Kern, 'Dynamic personalities of proteins', Nature 450, 964–972 (2007).
2. R. Baron and J. A. McCammon, 'Molecular Recognition and Ligand Association', Annu. Rev. Phys. Chem. (2013).
3. A. Bar-Even et al., 'The moderately efficient enzyme: Evolutionary and physicochemical trends shaping enzyme parameters', Biochemistry 50, 4402–4410 (2011).
4. P. W. Chan et al., 'Mapping the reaction coordinates of enzymatic defluorination'. J Am Chem Soc 133, 7461–7468 (2011).
5. T. H. Kim P. Mehrabi et al., 'The role of dimer asymmetry and protomer dynamics in enzyme catalysis'. Science. 355, eaag2355 (2017).
6. P. Mehrabi, C. Di Pietrantonio, T. H. Kim et al., 'Substrate-Based Allosteric Regulation of a Homodimeric Enzyme'. J. Am. Chem. Soc. 141, 11540–11556 (2019).
7. K. Moffat, 'Time-resolved crystallography'. Acta Crystallogr. A. 54, 833–41 (1998).
8. M. Levantino et al., 'Using synchrotrons and XFELs for time-resolved X-ray crystallography and solution scattering experiments on biomolecules'. Curr. Opin. Struct. Biol. 35, 41–48 (2015).

Original publications

'Liquid application method for time-resolved analyses by serial synchrotron crystallography', Nat. Methods 16, 979–982 (2019). DOI: 10.1038/s41592-019-0553-1

Pedram Mehrabi[1], Eike C. Schulz[1,3], Michael Agthe[5], Sam Horrell[5], Gleb Bourenkov[6], David von Stetten[6], Jan-Philipp Leimkohl[2], Hendrik Schikora[2], Thomas R. Schneider[6], Arwen R. Pearson[3,5], Friedjof Tellkamp[2] and R. J. Dwayne Miller[1,3,8]

'Time-resolved crystallography reveals allosteric communication aligned with molecular breathing', Science 365, 1167–1170 (2019). DOI: 10.1126/science.aaw9904

Pedram Mehrabi[1], Eike C. Schulz[1,3], Raison Dsouza[1,4], Henrike M. Müller-Werkmeister[1,12], Friedjof Tellkamp[2], R. J. Dwayne Miller[1,3,8], Emil F. Pai[7,9,10]

'The hit-and-return system enables efficient time-resolved serial synchrotron crystallography', Nat. Methods 15, 901–904 (2018). DOI: 10.1038/s41592-018-0180-2

Eike C. Schulz[1,3], Pedram Mehrabi[1,7,10], Henrike M. Müller-Werkmeister[1,12], Friedjof Tellkamp[2], Ajay Jha[1], William Stuart[1], Elke Persch[11], Raoul De Gasparo[11], François Diederich[11], Emil F. Pai[7,9,10] and R. J. Dwayne Miller[1,3,8]

1. Department for Atomically Resolved Dynamics, Max Planck Institute for Structure and Dynamics of Matter, Hamburg, Germany
2. Scientific Support Unit Machine Physics, Max Planck Institute for Structure and Dynamics of Matter, Hamburg, Germany
3. Centre for Ultrafast Imaging, Universität Hamburg, Hamburg, Germany
4. Department of Physics, Universität Hamburg, Hamburg, Germany
5. Institute for Nanostructure and Solid State Physics, Universität Hamburg, Hamburg, Germany
6. European Molecular Biology Laboratory, Hamburg Unit c/o Deutsches Elektronen-Synchrotron DESY, Hamburg, Germany
7. The Campbell Family Cancer Research Institute, Ontario Cancer Institute, Toronto, Ontario, Canada
8. Departments of Chemistry and Physics, University of Toronto, Toronto, Ontario, Canada
9. Departments of Biochemistry and Molecular Genetics, University of Toronto, Toronto, Ontario, Canada
10. Department of Medical Biophysics, University of Toronto, Toronto, Ontario, Canada
11. Laboratorium für Organische Chemie, ETH Zürich, Zürich, Switzerland
12. Institute of Chemistry - Physical Chemistry, University of Potsdam, Potsdam-Golm, Germany

New structural model could help in the development of more effective drugs

Structure of prodrug–transporter complex revealed

Prodrugs are inactive medications that are metabolised into an active, functional form within the human body. Some are able to hijack the human peptide transporters PepT1 or PepT2, which are involved in the food intake regulations, to hitch a ride directly into a cell. This process allows for the accelerated absorption of a drug into a patient's bloodstream. Although prodrugs are clinically effective, only little is known about the peptide transporters themselves on a molecular level. Our results provide new insights into the binding mode of prodrugs and will assist in the design of drugs with improved absorption rates.

We studied the peptide transporter DtpA from the bacterium *Escherichia coli* (*E. coli*), because this bacterial peptide transporter has a close evolutionary relationship with the human transporter PepT1 and PepT2 [1] with a highly conserved binding site and a similar substrate profile. These proteins are of great pharmacological interest due to their roles in intestinal uptake and reabsorption in the kidney of not only dietary peptides, but also drugs and prodrugs [2]. These transport proteins are known to be highly promiscuous with more than 8000 predicted substrates.

To produce well-diffracting crystals of DtpA suitable for single crystal structure determination, we made use of a DtpA-specific nanobody. This is a small fragment of naturally occurring heavy chain-only antibodies common in sharks and camelids. The DtpA specific nanobodies were selected by *in vitro* methods after immunisation of a llama with recombinant DtpA. The nanobodies increase the stability of membrane proteins such as DtpA and lock them in a given conformation (Fig. 1a), allowing the generation of high-quality crystals for macromolecular X-ray crystallography. Furthermore, they can be used as functional probes for in vivo applications.

Extensive screening of crystallisation conditions was necessary to produce micrometre sized crystals of DtpA in com-

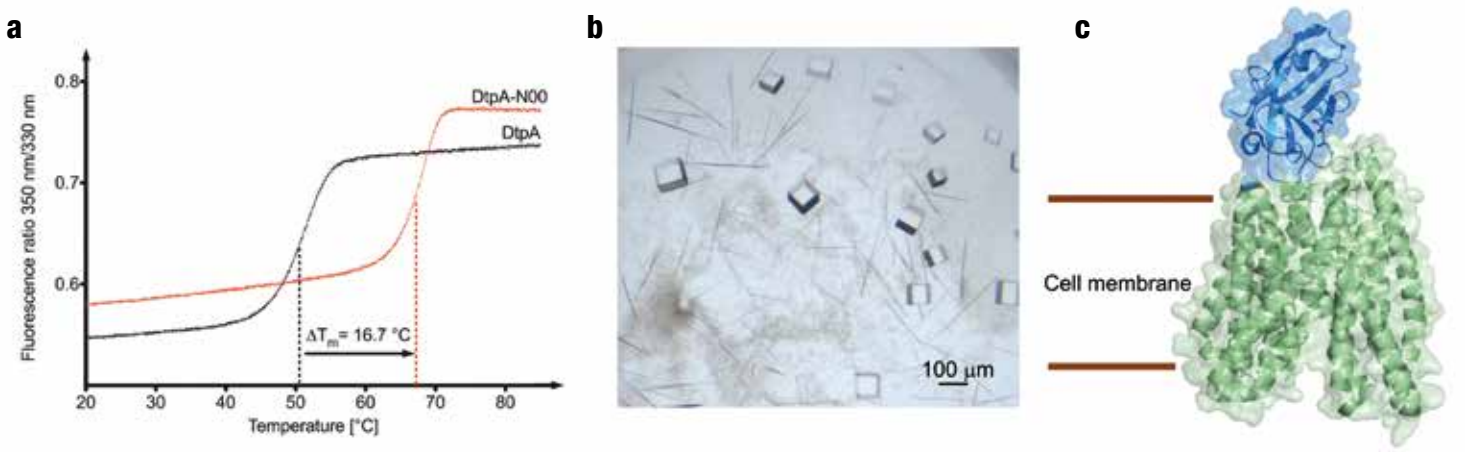

Figure 1

Crystal structure determination of DtpA in complex with nanobody N00 and the antiviral prodrug valganciclovir. a) N00 strongly stabilises DtpA against heat unfolding and locks the transporter in a specific conformation. b) Cubic and needle-shaped crystals of the DtpA-N00-valganciclovir complex were observed in crystallizsation experiments, which were used for data collection at the EMBL synchrotron beamlines. c) Cartoon representation of the structure of the peptide transporter DtpA (in green) stabilised by N00 (in blue). Membrane boarders are indicated.

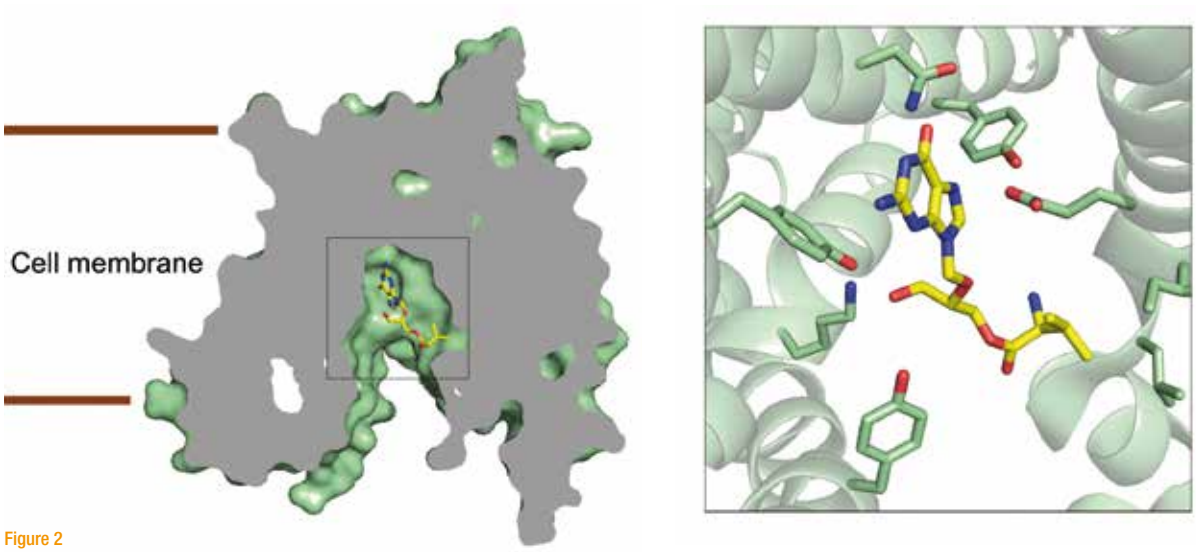

Figure 2

Binding mode of valganciclovir in the crystal structure of the DtpA-N00-valganciclovir complex. a) Valganciclovir is shown in sticks in the ligand-binding site of DtpA, which is illustrated as a surface model. The nanobody and transmembrane helices blocking the view to the binding site were omitted for clarity. b) Zoom in to the binding site of DtpA with valganciclovir shown in yellow and crucial interacting residues of DtpA in green sticks.

plex with a nanobody and a prodrug molecule at the European Molecular Biology Laboratory (EMBL) Sample Preparation and Characterisation facility in Hamburg (Fig. 1b). After cryo-cooling, thousands of crystals were screened and analysed at the EMBL operated beamlines P13 and P14 at PETRA III.

Our team determined the X-ray structure of DtpA in its free form and bound to valganciclovir at a resolution of 2.65 Ångstrom (Fig. 1c). The medicine valganciclovir is a prodrug that helps to combat certain viral infections [3]. DtpA follows the classical 'Major Facilitator Superfamily' fold with twelve hydrophobic transmembrane helices and two additional transmembrane helices of currently unknown function.

Our atomic structure revealed an unexpected result. In contrast to our predictions the orientation of the prodrug in the binding pocket was flipped by 180 degrees (Fig. 2 a, b). By using biophysical methods and *in vivo* transport assays, we also discovered that DtpA preferentially binds – and likely transports – tripeptides over dipeptides. Dipeptides are organic compounds of two amino acids joined together, whereas tripeptides consist of three amino acids. They originate from food break down in the stomach and small intestine.

By using innovative structural modelling methods we then created a structural model of the human PepT1 transporter in complex with valganciclovir, using the bacterial DtpA crystal structure as a guide. This structural model showed a high probability that human PepT1 binds valganciclovir in a similar way as DtpA and allowed us to pinpoint the exact amino acid groups responsible for binding. This understanding is likely to facilitate the development of new prodrugs with improved absorption rates, resulting in lower pharmacologically effective doses and reducing the negative side-effects experienced by patients.

Author contact:
Christian Löw, christian.loew@embl-hamburg.de
Yonca Ural-Blimke, yonca.uralblimke@embl-hamburg.de

References

1. D. Weitz, D. Harder, F. Casagrande, D. Fotiadis, P. Obrdlik, B. Kelety and H. Daniel, 'Functional and Structural Characterization of a Prokaryotic Peptide Transporter with Features Similar to Mammalian PEPT1', J. Biol. Chem. 282, 2832–2839 (2007).
2. M. Brandsch, I. Knütter and E. Bosse-Doenecke, 'Pharmaceutical and Pharmacological Importance of Peptide Transporters', J. Pharm. Pharmacol. 60, 543–585 (2008).
3. D. Jung and A. Dorr, 'Single-Dose Pharmacokinetics of Valganciclovir in HIV- and CMV-Seropositive Subjects', J. Pharm. Pharmacol. 39, 800–804 (1999).

Original publication

'Structure of Prototypic Peptide Transporter DtpA from *E. coli* in Complex with Valganciclovir Provides Insights into Drug Binding of Human PepT1',
J. Am. Chem. Soc. 141, 2404–2412 (2019). DOI: 10.1021/jacs.8b11343

Yonca Ural-Blimke[1], Ali Flayhan[1], Jan Strauss[1], Vasileios Rantos[1], Kim Bartels[1], Rolf Nielsen[1], Els Pardon[2,3], Jan Steyaert[2,3], Jan Kosinski[1,4], Esben M. Quistgaard[1,5,6] and Christian Löw[1,5]

1. Centre for Structural Systems Biology (CSSB), DESY and European Molecular Biology Laboratory Hamburg, Hamburg, Germany
2. Structural Biology Brussels, Vrije Universiteit Brussel (VUB), Brussels, Belgium
3. VIB-VUB Center for Structural Biology, VIB, Brussels, Belgium
4. Structural and Computational Biology Unit, European Molecular Biology Laboratory, Heidelberg, Germany
5. Department of Medical Biochemistry and Biophysics, Karolinska Institutet, Stockholm, Sweden
6. Department of Molecular Biology and Genetics–DANDRITE, Aarhus University, Aarhus C, Denmark

Cell death trigger in tuberculosis bacteria

Suicide system in tuberculosis bacteria might hold key to treatment

Tuberculosis is one of the top ten causes of death worldwide. In 2017, 1.3 million people around the world died of this disease and 10 million people were infected. The genome of the bacterium that causes tuberculosis holds a special toxin–antitoxin system with spectacular action: once the toxin is activated, bacterial cells die, stopping the disease. We investigated this promising feature for potential therapeutic targets.

Mycobacterium tuberculosis is the bacterium that causes tuberculosis (TB) in humans. Its genome holds 80 so-called toxin-antitoxin (TA) systems: sets of closely linked genes that encode both a toxic protein and an antitoxin: a toxin-neutralising antidote. When the bacteria are growing normally, the activity of the toxin is blocked by the presence of the antitoxin. However, under stress conditions such as scarcity of nutrients, dedicated enzymes rapidly degrade the antitoxin molecules. This activates many toxin proteins in the cell and slows down the growth of the bacteria, allowing them to survive in the stressful environment [1, 2].

One particular TA system has a more drastic effect: In the absence of the antitoxin, the toxin kills the bacteria. To understand the underlying mechanism, we studied this system in detail, as it holds great potential for the discovery of new therapeutic targets. We obtained the structure with a resolution of 1.8 Ångstrom, which revealed a large and compact system with a double-doughnut shape (Fig. 1). This structure was determined literally overnight by rapid X-ray collection on the EMBL beamline P14 at PETRA III, followed by experimental phasing and electron density interpretation in a few hours, in cooperation with the group of Thomas Schneider from EMBL. The structure of the toxin resembles the toxins of cholera and diphtheria. These diseases caused epidemics, with hundreds of thousands of people dying even within the past century. Complementary Small Angle X-ray Scattering (SAXS) data obtained at the EMBL beamline P12 at PETRA III were crucial to confirm and further characterise the oligomeric state of the complex.

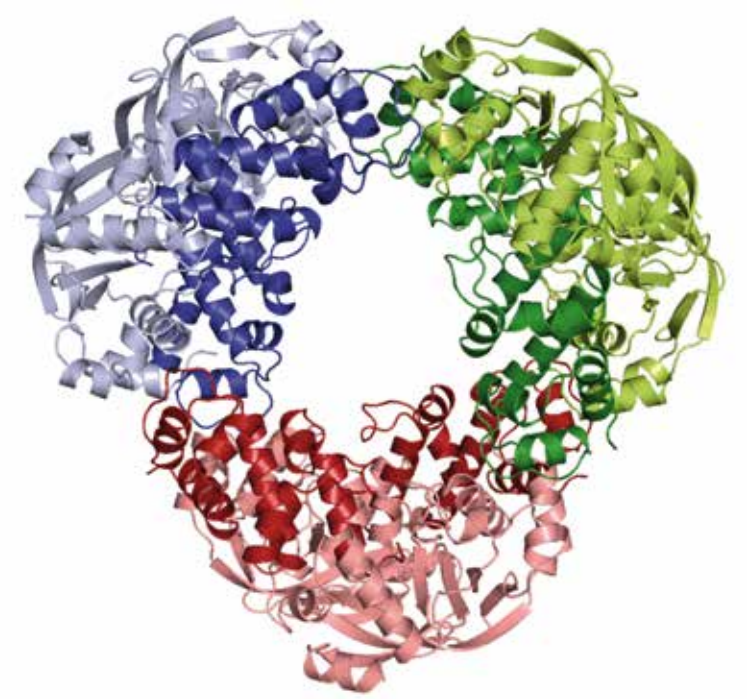

Figure 1

High-resolution structure of the *M. tuberculosis* MbcTA toxin/antitoxin complex. The complex is assembled by three $(Mbc_TMbc_A)_2$ hetero-tetramers that arranged into a ring-like hetero-dodecameric complex. The three $(Mbc_TMbc_A)_2$ sub-complexes are coloured in blue, red and green, where the toxin components are in dark colours and the antitoxin components are in light colours. The physiological relevance of the dodecameric assembly remains unknown at present. The toxin active site is blocked in the presence of antitoxin, thus active toxin requires complex disassembly. (Image: Matthias Wilmanns)

Knowledge of the structure gave important guidance for studying the system's biochemistry, which allowed us to discover the TA system's mode of action. When it dissociates, leading to unblocking of the toxin, it starts to modify the essential cellular metabolite Nicotinamide adenine dinucleotide (NAD+) by phosphorylation followed by subsequent deg-

radation steps (Fig. 2). NAD+ serves as an electron carrier in cellular metabolism and plays a crucial role in the maintenance of balanced redox homeostasis. The catalytic mechanism of this reaction has been without precedence in the literature, opening a new field of NAD chemistry. This activity literally removing NAD+ ultimately leads to the death of all bacterial cells. Lifetimes of mice infected with TB can be significantly extended, by inducing the expression of unblocked toxin.

Why the bacteria have such a suicide system is still unknown, but due to its strong effect on cell death it has potential to be exploited as a antimicrobial drug target. A molecule that could disrupt the native TA system, triggering the death of TB-causing bacteria, could become a promising drug. In a private–public partnership project with the biotech company Evotec supported by the Hamburg Investment Bank, we are currently working to screen thousands of small molecules to see if they have this capability.

To this end, it will also be crucial to unravelling natural conditions, under which this complex disassembles. The antitoxin component of this complex has also been predicted to have DNA binding properties and there are preliminary data pointing to binding its own promoter. As in the complete dodecameric complex (Fig. 1) the putative DNA binding site is blocked, we have recently produced a tetrameric sub-complex with an accessible DNA binding site. This could serve as a basis for a future structure of this toxin/antitoxin in the presence of DNA, providing insight on how DNA binding could regulate the activity of this toxin.

Taking all the data together, this work presents a highly interdisciplinary piece of research where we made use of a number of different X-ray based structural biology techniques, coupled by functional data from international collaborators from France and the United Kingdom, and financial support from the City of Hamburg to move this project into possible proprietary applications for future drug discovery.

Author contact:
Matthias Wilmanns, matthias.wilmanns@embl.org,
Annabel H. A. Parret, ahaparret@gmail.com,
Olivier Neyrolles, olivier.neyrolles@ipbs.fr

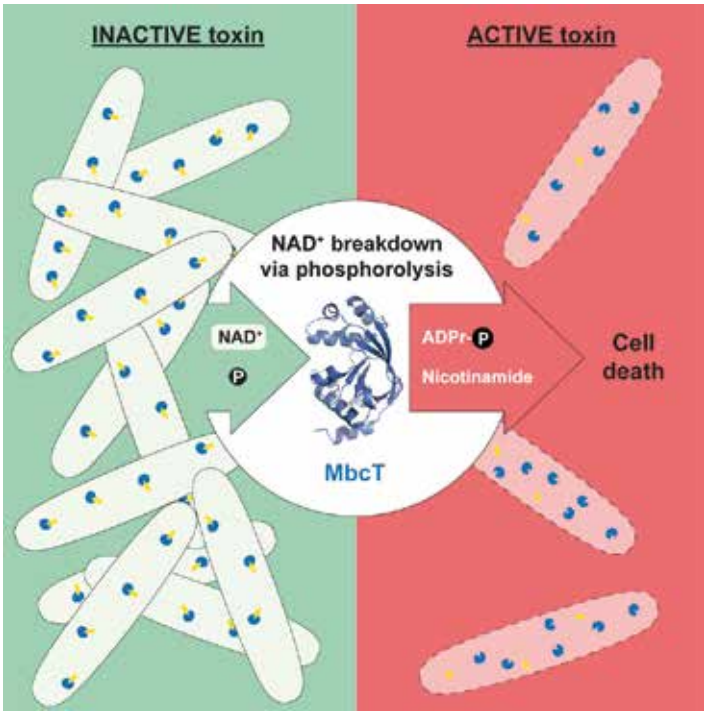

Figure 2

The bacterium *Mycobacterium tuberculosis* causes the disease tuberculosis (TB). Its genome holds many so-called toxin-antitoxin systems but one particular TA system has a very special effect. In the absence of the antitoxin, the toxin MbcT kills the bacteria. When this toxin dissociates from its antidote, it becomes activated and starts to degrade essential cellular metabolites called NAD+ molecules. This activity leads to the death of all bacterial cells. (This figure from the original publication is licensed under the Creative Commons Attribution-NonCommercial-No Derivatives 4.0. International License.)

References

1. H. S. Deter, R. V. Jensen, W. H. Mather and N. C. Butzin, 'Mechanisms for differential protein production in toxin–antitoxin systems', Toxins 9, 1–13 (2017).
2. A. M. Hall, B. Gollan and S. Helaine, 'Toxin-antitoxin systems: reversible toxicity', Curr. Opin. Microbiol. 36, 102–110 (2017).

Original publication

'An NAD+ Phosphorylase Toxin Triggers Mycobacterium tuberculosis Cell Death', Molecular Cell 73, 1282–1291 (2019). DOI: 10.1016/j.molcel.2019.01.028

Diana Mendes Freire[1] , Claude Gutierrez[2], Acely Garza-Garcia[3], Anna D. Grabowska[2,7], Ambre J. Sala[4], Kanchiyaphat Ariyachaokun[2,8], Terezie Panikova[1], Katherine S. H. Beckham[1], André Colom[2], Vivian Pogenberg[1], Michele Cianci[1,9], Anne Tuukkanen[1], Yves-Marie Boudehen[2], Antonio Peixoto[2], Laure Botella5, Dmitri I. Svergun[1], Dirk Schnappinger[5], Thomas R. Schneider[1], Pierre Genevaux[4], Luiz Pedro Sorio de Carvalho[3], Matthias Wilmanns[1,6], Annabel H. A. Parret[1] and Olivier Neyrolles[2]

1. European Molecular Biology Laboratory, Hamburg Unit, Hamburg, Germany
2. Institut de Pharmacologie et de Biologie Structurale, IPBS, Université de Toulouse, CNRS, Toulouse, France
3. Mycobacterial Metabolism and Antibiotic Research Laboratory, The Francis Crick Institute, London, UK
4. Laboratoire de Microbiologie et Génétique Moléculaires, Centre de Biologie Intégrative, Université de Toulouse, CNRS, Toulouse, France
5. Department of Microbiology and Immunology, Weill Cornell Medical College, New York, USA
6. University Hamburg Medical Centre Hamburg-Eppendorf, Hamburg, Germany
7. Present address: Department of Pathogen Molecular Biology, Faculty of Infectious and Tropical Diseases, London School of Hygiene and Tropical Medicine, London, UK
8. Present address: Department of Biological Science, Ubon Ratchathani University, Thailand
9. Present address: Department of Agricultural, Food and Environmental Sciences, Università Politecnica delle Marche, Ancona, Italy

X-ray fluorescence imaging enables pharmacokinetics

Localising functionalised nanoparticles

There is a strong need for a next-generation of pharmacokinetic: the in-vivo tracking of medical drugs. The efficacy of drugs strongly depends on the concentration with which they reach their target sites. Imagine that a newly developed medical drug does not reach the region where it is supposed to bind to druggable targets, then it is clear that it will not have the desired effect. However, it is not trivial to get a quantitative in-vivo information. Efficacy and also dosing studies today need a lot of pre-clinical and clinical testing. But if the pharmacokinetics could be measured at an early stage, the entire drug development could be faster and also less expensive. This envisaged breakthrough comes into reach when using X-ray fluorescence imaging at PETRA III that localizes nanoparticles functionalised with medical drugs.

Optical fluorescence imaging is well-known and widely used in biomedical research, however, it is limited to very short imaging depths that hinders its application for most pre-clinical and clinical studies. In contrast, X-ray Fluorescence Imaging (XFI) overcomes this limit as the incident and fluorescence photons energies are high enough for sufficient transmission. XFI is based upon the excitation of typically K-shell or L-shell fluorescence in high atomic number elements, such as gold. An incident photon can kick out an electron bound in the innermost shell of this atom, leaving a hole therein. Since atoms tend towards the minimum level of energy, electrons from outer shells, which are bound with less energy, drop down, fill the inner shell hole and give away the binding energy difference in form of an emitted photon. If high atomic number elements are used, their innermost electrons have strong binding energies, in the range of few tens of keV. Hence, when such an electron is ionised, the emitted photon has also an energy in this range. Even for objects of human-sized scales, this photon energy range is still sufficient for the incident photon to reach any depth inside the probe and also for the emitted photon to leave the probe.

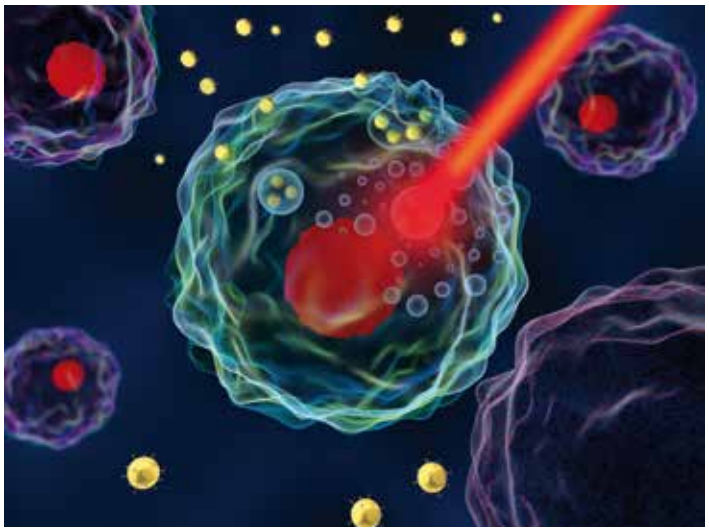

Figure 1

Artist view on an X-ray beam hitting a cell after uptake of functionalised gold nano-particles. (Credit: Meletios Verras)

Since usually no gold atoms are in our body, inert gold-nano-particles (GNPs) have been the first choice for XFI. If these GNPs are functionalised with pharmaceuticals, their local concentration can be accessed by measuring the amount of GNPs. In general, medical drugs consist of light elements which are not ‘XFI-visible’. However, scanning the probe and registering the emitted fluorescence photons at each scan position allows to localise GNPs carrying e.g. medical drugs or antibodies against cancer cells (Fig. 1). Indeed, XFI is a scanning imaging technique as the spatial resolution is only determined by the size of the X-ray beam. Whenever there is a sufficient amount of GNPs within the scanning pencil beam volume, a signal can be detected. It is this feature that makes XFI a perfect application case for synchrotron sources. One can show that the monochromatic and brilliant X-ray beams from a synchrotron source enable highest XFI detection sensitivity in terms of the minimum detectable local amount of GNPs.

In most cases pharmacokinetics requires a high sensitivity as the expected local GNP amounts are very small, in the order of 0.1 wt% (i.e. the GNP-weight compared to the weight of the tissue in which the GNPs are present). The basic concept of using XFI with functionalised GNPs came up in the mid 80s. Although, despite breakthroughs in imaging of small animals, for early-tumour diagnostics [1], XFI was regarded as effectively unusable in human patients due to an intrinsic

problem: incident photons undergo Compton-scattering inside the probe. For instance, a 90 keV photon has a mean free path length of about 6 cm before it scatters. Since human-sized scales are a multiple of this length, incident photons can scatter a few times, whereby changing direction and lowering their energy. While typical fluorescence lines are sharp peaks in measured X-ray spectra, Compton-scattering leads to a broad background (Fig. 2). Even in small probes, the statistical noise of this background can be larger than the amplitude of a fluorescence peak. The GNPs remain invisible in this case.

This long-standing background problem has not been solved – until recently, when we found 'spatial filtering' as a general solution as described in the publication. Our research team studied by numerical simulations and analytical models the angular flux distribution of the Compton-scattering background around the fluorescence peaks for a 30 cm large sphere. What we have discovered is a strong anisotropy for the case that the incident photon energy is close to the energy level of the gold K-edge. If the energy is higher, the degree of anisotropy vanishes as higher orders of Compton-scattering dominates, because the photons scatter more than just once. We discovered two key properties determining the background in a detector pixel. These are the total path length inside the probe and the pixel's solid angle relative to the position, where the photon was scattered. We developed a computer algorithm that chooses only those pixels whose sum spectrum shows a maximum in the statistical significance – if there is a signal at all. Our solution reduces the background in the signal energy region by a factor of more than 500.

For the first time we have also measured the spatial distribution of GNPs, which were functionalised with the cell adhesion peptide L1, along ex-vivo murine spinal cord samples from a study of the University Medical Center Hamburg-Eppendorf (UKE) on neuronal damage [3]. This experiment was performed at beamline P11 at PETRA III. We could show that the L1-GNPs were bound with a very high degree of localisation and, most surprisingly, the local amount was independent from the administered L1-dose. This measurement can be seen as a first demonstration on pharmacokinetics, whereby a separate run with non-functionalised GNPs showed no signal. Hence it were the L1-molecules which made the GNPs bound at the target site, not the GNPs by themselves. This pilot-study can pave the way to further medical imaging studies at PETRA III, extending research capabilities and application in the field of medical drug development.

Author contact: Florian Grüner, florian.gruener@uni-hamburg.de

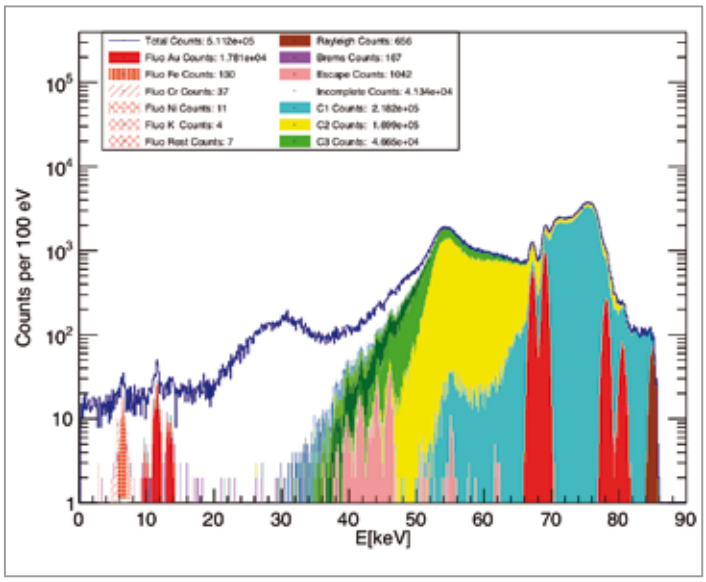

Figure 2

Numerical result of a simulated X-ray spectrum (photon counts vs. energy) with a computer voxel model of a rat, showing different orders of Compton-scattering, the gold K-shell and L-shell fluorescence lines as well as fluorescence lines from elements in a virtual target holder. One can clearly see the different background contributions depending on the photon energy. (courtesy of F. Blumendorf, Univ. Hamburg)

References

1. N. Manohar et al., 'Quantitative imaging of gold nanoparticle distribution in a tumor-bearing mouse using benchtop x-ray fluorescence computed tomography', Sci. Rep. 6, 22079 (2016).
2. F. Schulz et al., 'Gold nanoparticles functionalized with a fragment of the neural cell adhesion molecule L1 stimulate L1-mediated functions', Nanoscale 5, 10605–10617 (2013).
3. G. Loers et al., 'A Fab fragment directed against the neural cell adhesion molecule L1 enhances functional recovery after injury of the adult mouse spinal cord', Biochem. J. 460, 437–446 (2014).

Original publication

'Localising functionalised gold-nanoparticles in murine spinal cords by X-ray fluorescence imaging and background-reduction through spatial filtering for human-sized objects', Scientific Reports 8:16561 (2018)
DOI:10.1038/s41598-018-34925-3

Florian Grüner[1], Florian Blumendorf[1], Oliver Schmutzler[1], Theresa Staufer[1], Michelle Bradbury[2], Ulrich Wiesner[3], Tanja Rosentreter[4,12], Gabriele Loers[5], David Lutz[5], Bernadette Richter[6], Markus Fischer[6], Florian Schulz[7], Swantje Steiner[8], Martin Warmer[9], Anja Burkhardt[9], Alke Meents[10], Matthew Kupinski[11] and Christoph Hoeschen[12]

1. Universität Hamburg and Center for Free-Electron Laser Science, Hamburg, Germany
2. Department of Radiology and Molecular Pharmacology Program, New York, USA
3. Department of Materials Science and Engineering, New York, USA
4. Helmholtz Zentrum München GmbH, Neuherberg, Germany
5. Center for Molecular Neurobiology Hamburg, Hamburg, Germany
6. Hamburg School of Food Science, Hamburg, Germany
7. Institut für Physikalische Chemie, Hamburg, Germany
8. University Medical Center Hamburg-Eppendorf, Hamburg, Germany
9. Deutsches Elektronen-Synchrotron DESY, Hamburg, Germany
10. Center for Free-Electron Laser Science, Hamburg, Germany
11. College of Optical Sciences, Tucson, USA
12. Institute for Medical Technology, Magdeburg, Germany

First fossil late instar larva of Strepsiptera

Phase-contrast tomography reveals hidden details of endoparasitic fossil late instar larva

Microtomography with synchrotron radiation has an enormous potential to visualise otherwise unrecognisable details of fossils in the µm range. This was demonstrated investigating an insect larva embedded in Middle Eocene Baltic amber. The fossil is a late larval stage of the parasitic twisted-wing insects, the Strepsiptera. Due to turbidity and the position of the specimen in the amber, light microscopy did not allow determining morphological details, i.e., the presence of antennae, mouth parts or eyes, and whether it was a female or male larva. Microtomography with synchrotron radiation made structural details visible and also revealed the sex.

Twisted-wing insects (Strepsiptera) present a small group of parasitic insects with about 600 described species worldwide. The second instar larvae of all subgroups and the females of the vast majority of species (Stylopidia) are endoparasites of various insects, including silverfish, cicadas, wasps and many others. In combination with their parasitic lifestyle, they have evolved an extremely modified morphology and unusual patterns of life history. These include, for example, the extremely short-lived males with a lifespan of only a few hours and a bizarre mode of copulation, called traumatic insemination [1]. Striking features of the males are modified forewings resembling halteres of flies, fan-shaped hind wings, and 'raspberry' compound eyes. Females are always wingless. They are free-living, i.e. living outside the host, only in the most basal extant Mengenillidae. Their last larval stage is known to leave their host, as far as known at present exclusively primarily wingless silverfish. In contrast, females of Stylopidia (ca. 90% of the species) extrude only the anterior part of their body from the host's body wall. Strepsipterans are viviparous. The tiny primary larva – on average only about 0.2 mm long – search actively for suitable hosts [2].

Almost all fossil strepsipterans found so far were free-living males conserved in Burmese, Baltic or Dominican amber. They were likely trapped by the sticky surface of the fresh tree resin during their short wedding flight [3]. A remarkable finding was a miniaturised fossil primary larva from about 99 million years old Burmese amber from Myanmar [4]. This fossil revealed that parasitism has already evolved in the Mesozoic or even earlier in the group. Fossils of free-living females or of later free-living larval stages were not known so far. Therefore, the discovery of a well-preserved late free-living stage of an 'ancestral' species closed an important gap of knowledge.

The 4.4 mm long specimen investigated here was embedded in a piece of Middle Eocene Baltic amber (size approx. 24 × 15 × 3 mm, age approx. 42 - 54 Ma). Light microscopy

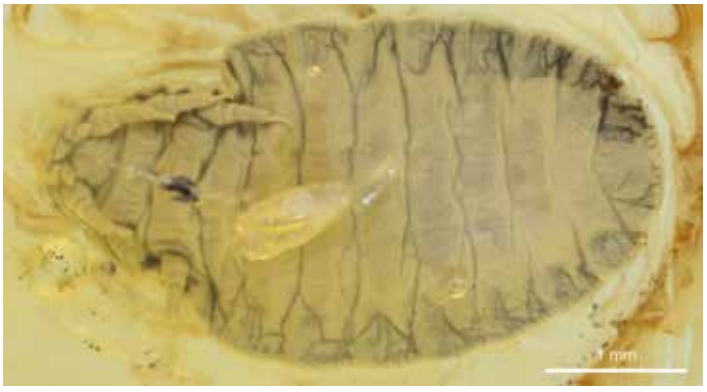

Figure 1

Microphotograph of the strepsipteran late instar larva in Baltic amber, ventral view.

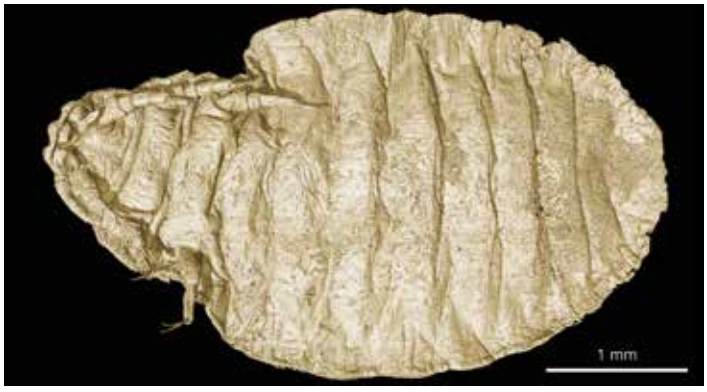

Figure 2

Volume-rendered 3D micrograph of the strepsipteran late instar larva, ventral view.

did not reveal structural details necessary to determine whether the specimen was a late male or female larval stage, or an adult female (Fig. 1). We therefore examined the fossil using microtomography with synchrotron radiation. The sample was scanned using the microtomography end station of the Imaging beamline P05 at PETRA III at an energy of 20 keV. The projections have been recorded with a slight edge enhancement placing the detector at 10 cm distance to the sample. The X-rays allowed imaging of the specimen at a resolution of 1.29 µm of the reconstructed volume and enabled an exceptionally detailed computer-based 3D reconstruction of the specimen (Figs. 2, 3).

The 3D reconstruction was used to conduct comprehensive phylogenetic analysis. In contrast to basal extant females, the antennal buds are short, the mandibles are not intercrossing in the midline, and the tarsi (not shown) are unsegmented. The low number of ommatidia of the compound eyes strongly suggests that it is an immature female. In summary, these features clearly indicate that the investigated specimen is not an adult female but a late larval instar.

The comparison with larvae of extant basal strepsipterans suggests that the specimen was probably in the third larval stage. Phylogenetic analyses of characters of late instar larvae indicate that the specimen is very likely an immature female of the extinct genus †*Mengea*, which is only known from Eocene Baltic amber.

It is remarkable that this fossil larva had left its host. This behaviour is otherwise only known from the extant Mengenillidae that infest silverfish, but has been postulated for the females of †*Mengea* [5]. In the process of emerging from their host, scales of the silverfish always adhere to the cuticle of extant last instar larvae. However, we found scales neither on the cuticle of the fossil larvae nor in the surrounding amber. It is therefore likely that the hosts were silverfish lacking scales, or alternative winged ground-living insects, such as for instance cockroaches. To clarify this issue it is required to find and investigate amber specimens that contain remnants of the host.

Author contact: Hans Pohl, hans.pohl@uni-jena.de
Jörg U. Hammel, joerg.hammel@hzg.de
Adrian Richter, adrian.richter@uni-jena.de
Rolf G. Beutel, rolf.beutel@uni-jena.de

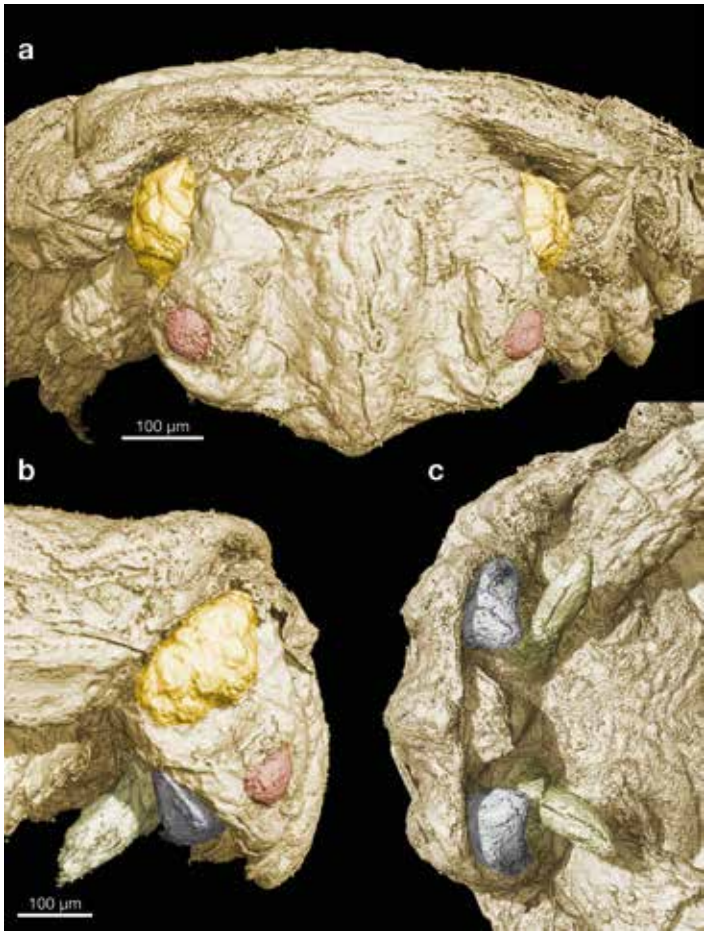

Figure 3

Volume-rendered 3D micrographs of the head of the strepsipteran late instar larva. a) frontal view. b) right lateral view. c) anteroventral view. Compound eye yellow, antenna dark red, mandible grey, maxilla light green.

References

1. M. Peinert, B. Wipfler, G. Jetschke, T. Kleinteich, S. N. Gorb, R. G. Beutel and H. Pohl, 'Traumatic insemination and female counter-adaptation in Strepsiptera (Insecta)', Scientific Reports 6, 25052 (2016).
2. H. Pohl and R. G. Beutel, 'The evolution of Strepsiptera (Hexapoda)', Zoology 111, 318–338 (2008).
3. H. Pohl, R. G. Beutel and R. Kinzelbach, 'Protoxenidae fam. nov (Insecta, Strepsiptera) from Baltic amber – a 'missing link' in strepsipteran phylogeny'. Zool. Scr. 34, 57–69 (2005).
4. H. Pohl, J. Batelka, J. Prokop, P. Müller, M. I. Yavorskaya and R. G. Beutel, 'A needle in a haystack: Mesozoic origin of parasitism in Strepsiptera revealed by first definite Cretaceous primary larva (Insecta)', PeerJ 6, e5943 (2018).
5. H. Pohl, B. Wipfler, D. Grimaldi, F. Beckmann and R. G. Beutel, 'Reconstructing the anatomy of the 42-million-year-old fossil *Mengea tertiaria* (Insecta, Strepsiptera)', Naturwissenschaften 97, 855–859 (2010).

Original publication

'The first fossil free-living late instar larva of Strepsiptera (Insecta)', Arthropod Systematics & Phylogeny 77, 125–140 (2019). DOI: 10.26049/ASP77-1-2019-06

Hans Pohl[1], Jörg U. Hammel[1,2], Adrian Richter[1] and Rolf G. Beutel[1]

1. Institut für Zoologie und Evolutionsforschung, Friedrich-Schiller-Universität Jena, Jena, Germany
2. Institute of Materials Research, Helmholtz-Zentrum Geesthacht, Outstation at DESY, Hamburg, Germany

Palladium is not always the active site for hydrogen evolution

Strain improves activity

The use of hydrogen, being the environmentally cleaner source of energy, may reduce the pressing problem of CO_2 emissions due to burning of conventional fossil fuels. The efficiency of hydrogen production from water depends upon the catalyst, which can be tuned through alloying, morphology change or strain engineering. Latter has been playing a vital role in modifying the activity of electrocatalysts. Incorporation of tensile strain into a Pd-based system usually requires substitution with larger atoms such as expensive and rare platinum. This work provides a unique strategy of introducing tensile strain by the substitution of small and low cost Cu (inverse strain effect) at the Pd sites of $Pd_{17}Se_{15}$. Detailed understanding of related processes will help tuning catalysts towards higher activity and stability.

In this work, we report on the synthesis of Cu substituted $Pd_{17}Se_{15}$ ($(CuPd)_{17}Se_{15}$) nanoparticles for hydrogen production. Combining experimental and theoretical approaches [1, 2] we have addressed the following three scientific points.

Exact site of substitution.
Contrary to the trend expected from the substitution by small Cu atoms, the interplanar distance in $Pd_{17}Se_{15}$ increases upon Cu substitution inducing a tensile strain into the system. This is evident from the comparison of powder X-ray diffraction (PXRD) profiles of the pristine and Cu substituted compound and is consistent with the negative shift of PXRD pattern (Fig. 1a, b). Simulated PXRD pattern clearly reflect the reversal of intensity of (330) and (331) planes as a function of Cu substitution in the unit-cell (Fig. 1c). Pd-Se bond distance increases as evident from the radial distribution function of extended X-ray absorption fine structure (EXAFS; measured at PETRA III beamline P64) spectra shown in Fig. 1d. $Pd_{17}Se_{15}$ has a single peak in *R*-space that splits into two peaks in case of $(CuPd)_{17}Se_{15}$ – with Se-Cu having lower and Se-Pd higher bond distances. This has been confirmed by the structural parameters extracted from fitting of the first coordination shell in Fig. 1d.

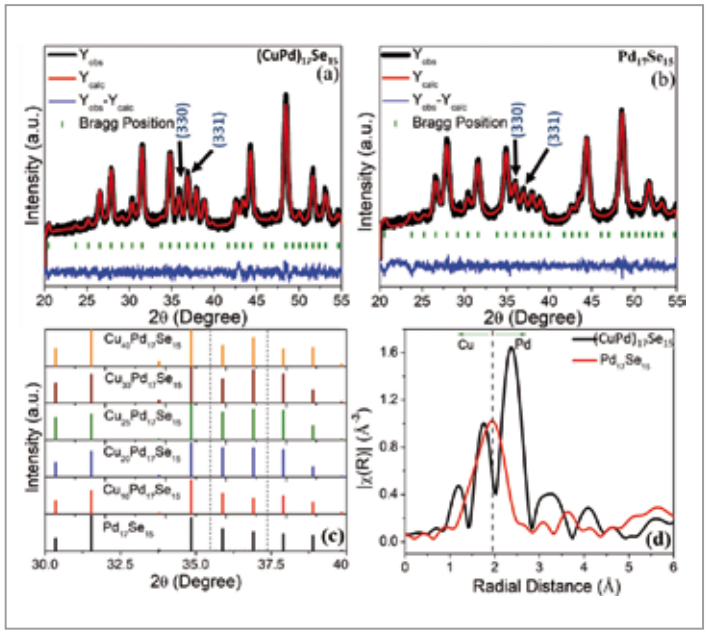

Figure 1

Profile matching of the PXRD pattern of a) $(CuPd)_{17}Se_{15}$ and b) pristine $Pd_{17}Se_{15}$ reveals that lattice parameters increased from 10.59 Å in pristine $Pd_{17}Se_{15}$ to 10.63 Å in $(CuPd)_{17}Se_{15}$. c) Simulated PXRD pattern with variation in Cu substitution. Vertical dotted lines enclose the (330) and (331) reflections. d) Fourier transformed R-space data showing the appearance of the Se-Cu peak at a lower and for the Se-Pd peak at a higher radial distance relative to the pristine compound.

Change in oxidation state upon copper substitution.
Pd atom being in +2 oxidation state adsorbs hydrogen very weakly, and Se in its elemental state binds weakly to H* adsorbate. However, the presence of Pd modulates the electronic structure of Se and favours the progress of the reaction. Cu substitution in $Pd_{17}Se_{15}$ further lowers the adsorption energy to an optimal value.

X-ray absorption fine structure (XAFS; P64) has been exploited to understand the driving force for the enhanced hydrogen evolution reaction (HER) activity upon Cu substitution. It was observed that Se in $(CuPd)_{17}Se_{15}$ has higher negative oxidation state compared to pristine $Pd_{17}Se_{15}$. Before electrochemical measurements, we activated our catalyst by cycling in a potential range of 0 to 0.8 V during which some amount of Cu dealloys out of the system creating vacancies. In order to investigate the chemical changes during the deal-

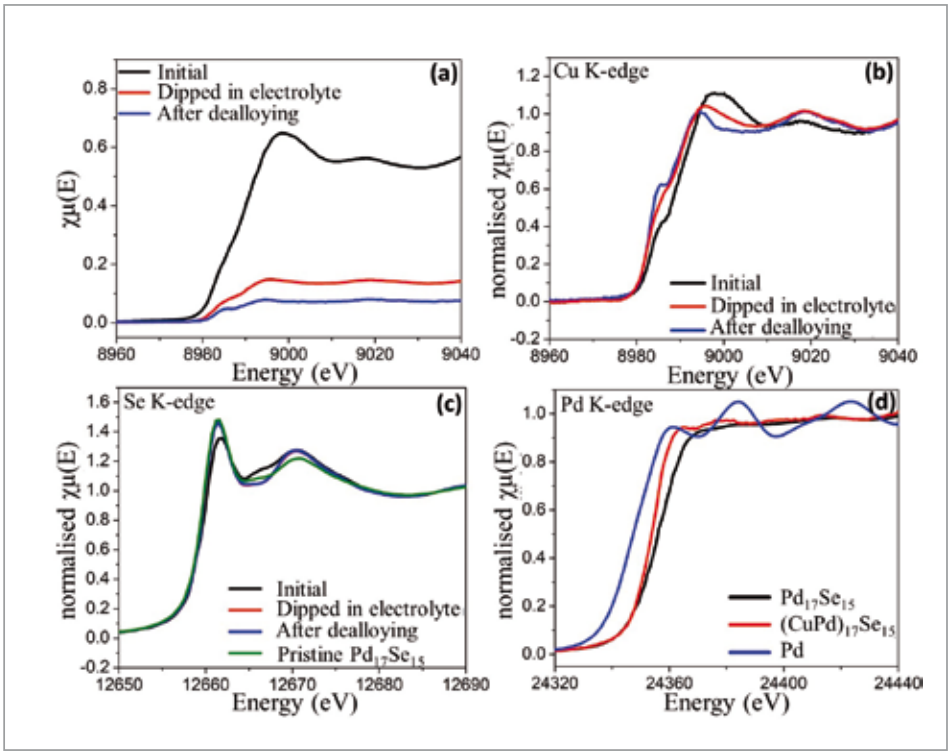

Figure 2

a) Raw Cu K-edge XANES spectra showing the chemical dissolution of Cu. b) Normalised Cu K-edge XANES spectra showing the shift in edge energy during the electrochemical process. c) Se K-edge XANES spectra showing the variation in oxidation state of Se. d) *Ex situ* Pd K-edge XANES spectra showing the intermediate oxidation state of Pd in $(CuPd)_{17}Se_{15}$.

loying process, *in situ* XAS study of the compound was performed. Figure 2a shows the raw data for Cu K-edge X-ray absorption near-edge spectroscopy (XANES; P64) of the compound before and after electrochemical measurements. Decrease in the edge jump of the spectra, when dipped in 0.5 M H_2SO_4 solution is attributed to the dissolution of Cu (II) in the acidic electrolyte, thus reducing the amount of Cu in the sample. Comparing the energy (E_0) in the normalised Cu K-edge XANES spectra (Fig. 2b), we find that Cu in the compound before the electrochemical treatment exhibits both +1 and +2 oxidation states. When dipped into the acidic electrolyte, Cu (II) dissolutes into the acidic electrolyte, leaving behind Cu in predominant +1 oxidation state in the catalyst. This is clearly detected in the shoulder peak, observed in the XANES pattern, attributed to 1s → $4p_z$ transition. The peak becomes predominant after the dealloying process.
Se K-edge XANES spectra show that when dipped in acidic electrolyte, the white-line intensity increases and reaches the same height as in pristine $Pd_{17}Se_{15}$, indicating Se in the same oxidation state as in $Pd_{17}Se_{15}$ (as shown in Fig. 2c). The comparison of Pd K-edge XANES spectra of Pd foil, pristine $Pd_{17}Se_{15}$ and $(CuPd)_{17}Se_{15}$ (Fig. 2d) reveals intermediate oxidation state between 0 and +2 for Pd in $(CuPd)_{17}Se_{15}$.

Driving force for enhancement of the activity.
Unexpected tensile stress induced by the Cu substitution and its electronic effect are the key reasons for the enhanced activity and stability compared to those of the pristine compound [3, 4]. Selective Cu dissolution further improves the activity.

In conclusion, we highlighted an in-depth understanding of the atomic strain engineering by Cu substitution in $Pd_{17}Se_{15}$ system. Cu imposes tensile stress to the system, which then enhances the activity of the system through modulation of the electronic structure. The obtained nanoparticles are highly stable for at least 30000 cycles of accelerated degradation test and have a record turn-over frequency value of 126.3 s^{-1} at an overpotential of 200 mV. Our results may help designing many new catalysts for HER and/or other electrochemical studies by atomic strain engineering through appropriate chemical substitution.

Author contact: Sebastian C. Peter, sebastiancp@jncasr.ac.in

References

1. T. Bhowmik, M. K. Kundu, S. Barman, 'Palladium nanoparticle–graphitic carbon nitride porous synergistic catalyst for hydrogen evolution/oxidation reactions over a broad range of pH and correlation of its catalytic activity with measured hydrogen binding energy', ACS Catal. 6,1929-1941 (2016).
2. X. Chia, N. A. A. Sutrisnoh, M. Pumera, 'Tunable Pt–MoS_x hybrid catalysts for hydrogen evolution', ACS Appl. Mater. Interfaces 10, 8702-8711 (2018).
3. K. Yan, S. K. Kim, A. Khorshidi, P. R. Guduru, A. A. Peterson, 'High elastic strain directly tunes the hydrogen evolution reaction on tungsten carbide', J. Phys. Chem. C121, 6177-6183 (2017).
4. Z. Han, G. Guohua, D. Mingliang, Z. Jinhui, W. Kai, W. Wenbo, C. Xu, L. Yong, M. Piming, D. Weifu, D. Fang, C. Mingqing, W. Guangming, W. Jiandong, Y. Haitao, G. Shaojun, 'Atomic-scale core/shell structure engineering induces precise tensile strain to boost hydrogen evolution catalysis', Adv. Mater. 30, 1707301 (2018).

Original publication

'Inverse strain effect in atomic scale – enhanced hydrogen evolution activity and durability in Cu-substituted palladseite', ACS Energy Letters 3, 3008-3014 (2018).
DOI: 10.1021/acsenergylett.8b01965

Saurav Ch. Sarma[1,2], Vidyanshu Mishra[1,2], K. A. Ann Mary[1], Soumyabrata Roy[1,2] and Sebastian C. Peter[1,2]

1. New Chemistry Unit, Jawaharlal Nehru Centre for Advanced Scientific Research, Bangalore, India
2. School of Advanced Materials, Jawaharlal Nehru Centre for Advanced Scientific Research, Bangalore, India

Collective Lamb shift of an X-ray L-edge

Using vacuum fluctuations to shift and control an X-ray transition in tantalum

One of the cornerstones of quantum optics is the idea that the vacuum is never quite empty. All the time, particles and photons are being created and destroyed, constantly floating in and out of existence. These processes are known as 'vacuum fluctuations'. The principle of energy conservation prevents them from lasting for long, but during their short lifetimes they often manage to briefly interact with each other and with their environment. Traces of these interactions can be measured in the form of minuscule spectroscopic shifts – the interaction with the vacuum has changed the properties of the atom, i.e. the way it absorbs and emits light.

Arguably the most famous spectroscopic trace of vacuum fluctuations is the Lamb shift, first measured in 1947 by Lamb and Retherford [1], a tiny shift of one hydrogen energy level with respect to another. The Lamb shift has a close relative in the collective Lamb shift. Here, the vacuum fluctuations induce an interaction between identical atoms within a larger ensemble, effectively a collective dipole-dipole interaction. The participation of so many atoms at the same time enhances the strength of the interaction leading to a measurable shift of the collective resonance energy. Nevertheless, after prediction of the collective Lamb shift in the 1970s, it was only observed in 2010 in ^{57}Fe [2], a Mössbauer nucleus whose narrow bandwidth resonance preordains it for the measurement of otherwise imperceptibly small shifts in spectroscopy. The field of X-ray spectroscopy, however, is also concerned with the much more common and broad-band transitions of electrons between atomic shells. From shifts in the absorption or emission spectra, information about the electronic structure and chemical environment of the atom can be inferred. The question whether quantum optical effects can cause similar shifts is obviously of some importance for the interpretation of these spectra. To search for this effect, an experiment similar to [2] was performed on tantalum. The L_{III} edge of this metal at 9.88 keV – a transition of a 2p electron to an empty 5d band – possesses a strong and unusually sharp resonance peak. This so-called 'white line' is indicative of some coupling between the excited electron and the hole it has left behind in an inner shell – in other words an exciton, very similar in principle to a discrete atomic energy level.

To maximise this shift, a nanometre sized thin layer of tantalum was placed in an X-ray cavity, as shown in a sketch of the setup in Fig.1. The cavity is a thin-film system in which two thin layers of a heavy metal, such as palladium or platinum, sandwich a wider core of carbon, in the centre of which the tantalum is embedded. At low glancing angles, X-rays are almost perfectly reflected by the platinum. If the light manages to tunnel into the cavity right at the correct incidence angle, it will bounce back and forth several times between the two metal layers constituting the cavity mirrors. In this way, a standing wave forms, and the intensity 'seen' by the atoms grows. This is not just applicable to light that illuminates the

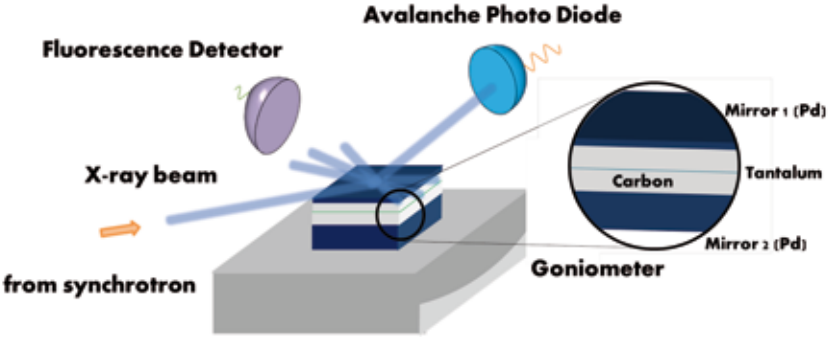

Figure 1

Sketch of the experimental setup. The cavity (detailed structure in the inset) is positioned onto a goniometer and rotated until the resonance condition is found. The incoming photon energy is scanned. A silicon drift fluorescence detector monitors the isotropic fluorescence, a diode the reflected radiation.

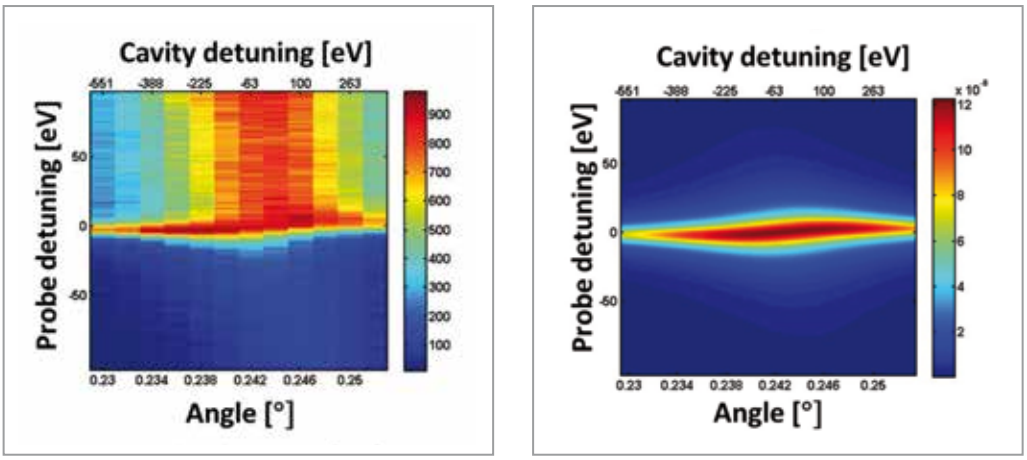

Figure 2

Collective Lamb shift of the tantalum L_{III} edge. Left: experiment, right: simulation. As the photon energy (y-axis) and the angle (x-axis) is varied, the fluorescence is collected with a fluorescence detector. A dispersion of the maximum, as well as a broadening at zero cavity detuning is clearly visible. The large signal at positive probe detuning is due to the continuum, which could not be included in the simulation.

cavity from outside, but also to the aforementioned vacuum fluctuations. They, too, grow much stronger inside the cavity, and so does the strength of their interaction with the tantalum. To probe this interaction, we illuminate a cavity with X-ray photons from the P09 beamline of PETRA III. Tunneling into the cavity, the light will encounter atoms whose interaction with photons is enhanced via vacuum fluctuations.

By changing the incoming angle and scanning the photon energy of the incoming beam we probe the resonances for every cavity setting. We observed both the reflectivity of the cavity, as well as the isotropic fluorescence. Dips in the former (not shown) indicate the presence of a resonant mode of the cavity-tantalum system – a kind of polaritonic state. An increase in the fluorescence for a particular photon energy indicates that this is the energy of the tantalum excitation. This particular result is shown in Fig. 2. As the angle is changed around the resonant mode, there is an energy shift of the peak. For some angles it occurs at higher, for others at lower incoming photon energies. The particular dispersion is well-understood in theory [3], which confirms that this is in fact the collective Lamb shift, and that it can be tailored by the choice of the cavity and its alignment. A related but distinct effect is single photon superradiance. At the position where the collective Lamb shift is zero, it is most obvious: a clear broadening of the bandwidth of the resonance. This is merely the energy-domain fingerprint of the shortened decay time: zero cavity detuning the excited electron relaxes into the ground state much faster than in free space.

All this is ample evidence that spectroscopic shifts and bandwidths, which are usually interpreted in terms of the chemical and electronic surroundings of the atom (neighbouring atoms, bonding types etc.), can also be induced by purely optical effects. More practically speaking, macroscopic structural properties can influence spectroscopic results. It has been known for a long time that the presence of a mirror close to an atom influences the latter's spectral properties. But the effect has not been observed in X-ray transitions so far. It is probably confined to situations where the energetic proximity to a resonance and the presence of a standing wave are both given. But there remain some interesting possible avenues for manipulating the X-ray matter interaction. For instance, the physical preconditions for the Lamb shift are rather close to those of the famed Purcell effect, which could be used for yield enhancement in the notoriously photon-hungry fluorescence spectroscopies.

Author contact: Ralf Röhlsberger, ralf.roehlsberger@desy.de

References

1. W. Lamb and R. Retherford, 'Fine Structure of the hydrogen atom by a microwave method', Phys. Rev. 72, 241 (1947)
2. R. Röhlsberger, K. Schlage, B. Sahoo, S. Couet and R. Rüffer, 'Collective Lamb shift in single photon superradiance', Science 328, 1248 (2010)
3. K. P. Heeg and J. Evers, 'X-ray quantum optics with nuclei embedded in thin-film cavities', Phys. Rev. A 88, 043828 (2013)

Original publication

'Spectral Control of an X-ray L-edge transition via a thin-film cavity', Phys. Rev. Lett. 122, 123608-123611 (2019). DOI: 10.1103/PhysRevLett.122.123608

Johann Haber[1], Jakob Gollwitzer[1], Sonia Francoual[1], Martin Tolkiehn[1], Jörg Strempfer[1] and Ralf Röhlsberger[1,2]

1. Deutsches Elektronen-Synchrotron DESY, Hamburg, Germany
2. The Hamburg Center for Ultrafast Imaging, Hamburg, Germany

Sensing chirality with fast electrons

Asymmetric electron emission from a chiral molecule at high kinetic energies

Chirality, etymologically derived from the Greek word 'cheir' for 'hand', is one of the fundamental mysteries in our understanding of the world we live in. A chiral system, like the human hand, can by definition not be superimposed with its mirror image through rotation or translation. The fact that all known living organisms are made of building blocks of one specific handedness is called homochirality. The human body's interaction with chiral molecules decides about odor perception, taste, and drug effects, to name few examples. Although this circumstance is well known and exploitable, it remains widely unclear why nature made this choice and what the fundamental mechanisms behind it are.

Chiral molecules are forming life of any known kind. Human bodies are in fact macrostructures puzzled together from small chiral building blocks. As a consequence, human senses like smell and taste are enantiomerically selective. Mirror images of chiral molecules, so-called enantiomers share almost all of their chemical and physical characteristics. They can practically only be distinguished via the interaction with other chiral objects or receptors.

For studying the fundamentals of chiral molecules in terms of their structure and also their chemical properties and dynamics, a very nicely controllable probe that also possesses a handedness is circularly polarised light. The distinct difference for a chiral compound between absorbing a left-handed or a right-handed photon can provide stereochemical information and is called circular dichroism (CD). As for many other phenomena of light-matter interaction, the efficiency of this CD effect is depending on the wavelength of the photon that 'maps out' the chiral structure. It is remarkable that this effect persists even with randomly oriented enantiomers. One can understand this by imagining randomly aligned screws flying around and rotating nuts that approach an ensemble of these screws. The nuts cannot attach to the wrong chirality of the screws' threads at all, whereas there may be a little chance to hit the right screw at the right angle to engage. As in this illustrative example, the effect strength of CD is rather small and typically requires extremely accurate measurements of photon transmission probabilities.

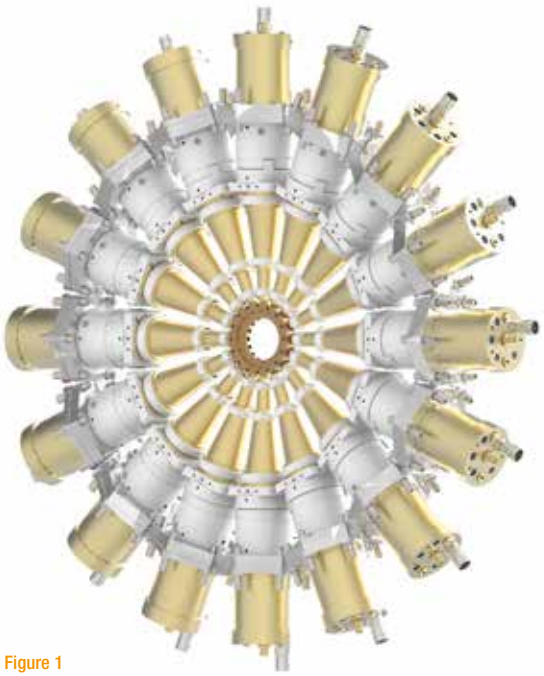

Figure 1

The employed angle-resolving spectrometer built at beamline P04 at DESY.

Theoretically predicted about four [1] and experimentally proven about two decades ago [2], it was shown that ejecting a relatively slow electron from a chiral system via photoionisation with circularly polarised light can lead to an asymmetric emission of this electron. In this scheme, the electron carries the handed nature of the light and therefore can also map out the chiral structure. The characteristic of this chiral sensitivity of the electron is a forward-backward asymmetry in its emission with respect to the propagation direction of the light in the laboratory frame. This so-called photoelectron circular dichroism (PECD) is superior in its strength over the traditional CD, because it is a pure electric-dipole effect. This fact, together with its enantioselectivity, has established PECD as a very versatile and powerful tool for investigations of chiral structures as well as dynamics. The latter is currently evolving as a new scientific field at ultrashort light sources such as free-electron lasers.

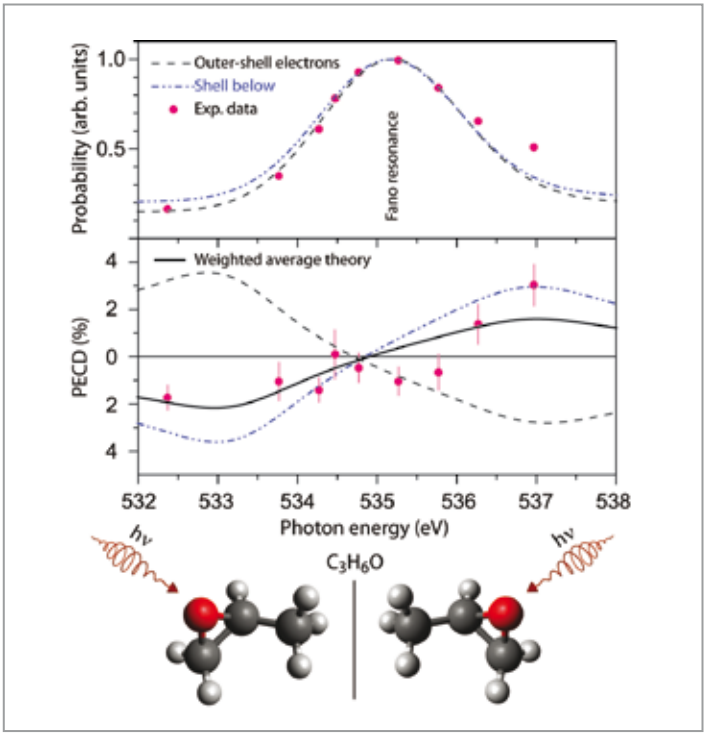

Figure 2

Relative probabilities (upper panel) for the population of the outer shells of the chiral molecule methyloxirane (C_3H_6O) together with the respective PECD (middle panel) computed as functions of the exciting-photon energy in the vicinity of the lowermost O 1s excitation of methyloxirane (see cartoon at the bottom). The energy position of the resonance E_r = 535.11 eV [4] is indicated by the vertical text in the upper panel. Circles with error bars represent the present experimental data measured for the two unresolved outermost electron bands. Solid curves represent the weighted average theoretical results. A characteristic feature of this effect is an anomalous dispersion of PECD, i.e., a chiral asymmetry changes its sign across the resonance.

The wavelength of the probing projectile, i.e. the electron for PECD compared to a photon for CD, acts here also as a crucial factor that largely determines the effect strength. Simplified, one could say that the electron 'needs time' to scatter in the asymmetric chiral potential of the molecule in order to accumulate its asymmetry. This limits the sensitivity of the method to slow electrons in the order of few to few tens of eV kinetic energy. It has been shown that PECD can be observed for valence electrons but also for highly bound inner-shell electrons that then allow for a site-specific view on the structural properties of the target. Experimentalists have been exploiting and advancing this method e.g. to strong-field physics, non-linear photon absorption, and ultrafast measurements of dynamics [3 and refs. therein], but the requirement for slow electrons persisted to limit the versatility of this method, so far.

Now, circularly polarised light from the P04 beamline at PETRA III was used by a group of researchers from DESY, the universities of Kassel, Kiel, and Frankfurt, as well as the European XFEL, the Fritz-Haber-Institut, and the Helmholtz-Zentrum Berlin to prove a theoretical ab initio calculation which predicts that resonances in the photoionisation process can be used to recover the full strength of PECD even for very fast electrons, here for high photoelectron kinetic energies as large as 520 eV. This exceeds the previously accessible kinetic energies for chiral sensitivity by two orders of magnitude. A so-called Fano interference between direct and resonant photoionisation pathways is the key to recover PECD at such high energies. It can be understood as asymmetry mediator that preserves the information of the PECD effect and imprints it into the fast electrons. Using an angle-resolving electron spectrometer (see Fig. 1), the resonance reveals its dramatic enhancement of the PECD amplitude of also about two orders of magnitude compared to the non-resonant case. Figure 2 summarises the results. They yield a new perspective for chirality studies with highly energetic light and broaden the applicability of one of the most important tools for investigations of chiral matter in general.

Author contact: Florian Trinter, florian.trinter@desy.de
Markus Ilchen, markus.ilchen@xfel.eu

References

1. B. Ritchie, 'Theory of the angular distribution of photoelectrons ejected from optically active molecules and molecular negative ions', Phys. Rev. A 13, 1411 (1976).
2. N. Böwering, T. Lischke, B. Schmidtke, N. Müller, T. Khalil and U. Heinzmann, 'Asymmetry in photoelectron emission from chiral molecules induced by circularly polarized light', Phys. Rev. Lett. 86, 1187 (2001).
3. M. Wollenhaupt, 'Photoelectron circular dichroism in different ionization regimes', New J. Phys. 18, 121001 (2016).
4. M. N. Piancastelli, T. Lischke, G. Prümper, X. J. Liu, H. Fukuzawa, M. Hoshino, T. Tanaka, H. Tanaka, J. Harries, Y. Tamenori, Z. Bao, O. Travnikova, D. Ceolin and K. Ueda, 'Electronic structure of core-excited and core-ionized methyl oxirane', J. Electron Spectrosc. Relat. Phenom. 156-158, 259 (2007).

Original publication

'Recovery of high-energy photoelectron circular dichroism through Fano interference', Physical Review Letters 123, 043202 (2019). DOI: 10.1103/PhysRevLett.123.043202

Gregor Hartmann[1], Markus Ilchen[1,2], Philipp Schmidt[1], Catmarna Küstner-Wetekam[1], Christian Ozga[1], Frank Scholz[3], Jens Buck[3,4], Florian Trinter[3,5], Jens Viefhaus[3,6], Arno Ehresmann[1], Markus S. Schöffler[7], André Knie[1], Philipp V. Demekhin[1]

1. Institut für Physik und CINSaT, Universität Kassel, Kassel, Germany
2. European XFEL GmbH, Schenefeld, Germany
3. Deutsches Elektronen-Synchrotron DESY, Hamburg, Germany
4. Institut für Experimentelle und Angewandte Physik, Universität Kiel, Kiel, Germany
5. Molecular Physics, Fritz-Haber-Institut der Max-Planck-Gesellschaft, Berlin, Germany
6. Helmholtz-Zentrum Berlin (HZB), Berlin, Germany
7. Institut für Kernphysik, J. W. Goethe-Universität, Frankfurt am Main, Germany

Molecular footballs torn apart by X-ray FEL pulse

Time-resolved study reveals the X-ray laser-induced fragmentation dynamics of a molecule consisting of 60 carbon atoms

What do X-ray-induced disintegration of fullerenes and Serial Femtosecond Crystallography (SFX) of proteins have in common? Seemingly not more than using the same X-ray source, an X-ray Free-Electron Laser (XFEL). However, in fact, the disintegration of the carbon molecules and the radiation damage of nanocrystals of light atoms, induced in both cases by the X-rays, evolve due to very similar elementary physical phenomena in terms of ionisation and chemical bonding. A time-resolved spectroscopy experiment together with simulations performed using advanced theoretical tools developed in the DESY Photon Science division reveals details of the molecular disintegration of C_{60}, thereby deepening the understanding of the radiation damage process.

Buckminsterfullerene, C_{60}, as a target molecule, has several advantages when aiming for detailed understanding of the XFEL-induced dynamical processes in biological systems. In both SFX and the new study on C_{60}, photon-induced ionisation, which is responsible for breaking up the atomic arrangement, happens at similar rates. Further, the carbon atoms in fullerene are held together (at least initially) by chemical bonds having similar length and strength to the ones found, e.g., in proteins, which are key target systems for ultrafast X-ray imaging. Surviving chemical bonds may contribute to transient stabilisation of the molecular structure. Moreover, C_{60} offers the practical advantages of easy and reliable production for experiment and a relatively small size (though still with sufficient complexity) for reasonably fast simulation runs. The latter is critical when exploring different modelling scenarios. In an earlier time-unresolved, high-intensity study [1], the molecules underwent extreme ionisation initiating the explosion of the atoms surrounded by a nano-size electron plasma. While such violent conditions are available at nanofocus hard-X-ray FEL setups, a micrometre-focus arrangement nowadays routinely used in SFX experiments creates milder ionisation.

In this work a collaboration between experimental and theoretical researchers aimed for a time-resolved study of XFEL-induced dynamics of gas-phase C_{60} molecules. The experiment was carried out at the Linac Coherent Light Source (LCLS) at SLAC National Accelerator Laboratory, exploiting its novel capability of producing two consecutive

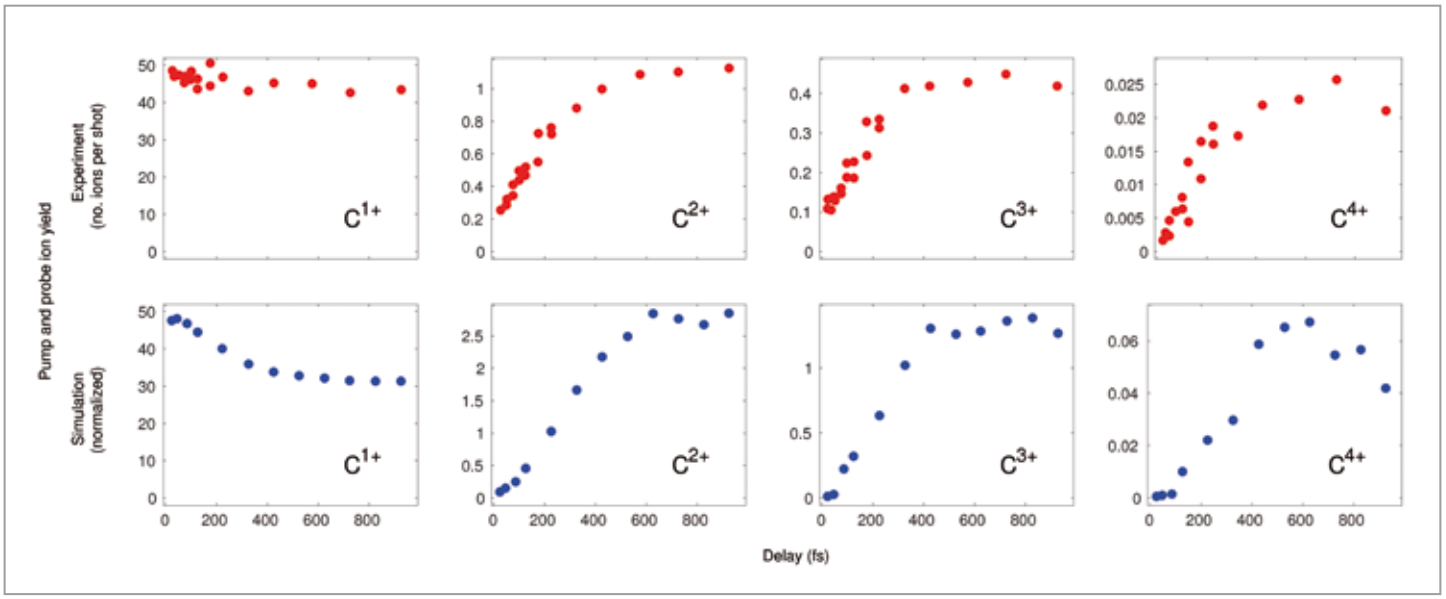

Figure 1

Yield of atomic ion fragments as a function of pump-probe delay. Upper panels (red colour): experimental results, lower panels: simulation data. According to the simulations the delay dependent yields of C^{2+} and C^{3+} reflect the temporal evolution of the formation of neutral and singly charged atomic fragments following the pump pulse.

ultrashort (~20 fs duration) XFEL pulses of ~600 eV photons. The first (pump) pulse initiated the dynamics of the molecule, whereas the second (probe) pulse arriving tens or hundreds of femtoseconds later altered the system further. The change induced by the probe pulse depends on the degree of disintegration that has already taken place. The pump-probe delay dependent yields of the produced fragment ions were collected and analysed. An understanding of the experimental data was made possible through simulations done using the computational tool XMDYN [2].

The experimental and simulation data agree very well, validating the applied model. Among the observables the most remarkable delay dependence was exhibited by the yield of C^{2+}, C^{3+} and C^{4+} highly charged atomic ion fragments (Fig. 1), suitable for the characterisation of the molecular time evolution. The simulations also show that the measured signal corresponds to the time evolution of molecules charged up by the pump pulse to an overall charge of +13 (an average charge of ~0.2 per carbon atom), which corresponds to the milder ionisation condition of SFX experiments.

A few snapshots from a typical simulated trajectory, showing the dynamics initiated by the pump pulse (but before the arrival of the probe pulse), are depicted in Fig. 2. The first observation is that even well after the pump pulse (e.g. at t = +60 fs), the system has not expanded significantly. In fact, during irradiation the maximum atomic displacement stays below 2 Å, a resolution limit widely used in experimental structural biology. This demonstrates the stabilisation effect of the chemical bonds against the Coulomb forces driving molecular disintegration. Another observation is that the charge states of the atoms change dynamically due to interatomic electron transfer, a phenomenon recently introduced in XMDYN [3]. The rapid charge redistribution is responsible for more efficient energy redistribution among the atomic sites, thus giving rise to a smaller maximum atomic displacement at a given time. Yet another observation is that not only charged atomic fragments are formed, but neutral atoms (grey colour) leave the system as well. In fact, the simulations show that the probe pulse creates C^{2+} and C^{3+} ions mainly from neutral atoms and singly charged atomic ions, respectively (C^{4+} is generated from both C^{0+} and C^{1+}). However, when a parent neutral atom (or singly charged ion) is still close to other atoms at the time of the arrival of the probe pulse (i.e., at short time delay), the charge of the resulting multiply ionised carbon atom quickly gets reduced due to interatomic electron transfer. Otherwise (i.e., at long time delay), the created high charge state remains unchanged. Thus, e.g., by analysing the C^{2+} yield as a function of the pump-probe delay, the real-time emission dynamics of neutral carbon atoms is captured. This highlights a remarkable property of the current experiment, namely, that the ion signal detected as a function of the pump-probe delay time can be mapped to the real-time fragmentation dynamics triggered by the pump pulse.

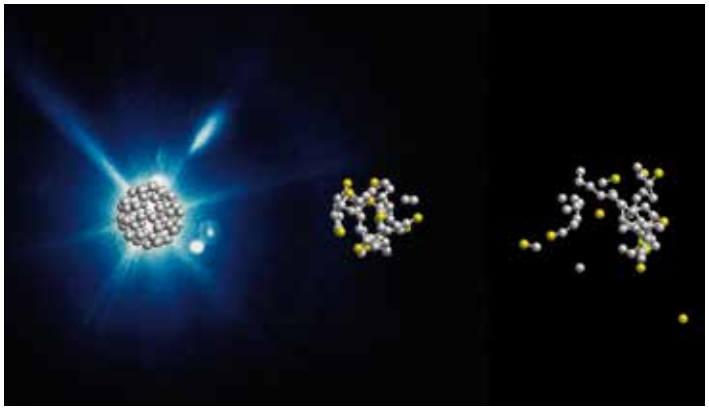

Figure 2

Simulated snapshots of C_{60} disintegrating due to a 20-fs XFEL pump pulse only at 0 fs, 60 fs and 240 fs. The colours grey and yellow refer to atomic charges +0 and +1, respectively. Due to the chemical bonds and the energy redistribution driven by valence-electron transfer, the system undergoes slow multistep fragmentation releasing its final fragments with a delay of a few hundred femtoseconds. This phenomenon plays a role in stabilising polyatomic systems against radiation damage under SFX conditions.
Image: Zoltan Jurek

The current study is an important contribution to the quantitative validation of the modelling approach implemented in XMDYN. The availability of such a software tool is essential for ongoing key applications of XFELs, such as for atomic-resolution imaging of nanosize periodic and non-periodic samples. Because of its predictive capabilities, XMDYN has been integrated in a comprehensive software suite, coordinated by the European XFEL, targeting the simulation of the complete single-molecule-imaging pipeline from start to end [4].

Author contact: Zoltan Jurek, zoltan.jurek@cfel.de
Robin Santra, robin.santra@cfel.de

References

1. B. F. Murphy et al., 'Femtosecond X-ray-induced explosion of C_{60} at extreme intensity', Nat. Commun. 5, 4281 (2014).
2. Z. Jurek, S.-K. Son, B. Ziaja and R. Santra, 'XMDYN and XATOM: versatile simulation tools for quantitative modeling of X-ray free-electron laser induced dynamics of matter', J. Appl. Cryst. 49, 1048–1056 (2016).
3. Y. Kumagai et al., 'Radiation-induced chemical dynamics in Ar clusters exposed to strong X-ray pulses', Phys. Rev. Lett. 120, 223201 (2018).
4. C. H. Yoon et al., 'A comprehensive simulation framework for imaging single particles and biomolecules at the European X-ray Free-Electron Laser', Sci. Rep. 6, 24791 (2016).

Original publication

'Femtosecond-resolved observation of the fragmentation of buckminsterfullerene following X-ray multiphoton ionization', Nature Physics 15, 1279–1283 (2019).
DOI: 10.1038/s41567-019-0665-7

Nora Berrah, Alvaro Sanchez-Gonzalez, Zoltan Jurek, Razib Obaid, Hui Xiong, Richard J. Squibb, Timur Osipov, Alberto Lutman, Li Fang, Thomas Barillot, John D. Bozek, James Cryan, Thomas J. A. Wolf, Daniel Rolles, Ryan Coffee, Kirsten Schnorr, Sven Augustin, Hironobu Fukuzawa, Kenta Motomura, Mario Niebuhr, Leszek J. Frasinski, Raimund Feifel, Claus Peter Schulz, Koudai Toyota, Sang-Kil Son, Kiyoshi Ueda, Thomas Pfeifer, Jon P. Marangos and Robin Santra

Affiliation details at https://www.nature.com/articles/s41567-019-0665-7

Distorted atoms

Intense XUV fields modify electronic transitions

Spectral lines provide a characteristic fingerprint of light-matter interaction within atoms. Dating back about 200 years, Wollaston and Fraunhofer already identified discrete absorption lines in the solar emission spectrum. Half a century later a systematic spectral analysis of the elements in flame emission was carried out by Kirchhoff and Bunsen in Heidelberg. Light-matter interaction is thus the key to our modern understanding of the microscopic world via quantum mechanics. Short-wavelength extreme-ultraviolet (XUV) light lets us access the innermost structure and dynamics of atoms. With such intense XUV light from the free-electron laser FLASH it is now possible to enter the nonlinear regime: It allows one to decisively distort transitions of single and correlated pairs of electrons. This was just measured using Fraunhofer's approach, however, with absorption lines that look different when viewed in intense XUV light.

Absorption spectroscopy is a powerful tool to visualise the structure of bound electrons in matter. The concept is very simple (see Fig. 1a). Use a spectrally broadband light source and transmit it through a dense enough medium. The transmitted light is then spectrally dispersed and resolved. The target medium thus leaves its internal quantum-dynamical fingerprint in the transmitted radiation. Depending on the spectral band used, different characteristics are accessible. Molecular vibrations are typically found in the infrared region, while electronic transitions within the valence shell of atoms and molecules are located in the visible to UV part of the electromagnetic spectrum. Going further, the extreme ultraviolet (XUV) and even X-ray region of the electromagnetic spectrum allows for multi-electron excitations and core-to-valence transitions. These transitions are very specific to each atomic element and its local environment.
Using intense short-wavelength pulses generated by free-electron lasers it is now possible to drive such transitions into

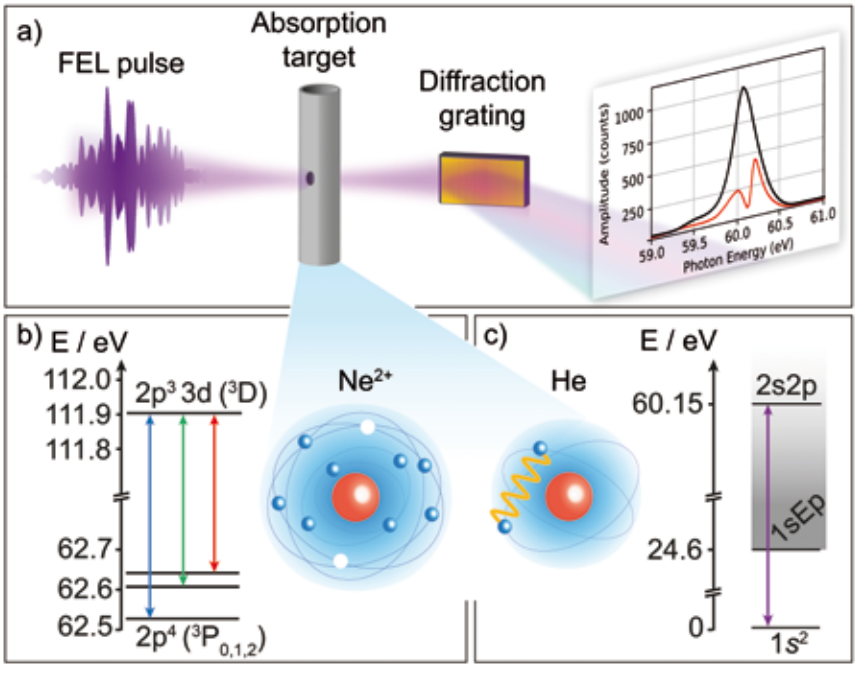

Figure 1

Measurement scheme for resonant XUV nonlinear dressing of helium and neon atoms. (a) FEL pulses are focused into a moderately dense gas target (atomic number density approximately 10^{18} cm^{-3}) and subsequently spectrally resolved with a grazing-incidence diffraction grating. The inset plot shows FEL spectra averaged over multiple single shots without (black curve) and with (red curve) helium target gas in the cell. (b) Energy level scheme of FEL-produced Ne^{2+} ions, denoting FEL-driven resonant $2p^4$ (^{3}P) – $2p^3$3d (^{3}D) multiplet transitions. (c) Energy level scheme of helium for intense FEL pulses dressing the $1s^2$ – 2s2p autoionising two-electron transition.

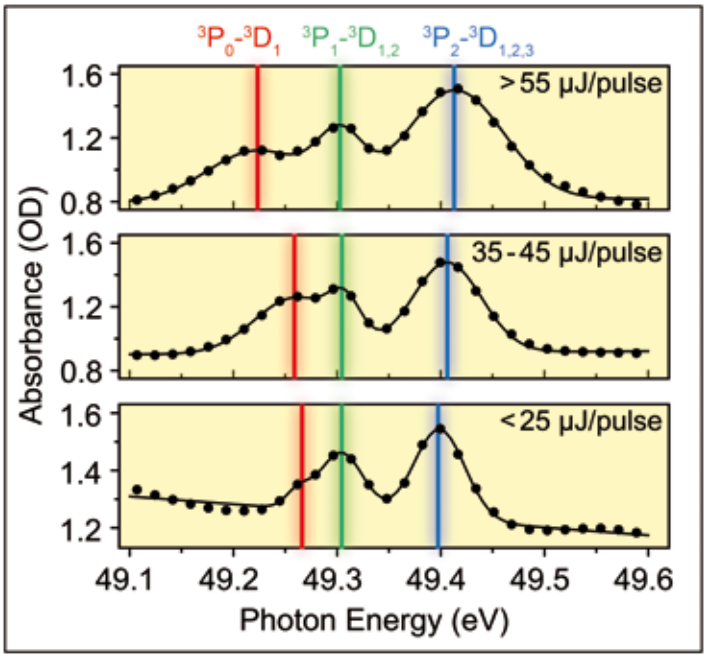

Figure 2

XUV-induced ac Stark shifts of the $2p^4$ (^3P) – $2p^3 3d$ (^3D) multiplet transition in FEL-produced doubly charged neon Ne^{2+} ions, measured through nonlinear XUV absorption spectroscopy. The red, green and blue vertical lines trace the peaks of the Stark-shifted resonant transitions for increasing FEL pulse energy (bottom to top).

the nonlinear regime of light-matter interaction. Such nonlinear interactions unlock quantum control protocols [1], but are currently only well established at longer wavelengths where conventional lasers exist. One crucial phenomenon is the so called ac Stark effect through the laser-induced shifting of energy levels which is due to the strong coupling of an electronic transition to the laser field. It is accompanied by Rabi oscillations and enables complete population transfer among different quantum states.

Such strong-field induced resonant nonlinear couplings remained elusive in the short-wavelength XUV domain. Hereby, one main obstacle is the loss of coherence due to ionisation. Figuratively speaking, one has to be quick before ionisation takes place, with the excited-state and/or core-hole lifetime being typically on the order of femtoseconds and even below, down to attoseconds. Another technical challenge is certainly the availability of intense ultrafast pulses in the XUV wavelength regime. In the past, combining weak attosecond XUV with strong near-visible femtosecond laser pulses it has been possible to resolve the ultrafast build-up of an absorption line in helium [2] and modify its shape [3] which allows one to laser-control a two-electron wavepacket [4]. Attosecond XUV absorption spectroscopy combined with near-visible laser pulses also shed light on the coupling dynamics of dipole-allowed and dipole-forbidden inner-valence transitions in neon [5].

Now, in two recent experiments performed at FLASH we have observed resonant XUV-induced nonlinear effects in

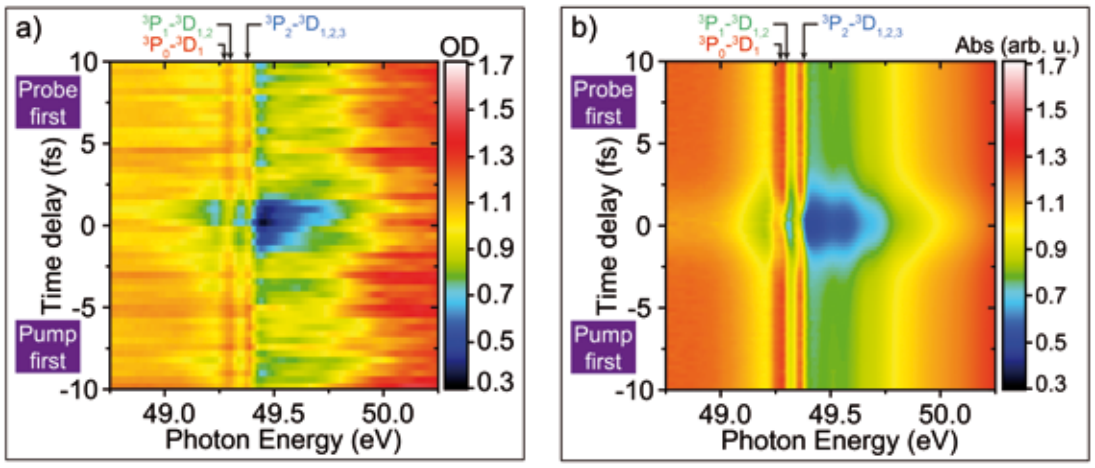

Figure 3

XUV-pump XUV-probe transient absorption spectroscopy of neon. (a) The measurement reveals a coherence-induced enhancement of transparency for precise temporal overlap of the SASE FEL pulses on the few-femtosecond timescale. (b) A nonlinear numerical model, including the near-resonant coupling of ionic transitions and plasma-induced XUV diffraction, reproduces and confirms the experimental observation.

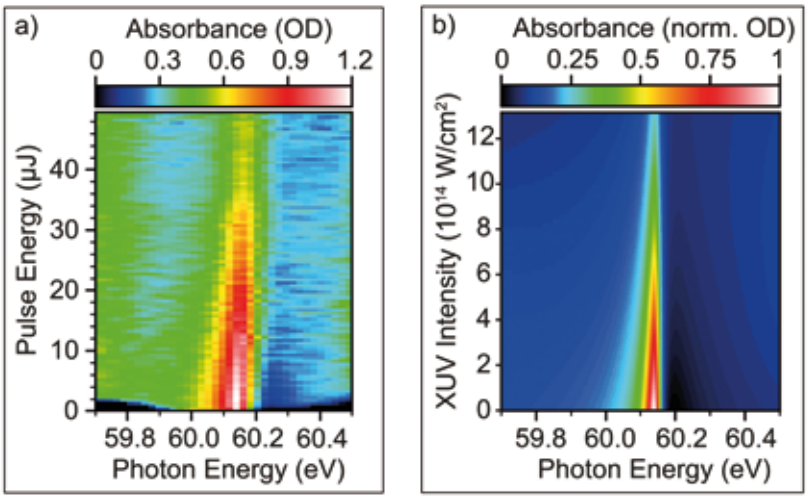

Figure 4

XUV-induced resonant nonlinear effects in helium. (a) The resonant absorption across the 2s2p two-electron transition shows characteristic asymmetry changes of the Fano lineshape for increasing FEL pulse energy. (b) Model calculation of the resonant absorbance in helium for increasing intensity of a Gaussian pulse (duration 5 fs, FWHM) centered at 60.10 eV photon energy.

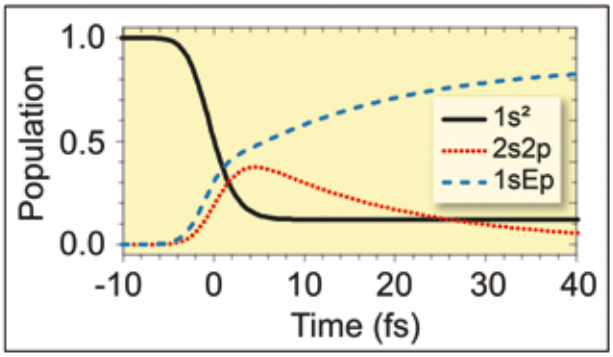

Figure 5

Resonantly driven two-electron population dynamics in helium, revealed by the model simulation for XUV intensity 1.1×10^{15} W/cm^2 and FWHM pulse duration of 5 fs.

atomic transitions. To deliver intense enough XUV light into the atom and resolve its effect on resonant transitions we have followed two different strategies. In a first experiment, performed at around 50 eV photon energy, the FEL pulse was temporally split in two parts. The first part is responsible to sequentially ionise the neon atom to its doubly charged Ne^{2+} ion, which represents the target for the second and more intense FEL pulse (see Fig. 1b). Tuning the intensity of the second FEL pulse reveals an XUV-induced shift of various resonant transitions that belong to the valence $2p^4$ (^{3}P) – $2p^3$ 3d (^{3}D) multiplet of the Ne^{2+} ion (see Fig. 2).

Going further and analysing more closely the production of the doubly charged Ne^{2+} ions, we measured the XUV-optical response of the system by XUV-pump XUV-probe transient absorption spectroscopy across the precise temporal overlap of both pulses. As can be seen in Fig. 3a, an all-XUV-optical coherence enhancement is observed, which is mainly due to plasma-induced diffraction of XUV light on the few-femtosecond timescale. This experimental observation is supported by a numerical model shown in Fig. 3b. The characteristic SASE (self-amplified spontaneous emission) build-up of brilliant XUV light at FLASH, producing intense temporal spikes on the few-femtosecond timescale according to an average spectral bandwidth of about 1 eV is a crucial ingredient for this observation. Our findings represent a significant step towards site-specific multidimensional nonlinear spectroscopy protocols for atomic and molecular systems in the gas phase.

In a second experiment, also performed at FLASH at around 60 eV photon energy, we again made use of the intrinsic few-femtosecond timing structure of the SASE generation process. This timescale is short enough to beat the natural autoionisation decay of the 2s2p two-electron excited state in helium, which has been the target of this experiment (see Fig. 1c). Hence it is possible to observe FEL-induced non-trivial modifications of the asymmetric Fano absorption lineshape of the $1s^2$ – 2s2p transition of a correlated electron pair in helium (see Fig. 4a), which are revealed by increasing the FEL intensity. Supported by a quantum model (see Fig. 4b), the simulations also predict a population inversion of the electron pair (see Fig. 5), boosting the population of the 2s2p excited state above the one of the $1s^2$ ground state. This happens despite the presence of the single-electron ionisation loss into the 1sEp channel, where one electron escapes into the continuum (with kinetic energy E) and leaves the He^+ ion in the 1s ground state. Once again, the intrinsic temporal structure of SASE FEL pulses is crucial for this experimental observation, where we have identified the nonlinear interaction

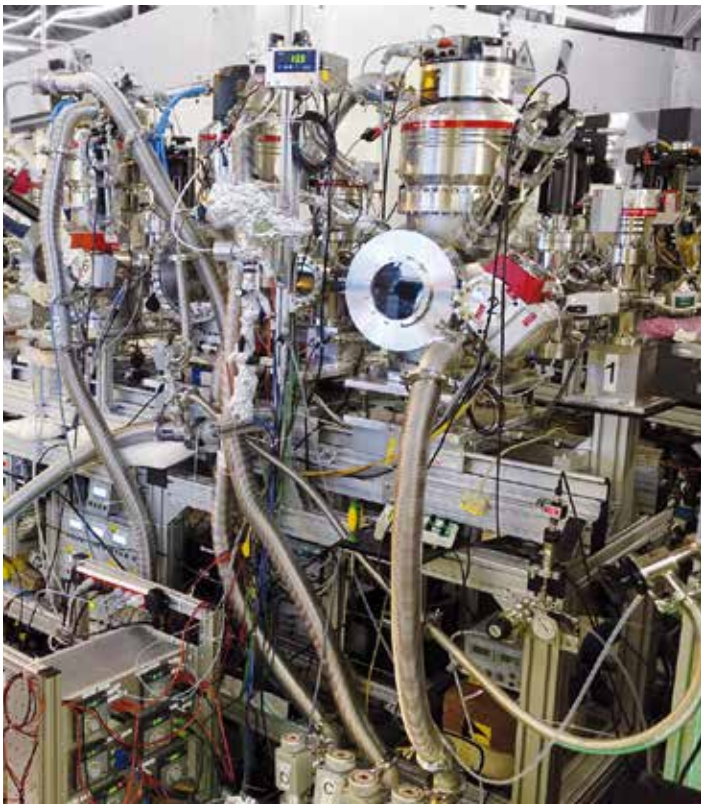

Figure 6

Experimental setup for nonlinear XUV absorption spectroscopy, installed at the open-port beamline BL2 at FLASH.

of a single few-femtosecond temporal intensity spike as the leading contribution to the observed lineshape modification in helium.

In the future, we expect the here presented novel experimental schemes of all-XUV-optical nonlinear absorption spectroscopy for gas-phase target systems to greatly benefit from FEL operation modes which allow one to produce isolated few-femtosecond and even sub-femtosecond single pulses. Being directly sensitive to its temporal structure, our experimental approach can also be a useful tool for the characterization of such FEL pulses.

Both experiments demonstrate the feasibility of quantum control of specific transitions characteristic to each atom, which includes also the steering of an electron pair. The results also pave the road towards site-specific quantum control of molecular dynamics and chemical reactions by using intense and ultrashort FEL pulses.

Author contact: Christian Ott, christian.ott@mpi-hd.mpg.de
Thomas Ding, thomas.ding@mpi-hd.mpg.de
Thomas Pfeifer, thomas.pfeifer@mpi-hd.mpg.de

References

1. Y. Silberberg, 'Quantum coherent control for nonlinear spectroscopy and microscopy', Annu. Rev. Phys. Chem. 60, 277–292 (2009).
2. A. Kaldun, A. Blättermann, V. Stooß, S. Donsa, H. Wei, R. Pazourek, S. Nagele, C. Ott, C. D. Lin, J. Burgdörfer and T. Pfeifer, 'Observing the ultrafast buildup of a Fano resonance in the time domain', Science 354, 738–741 (2016).
3. C. Ott, A. Kaldun, P. Raith, K. Meyer, M. Laux, J. Evers, C. H. Keitel, C. H. Greene and T. Pfeifer, 'Lorentz meets Fano in spectral line shapes: A universal phase and its laser control', Science 340, 716–720 (2013).
4. C. Ott, A. Kaldun, L. Argenti, P. Raith, K. Meyer, M. Laux, Y. Zhang, A. Blättermann, S. Hagstotz, T. Ding, R. Heck, J. Madroñero, F. Martín and T. Pfeifer, 'Reconstruction and control of a time-dependent two-electron wave packet', Nature 516, 374–378 (2014).
5. T. Ding, C. Ott, A. Kaldun, A. Blättermann, K. Meyer, V. Stooß, M. Rebholz, P. Birk, M. Hartmann, A. Brown, H. van der Hart and T. Pfeifer, 'Time-resolved four-wave-mixing spectroscopy for inner-valence transitions', Optics Letters 41, 709–712 (2016).

Original publications

'Nonlinear Coherence Effects in Transient-Absorption Ion Spectroscopy with Stochastic Extreme-Ultraviolet Free-Electron Laser Pulses', Physical Review Letters 123, 103001 (2019). DOI: 10.1103/PhysRevLett.123.103001

Thomas Ding[1], Marc Rebholz[1], Lennart Aufleger[1], Maximilian Hartmann[1], Kristina Meyer[1], Veit Stooß[1], Alexander Magunia[1], David Wachs[1], Paul Birk[1], Yonghao Mi[1], Gergana D. Borisova[1], Carina da Costa Castanheira[1], Patrick Rupprecht[1], Zhi-Heng Loh[2], Andrew R. Attar[3], Thomas Gaumnitz[4], Sebastian Roling[5], Marco Butz[5], Helmut Zacharias[5], Stefan Düsterer[6], Rolf Treusch[6], Stefano M. Cavaletto[1], Christian Ott[1] and Thomas Pfeifer[1]

1. Max-Planck-Institut für Kernphysik, Heidelberg, Germany
2. Division of Chemistry and Biological Chemistry, School of Physical and Mathematical Sciences, Nanyang Technological University, Singapore
3. Department of Chemistry, University of California, Berkeley, California, USA
4. Laboratorium für Physikalische Chemie, ETH Zürich, Zürich, Switzerland
5. Physikalisches Institut, Westfälische Wilhelms-Universität, Münster, Germany
6. Deutsches Elektronen-Synchrotron DESY, Hamburg, Germany

'Strong-Field Extreme-Ultraviolet Dressing of Atomic Double Excitation', Physical Review Letters 123, 163201 (2019). DOI: 10.1103/PhysRevLett.123.163201

Christian Ott[1], Lennart Aufleger[1], Thomas Ding[1], Marc Rebholz[1], Alexander Magunia[1], Maximilian Hartmann[1], Veit Stooß[1], David Wachs[1], Paul Birk[1], Gergana D. Borisova[1], Kristina Meyer[1], Patrick Rupprecht[1], Carina da Costa Castanheira[1], Robert Moshammer[1], Andrew R. Attar[2], Thomas Gaumnitz[3], Zhi-Heng Loh[4], Stefan Düsterer[5], Rolf Treusch[5], Joachim Ullrich[6], Yuhai Jiang[7], Michael Meyer[8], Peter Lambropoulos[9] and Thomas Pfeifer[1]

1. Max-Planck-Institut für Kernphysik, Heidelberg, Germany
2. Department of Chemistry, University of California, Berkeley, California, USA
3. Laboratorium für Physikalische Chemie, ETH Zürich, Zürich, Switzerland
4. Division of Chemistry and Biological Chemistry, School of Physical and Mathematical Sciences, Nanyang Technological University, Singapore
5. Deutsches Elektronen-Synchrotron DESY, Hamburg, Germany
6. Physikalisch-Technische Bundesanstalt PTB, Braunschweig, Germany
7. Shanghai Advanced Research Institute, Chinese Academy of Sciences, Shanghai, China
8. European XFEL, Schenefeld, Germany
9. Department of Physics, University of Crete and IESL-FORTH, Heraklion, Greece

Quantum-rotational dance floor

Molecular movie and quantum-carpet of rotational dynamics of carbonylsulfide

Making a molecular movie with a spatial and temporal resolution down to a few picometres and a few femtoseconds has been a long-standing dream in the molecular sciences. In our study, the rotational dynamics of quantum-state selected OCS molecules induced by an optimised two-pulse sequence was monitored by Coulomb-explosion imaging following ionisation with an intense mid-infrared laser pulse. We recorded a high-resolution and high-fidelity molecular movie over more than one-and-a-half periods of the laser-induced rotational dynamics of OCS. In addition, we demonstrated the highest experimentally achieved degree of field-free molecular alignment.

Watching molecules at work by recording the so-called molecular movie is challenging. Femtosecond diffractive imaging studies with intense short-wavelength pulses or with ultrashort electron bunches became possible just recently with the advent of X-ray free-electron lasers or relativistic electron guns. However, for gas-phase molecules that rotate freely in space, most of the structural information that is contained in X-ray or electron diffraction experiments is averaged out. This effect can be circumvented using laser-induced alignment to fix-in-space one or more molecular axes along specific directions in the laboratory frame. When the pulse duration of the laser becomes shorter than the rotational period of the molecule, a rotational wavepacket is formed that freely evolves after the laser pulse. This *field-free* rotational-wavepacket dynamics is responsible for a rich time-dependent modulation of the angular probability distribution that becomes angularly confined along the laser polarisation direction at specific times [1].

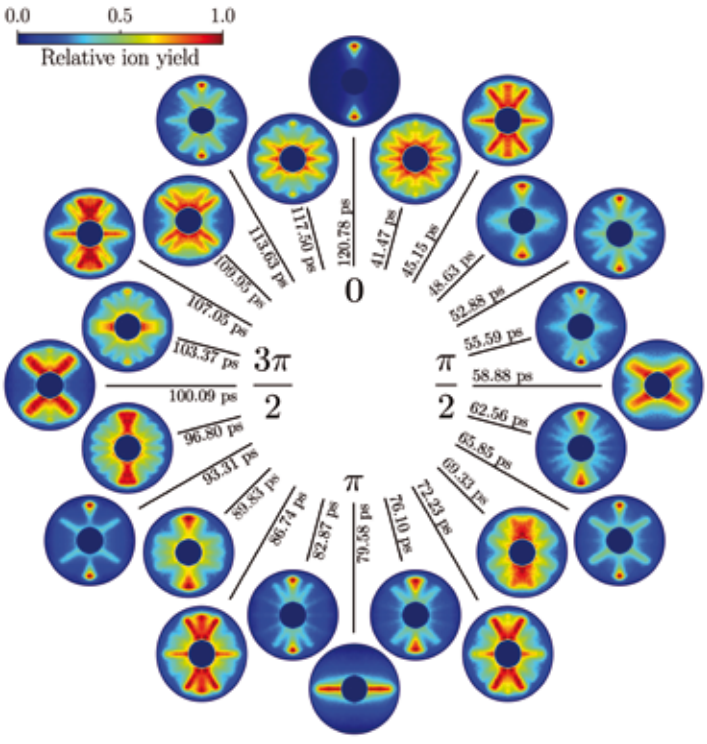

Laser-induced alignment of isolated molecules provides not only an important step towards high-resolution imaging of molecular structure and dynamics, it provides also an interesting and important testbed for making a molecular movie in which direct access to angular coordinates is required. During the last two decades, rotational quantum dynamics induced by intense laser fields has been observed and characterised using various techniques, for instance, by time-delayed Coulomb-explosion ion imaging [2], photoelectron imaging [3], or ultrafast electron diffraction [4]. Also, methods based on multiple pulses or tailored laser pulses to enhance the degree of alignment have been successfully tested [5].

We demonstrated the direct experimental high-resolution imaging of the time-dependent angular probability density of a rotational wavepacket in carbonylsulfide (OCS). This provided, to the best of our knowledge, the highest fidelity movie of the quantum rotational dynamics of an isolated molecule. The electric deflector selected OCS molecules initially in their absolute ground state [6]. These were kicked with two 250 fs short laser pulses, separated by 38.1 ps, to create the rotational wavepacket. The resulting time-dependent angular-

Figure 1

Rotational clock depicting the molecular movie of the observed quantum dynamics. Individual experimental O^+ ion-momentum distributions depicting snapshots of the rotational wavepacket dynamics over one full period. The displayed data was recorded from the prompt alignment at 38.57 ps to the first full revival at 120.78 ps. See https://doi.org/10.1038/s41467-019-11122-y for the full movie (supplementary movie 1).

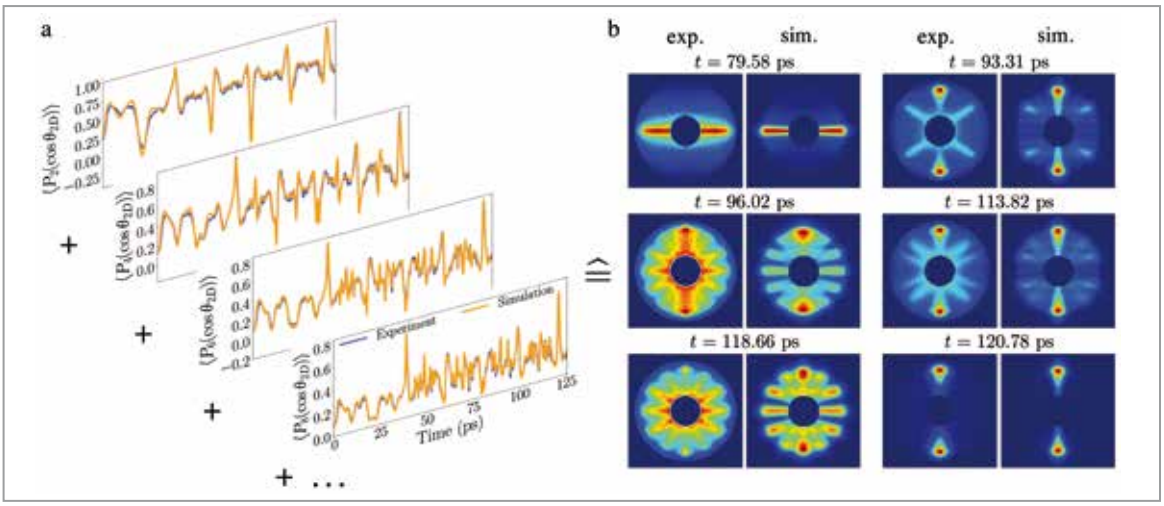

Figure 2

Decomposition of angular distributions into their moments. a) Comparison of the decomposition of the experimental and theoretical angular distributions in terms of Legendre polynomials. b) Simulated and experimental angular distribution at selected time delays; we note that the radial distributions in the simulations were extracted from the experimental distribution at 120.78 ps.

probability-density distributions of OCS were probed through Coulomb-explosion imaging following multiple ionisation using a third, 60 fs short, mid-infrared laser pulse. The molecules dissociated quickly into O^+ and the CS^+ counter-ion, with the two fragments recoiling back-to-back along the molecular axis due to their mutual Coulomb repulsion. The angularly-resolved O^+ ion-momentum distributions were recorded using a velocity map imaging spectrometer, providing a mapping of the angular probability distribution of the molecules at the moment of dissociation. Figure 1 displays snapshots of these measured angle-resolved distributions for various time delays between the alignment and the probe laser pulses over one rotational period of the OCS molecule. The strong angular confinement of the O^+ ion momentum distribution along the vertical direction observed at a time delay of 120.78 ps in Fig. 1 corresponds to an unprecedented degree of field-free alignment of $\langle\cos^2\theta_{2D}\rangle = 0.96$. The rich angular structures observed in the ion-momentum distributions at other time delays are a direct manifestation of the complex time-dependent rotational wavepacket dynamics, which is further enhanced by the quantum-state-selected ultracold initial sample exploited in our measurements. Such rich dynamics would be largely lost in the incoherent summation of wavepackets from even a few initial states.

The complete characterisation of the rotational wavepacket, i.e., including the population and the relative phases of the rotational states populated by the two-pulse excitation, was retrieved from the molecular movie shown in Fig. 1. To do so, we solved the time-dependent Schrödinger equation using the experimentally determined parameters and computed the angular probability distribution of the molecule at various time delays after the two-pulse excitation. Figure 2a shows an expansion of the angular distributions from both, experiment and simulation, in terms of Legendre polynomials for the first 4 even-order polynomials. Figure 2b displays a comparison between simulated and experimental angular distribution at selected time delays. The agreement is excellent for all orders and at all times. This emphasises that we can retrieve the complete wavepacket with its populations and relative phases at all times.

The exact knowledge of the rotational wavepacket and the unprecendented degree of field-free alignment achieved experimentally pave the way towards the time-resolved imaging of chemical dynamics in OCS, e.g., building also on picometre-resolution laser-induced-electron-diffraction approaches [7]. The extension of these methods to align more complex and biologically relevant molecules is currently investigated.

Author contact: Evangelos Thomas Karamatskos, evangelos.karamatskos@cfel.de
Arnaud Rouzée, arnaud.rouzee@mbi-berlin.de
Jochen Küpper, jochen.kuepper@cfel.de

References

1. H. Stapelfeldt and T. Seideman, 'Colloquium: Aligning molecules with strong laser pulses', Rev. Mod. Phys. 75, 543–557 (2003).
2. F. Rosca-Pruna and M. J. J. Vrakking, 'Experimental observation of revival structures in pico second laser-induced alignment of I_2', Phys. Rev. Lett. 87, 153902 (2001).
3. L. Holmegaard et al., 'Photoelectron angular distributions from strong-field ionization of oriented molecules', Nat. Phys. 6, 428 (2010).
4. J. Yang, J. Beck, C. J. Uiterwaal and M. Centurion, 'Imaging of alignment and structural changes of carbon disulfide molecules using ultrafast electron diffraction', Nat. Commun. 6, 8172 (2015).
5. O. Ghafur et al., 'Impulsive orientation and alignment of quantum-state-selected NO molecules', Nat. Phys. 5, 289–293 (2009).
6. Y.-P. Chang, D. A. Horke, S. Trippel and J. Küpper, 'Spatially-controlled complex molecules and their applications', Int. Rev. Phys. Chem. 34, 557–590 (2015).
7. E. T. Karamatskos et al., 'Atomic-resolution imaging of carbonyl sulfide by laser-induced electron diffraction', J. Chem. Phys. 150, 244301 (2019).

Original publication

'Molecular movie of ultrafast coherent rotational dynamics of OCS',
Nature Communications 10, 3364 (2019). DOI: 10.1038/s41467-019-11122-y

Evangelos T. Karamatskos[1,2], Sebastian Raabe[3], Terry Mullins[1], Andrea Trabattoni[1,2], Philipp Stammer[3], Gildas Goldsztejn[3], Rasmus R. Johansen[4], Karol Długołecki[1], Henrik Stapelfeldt[4], Marc J.J. Vrakking[3], Sebastian Trippel[1,5], Arnaud Rouzée[3] and Jochen Küpper[1,2,5]

1. Center for Free-Electron Laser Science, DESY, Hamburg, Germany
2. Department of Physics, Universität Hamburg, Hamburg, Germany
3. Max Born Institute, Berlin, Germany
4. Department of Chemistry, Aarhus University, Aarhus, Denmark
5. The Centre for Ultrafast Imaging, Universität Hamburg, Hamburg, Germany

Tailored optical centrifuge sets molecules spinning rapidly about selected axes

Coherent control of molecular rotation axis

Molecules exhibit different reactivities depending on their orientation, which makes the outcome of elastic, inelastic, and chemically-reactive collisions strongly dependent on the reactants' rotational motion. In recent years, the control of molecular rotation has made tremendous progress due to the development of innovative techniques in strong-field laser physics. Here, we computationally demonstrate a new type of coherent control by exciting the rotation of an asymmetric-top molecule about two entirely different molecular axes. This is achieved using tailored laser pulses that act as a centrifuge and excite the prototypical H_2S molecules along separate pathways of rotational states. This scheme for strongly controlling the angular-momentum alignment of molecules can be readily adapted to virtually any molecular system.

Advances in molecular-beam and laser technologies led to considerable progress in the optical control of molecular rotation, ranging from the alignment and orientation of molecular axes, where molecules can be spatially fixed in the laboratory frame [1, 2], to the creation of unidirectional rotating molecular ensembles that possess oriented angular momentum [3]. A highly efficient technique to induce large angular momenta is the optical centrifuge [4, 5], which is a strong, nonresonant, linearly- or elliptically-polarised laser pulse that performs accelerated rotation of its polarisation about the direction of propagation. Such optical centrifuges can excite molecules into rotational states with large angular momentum. The created molecular superrotors have revealed interesting properties, for instance, they can provide significant energy to collisions and, at the same time, behave like tiny gyroscopes that are fairly resistant to collisions and reorientation.

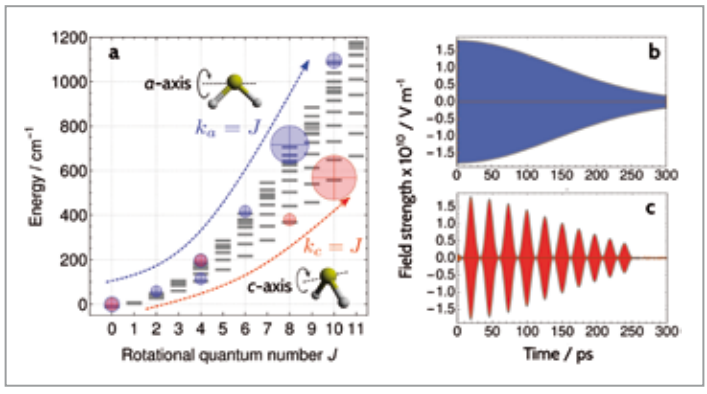

Figure 1

Controlling the molecular axis of rotation in H_2S by exciting along different pathways of rotational states with an optical centrifuge. (b) A Gaussian pulse envelope that produces rotation about the principal *c*-axis. (c) Using an optimised sinc function combined with a Gaussian profile for the pulse envelope leads to rotation about the principal *a*-axis. The populations of rotational states obtained with the Gaussian and sinc pulse envelopes are plotted on panel (a) with the red and blue circles, respectively, where the circle size reflects the relative population.

The populations of rotational states in a molecule upon excitation with the laser centrifuge are primarily excited through $\Delta J=2$ and $\Delta m=\pm 2$ rotational Raman transitions, where the sign of Δm depends on whether the centrifuge rotates in clockwise or anticlockwise direction. J and m denote the quantum numbers of the total angular momentum and its projection onto the laboratory *Z* axis, respectively. These quantum numbers fully characterise the rotational dynamics of linear molecules. In non-linear molecules, the rotational states are described by two additional pseudo-quantum numbers, k_a and k_c, that denote projections of the total angular momentum onto the inertial *a*- and *c*-axis, respectively. For instance, the rotational energies of hydrogen sulfide (H_2S) are plotted as a function of J in Fig. 1a. The highest-energy states within each J multiplet correspond to $k_a=J$ and in these states the molecule rotates about the *a*-axis. The lowest-energy states correspond to rotation about the *c*-axis with $k_c=J$.

The majority of studies have involved diatomic and triatomic linear molecules, which have only one, albeit degenerate, unique axis of stable rotation. Less explored are asymmetric-top molecules, which can stably rotate about two different molecular axes, *a* and *c*; we note that no body can stably rotate about the third axis, *b*. So far, when an optical centrifuge was applied to an asymmetric-top molecule, it would

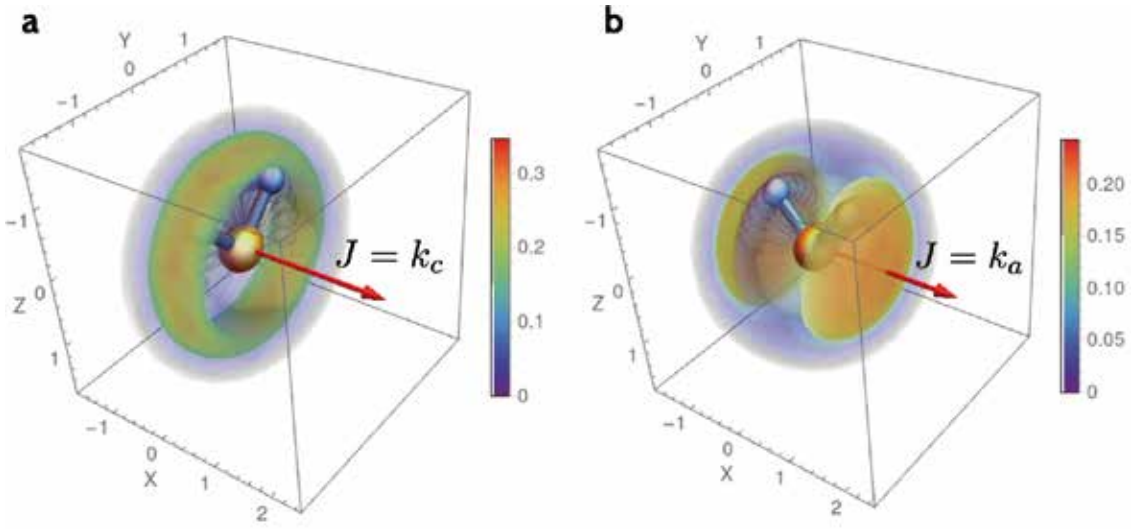

Figure 2

The probability density distributions of the hydrogen atoms in H_2S in the laboratory frame after the end of the laser centrifuge pulse with the Gaussian (a) and sinc (b) function envelope at a time of 70 ps and 120 ps, respectively. The laser polarisation rotates in the *YZ* plane.

make it rotate about only one specific axis, depending on the inertial shape of the molecule. For H_2S, the standard laser centrifuge with a single-pulse envelope excites molecules along a pathway of lowest energy rotational states, see Fig. 1b, i.e., those corresponding to rotation about the molecular *c* axis. The populations of rotational states at a time of 70 ps are marked with the red circles in Fig. 1a, where the circle size is proportional to the normalised populations. The probability density distribution of hydrogen atoms in the laboratory frame, plotted in Fig. 2a, has a ring-shape, which means that the H–S–H plane is confined to the plane of the laser polarisation and the molecule rotates about the *c*-axis.

In 2018, our group at CFEL and Universität Hamburg, theoretically and computationally devised a sophisticated optical centrifuge approach that makes molecules rotate rapidly about a chosen molecular axis. The new scheme lets us select between *a*-axis and *c*-axis rotation through excitation along different pathways of rotational states. This was achieved using a laser centrifuge with a modified pulse envelope. The laser field was repeatedly turned on only when the angular frequency of the centrifuge is in resonance with the desired transition frequency between two states, thus enabling population transfer. The field was turned off as the angular frequency increases and sweeps through resonance with undesired transitions, before being turned on again at a later time when in resonance with the next desired transition.

The study demonstrated how for H_2S fast rotation about the *a*-axis, instead of the normal *c*-axis rotation, can be induced through modifications of the pulse envelope of the optical centrifuge. Here, this was achieved through a series of prototypical sinc-type-function modulations of the temporal envelope of the laser pulses, shown in Fig. 1c. The resulting populations of rotational states at a time of 120 ps are indicated by blue circles in Fig. 1a. The excitation along the highest-energy pathway of rotational states was produced. The plot of the probability density distribution of hydrogen atoms in Fig. 2b attests to a rotation of the molecule about the *a*-axis.

This study demonstrates that sophisticated coherent control schemes could be developed to transfer arbitrary molecules into specific highly-excited states or to create specific angular probability distributions. The novel scheme to control the angular momentum alignment of a molecule could be useful in studies of molecule-molecule or molecule-surface scattering, where it would control the outcome and the stereodynamics of a scattering event. Equally beneficial is the large amount of energy associated with superrotors, which can also be controlled by changing the duration of the optical centrifuge pulse.

Author contact:
Andrey Yachmenev, andrey.yachmenev@cfel.de
Jochen Küpper, jochen.kuepper@cfel.de

References

1. H. Stapelfeldt and T. Seideman, 'Colloquium: aligning molecules with strong laser pulses', Rev. Mod. Phys. 75, 543 (2003).
2. E. T. Karamatskos et al., 'Molecular movie of ultrafast coherent rotational dynamics of OCS', Nat. Commun. 10, 3364 (2019), arXiv:1807.01034 [physics]; see also page 60 in this report.
3. A. Owens et al., 'Climbing the rotational ladder to chirality', Phys. Rev. Lett. 121, 193201 (2018), arXiv:1802.07803 [physics].
4. D. M. Villeneuve et al., 'Forced molecular rotation in an optical centrifuge', Phys. Rev. Lett. 85, 542, (2000).
5. A. Korobenko et al., 'Direct observation, study, and control of molecular superrotors' Phys. Rev. Lett. 112, 11300 (2014).

Original publication

'Coherent control of the rotation axis of molecular superrotors', The Journal of Physical Chemistry Letters 9, 4206–4209 (2018). DOI: 10.1021/acs.jpclett.8b01689; arXiv:1807.04016 [physics]

Alec Owens[1,2], Andrey Yachmenev[1,2] and Jochen Küpper[1,2,3]

1. Center for Free-Electron Laser Science, DESY, Hamburg, Germany
2. Center for Ultrafast Imaging (CUI), Universität Hamburg, Hamburg, Germany
3. Department of Physics, Universität Hamburg, Germany

Hard X-ray photoelectron spectroscopy at 2.5 bar

Investigating catalytic reactions under industrially realistic conditions

Catalyst materials are found in nearly all industrial processes of the chemical industry and are considered as key technology for chemical transformation. This includes very topical societal needs such as energy production, energy storage and technology for environmental protection. Even though considerable effort has been undertaken to understand the underlying processes of how molecules transform from one species to an other, necessary insight is still missing. Large progress has been made using experimental attempts under well-controlled conditions in vacuum. However, the catalytically relevant processes happen at pressures of several bar and at elevated temperatures and need to be studied there. We have been able to improve the dection limit by more than 3 orders of magnitude, enabling us to answer fundamental scientific questions about catalytic reactions as they realistically occur. We hope to spark new scientific discoveries leading to optimisation of catalysis even on the industrial scale.

X-ray photoelectron spectroscopy (XPS) is a technique that allows investigating the chemical composition of materials and molecules on surfaces. It is traditionally used almost exclusively in the high or ultrahigh vacuum regime because electrons are scattered inelastically in the gas atmosphere. Continuous developments made it possible for scientists to access the low 1 mbar pressure regime. However, many important catalytic reactions take place at several bar, which were still not accessible.

This presents a real challenge, as the typical design intent of vacuum chambers is to have low pressure inside and atmospheric pressures outside. Having a high pressure inside the vacuum chamber is a contradiction and has driven us towards finding new approaches. Thus we have developed a new experimental end station where we combine traditional surface-science vacuum-technology with high-pressure XPS (Fig. 1, left). The newly developed high-pressure XPS instrument can be used in a multi-bar pressure regime while at the same time controlling the catalyst temperature up to 500 °C. In this regime relevant processes such as Fischer-Tropsch reactions can be studied in detail.

The heart of the instrument is the virtual cell (Fig. 1, right). Here the reaction mixture is guided directly onto the sample surface, creating a locally defined high-pressure region. We utilize high kinetic energy photoelectrons created by the hard X-rays from beamline P22 to decrease scattering in the gas. Simultaneously, the distance between the sample and the electron-spectrometer inlet is minimised (typically 30 µm) and controlled with submicrometer precision. This puts strict requirements on the design; especially vibrations and thermal expansion need to be taken into account in order to allow for precise thickness control of the gas cushion.

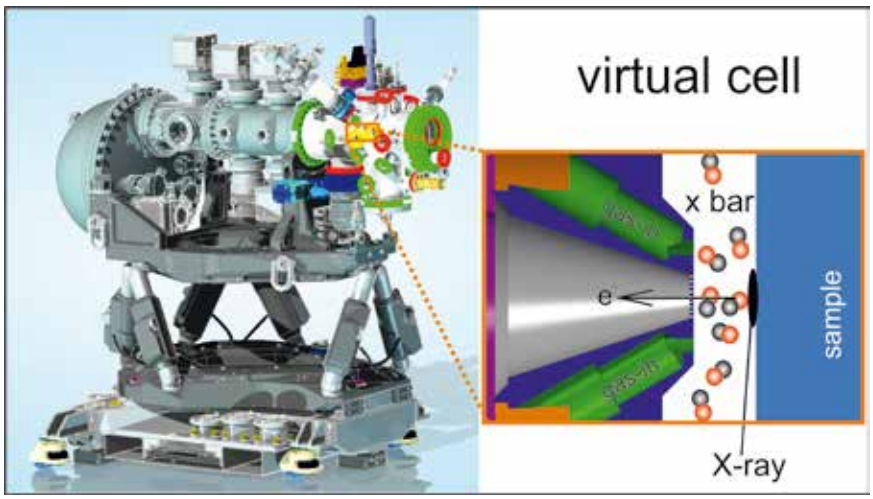

Figure 1
3D rendering of the POLARIS end station (left) and cartoon drawing of the virtual cell (right). In the virtual cell, premixed gas is directed onto the sample surface and creates a local high-pressure cushion. Grazing incidence hard X-rays are used to excite the photoelectrons which are detected in the electron analyser.

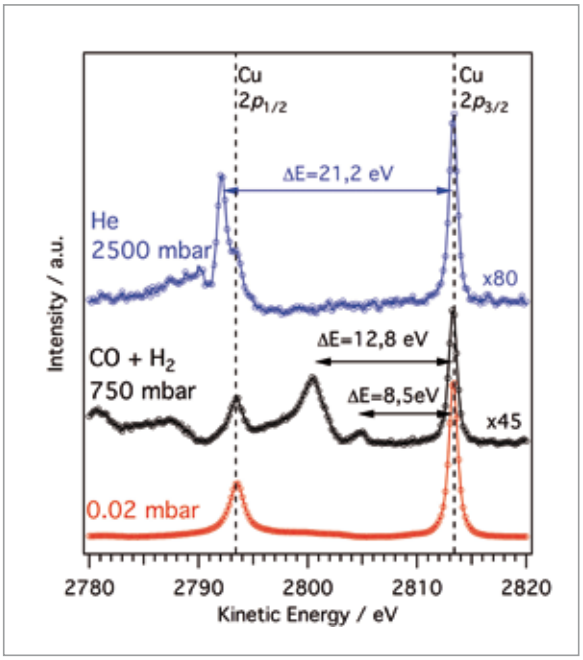

Figure 2

Copper *2p* X-ray photoelectron spectra acquired at high-pressure conditions. We compare measurements in vacuum conditions (red), 750 mbar of a CO : H_2 = 1 : 3 gas mixture (black) and 2.5 bar He (blue). The arrows indicate distinct electron energy loss features that arise when the electrons are transmitted through the gas phase in the virtual cell.

A thin foil separates the vacuum in the electron spectrometer from the reaction region where gas at multiple bars is present. The foil is perforated with apertures and trades off high electron transmission and low gas permeation. Simulations of the pressure around the sample surface clearly show that at pressures exceeding several hundreds of mbar the sample-to-aperture distance can be reduced below the commonly established values. Being able to approach the inlet further than previously believed further enhances the electron transmission through the gas phase.

Commissioning experiments took place at beamline P22 of PETRA III. The specific characteristics of this beamline allowed measurements at grazing incidence of 0.3°, which is below the angle of total reflection. In our publication we show on an Rh single crystal that this leads to a considerable enhancement of the surface sensitivity compared to large incidence geometries.

To demonstrate the effectiveness of our design we have performed an highlighting experiment on a copper single crystal at an absolute pressure of 2.5 bar. In Fig. 2 we compare spectra taken at vacuum conditions, at 2.5 bar of He and 750 mbar of reaction mixture (H_2 : CO = 3 : 1). The figure shows that these conditions can be effectively studied inside the POLARIS end station. We detect distinct features due to gas-type dependent electron energy loss processes. The observation of spectra at such high pressures has not been possible before and opens up the path to scientifically address relevant catalytic processes in an *operando* fashion.

Catalysis experiments are challenging for a fundamental reason: many materials can be catalytically active. Therefore parasitic reactions could potentially obscure the catalytic reaction on the sample surface. Using the virtual cell approach the gas influx continuously pushes the gas away from the interaction region, thereby limiting the exposure to the sample surface and minimising the contribution from extraneous reactions effectively. Also by using a gas stream that is directly pointed at the sample, processed gas molecules are quickly pushed away from the interaction region allowing to operate the reaction in a regime that is not mass transfer limited. The compact design of the high-pressure environment further helps to reduce losses that occur due to scattering of photons and electrons in the measurement process. In addition, the virtual cell approach allows the usage of X-ray standing waves and the combination with other spectroscopic techniques.

Author contact: Peter Amann, peter.amann@fysik.su.se

Original publication

'A high-pressure X-ray photoelectron spectroscopy instrument for studies of industrially relevant catalytic reactions at pressures of several bars', Review of Scientific Instruments 90, 103102 (2019); DOI: 10.1063/1.5109321

Peter Amann[1], David Degerman[1], Ming-Tao Lee[1], John D. Alexander[1], Mikhail Shipilin[1], Hsin-Yi Wang[1], Filippo Cavalca[1], Matthew Weston[1], Jörgen Gladh[1], Mikael Blom[1], Mikael Björkhage[1], Patrik Löfgren[1], Christoph Schlueter[2], Patrick Lömker[2], Katrin Ederer[2], Wolfgang Drube[2], Heshmat Noei[3], Johann Zehetner[3], Henrik Wentzel[4], John Åhlund[5] and Anders Nilsson[1]

1. Department of Physics, Stockholm University, Stockholm, Sweden
2. Deutsches Elektronen-Synchrotron DESY, Hamburg, Germany
3. Research Centre for Microtechnology, University of Applied Sciences, Dornbirn, Austria
4. Teknikvetenskap Royal Institute of Technology (KTH), Stockholm, Sweden
5. Scienta Omicron AB, Uppsala, Sweden

Superfluorescent extreme ultraviolet emission

Free-electron laser FLASH drives Xe to collective spontaneous emission

Superfluorescence is a quantum optical phenomenon that was first discovered in the infrared range in the 1970s, and later demonstrated for microwaves and optical wavelengths. For the first time, we observed superfluorescence in the extreme ultraviolet (XUV) spectral range using the free-electron laser (FEL) FLASH. The FEL prepares xenon atoms in excited states by inner-shell photoionisation. The inner-shell hole decays by Auger process, leading to a population inversion in the residual ions. In the absence of decoherence processes, a macroscopic polarisation builds up in the medium, leading to emission of directed, highly amplified, and coherent pulses of XUV light. The present comprehensive experimental and theoretical study deepens our understanding of the process of superfluorescence in general and could lead to new applications in the future.

Superfluorescence or superradiance describes the spontaneous, collective decay of a macroscopic ensemble of excited atoms or ions, which have been prepared in a population-inverted state, resulting in emission of collimated, high-intensity radiation pulses [1]. Superfluorescence was first demonstrated in 1972 in the infrared range [2], and later also in the microwave and visible spectral regions [3]. With the advent of free-electron lasers, it became possible to efficiently pump, i.e., ionise inner-shell levels. In 2012, strong X-ray K_α superfluorescence following ionisation of the 1s shell in neon gas with an X-ray FEL (LCLS) has been demonstrated [4,5].

This work represents the first demonstration of superfluorescence in the XUV region, following inner-shell ionisation of xenon gas. It is particularly difficult to obtain amplification by stimulated emission in the XUV region due to two competing processes: electronic Auger decay and radiative relaxation. The dominant decay of an inner-valence vacancy proceeds along the Auger process with an associated time scale of femtoseconds, or even sub-fs (for Coster-Kronig decays).

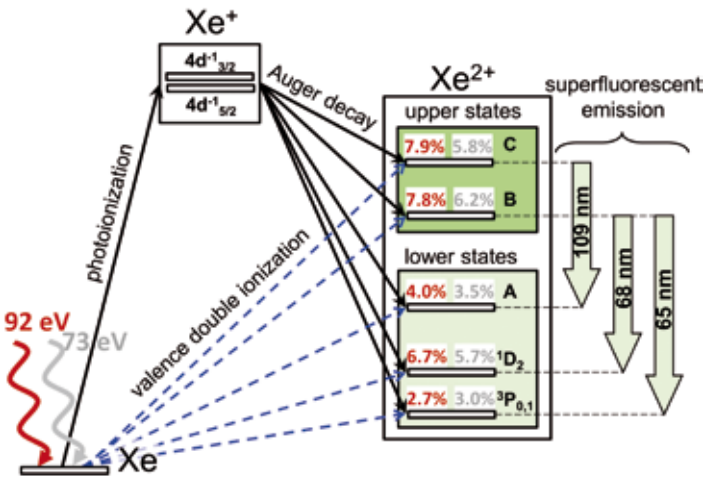

Figure 1

The FEL pulse photoionises the 4d shell of the Xe ground state. The resulting Xe^+ $4d^{-1}$ vacancies decay via Auger process into various Xe^{2+} and Xe^{3+} (not shown) states. Population inversion in Xe^{2+} is established between the upper (B, C) and lower (A, $^1D_2$, and $^3P_{0,1}$) states of the observed transitions. Valence double ionisation (dashed blue arrows) contributes to the population of the Xe^{2+} states. The population branching ratios of each state, relative to all Xe^+, Xe^{2+}, and Xe^{3+} states as deduced from our coincidence measurements are given in red (grey) for pump photon energy 92 eV (73 eV).

On the contrary, the radiative transition times are nanoseconds; thus, radiative transition rates are several orders of magnitude smaller than nonradiative ones. It sets a difficult starting position for amplification by stimulated emission.

Using the FEL FLASH, it is possible to create a relatively long lived population inversion, via Auger pumping [6]: Photoionisation of the 4d shell in Xe is followed by fast Auger decay to a manifold of Xe^{2+} and Xe^{3+} ions in excited states. The branching ratios of the decays are such that population inversion is created between several states in the dication. The process is shown in Fig. 1. These long lived states allow for the build-up of a macroscopic polarisation that sustains coherent, collective emission. Here, FELs offer clear advantages. Their ultrashort, highly intense pulses guarantee an almost instantaneous population inversion, and their transversal coherence allows for tight focusing and longitudinal pump geometry, which is ideal for superfluorescence.

The experiment was performed using the CAMP end station at FLASH. The FEL pulses (90 fs, up to 90 µJ, photon energy 73 eV or 92 eV, below and on the giant 4d resonance) where focused into a cell of xenon gas at nearly atmospheric pressure, creating a pencil-shaped, pumped medium of 4.5 mm length and about 40 µm diameter. The transmitted FEL radia-

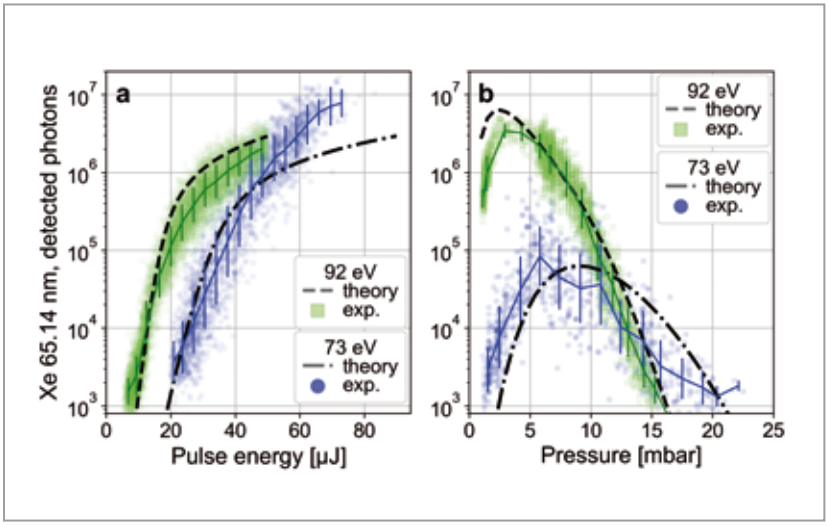

Figure 2

Emission yield of the 65 nm line as a function of (a) FEL-pulse energy E_P for pump photon energy ω_P = 73 eV (at 7 mbar Xe) and 92 eV (at 3.5 mbar Xe) and (b) pressure for fixed E_P = 30 μJ for ω_P = 73 eV and E_P = 75 μJ for ω_P = 92 eV. Symbols: Experimental single-shot data. For each data set, the solid line and error bars are the geometric mean and standard deviation, the black lines are the result of the theory.

tion and XUV emission were analysed by a high-resolution spectrometer downstream of the experimental chamber, allowing to simultaneously measure both the FEL spectrum and the superfluorescence. Using this setup, intense XUV emission lines at wavelengths of 65, 68 and 109 nm were observed in the forward direction (see Fig. 1).

For the strongest lines at 65 and 68 nm the dependence of the emission parameters on changes in gas pressure and FEL fluence was investigated. Fig. 2 shows the 65 nm line. When varying the FEL-pulse energy from 10 to 60 μJ, the emission yield of the 65 nm line increases exponentially over four orders of magnitude until reaching saturation. Increasing the pressure inside the gas cell (and thus the number of possible emitters), the yield increases at first, then saturates, and in the end decreases again due to reabsorption of the emitted photons in the gas.

A novel theoretical approach [7], based on a quantum treatment of the atomic system and the irradiated field, was compared to the experimental results, as shown in Fig. 2. The quantitative agreement obtained with the experiment supports the interpretation of superfluorescent emission. For the temporal evolution of the emitted radiation, calculations show delayed peak-like behaviour that is characteristic for superfluorescence [1]. For the spectral properties of the emitted radiation, calculations predict broadening of the emission line and the emergence of shoulders that are a consequence of Rabi-like oscillations. The predicted line broadening with increasing emission yield was experimentally observed and provides additional evidence for the superfluorescent nature of the emitted radiation.

In conclusion, this research combines the first experimental, spectroscopic evidence for superfluorescence in the XUV region and a new theoretical approach that supports the interpretation of superfluorescence. The fact that saturation of XUV emission can also be reached using plasma sources, instead of an FEL for pumping, holds promise for future applications and development of high brilliance table-top XUV sources.

Author contact:
Andrei Benediktovitch, andrei.benediktovitch@desy.de
Laurent Mercadier, laurent.mercadier@xfel.eu
Benjamin Erk, benjamin.erk@desy.de
Nina Rohringer, nina.rohringer@desy.de

References

1. R. Bonifacio et al., 'Steady-state pulses and superradiance in short-wavelength, swept-gain amplifiers', Phys. Rev. A 12, 2568–2573 (1975).
2. N. Skribanowitz et al., 'Observation of Dicke superradiance in optically pumped HF gas', Phys. Rev. Lett. 30, 309–312 (1973).
3. M. Gross and S. Haroche, 'Superradiance: an essay on the theory of collective spontaneous emission', Phys. Rep. 93, 301–396 (1982).
4. N. Rohringer et al., 'Atomic inner-shell x-ray laser at 1.46 nanometres pumped by an X-ray free-electron laser', Nature 481, 488–491 (2012).
5. C. Weninger et al., 'Stimulated electronic X-ray Raman scattering', Phys. Rev. Lett. 111, 233902 (2013).
6. E. J. McGuire, 'Soft-X-ray amplified spontaneous emission via the Auger effect', Phys. Rev. Lett. 35, 844–848 (1975).
7. A. Benediktovitch, V. P. Majety and N. Rohringer, 'Quantum theory of superfluorescence based on two-point correlation functions', Phys. Rev. A 99, 013839 (2019).

Original publication

'Evidence of extreme ultraviolet superfluorescence in xenon', Phys. Rev. Lett. 123, 023201 (2019). DOI: 10.1103/PhysRevLett.123.023201

L. Mercadier, A. Benediktovitch, C. Weninger, M. A. Blessenohl, S. Bernitt, H. Bekker, S. Dobrodey, A. Sanchez-Gonzalez, B. Erk, C. Bomme, R. Boll, Z. Yin, V. P. Majety, R. Steinbrügge, M. A. Khalal, F. Penent, J. Palaudoux, P. Lablanquie, A. Rudenko, D. Rolles, J. R. Crespo López-Urrutia and N. Rohringer

Affiliation details at
https://journals.aps.org/prl/abstract/10.1103/PhysRevLett.123.023201

When an X-ray free-electron laser behaves as a real laser

Hanbury Brown and Twiss interferometry at a seeded free-electron laser

X-ray free-electron lasers (XFELs) provide very bright coherent X-ray radiation and are considered to be laser sources at these photon energies. XFELs are highly spatially coherent to the first order but in spite of their name, they behave statistically as chaotic sources. Here, we demonstrate experimentally, by combining Hanbury Brown and Twiss (HBT) interferometry with spectral measurements, that the externally-seeded XUV FERMI source does indeed behave statistically as a laser.

Glauber in his pioneering work [1] stated that a truly coherent source of radiation should be coherent in all orders of intensity correlation functions. Single-mode or phase-locked optical lasers are not only coherent in the first order, but also in the second order of intensity correlation functions [2]. This distinguishes laser sources from chaotic radiation sources, a difference especially important for quantum-optics experiments that are extended now to classical fields [3], in which high-order coherence properties of the source play an important role. The possibility of employing similar properties of sources in the X-ray range with extremely high brightness is the main attraction for completely new and exciting applications of XFELs.

Most of the presently operating XFELs generate radiation using the self-amplified spontaneous emission (SASE) process, where the radiation is produced stochastically by the electron-bunch shot noise. As a result, SASE FELs are spatially highly coherent sources in first order, but, from a statistical point of view, they behave as chaotic sources of radiation [4]. FERMI is the first externally-seeded single-pass FEL in the XUV regime [5]. A question naturally arises: Is the seeded FERMI FEL coherent in higher orders, thus satisfying the definition of Glauber?

The basic idea behind HBT interferometry [6] is to extract statistical properties of radiation from the normalised second-order intensity correlation function

$$g^{(2)}(r_1, r_2) = \frac{\langle I(r_1) \cdot I(r_2)\rangle}{\langle I(r_1)\rangle\langle I(r_2)\rangle}, \qquad (1)$$

where $I(r_1)$ and $I(r_2)$ are intensities at different spatial positions measured simultaneously, and the brackets $\langle \ldots \rangle$ denote averaging over a large ensemble of different radiation pulses. The statistical behaviour of the $g^{(2)}$-function is fundamental in quantum optics [2] and strongly depends on the radiation type. For example, for coherent laser sources the $g^{(2)}$-function is equal to one, but for chaotic sources it behaves quite differently [2].

The experiment was performed at the DiProI end station of FERMI and acquiring simultaneously data from the online spectrometer PRESTO (Fig. 1). Importantly, FERMI operation can be switched from seeded to SASE mode. We first analysed the X-ray intensity distribution of the FEL pulses in the seeded and SASE regimes of FERMI by employing HBT correlation analysis using Eq. (1) (Fig. 2a–d). The contrast values $\zeta = g^{(2)}(0,0) - 1$ were on the order of 0.03–0.04 for the seeded beam and significantly higher, at about 0.1–0.15 for the SASE mode. This difference between the two regimes of operation becomes more evident by analysis of the corresponding spectral profiles.

Both, in the seeded and SASE regimes of FERMI operation, the average spectrum was Gaussian in shape but with a relative bandwidth of $4.6 \cdot 10^{-4}$ (seeded mode) and $6 \cdot 10^{-3}$ (SASE) that was an order of magnitude broader (Fig. 2c,d). From our online spectrometer measurements, we observed in the seeded regime from one to five modes, varying from pulse to pulse, with one mode usually dominating. This should provide values of contrast close to 2 for a chaotic source and does not match the low value of contrast ζ determined in the experiment. At the same time, the values

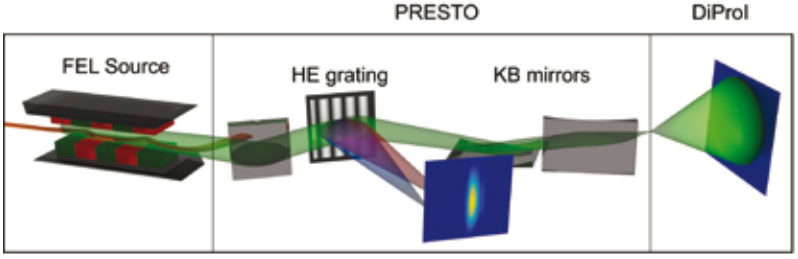

Figure 1

Schematic layout of the experiment. Radiation generated in the undulators is focused by Kirkpatrick–Baez mirrors into the DiProI end station and the detector is installed out of focus to observe the direct beam. Radiation from each pulse is partially diffracted by a grating to the PRESTO spectrometer detector to observe online pulse spectra.

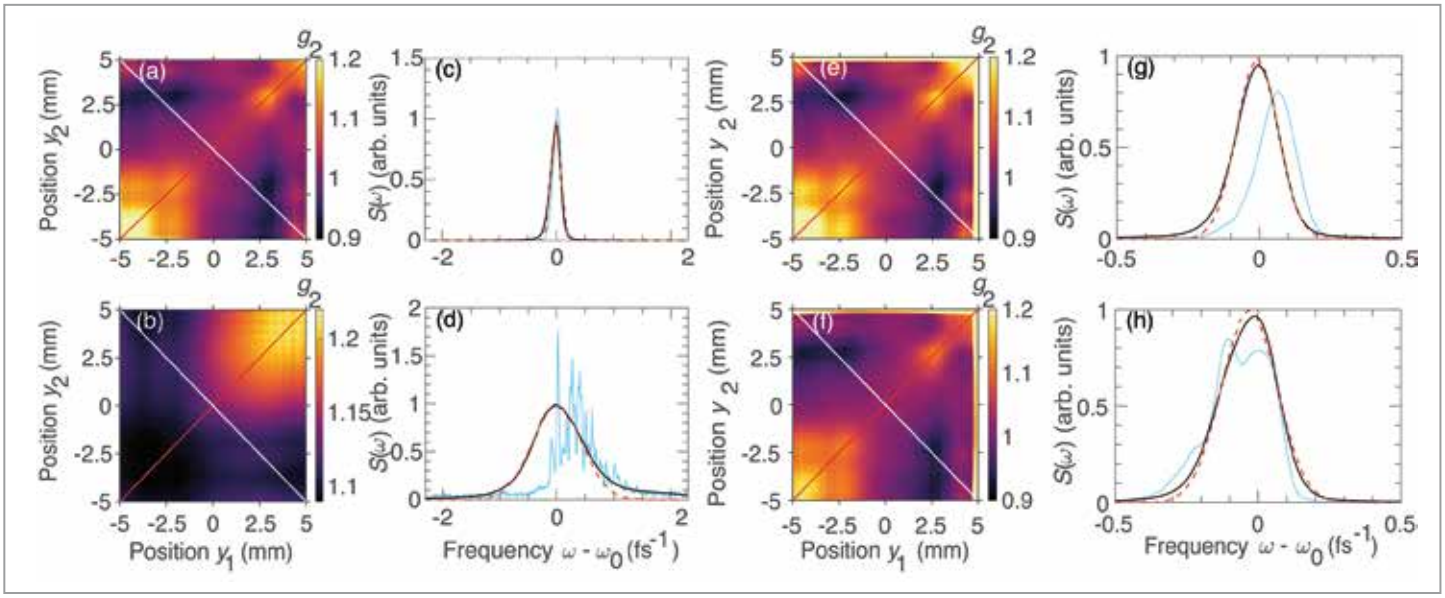

Figure 2

(a-d) Correlation functions and spectra measured in the seeded and SASE modes of operation. Intensity correlation functions for seeded (a) and SASE (b) regimes of operation in vertical directions. (c-d) Spectral structure of an individual pulse (blue line), average spectrum (black line), and Gaussian fit (red dashed line) for seeded (c) and SASE (d) regimes. (e-h) Seeded-mode single and multiple-pulse analysis. Intensity correlation functions (e, f) and spectral structure (g, h) for the sorted pulses with the lowest (e, g) and highest (f, h) number of modes. In (g, h) representative single pulses are shown by blue lines, an average over 10^3 pulses is shown by black lines, and Gaussian fit by red dashed lines.

of contrast ζ obtained in SASE mode match the number of observed spectral modes (about 10), supporting the assumption of chaotic character of the source in the SASE regime.

Next, we analysed the spectral dependence of the $g^{(2)}$-function in the seeded regime of operation by implementing a sorting procedure. Two data sets were then considered: Pulses with the largest contribution of the main mode and pulses with the smallest contribution. Intensity correlation functions (Eq. (1)) are shown in Fig. 2 (e,f) and cases of the single and multi-mode pulses are given in Fig. 2 (g,h). Remarkably, these two data sets produce correlation functions with low values of contrast ζ of about 0.02 and 0.07 for both data sets. As such, we conclude that the seeded FERMI source is behaving as a laser source, even in the case when several modes are present in the spectrum. This implies that the spectral modes are potentially phase locked, which is an important finding for coherent-control experiments.

A combination of HBT interferometry and spectral measurements has allowed us to demonstrate that a seeded FEL is fundamentally different in its statistical properties from a SASE-based FEL. These measurements are a decisive step forward in understanding the basic properties of FELs. While SASE FELs behave statistically as chaotic sources, the seeded FERMI FEL is equivalent in its statistical properties to a coherent laser in the definition of Glauber. By that, we foresee that seeded FELs are opening new opportunities for quantum-optics experiments and for the design and operation of next-generation XFEL sources.

Author contact: Ivan Vartaniants, ivan.vartaniants@desy.de

References

1. R. J. Glauber, 'The quantum theory of optical coherence', Phys. Rev. 130, 2529–2539 (1963).
2. R. Loudon, 'The quantum theory of light', 3rd edn, (Oxford University Press, Great Britain, 2000).
3. R. Schneider et al., 'Quantum imaging with incoherently scattered light from a free-electron laser', Nat. Phys. 14, 126–129 (2018).
4. A. Singer et al., 'Hanbury Brown-Twiss interferometry at a free-electron laser', Phys. Rev. Lett. 111, 034802 (2013). Erratum: 117, 239903(E) (2016).
5. E. Allaria et al., 'Two-stage seeded soft-X-ray free-electron laser', Nat. Photon. 7, 913–918 (2013).
6. R. Hanbury Brown and R. Q. Twiss, 'A test of a new type of stellar interferometer on Sirius', Nature 178, 1046–1048 (1956).

Original publication

'Seeded X-ray free-electron laser generating radiation with laser statistical properties', Nature Communications, 9, 4498 (2018). DOI: 10.1038/s41467-018-06743-8

Oleg Yu. Gorobtsov[1,9], Giuseppe Mercurio[2,10], Flavio Capotondi[3], Petr Skopintsev[1,11], Sergey Lazarev[1,4], Ivan A. Zaluzhnyy[1,5,12], Miltcho B. Danailov[3], Martina Dell'Angela[6], Michele Manfredda[3], Emanuele Pedersoli[3], Luca Giannessi[3,7], Maya Kiskinova[3], Kevin C. Prince[3,8], Wilfried Wurth[1,2] and Ivan A. Vartanyants[1,5]

1. Deutsches Elektronen-Synchrotron DESY, Hamburg, Germany
2. Department of Physics, University of Hamburg and Center for Free Electron Laser Science, Hamburg, Germany
3. Elettra-Sincrotrone Trieste, Basovizza (Trieste), Italy
4. National Research Tomsk Polytechnic University (TPU), Tomsk, Russia
5. National Research Nuclear University MEPhI (Moscow Engineering Physics Institute), Moscow, Russia
6. CNR-IOM – Istituto Officina dei Materiali, Trieste, Italy
7. ENEA C.R. Frascati, Frascati, Rome, Italy
8. Centre for Translational Atomaterials, Department of Chemistry and Biotechnology, School of Science Swinburne University of Technology, Melbourne, Australia
9. Present address: Department of Materials Science and Engineering, Cornell University, Ithaca, USA
10. Present address: European XFEL GmbH, Schenefeld, Germany
11. Present address: Laboratory for Biomolecular Research, Division of Biology and Chemistry, Paul Scherrer Institute, Villigen, Switzerland
12. Present address: Department of Physics, University of California San Diego, La Jolla, USA

The taming of the light screw

A new knob to control and create higher-order harmonic light from solids

The study of lightwave-driven electronic dynamics occurring on sub-optical-cycle time scales in condensed matter and nanosystems is a fascinating frontier of attosecond science, which was originally developed in atoms and molecules. Adapting attosecond metrology techniques to observe and control the fastest electronic dynamics in the plethora of solids and novel quantum materials is very promising for studying correlated electronic dynamics on atomic length and ultrashort time scales, thereby potentially impacting future technologies such as petahertz electronic signal processing or strong-field optoelectronics. Here, we introduce polarisation-state-resolved high-harmonic spectroscopy of solids, which opens up new avenues for spectroscopic studies of strongly correlated, topological, and magnetic materials.

When atoms and molecules interact with strong laser pulses they emit high-order harmonics of the fundamental driving laser field. This high-order harmonic generation (HHG) in gases is one of the cornerstones of attosecond science and nowadays routinely used to produce isolated attosecond pulses and coherent radiation ranging from the visible to soft X-rays. Because of their higher electronic density, solids are one promising route towards compact, brighter HHG sources allowing for many new applications. However, whereas the HHG process in gases is well understood within the intuitive three-step model of HHG, the underlying microscopic mechanism in solid materials is still the subject of scientific controversy [1]. Here, by combining HHG experiments and state-of-the-art time-dependent density functional theory (TDDFT) simulations, we introduce polarisation-state-resolved high-harmonic spectroscopy of solids, which permits deeper insights into both electronic and structural dynamics due to its inherent sub-optical-cycle temporal resolution.

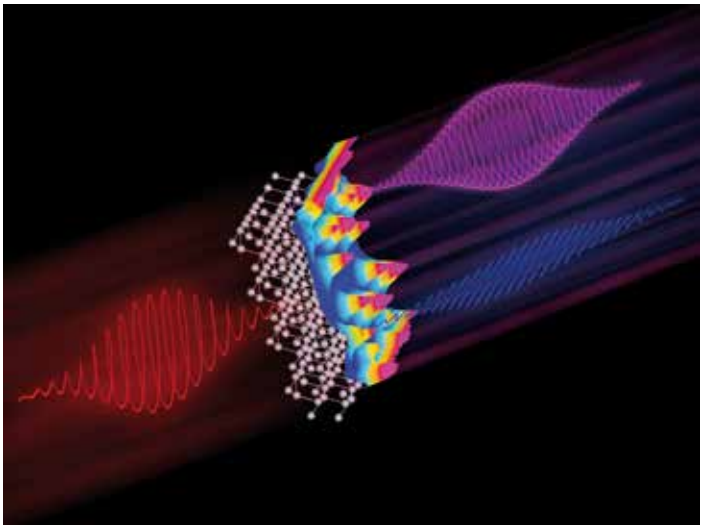

Figure 1

When an intense laser field (red) interacts with a crystalline solid (white), higher-order harmonic fields (blue and magenta) are emitted, whose polarization states (linear, elliptic or circular) are determined by crystal symmetry and can be controlled by the strong-field dynamics. The colormap surface shows the ellipticity of the ninth harmonic (HH9) from silicon. Image: Jörg Harms / MPSD.

In 2017, we predicted [2] that by using elliptically polarised driving pulses, it should be possible to unravel the complex interplay between the two mechanisms – interband and intraband electronic dynamics – responsible for HHG in solids. By means of *ab initio* TDDFT simulations we have shown how these two mechanisms are strongly and differently affected by the ellipticity of the driving laser field. The interplay between these effects can be used to tune and optimize harmonic emission in solids. We also predicted the possibility of generating circularly polarised harmonics with alternating helicities from a single circularly polarised driving field. In principle, such a process is symmetry forbidden in atoms. In fact, as illustrated in Fig. 1, we theoretically predicted and experimentally observed in silicon and quartz that the emitted harmonic fields can oscillate in a linear fashion, or they can rotate elliptically or circularly with clockwise or anticlockwise helicity, just like a screw of light, sensitively depending on the complex electronic dynamics in the crystal.

In our HHG experiments shown in Figs. 2 and 3, we irradiated free-standing 2 µm thin (100)-cut silicon samples with 120 fs, 2.1 µm pulses obtained from an optical parametric amplifier with tunable ellipticity ε and peak intensities up to 0.7 TW/cm^2 in vacuum. For the highest driver intensities one enters

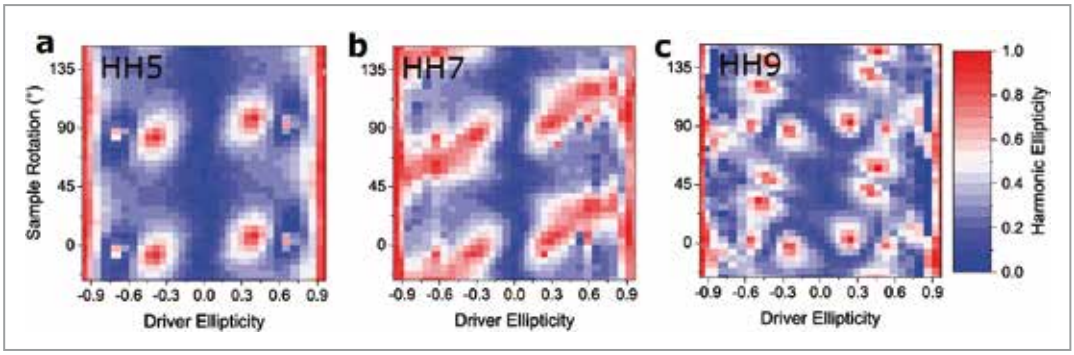

Figure 2

(a) Measured harmonic ellipticity $|\varepsilon_{HH}|$ of the fifth harmonic HH5, the seventh harmonic HH7 (b), and the ninth harmonic HH9 (c) from silicon as function of driver pulse ellipticity and sample rotation. The peak driving intensity is 0.6 TW/cm² in vacuum.

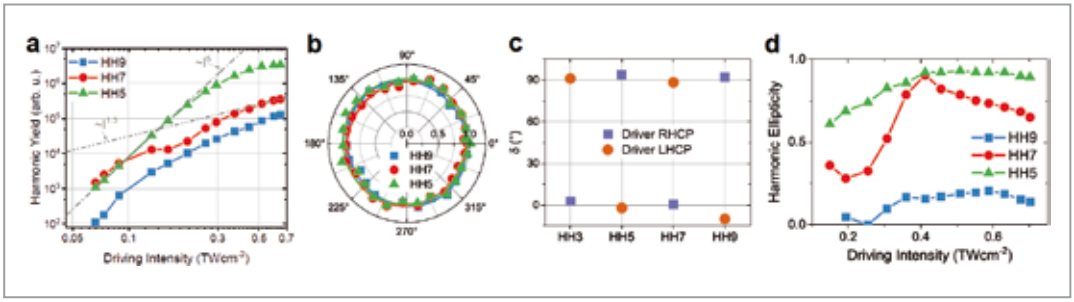

Figure 3

High-order harmonic generation from silicon: (a) Measured harmonic yields versus driving intensity for driving ellipticity $\varepsilon = 0$. For the highest intensities, one enters the nonperturbative strong-field interaction regime. (b) Normalised harmonic intensity versus polariser rotation angle, indicating circular polarisation (also confirmed by Stokes parameter measurements). (c) Analysis of harmonic helicities, the angle $\delta = 90°/0°$ corresponds to right/left-handed circular polarisation (RHCP/LHCP). (d) Harmonic ellipticities $|\varepsilon_{HH}|$ versus driving intensity for driving ellipticity $\varepsilon = 0.4$ and sample rotation $\theta = \Gamma X + 10°$, indicating strong-field control of the harmonic ellipticities.

the nonperturbative strong-field interaction regime as can be seen in Fig. 3a. We measured the harmonics' intensities (not shown) and ellipticities (see Fig. 2) as a function of driver pulse ellipticity ε and sample rotation θ. Interestingly, all harmonics shown in Fig. 2 respond in a distinctly different way to the driver pulse ellipticity ε, which can be explained by the different response of interband and intraband dynamics to driver ellipticity. Our experiments reveal that the polarisation states of the harmonics, i.e. the harmonics' ellipticities (Fig. 2 and Fig. 3b) and helicities (Fig. 3c) are not only determined by crystal symmetries, but can be dynamically controlled (Fig. 3d), as a consequence of the intertwined interband and intraband electronic dynamics. We exploit this symmetry-dynamics duality to efficiently generate coherent circularly polarised harmonics from elliptically polarised pulses. Finally, we have also experimentally confirmed the harmonics' temporal and spatial coherence in silicon.

The present work investigates the prototype materials silicon and quartz to establish this new spectroscopic technique. Yet the method is versatile and expected to find important applications in future studies of novel quantum materials such as strongly correlated materials [3, 4], topological insulators [5], and magnetic materials. Moreover, compact sources of bright circularly polarised harmonics in the XUV regime might advance our tools for the spectroscopy of chiral systems and 2D materials with valley selectivity.

Author contact: Oliver D. Mücke, oliver.muecke@cfel.de
Nicolas Tancogne-Dejean, nicolas.tancogne-dejean@mpsd.mpg.de
Franz X. Kärtner, franz.kaertner@cfel.de
Angel Rubio, angel.rubio@mpsd.mpg.de

References

1. N. Tancogne-Dejean, O. D. Mücke, F. X. Kärtner and A. Rubio, 'Impact of the electronic band structure in high-harmonic generation spectra of solids', Phys. Rev. Lett. 118, 087403 (2017)
2. N. Tancogne-Dejean, O. D. Mücke, F. X. Kärtner and A. Rubio, 'Ellipticity dependence of high-harmonic generation in solids originating from coupled intraband and interband dynamics', Nature Commun. 8, 745 (2017)
3. N. Tancogne-Dejean, M. A. Sentef and A. Rubio, 'Ultrafast modification of Hubbard *U* in a strongly correlated material: *Ab initio* high-harmonic generation in NiO', Phys. Rev. Lett. 121, 097402 (2018)
4. R. E. F. Silva, I. V. Blinov, A. N. Rubtsov, O. Smirnova and M. Ivanov, 'High-harmonic spectroscopy of ultrafast many-body dynamics in strongly correlated systems', Nature Photonics 12, 266 (2018)
5. R. E. F. Silva, Á. Jiménez-Galán, B. Amorim, O. Smirnova and M. Ivanov, 'Topological strong-field physics on sub-laser-cycle timescale', Nature Photonics 13, 849 (2019)

Original publication

'Polarization-state-resolved high-harmonic spectroscopy of solids', Nature Commun. 10, 1319 (2019). DOI: 10.1038/s41467-019-09328-1

N. Klemke[1,2], N. Tancogne-Dejean[1,3], G. M. Rossi[1,2], Y. Yang[1,2], F. Scheiba[1,2], R. E. Mainz[1,2], G. Di Sciacca[1], A. Rubio[1,2,3,4,5], F. X. Kärtner[1,2,4] and O. D. Mücke[1,4]

1. Center for Free-Electron Laser Science CFEL, Deutsches Elektronen-Synchrotron DESY, Hamburg, Germany
2. Physics Department, University of Hamburg, Hamburg, Germany
3. Max Planck Institute for the Structure and Dynamics of Matter MPSD, Hamburg, Germany
4. The Hamburg Centre for Ultrafast Imaging CUI, University of Hamburg, Hamburg, Germany
5. Center for Computational Quantum Physics CCQ, The Flatiron Institute, New York, USA

Ultraviolet ‘speed camera’

A new tool to access DNA damage on the electronic time scale

In the last few decades, ultrashort laser pulses have been exploited for the investigation of the microscopic world, allowing for faster and faster physical processes to be captured in real-time. Electron dynamics in molecules following UV light absorption is expected to be the basis of many biological processes, such as DNA damage and photo-protection. An extremely high temporal resolution is required to track these processes at their natural time scale, typically ranging from few femtoseconds down to attoseconds.

In a prototypical laser-assisted time-resolved experiment, a first light burst is used to illuminate the target under study and potentially trigger a dynamical response, which is then probed by a second delayed light burst. After light absorption, a molecular system can react on a time scale which ranges from seconds – for instance when considering structural changes in large proteins – down to attoseconds (10^{-18} s) when considering the pure electronic rearrangement [1].

While the real-time investigation and control of the electron dynamics may provide a unique tool to access the molecular reactivity at extreme time scales and to enable new functionalities, this field of research is still at its infancy. So far, electron dynamics has been only addressed using sub-femtosecond light pulses generated via the extremely non-linear process referred to as high-order harmonic generation [2]. Although this method is very effective for the generation of sub-femtosecond pulses, it has the drawback of low conversion efficiency and it is mostly limited to the extreme-ultraviolet (XUV) or soft X-ray spectral ranges [3].

Nevertheless, a number of processes relevant for photochemistry and photobiology are triggered by the interaction with much less energetic photons, typically in the UV spectral region. In most molecules for example, the excess of energy gained by absorbing a UV photon is often dissipated via non-radiative decay. Upon UV excitation, ultrafast conversion of electronic energy into vibrational modes has been demonstrated to be at the core of fundamental processes such as DNA damage and photoprotection [4].

Nowadays, the generation of ultrashort deep UV (200 - 300 nm) pulses is still extremely challenging. Typically, such pulses are produced by up-converting a near-infrared (NIR) laser pulse in a nonlinear crystal. With this method, the shortest achievable UV pulse is limited by optical dispersion and phase matching constraints in the crystal, making durations shorter than 10 fs hardly reachable. To circumvent this limitation, we developed a novel method based on third harmonic generation (THG) of a 5 fs NIR pulse in a gas target, where dispersion effects are dramatically reduced. With this approach, we demonstrated the generation of 1.9 fs duration deep UV pulses, with a spectrum extending from 210 nm to 340 nm, and an energy of 150 nJ per pulse.

We implemented this setup within an ultra-high vacuum (UHV) beamline, that allows the deep UV pulses to be

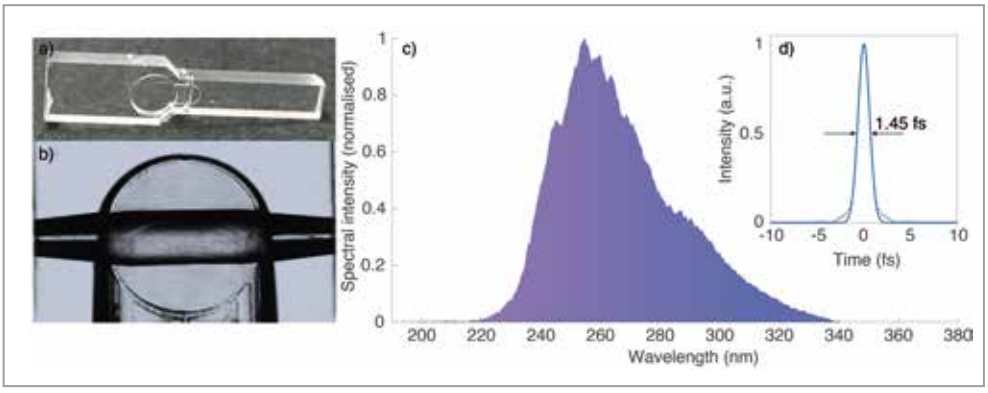

Figure 1

(a) Gas cell used to generate the UV pulses. (b) Magnified image of the channel through which the laser is propagating. (c) Measured UV spectrum at the maximum efficiency. (d) Transform limited temporal profile of the spectrum in (c) (grey dots) and correspondent Gaussian fit (blue solid line) showing a duration of 1.45 fs (FWHM).

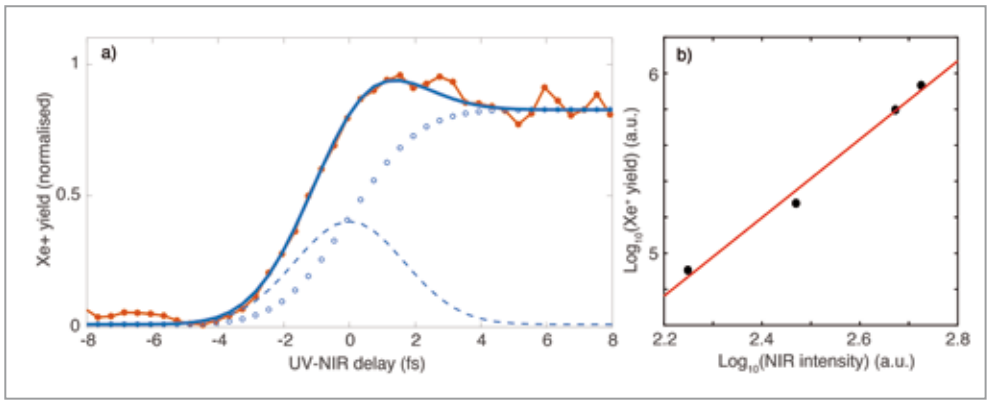

Figure 2

(a) UV-NIR cross-correlation signal acquired in xenon (red dotted line). The blue solid line shows the fit consisting of two contributions: (i) Gaussian-like UV+NIR direct ionisation (blue dashed line), (ii) error-function-like resonance-enhanced transition (blue circles). (b) Scaling (black dots) of the peak cross-correlation signal as a function of the NIR intensity in bi-logarithmic scale. The trend is fitted with a linear function (red solid line), showing a dominant 2-NIR-photon absorption (slope m = 2.18 ± 0.35).

combined with isolated XUV attosecond pulses in a UV-pump XUV-probe measurement scheme in an interferometric approach, allowing for unprecedented time resolution. The NIR beam used to generate the UV radiation was focused into a gas cell filled with argon where the THG process was obtained. The gas cell, shown in Fig. 1a,b, has been fabricated in a fused silica slab using femtosecond laser irradiation followed by chemical etching (FLICE). The use of a laser-machined fused silica cell presents several advantages with respect to more traditionally employed metallic ones: (1) the geometry can be arbitrarily set with extremely high precision (few μm); (2) contrary to metals, glass offers a high transmittance for VIS-NIR radiation, preventing the cell to be damaged by the impinging ultra-intense laser beam; (3) if embedded in a differential pumping system, a high gas pressure (several bars) can be used.

Figure 1c shows the measured spectrum of the UV pulses generated with the maximum efficiency at an argon gas pressure of 1.2 bar. The spectrum extends from 210 to 340 nm, corresponding to a transform limited (TL) duration (Fig. 1d) of 1.45 fs. The temporal characterisation of the UV pulses was performed through cross-correlation with a residual portion of the 5 fs NIR pulses used for THG by ionising a Xe gas target and collecting the UV-NIR delay-dependent yield of Xe^+ ions. In Fig. 2a the cross-correlation signal (red dotted line) and the correspondent fitting curve (blue solid line) are plotted. The ionisation process – as well as the fit model – consists of two main contributions, i.e. a Gaussian-like direct photo-ionization contribution (blue dashed line) and a resonance-enhanced contribution (blue circles). The latter – modelled as an error function – originates from a two-UV-photon excitation of a long-lived Rydberg state of Xe. Both terms involve the absorption of two NIR photons, highlighted by the linear trend with slope m = 2.18 ± 0.35 of the bi-logarithmic NIR intensity scaling of the cross-correlation signal in Fig. 2b.

From the cross-correlation measurement we retrieved a duration of 1.9 ± 0.3 fs (FWHM) for the UV pulses, very close to the transform limited duration thus indicating a limited dispersion acting on the generated UV pulses. Our scheme opens up new perspectives for investigating the role of the electron dynamics in the photochemical processes activated by the absorption of UV light, thus paving the way for a future attosecond time-resolved ultraviolet molecular spectroscopy.

Author contact: Andrea Trabattoni, andrea.trabattoni@desy.de
Francesca Calegari, francesca.calegari@desy.de

Reference

1. F. Lepine et al., 'Attosecond molecular dynamics: fact or fiction?', Nature Photonics 8, 195–204 (2014).
2. P. B. Corkum, 'Plasma perspective on strong field multiphoton ionization', Phys. Rev. Lett. 71, 1994 (1993).
3. F. Calegari et al., 'Advances in attosecond science', J. Phys. B 49, 062001 (2016).
4. C. E. Crespo-Hernandez et al., 'Base stacking controls excited-state dynamics in A·T DNA', Nature 436, 1141 (2005).

Original publication

'Generation of deep ultraviolet sub-2-fs pulses', Opt. Lett. Vol. 44, No. 6, 1308–1311 (2019). DOI: 10.1364/OL.44.001308

Mara Galli[1,2,3], Vincent Wanie[1,4], Diogo Pereira Lopes[2], Erik P. Månsson[1], Andrea Trabattoni[1], Lorenzo Colaizzi[1], Krishna Saraswathula[1], Andrea Cartella[5], Fabio Frassetto[6], Luca Poletto[6], François Légaré[4], Salvatore Stagira[2,3], Mauro Nisoli[2,3], Rebeca Martínez Vázquez[3], Roberto Osellame[3] and Francesca Calegari[1,3,5,7]

1. Center for Free-Electron Laser Science (CFEL), DESY, Hamburg, Germany
2. Physics Department, Politecnico di Milano, Milano, Italy
3. Institute for Photonics and Nanotechnologies, IFN-CNR, Milano, Italy
4. Institut National de la Recherche Scientifique, Centre Énergie Matériaux et Télécommunications, Varennes, Canada
5. The Hamburg Centre for Ultrafast Imaging, Universität Hamburg, Hamburg, Germany
6. Institute for Photonics and Nanotechnologies, IFN-CNR, Padova, Italy
7. Department of Physics, Universität Hamburg, Hamburg, Germany

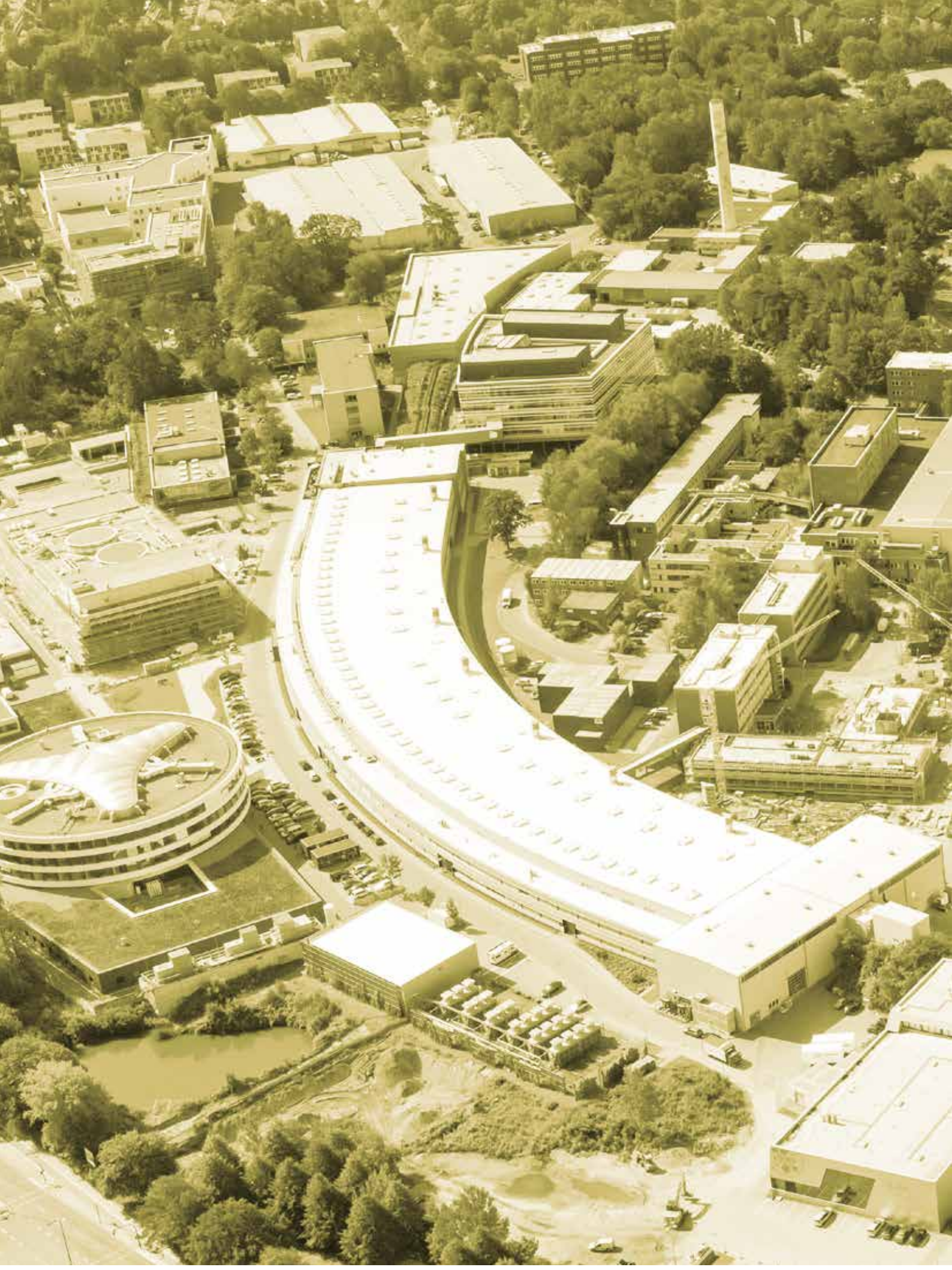

Light Sources

FLASH

Seeds for the future

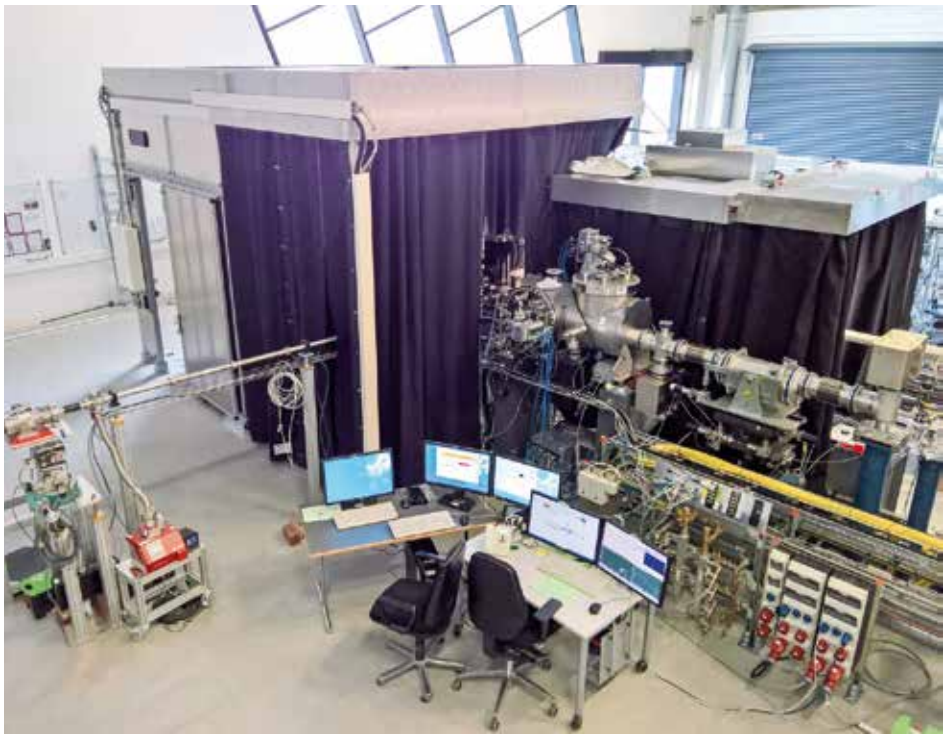

Figure 1
End of the FLASH2 beamline FL24 with a large (~18 m²) laser hutch at left housing the users' experimental chamber and a smaller laser hutch (at right, behind the last beamline mirrors) where the final compression and generation of laser harmonics takes place, just before coupling the laser into the FEL beamline towards the experiment. The tubes at the lower left are a 'side arm' of the FEL beamline with a wavefront sensor at its end which is used to characterise the experiment's focus shape and size of the FEL beam.

In 2019, successful and stable user operation at FLASH was provided at both undulator lines, FLASH1 and FLASH2, with an all-time high of about 4600 hours machine operation for users in total and a record machine availability of 98%. Free-electron laser (FEL) beam was provided for about 3700 hours into the 'Albert Einstein' experimental hall (FLASH1) and for about 2750 hours into the 'Kai Siegbahn' hall (FLASH2).

In parallel, we further ramped up the experimental capabilities in the 'Kai Siegbahn' hall, now also delivering the optical laser for time resolved experiments to users at beamline FL24, starting operation of a dedicated terahertz (THz) streaking beamline FL21 for pulse length diagnostics, bringing a vacuum-ultraviolet (VUV) high harmonics generation (HHG) laser source into operation at the Reaction Microscope at beamline FL26, and finalising our plans for a monochromator beamline FL23 that will preserve the short FEL pulse length. In addition to the day-to-day machine operation and all the new installations for our present user facility portfolio, the plans for the future of FEL science at FLASH within the FLASH2020+ upgrade programme were also further refined. The conceptual design report (CDR) is finalised and currently a detailed technical design is in preparation.

Optical pump-probe laser now available at FLASH beamline FL24
Since spring 2019, the FLASH2 optical pump-probe laser is now also available at beamline FL24 and has been successfully used in eight experiments already. Figure 1 shows the hutches for laser protection at the end of beamline FL24. On the left, a large laser hutch for user experiments and on its right side and closely linked, a smaller laser hutch called MOD (modular optical delivery station) is set up. Here, the optical laser pulses are compressed to their final length and harmonics of the 800 nm fundamental are generated according to users' needs before focusing and coupling the laser into the FEL beamline towards the experiment.

New beamline FL21 with a dedicated THz streaking end station
The new beamline FL21 was recently installed in the FLASH2 experimental hall. It is featuring two branches: the straight beamline provides an unfocused FEL beam that can be used for non-permanent photon diagnostics or exploratory experimental setups (Fig. 2, right beamline in CAD drawing). The second branch leads to a dedicated FEL pulse duration lab (Fig. 2) in its own 2.5 × 4 m² laser safety enclosure (photo in Fig. 2). A splitting mirror at the branching can be used to geometrically cut a freely selectable fraction of the incident FEL beam and reflect it towards the pulse length diagnostics setup based on the THz streaking technique [1 and references therein]. The FEL beam is focused by a toroidal mirror into a permanently installed experimental chamber containing a gas jet, several electron time-of-flight (TOF) detectors and other diagnostics. Single-cycle THz pulses generated by an infrared (IR) drive laser are used for the pulse duration measurement.

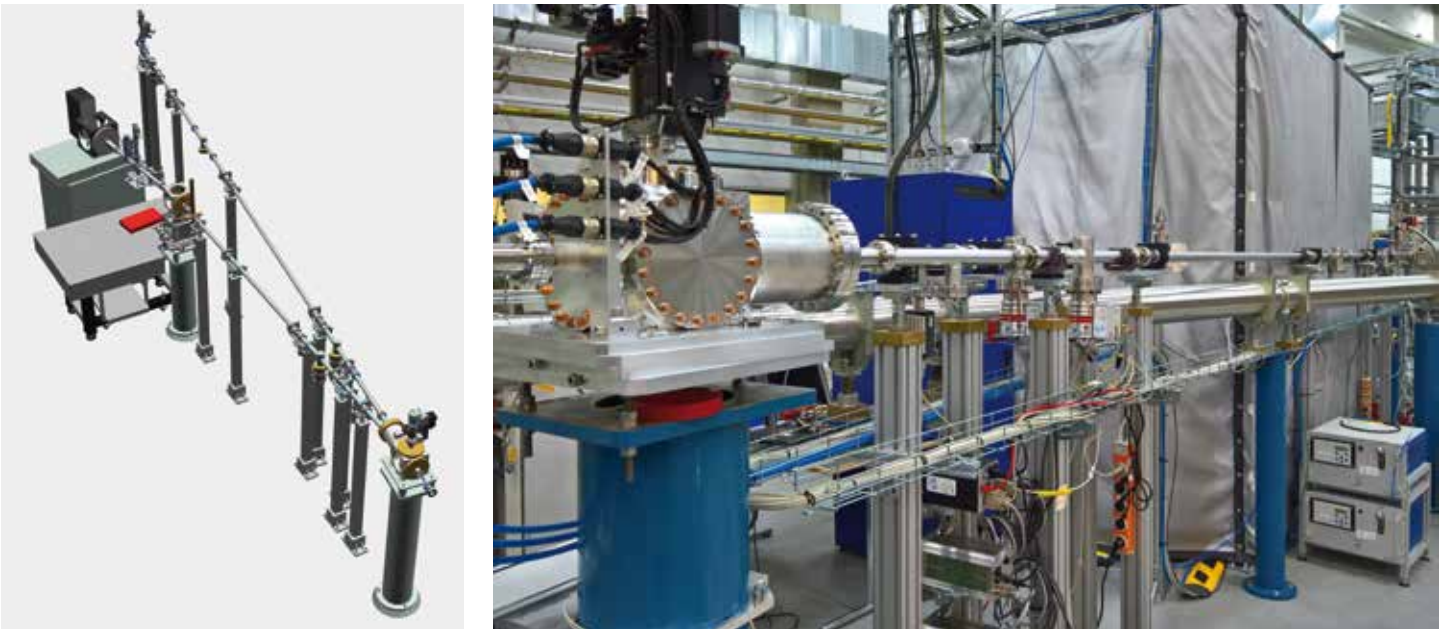

Figure 2

Left: CAD drawing of the end of the FLASH2 beamline FL21 (FEL beam coming from bottom) with 2 branches: pulse length diagnostics (left) and open port for exploratory setups (right). Right: photo of the same area, now with laser tent around pulse length diagnostics (FEL entering from left side).

Further experience with the THz streaking technique, in particular concerning measurement uncertainties and achievable resolution shall be gained at FL21. The goal is to provide a reliable pulse duration measurement setup in the medium term. Thanks to the splitting mirror, an online-measurement of the pulse duration parallel with an experiment in the straight branch at right is feasible. First THz streaking measurements in autumn 2019 were not only used for FEL pulse length determination but also turned out to be quite suitable for monitoring the pulse arrival time. Comparing the peak position of the streaking signal in time with a beam arrival monitor (BAM) signal for the electrons in the accelerator yielded a remarkable agreement. Both signals coincide within better than 20 fs (rms) over a time scale of tens of minutes.

New HHG laser source at FLASH beamline FL26

An HHG source driven by the FLASH2 pump-probe laser has recently been incorporated in the beamline FL26 at FLASH2. It was realised within the framework of a BMBF collaborative research ('Verbundforschung') project, named SynVLiFL ('Synchrone VUV Lichtquelle an FLASH2'), led by the Leibniz Universität Hannover (Uwe Morgner, Milutin Kovacev et al.) with strong involvement of the 'Laser Science and Technology' group at DESY. The HHG performance is currently being optimised with the aim of carrying out first pump-probe experiments in conjunction with the FEL at the FL26 Reaction Microscope end station (ReMi).

The HHG beamline consists of four main parts (Fig. 3a):

- The HHG chamber, where high harmonics can be generated either in a semi-infinite gas cell (SIGC) or in a gas jet.
- A double filter wheel (FW), with thin metal filters to block the remaining IR driving radiation and/or select different harmonics regions.
- An in-coupling mirror chamber (IM), where a hyperboloidal C-coated mirror reflects and collimates the higher harmonics beam, blocking at the same time the upper half of the FEL beam. The lower half of the FEL propagates below the mirror, parallel to the higher harmonics (Fig. 3b).
- A transmission spectrometer (SM) for the spectral analysis of the harmonics beam [2].

Behind the in-coupling chamber the FEL and harmonics beams co-propagate across the split-and-delay unit mirrors (SDM) (Fig. 3b) and the ellipsoidal mirror (FM) of FL26 which focuses both beams in the ReMi.

So far, harmonics up to the 23rd order (34 nm) driven by 800 nm in the SIGC have been clearly observed (Fig. 3c). The beam was successfully steered and focused into the ReMi and could be observed on the interaction screen there. Along with the HHG source commissioning, first measurements in the REMI, where argon atoms were ionised and the energy spectra of the released electrons were recorded, already

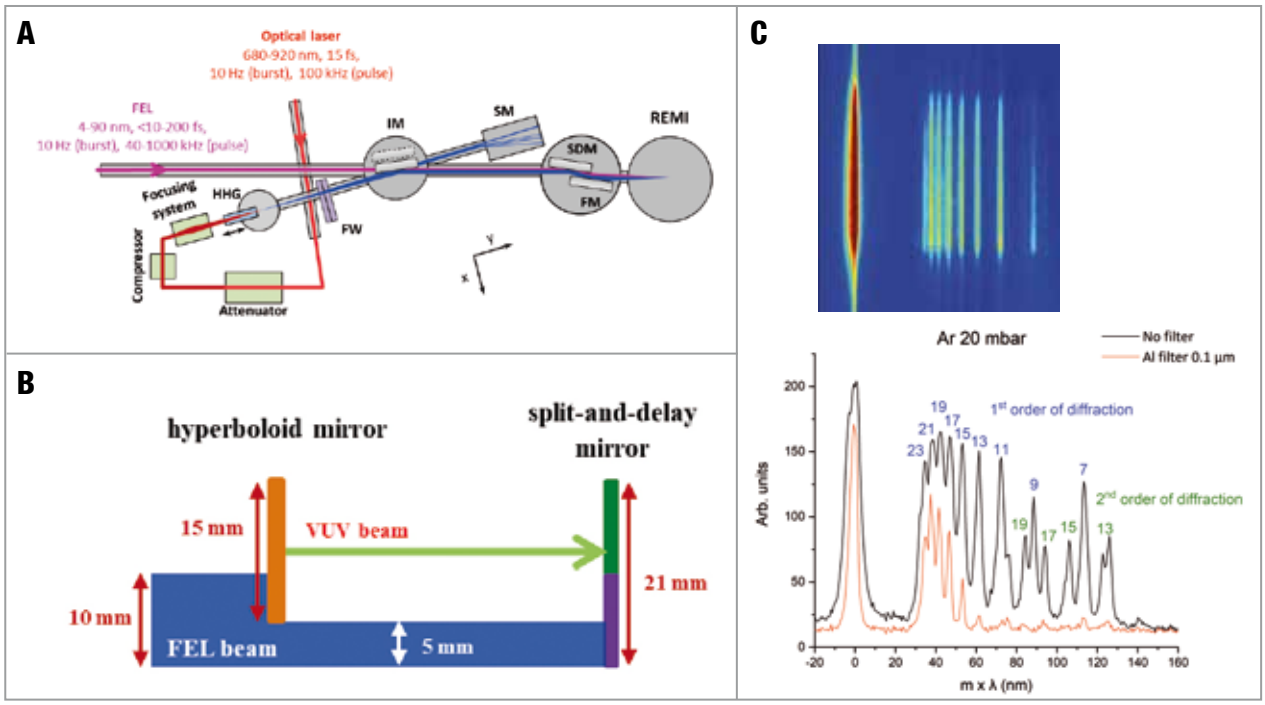

Figure 3

a) HHG beamline incorporated in the FL26 beamline at FLASH. HHG: High Harmonic Generation chamber, FW: filter wheel, IM: in-coupling mirror chamber, SM: spectrometer, SDM: split-and-delay mirror, FM: focusing ellipsoidal mirror. b) The lower part of the FEL beam is centred in the lower half of the split-and-delay mirror. c) Harmonics spectrum on the phosphor screen, calibrated with respect to m × λ (m: order of diffraction, λ: wavelength).

demonstrate the potential of this new laser source, as well as its long-term stability [3].

As next steps, the HHG generation is being optimised in terms of the focus position in the SIGC, the gas parameters as well as the driving wavelengths (using shorter driver wavelengths). After these optimisations the generation efficiency is expected to increase [4] and the HHG source will be exploited in some first test experiments together with the ReMi team.

Further detailed source specifications will be available for all potential users once the HHG source is fully characterised and ready for user experiments.

Time-delay compensating monochromator beamline planned as FLASH beamline FL23

For many research areas which require a narrower spectral bandwidth of the photon pulse than the 'natural' bandwidth of FLASH, ultra-short pulse-length below 50 fs and high peak brightness are still prerequisites. However, by using a monochromator with a single grating, the FEL pulse is stretched proportionally to the required resolution, according to the number of illuminated lines of the grating. Typical FLASH wavelengths and resolving powers of a few thousands result in pulse lengths stretched to a few hundred femtosconds. By using a two-grating monochromator design [5, 6 and references therein] instead, the initial ultra-short pulse length of FLASH can be preserved. The requirements of user experiments for such a 'time-delay compensating monochromator' (TDCM) were evaluated in a workshop in July 2017 and are summarised in the table below.

Wavelength (incl. harmonics)	(nm)	1.2 - 20.0
Pulse length	(fs)	< 50
Resolution	(λ/ Δλ)	≥ 2000
Flux at beamline end	(photons/pulse)	10^{10}

The simulations in reference [5] show that these required performance values can mostly be reached. At the long wavelength end, however, one might have to trade pulse length for resolution, because one reaches the Fourier limit.

To maximise the beamline throughput and the transmission efficiency, the number of optical elements was minimised in the TDCM beamline (see Fig. 4).

Meanwhile this new TDCM beamline FL23 at FLASH2 is in the technical design and procurement phase. It is expected to be installed and commissioned in late 2021. With its medium resolution while preserving the pulse length and with its focus on the short wavelength range, it will complement the high resolution monochromator beamline PG at FLASH1.

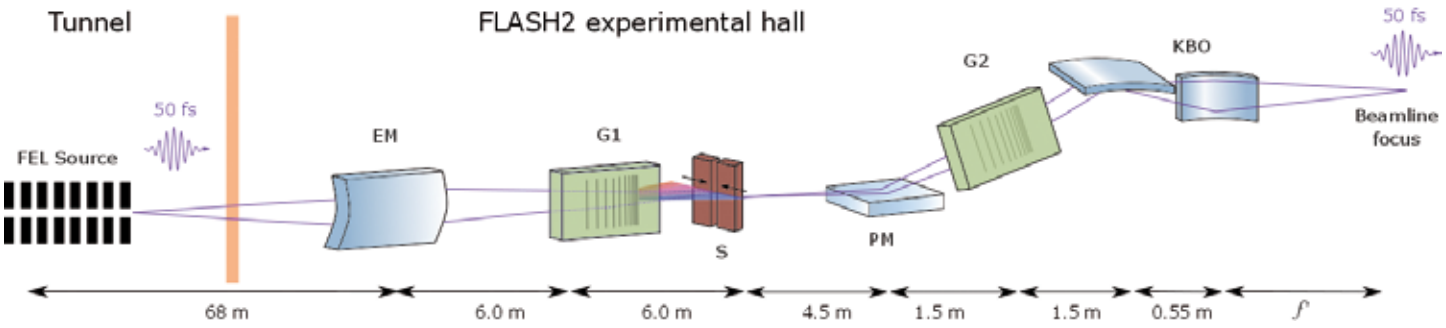

Figure 4

Schematic of the time-delay compensating monochromator at the FLASH beamline FL23. The TDCM is equipped with six optical elements: a planar elliptical mirror (EM), two variable line spacing gratings (G1, G2) in reflection mode, a slit (S), a planar mirror (PM) and a bendable Kirkpatrick-Baez (KB) focusing system.

Future upgrades – the FLASH2020+ project

Within the FLASH2020+ upgrade project, substantial improvements to the photon beam parameters are planned, as highly requested by the user community. In an initial step, FLASH2 will gain flexibility in photon beam polarisation by the installation of an APPLE-III type afterburner undulator. Together with a small increase in electron beam energy to 1.35 GeV, this will extend the wavelength range up to the oxygen K-edge, in order to cover important elemental resonances for energy research and the entire water window for research on biological samples.

In a second step, FLASH1 shall be equipped with a complete set of fully (gap as well as polarisation) tunable undulators. The wavelength tunability via undulator gap at both undulators lines will finally allow for more efficient parallel operation of both FEL lines with flexible wavelengths. Currently – with the fixed gap undulators – the wavelength requested for experiments at FLASH1 determines the electron beam energy of the accelerator and thus also the working point for FLASH2.

In addition, FLASH1 will be externally seeded at the full repetition rate that FLASH can provide in burst mode, making it the only high repetition rate FEL with full longitudinal coherence. Within the FLASH2020+ project, also novel FEL lasing concepts will be exploited at FLASH2 in the future. They are based on variable undulator configurations to, e.g., produce multiple FEL 'colours' or shorten the pulse duration and enable attosecond experiments.

The FLASH2020+ CDR was presented to the DESY advisory bodies Photon Science Committee (PSC), Machine Advisory Committee (MAC) and Laser Advisory Committee (LAC) in spring 2019. All three committees are very supportive and suggested to start with the upgrade plans as soon as possible. Presently, the detailed design/construction phase has started while all critical technical details are compiled in a technical design report (TDR). FLASH2020+ is well on track.

Contact: Rolf Treusch, rolf.treusch@desy.de

References

1. R. Ivanov et al., 'FLASH free-electron laser single-shot temporal diagnostic: terahertz-field-driven streaking', J. Synchrotron Rad. 25, 26–31 (2018). DOI: 10.1107/S160057751701253X.
2. S. J. Goh et al., 'Fabrication and characterization of free-standing, high-line-density transmission gratings for the vacuum UV to soft X-ray range', Opt. Exp. 23, 4421–4434 (2015). DOI: 10.1364/OE.23.004421.
3. Elisa Appi, Christina C. Papadopoulou et al., A synchronized VUV light source based on high-order harmonic generation at FLASH, submitted to special issue of Nature Scientific Reports on "Intense ultra-short pulses from femtosecond to attosecond" (Dec. 2019).
4. C. Heyl et al., 'Introduction to macroscopic power scaling principles for high-order harmonic generation', J. Phys. B: At. Mol. Opt. Phys. 50, 013001 (2017). DOI: 10.1088/1361-6455/50/1/013001.
5. L. Poletto et al., 'Double-grating monochromatic beamline with ultrafast response for FLASH2 at DESY', J. Synchrotron. Rad. 25, 131–137 (2018). DOI: 10.1107/S1600577517013777.
6. M. Ruiz Lopez et al., 'Wavefront propagation simulations supporting the design of a time-delay compensating monochromator beamline at FLASH2', J. Synchrotron Rad. 26, 899–905 (2019). DOI: 10.1107/S160057751900345X.

PETRA III

Successful operation and new installations

Figure 1

Left: The previous 2 m long standard undulator at the 'High Energy Materials Science' beamline P07. Right: the new in-vacuum undulator recently installed at the same place.

In the year 2019 about 3200 individual users performed experiments at PETRA III beamlines. In total, 22 beamlines were open for proposal submission. The operation time of PETRA III was split in two periods in 2019, one from mid of March until mid of July and a second from beginning of August until end of December. Overall, 3802 hours were available for proposals of users at each of the beamlines P01-P14 in the PETRA III experimental hall 'Max von Laue', P21.1-P24 in the hall 'Ada Yonath' and P64-P65 in the hall 'Paul Peter Ewald'. In 2019, a record number of 1600 proposals were submitted, including about 200 proposals that have been collected for the EMBL beamlines P12-P14.

PETRA III – Successful cooperations

Both independent beamlines P21.1 and P21.2 of the 'Swedish Materials Science beamline' at PETRA III successfully started user operation after the summer shutdown. At the 'Damping Wiggler Section North' of PETRA III, the 'High Energy X-ray Beamline' P61 for materials and high-pressure science had the first beam for commissioning. First regular users are expected for the second half of 2020. The construction of the undulator beamline for 'Anomalous Small Angle X-Ray Scattering' P62 made very good progress. The commissioning will also start in 2020.

The user community of PETRA III was very successful in raising third-party funding from the Federal Ministry of Education and Research (BMBF). This funding ('Verbundforschung') is intended to foster cooperation between German universities and large-scale research infrastructures. The instrumentations or applications suggested in the successful proposals aim for enabling excellent research from which proposers and the research community will benefit. A total of 36 proposals with strong engagement at PETRA III beamlines have been approved and are funded with roughly 18 million Euro for the next 3 years.

Two strategic PETRA III cooperations went into the second phase. The extremely productive cooperation with the Jawaharlal Nehru Centre for Advanced Scientific Research (JNCASR) in Jakkur (India), has been extended for another 5 years. In return for the major investments within this cooperation, users from India receive beamtime.

After the 'Swedish Materials Science beamline' has successfully started operation, as a next step, the coopera-

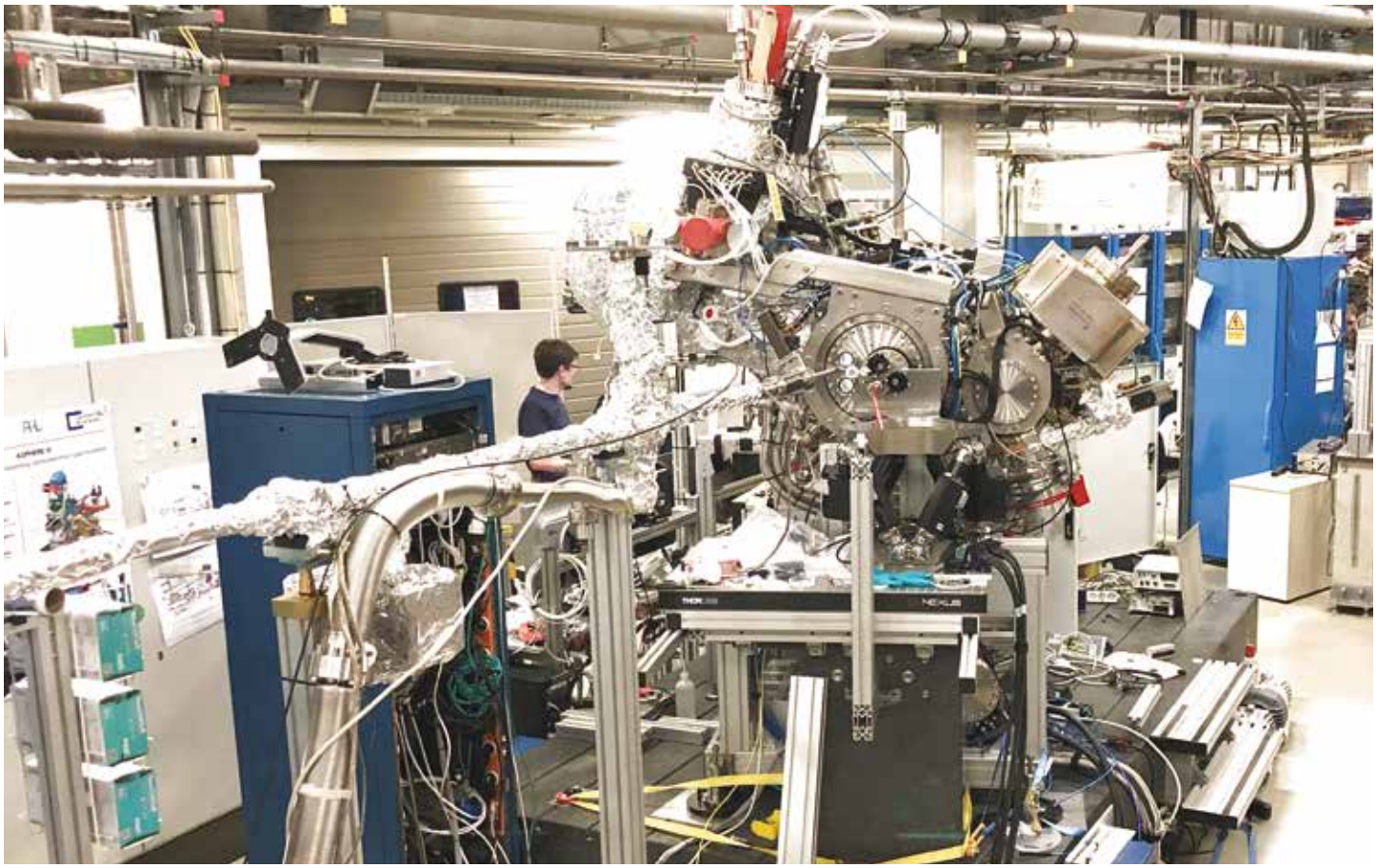

Figure 2

ASPHERE III, the setup for angle-resolved photoemission, at the PETRA III beamline P04.

tion between the Swedish Research Council and DESY handling the Swedish user access has been initiated.

Academic hosting of this beamline is provided by the Royal Institute of Technology (KTH) and Linköping University (LiU) through the newly founded Center for X-rays in Swedish Materials Science (CeXS). First beamtimes within this cooperation were allocated to Swedish users in August 2019.

PETRA III – Machine operation

The availability of the PETRA III storage ring was 98.5% with a mean time between failures of 64 h 39 min (as of November 25, 2019) reflecting the very good performance parameters of PETRA III in 2019.

As in the previous years, different bunch filling modes in the PETRA III storage ring were offered: a 'time resolved' mode with 40 bunches and a 'continuous' mode with 480 bunches both with approximately the same share. This bunch mode distribution has proven to be an optimal scenario for providing a maximum number of 'timing mode' shifts while minimising radioactive activation of ring components as well as radiation damage of undulators.

In the shutdown period at the beginning at 2019, the second in-vacuum undulator at PETRA III was installed at the Helmholtz-Zentrum Geesthacht (HZG)/DESY beamline P07 for High Energy Materials Science (Fig. 1), replacing the interim 2 m long undulator. The new device with a period length of 21 mm and a total length of 4 m is optimised for generating bright high energy X-rays in the range 40 – 150 keV. It delivers a factor of 5 more flux as compared to the previous 2 m device. Also, in January 2019 the frontend components of beamlines P61 – P63 have been installed.

During the summer break, the half metre undulator at P21.1 has been replaced by the final 2 m undulator. A short test run of PETRA III with reduced particle energy of 3 GeV instead of the usual 6 GeV was offered to some beamlines. It was used to characterise the horizontal emittance parameter which was approximately 700 pmrad at 50 mA current. This value is roughly half of the value of 1.3 nmrad at 6 GeV and was expected taking interbeam scattering effects into account.

The winter shutdown of 9 weeks began on 20 December 2019 and will be used to install the undulator of beamline P62 and to prepare the frontends of the bending magnet

Figure 3

The two detectors stages for simultaneous powder diffraction and pair distribution function measurements at the PETRA III beamline P02.1. In front on the left the Perkin Elmer detector, in the back the Varex detector.

Figure 4

Eulerian cradle diffractometer with PILATUS3 X CdTe 1M installed on the detector arm at the PETRA III beamline P24.

beamline P66 for time-resolved luminescence spectroscopy ('Superlumi').

PETRA III – Beamlines and experiments

In the PETRA III experimental hall 'Max von Laue', the ASPHERE III experiment (Fig. 2) which is funded by several BMBF 'Verbundforschung' projects of Kiel University and University of Würzburg has been transferred to its final position at the first branch of the soft X-ray beamline P04. ASPHERE is an instrument for spin and angle-resolved photoelectron spectroscopy and will be extended by an MBE growth-chamber in the near future.

At the PETRA III beamline for powder diffraction and total scattering P02.1, a second detector stage has been installed with a Varex flat panel detector in addition to the already existing stage with the Perkin Elmer flat panel detector (Fig. 3). This new setup was recommended at a beamline review in April 2018 and enables a seamless adaptation of the resolution in reciprocal space by moving the detectors close or far from the sample. This allows for simultaneous measurements of the pair distribution function (PDF) with one detector at small distances and of the high resolution powder diffraction at large distances. For this it is beneficial that the Varex detector has a very small outer frame with only 17 mm width. Alternatively, the Varex detector can be used for powder diffraction with high resolution as the pixel size is only 100 µm x 100 µm, and hence 4 times smaller than offered by the Perkin Elmer detector. This setup is shown in Fig. 3.

At PETRA III beamline P02.1 a rapid access scheme for users has been tested. Motivation for this new access route is the request from users for short-notice powder diffraction or total scattering experiments with a duration of 4 hours or less for a small set of standard samples. For rapid access beamtimes, the samples have to be mounted on standardised holders, similar to the well-known puck system of biocrystallography beamlines, and shipped to DESY. During the experiment the sample robot of P02.1 mounts the samples to the diffractometer where the alignment and the data collection are done automatically. The raw as well as the pre-analysed data are returned to the users after the measurement. The users are usually not present during the measurements. It is planned to conduct the experiments six weeks after the application at the latest. The first test call for rapid access in August 2019 resulted in 80 proposals of this kind which have been processed in the weeks thereafter. The first regular call for rapid access proposals at P02.1 will be opened in summer 2020.

In the PETRA III experimental hall 'Ada Yonath', the plans for installing an imaging experiment at the nano-diffraction beamline P23 are very advanced. This project is led by the Karlsruhe Institute for Technology (KIT) in cooperation with the P23 team and would relocate the state-of-the-art X-ray imager MiQA (Microscope and Quality Assurance) from the Karlsruhe synchrotron radiation source KARA (the former ANKA user facility) to PETRA III. This experiment, then called 'HIKA', will allow for materials science and medical imaging measurements making use of the excellent beam parameters of P23. In particular, it is optimised for laminography, a tomography method for flat samples, which is not available at PETRA III so far. The first experiments are planned for 2022.

At the beamline P24 for chemical crystallography, a PILATUS3 X CdTe 1M has been purchased and commis-

Figure 5

New chemistry user lab in PETRA III experimental hall 'Ada Yonath'. Left the fridges and the clean water facilities, right the fume hoods and the wet bench.

sioned as part of the strategic cooperation with the Max Planck Society (MPG). Beamline P24 at PETRA III is dedicated to detailed crystal structure investigation of small molecules under ambient and non-ambient conditions, in different sample environments for low and high temperatures, external fields and *in situ* experiments. For high resolution studies of single crystals, P24 provides photon energies between 15 keV and 44 keV allowing for collection of large q-space data with sufficiently high q-resolution. In this energy range silicon based pixel-detectors are inefficient. Usually image plate or CCD detectors are used as they have high efficiency, small pixel size and no gaps between modules. However, these detectors do not reach the high quantum efficiency of a modern CdTe-based detector, are relatively slow and do not allow single photon counting. In addition to the higher resolution CCD detector, the CdTe-based pixel detector Pilatus from Dectris is employed at P24 to close this gap (Fig. 4).

A new chemistry user lab went into operation in the PETRA III experimental hall 'Ada Yonath'. This chemistry lab is similarly equipped as the chemistry user lab in the PETRA III experimental hall 'Max von Laue' with fume hoods and wet benches and can be used for chemical preparation of samples for experiments at PETRA III beamlines (Fig. 5). Users can request access to chemistry labs online via DOOR (https://door.desy.de).

In the PETRA III experimental hall 'Paul P. Ewald', beamline P61 for materials and extreme conditions science is now in the commissioning phase and has received the first beam in October 2019 (Fig. 6). Beamline P61 is shared between HZG (EH1) focusing on materials sciences and DESY (EH2) with a large volume press (LVP) installed. The experimental

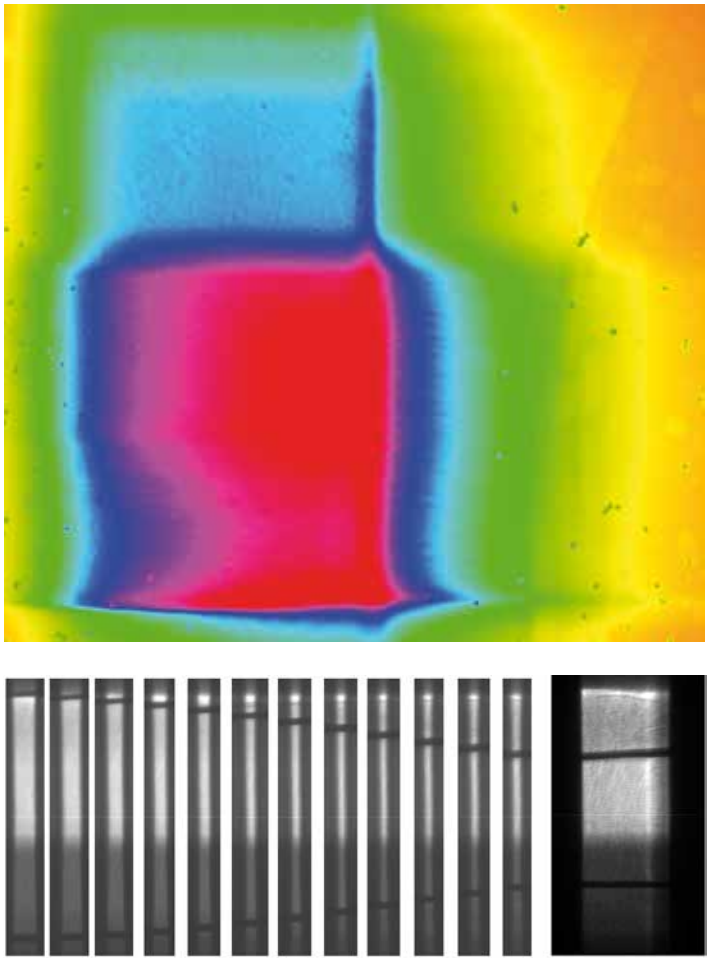

Figure 6

Top: Image of the first X-ray beam in the large volume press (LVP) hutch of the PETRA III beamline P61. The width of the beam shown on the left is approximately 2 mm. Bottom left: Series of radiographs from a marble rod under uniaxial compression from 1 bar to 45 kbar (from left to right) ending up into a condition of 50% strain. Bottom right: Radiograph of the marble rod after decompression back to 1 bar.

Figure 7

Left: image of the open P62 optics hutch with girders installed. Right: view on the PETRA III beamline P62. In the front the control hutch, in the back the experimental hutch.

hutch EH2 is operated by DESY, in collaboration with the Bavarian Research Institute of Experimental Geochemistry and Geophysics (BGI) of the University Bayreuth. The radiation source of P61 is a high energy wiggler section which has two functions. The wigglers deliver a white X-ray spectrum of which the range from 30 keV to 200 keV is used at the experiments at P61. Moreover the wigglers serve as damping wigglers to reduce the horizontal emittance of PETRA III from horizontally 4 nmrad down to the present 1.3 nmrad. Therefore, all wigglers are always closed with fixed gap. This does not restrict the operation of beamline P61. First users for regular beamtime are expected in summer of 2020.

In the open sector 2 of PETRA III experimental hall 'Paul P. Ewald', the construction of the new beamline P62 for small angle X-ray scattering for materials research with options of anomalous scattering and SAXS CT is in a very advanced state. All hutches are already constructed; the electronics, IT-infrastructure and interlock are almost finished (Fig. 7). In the optics hutch, the supports for the optics are installed, the design of the instrumentation is complete and the critical parts are ordered. The undulator will be installed in 2020. The monochromator (3.5 - 35.0 keV), the compound refractive lenses and the mirrors will be assembled in spring 2020. The SAXS instrument will have an in-vacuum EIGER2 X 9M detector installed inside a 13 m long SAXS flight tube and a customised EIGER2 X 4M-DESY for WAXS applications. The delivery of the WAXS detector is planned for mid 2020. The SAXS detector is scheduled for a later date, however, a spare PILATUS 6M is available for commissioning from early summer 2020 on. First operation for users is planned for late 2020.

PETRA IV

In the frame of the PETRA IV project at DESY, a diffraction-limited light source for hard X-ray radiation is being developed. PETRA IV will yield three dimensional images of matter with up to 100 times higher spatial and up to 10000 times higher temporal resolution compared to what is possible at PETRA III today. This improvement will be made possible by upgrading the existing PETRA III facility with the recent revolutionary developments in accelerator and undulator technology. The gain in brightness, the key parameter to characterise the quality of X-ray beams, will be a factor 100 for photon energies of 10 keV and a factor of almost 1000 at higher energies of 80 keV. Moreover, the beams of the lower energy range of PETRA IV would be diffraction limited. They

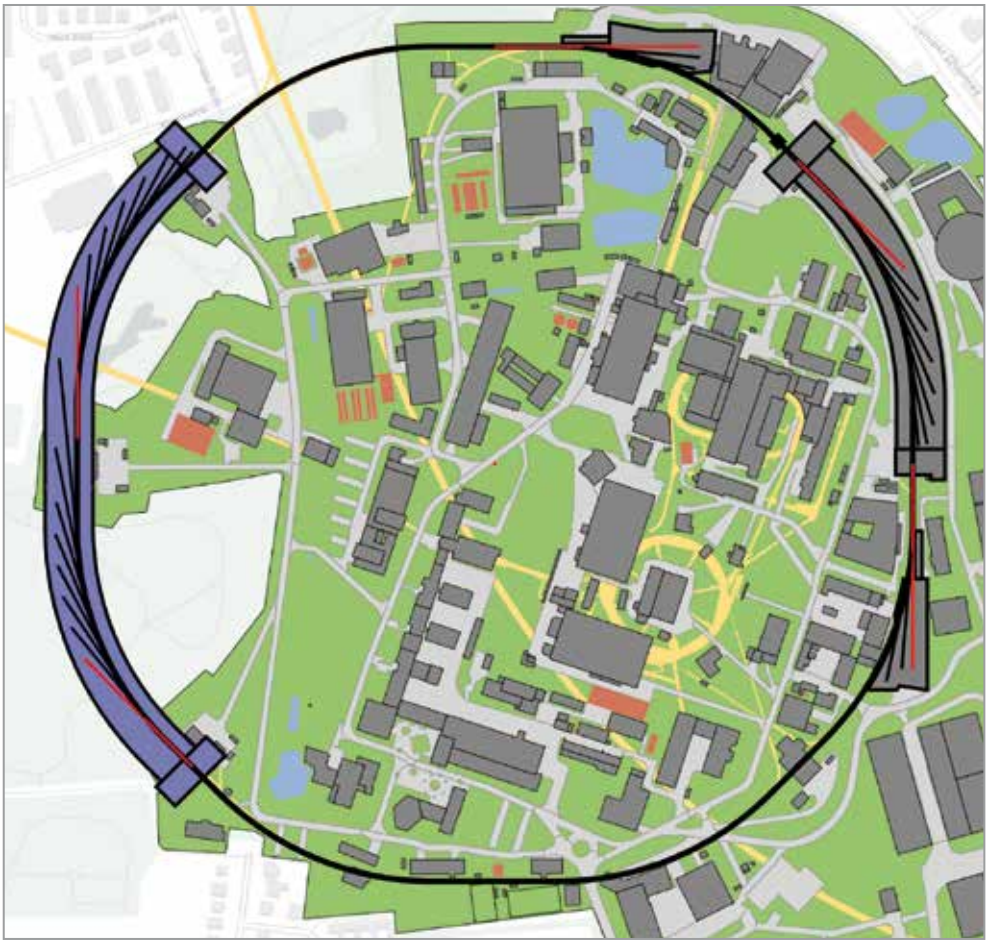

Figure 8

Possible realisation of the future PETRA IV light source (storage ring in black) with 30 beamlines, thereof 5 beamlines with 10 m undulators (red). The blue hall is the planned new PETRA IV hall.

can then be focused without severe losses to nanometre spot sizes achieving ultimate spatial resolution. For photon energies of about 40 keV, the coherence of the beam is comparable to today's PETRA III 10 keV photons.

After detailed studies of different options for the PETRA IV lattice, a solution based on the ESRF-type hybrid multi-bend achromat has been selected. These results were published in the PETRA IV conceptual design report (CDR). This option allows for two possible modes of operation: a brightness mode with 1600 bunches at 200 mA ring current and a timing mode with 80 bunches at 80 mA ring current. The expected emittance of PETRA IV for these two operation modes are listed in the table below.

	Brightness mode	Timing mode
No. of bunches	1600	80
Ring current	200 mA	80 mA
Emittance (horizontal)	< 20 pmrad	< 50 pmrad
Emittance (vertical)	< 4 pmrad	< 10 pmrad

For PETRA IV a fourth experimental hall hosting 16 undulator beamlines is planned opposite to the 'Max von Laue' hall (Fig. 8). It is expected that the canting of undulator beamlines, as realised at PETRA III where two beamlines share one sector, will no longer be possible. Therefore, 8 sectors with only 8 beamlines may fit into the experimental hall 'Max von Laue'. At PETRA IV, in total 30 undulator beamlines would be available in 4 experimental halls around the ring; thereof up to 5 beamlines with long 10 m insertion devices.

The conceptual design report of the PETRA IV project is finalised. As a next step, it will be submitted to the Helmholtz Committee for Research Infrastructures (FIS) for evaluation in spring 2020. In parallel, the technical design report (TDR) phase for PETRA IV will be initiated; it will be completed by the end of 2022. In expectation of positive project evaluation and funding around 2022/2023, PETRA IV will be built according to the present plan by 2027. DESY will then operate the most brilliant and powerful storage ring based X-ray source worldwide again.

Contact: Oliver Seeck, oliver.seeck@desy.de
Hans-Christian Wille, hans-christian.wille@desy.de

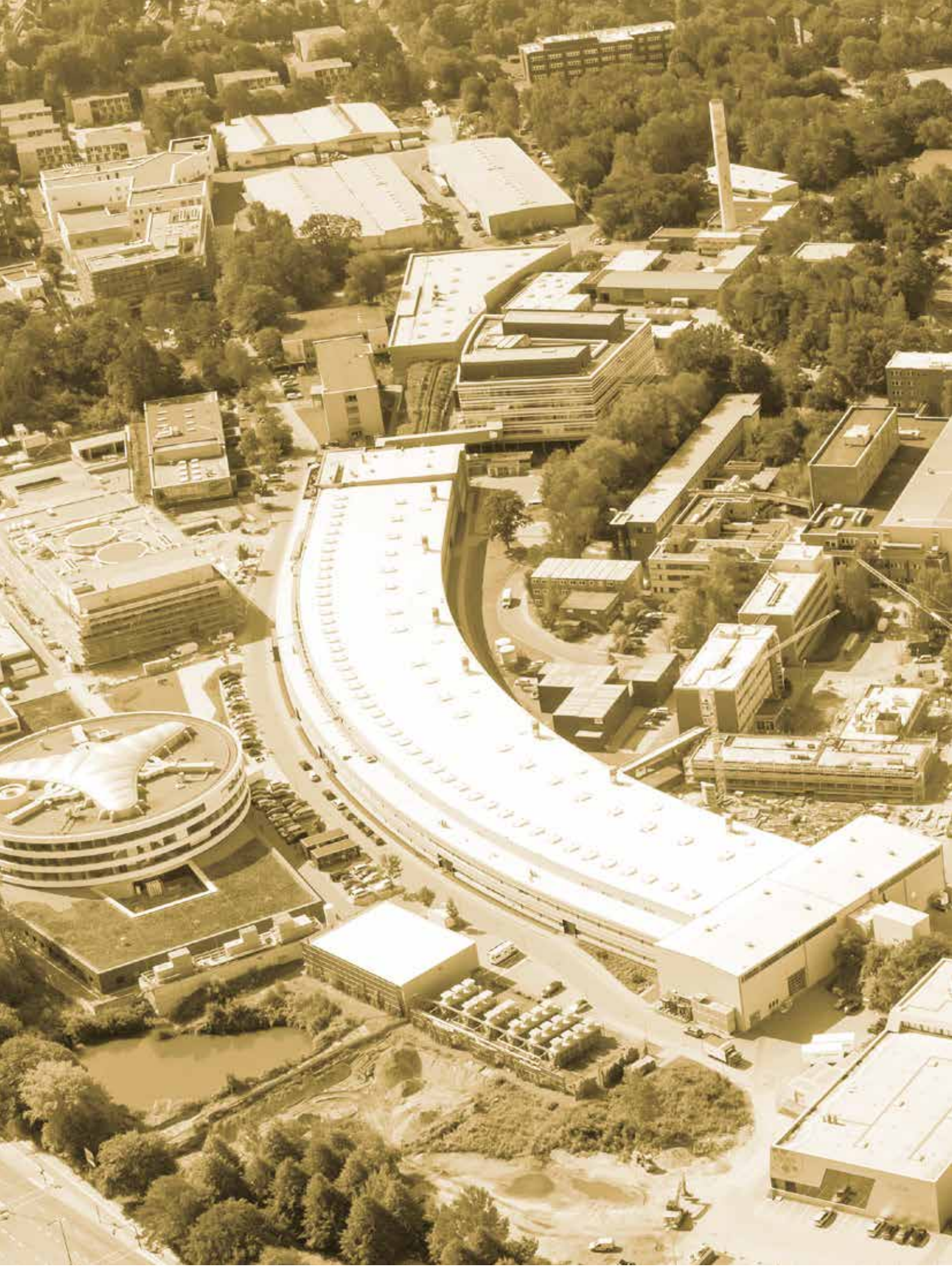

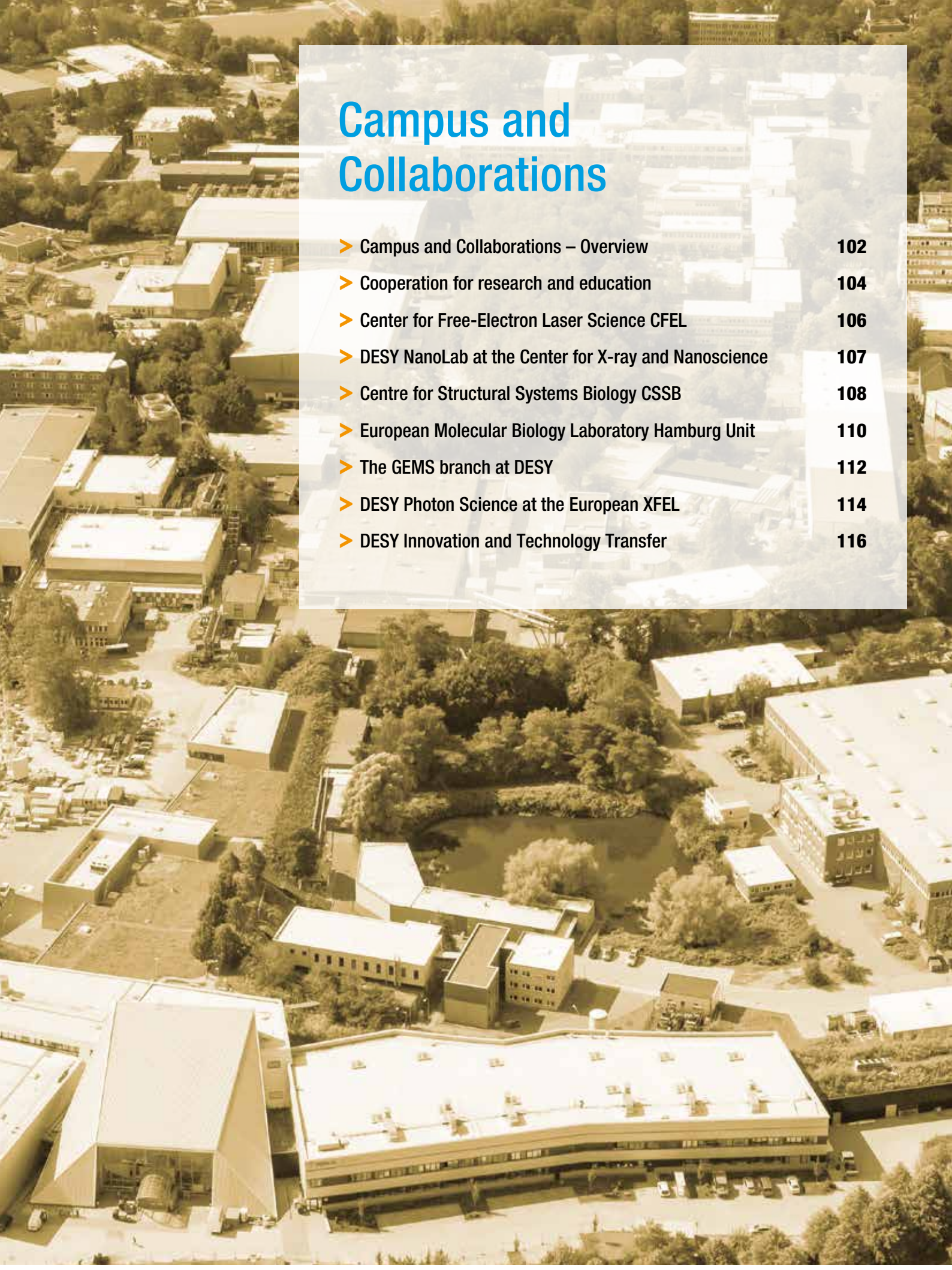

Campus and Collaborations

Campus and Collaborations – Overview

DESY Photon Science is part of a worldwide collaborative network. Cooperation creates new scientific and technological opportunities at DESY's facilities, increases the pool of talents and is also indispensable to further coordinate research roadmaps and agendas. The collaboration landscape at DESY Photon Science is diversified and involves local as well as national and international partners.

Universities

A strong connection to the Universität Hamburg (UHH) is established through the 'Partnership for Innovation, Education and Research' (PIER). This structural cooperation has provided the ground for a joint graduate school (PIER Helmholtz Graduate School, PHGS), joint professorships and research projects. DESY cooperates with UHH and further German universities through joint professorships, common research projects, collaborative research centres (SFBs) and BMBF Collaborative Research at PETRA III and FLASH. With some of the universities joint laboratories and outstations on the DESY campus are formed. Examples of current partner institutions are the Technische Universität Hamburg, and the Universities of Göttingen, Kiel and Erlangen-Nürnberg.

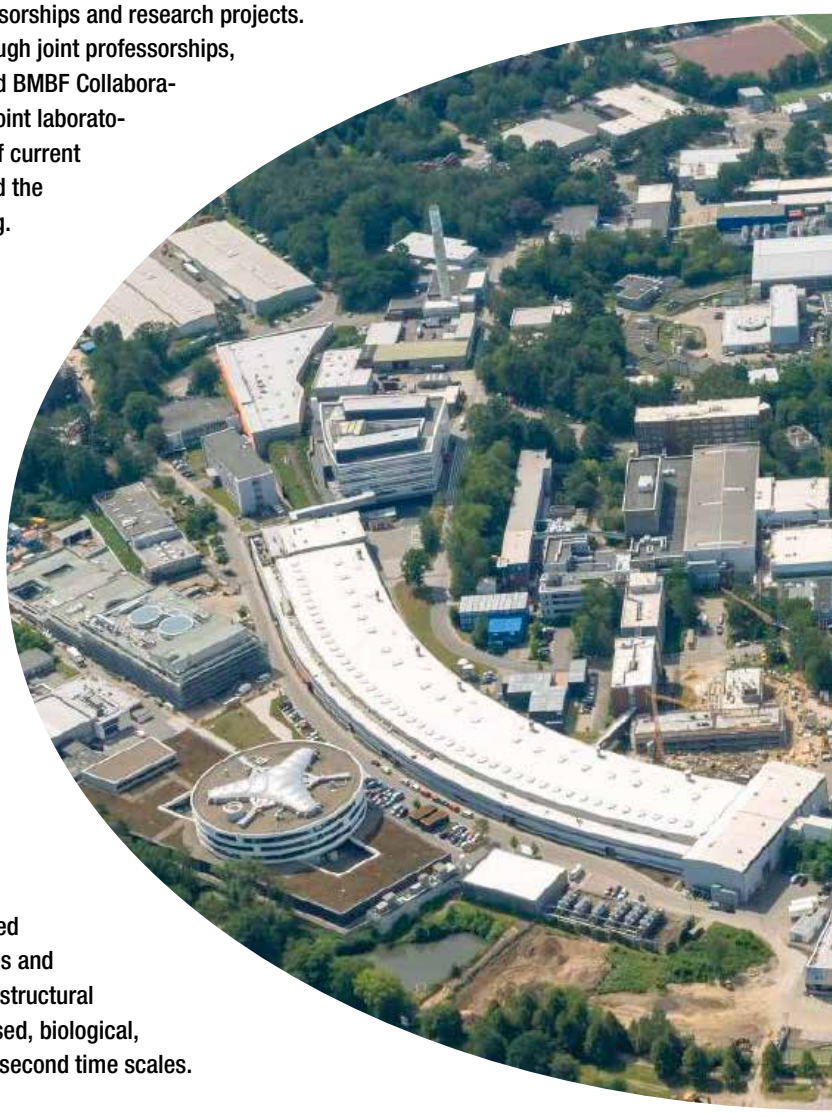

Interdisciplinary research platforms

Cooperation between the research fields, links to other divisions at DESY and joint projects with external partners are of decisive importance for the interdisciplinary research at DESY Photon Science. Connections are established for example in joint centres via common thematic focus points:

Within the Centre for Structural Systems Biology (CSSB) scientists use a novel approach which combines integrative structural biology with systems biology to advance our understanding of the molecular mechanisms of some of the world's most widespread infections.

The Center for Free-Electron Laser Science (CFEL) as a joint enterprise of DESY, the Max Planck Institute for the Structure and Dynamics of Matter (MPSD) and the Universität Hamburg is designed to advance science with next generation light sources and lasers. The three partners join forces to explore structural changes of atoms, molecules, condensed, biological, or warm dense matter on femtosecond time scales.

The building of the Center for X-ray and Nano Science (CXNS) is constructed in cooperation with the Helmholtz-Zentrum Geesthacht (HZG) and the Christian-Albrechts-Universität zu Kiel (CAU). In addition to several DESY research groups, the building will also house the DESY NanoLab.

Further centres in the planning phase are the Centre for Molecular Water Science (CMWS), the Centre for Data and Computing Science (CDCS), and the Wolfgang-Pauli-Centre (WPC) for theoretical physics.

DESY within User Consortia at the European XFEL

Besides being responsible for the construction and the operation of the European XFEL linear accelerator, DESY plays an important role as user of the European XFEL. DESY is partner in several user consortia; among them are:

- the Serial Femtosecond Crystallography (SFX) user consortium,
- the Helmholtz International Beamline for Extreme Fields (HIBEF),
- the Heisenberg Resonant Inelastic X-ray Scattering (h-RIXS) user consortium,
- the DataXpress consortium for data analysis,
- the consortium on state-, size-, and isomer-selected samples of polar molecules and clusters at the European XFEL (COMO).

Moreover, DESY scientists develop lasers and detectors for usage at the European XFEL.

European Molecular Biology Laboratory (EMBL) Hamburg

At EMBL Hamburg, scientists investigate the structure of challenging molecules that impact human health. The Hamburg site's service teams develop methods and software to support scientists from around the world in every step of biological structure determination. EMBL runs three beamlines at PETRA III: one for Small Angle X-ray Scattering experiments and two for Macromolecular Crystallography.

Helmholtz-Zentrum Geesthacht (HZG)

The German Engineering Materials Science Centre (GEMS) is a user platform of HZG for the complementary research with photons and neutrons with an outstation at DESY. GEMS research groups work in X-ray diffraction and imaging on the DESY campus. HZG operates several beamlines and end stations at PETRA III focusing on research in the field of engineering materials science.

DESY Innovation and Technology Transfer

With support of the DESY department for Innovation and Technology Transfer (ITT) scientists from DESY Photon Science contribute to the DESY innovation strategy including the transfer of knowledge and technology from the laboratory to industry.

International cooperation

DESY is engaged in international cooperation and user consortia, for example to leverage new resources and contributions to DESY facilities and installations. Significant examples for DESY Photon Science in that respect are the international contributions to PETRA III by Sweden in connection to the Röntgen-Angström-Cluster (RAC) and by India via the India@DESY collaboration.

Cooperation for research and education

News from the partner universities

Figure 1
Horst Weller (UHH, Department of Chemistry) explains to a public audience at the 'Summer of Knowledge', how nanoscience impacts the world.
Photo: UHH, RRZ/MCC, Mentz

Universität Hamburg (UHH)
In January 2019 Hamburg's First Mayor Peter Tschentscher presented plans to develop the University Campus next to DESY in the frame of the 'Science City Bahrenfeld'. The expanded area shall provide the space for accommodating the Department of Physics as well as parts of the Departments of Chemistry and Biology. This will further strengthen the cooperation between these disciplines and their links to DESY and the Max Planck Institute for the Structure and Dynamics of Matter (MPSD). On-site teaching facilities will establish true campus life.

Encouraged by the success of previous years, in April another round of 'Science on tap' brought scientists of the UHH, DESY and other partners to more than 50 pubs in Hamburg to talk about their research in a relaxed atmosphere. Again, thousands of interested citizens were attracted by first-hand impressions on contemporary science, communicated by enthusiastic scientists in an unconventional setting.

In 2019, the UHH celebrated the 100th anniversary of its foundation. One of the central activities was the 'Summer of Knowledge', held in June on the large square in front of the city hall. Over four days, Hamburg's citizens and guests were invited to meet researchers in specially erected large tents and to enjoy talks on modern science or try out hands-on experiments (Fig. 1). About 50000 people joined the event. The Mildred Dresselhaus Guest Professorships 2019 for female scientists were awarded to Ruth Signorell from ETH Zürich, and Alicia Palacios, Universidad Autónoma de Madrid. Their anticipated stay in Bahrenfeld will give local scientists ample opportunity for establishing and strengthening collaborations with these distinguished colleagues.

Since 2011 scientists from the Department of Physics together with colleagues from DESY, the MPSD and the European XFEL have worked within the collaborative research centre SFB 925 on light-induced dynamics and control of correlated quantum systems. This SFB was now successfully evaluated by the DFG and will receive continued funding for a third four-year period until 2023.

Since 2019 two Clusters of Excellence, one ('Advanced Imaging of Matter AIM') in photon science and the second one ('Quantum Universe') in astro-particle physics put Hamburg's Department of Physics into a unique position among the German physics departments. Completion with another two clusters in climate research ('Climate, Climatic Change, and Society') and in the humanities ('Understanding Written Artifacts'), has entitled the University to apply for additional funding for top-level universities in Germany. In July, the UHH was selected as one of eleven German universities to be awarded the status of a 'University of Excellence'. Two of the clusters (AIM and 'Understanding Written Artifacts') include contributions by DESY Photon Science research groups. The high international visibility expected to come with this status will also help to attract talented students to Hamburg. The early integration of students from foreign countries will be supported by the newly established 'International MSc. in

Figure 2
Financed by the BMBF, a high-power laser as excitation offers the possibility to investigate interfaces between liquids and gases on short time scales by means of X-rays at the LISA instrument (PETRA III beamline P08). Photo: C. Lemke, CAU

Physics' course programme, which has started in the winter term 2019/2020.

Christian-Albrechts-Universität zu Kiel (CAU)
In the frame of the Ruprecht-Haensel-Laboratory – a cooperation between CAU and DESY – scientists from Kiel physics department received substantial funding via BMBF. Focused on developing new instruments and experimental methods with especially intensive X-ray beams and using them for research in advanced materials and life science, the collaborative projects are:

- HESEC: new methods for energy research using high energy photons,
- LISA Dynamics: understanding ultrafast dynamics of water interfaces and cell membranes (Fig. 2),
- QM-MBE-SXPES: design and *in situ* characterisation of novel quantum materials,
- XFEL-k-Spin-multi-D: understanding and controlling ultra fast dynamics of quantum matter.

The funded projects could create important foundations for customised quantum materials, new electrodes in fuel cells and electrolysers, controlled release of medicines or the understanding of chemical reactions.

Georg-August-Universität Göttingen (GAU)
After twelve years of successful collaborative research, the 'seed' of the cooperation in photon science between GAU and DESY – the SFB 755 '*Nanoscale photonic imaging*' – closed in 2019 with an international conference. SFB 755 started in 2007, during a time when it was unclear where high flux X-ray sources will bring the scientific community in the future. A decade later the SFB with its spokespersons Tim Salditt and Sarah Köster celebrated together with colleagues from CFEL/UHH and DESY the manifold reached milestones in optical to X-ray photon science. Starting from the methodological base, which was set in frame of the SFB 755 research, future activities will point, on the one hand, towards biophysical and medical analysis. In this context Sarah Köster has been awarded with the EPS-Emmy Noether Distinction for Women in Physics for her seminal contributions to the physics of biological cells and biopolymers. And on the other hand, future developments aim at the design and real-time characterisation of smart bio-based and water-transforming energy materials, which is one international collaboration topic within the future Centre for Molecular Water Science (CMWS).

Technische Universität Hamburg (TUHH)
There are several joint research projects of scientists at DESY Photon Science and the TUHH.

Within the joint project '*In situ* XANES and EXAFS of titanium silicalites during the epoxidation of propylene to propylene oxide' as part of the 'Landesforschungsförderung' the method of XANES (X-ray absorption near edge structure) imaging was implemented at PETRA III, for imaging the chemical state of a catalyst under working conditions. In parallel, the chemical reactor developed at TUHH was recently used at PETRA III to follow the oxidation of carbon monoxide over a molybdenum based catalyst. In a next step, *operando* imaging of the catalyst in two and three dimensions will be implemented.

The DESY NanoLab continues its fruitful cooperation with the materials science departments of the TUHH within the SFB 986 'Tailor-made Multi-scale Material Systems', funded by the German Science Foundation (DFG). The two currently funded projects aim at a better understanding of structure-functionality relations in bottom up-fabricated materials. The fruitful cooperation resulted in a number of joint publications. The application for the third and final funding period of the SFB 986 has already been prepared and has been submitted by the end of 2019.

To further deepen their cooperation in the field of materials science, the TUHH and DESY have jointly submitted a 'Hamburg X proposal' together with UHH and HZG for a Center for Integrated Multiscale Materials Systems (CIMMS). Within CIMMS TUHH and DESY decided to support long term funding of a W3 professorship for materials imaging.

Contact: Markus Drescher, UHH, markus.drescher@uni-hamburg.de
Bridget Murphy, CAU, murphy@physik.uni-kiel.de
Simone Techert, GAU and DESY, simone.techert@desy.de
Christian Schroer, UHH and DESY, christian.schroer@desy.de
Andreas Stierle, UHH and DESY, andreas.stierle@desy.de

Center for Free-Electron Laser Science CFEL

Three institutions working successfully together

The inter-institutional and cooperative nature of CFEL – a joint enterprise of DESY, Universität Hamburg (UHH) and the Max Planck Institute for the Structure and Dynamics of Matter (MPSD) – fosters outstanding research results, of which a few recent ones are presented in the following.

In a pioneering experiment, a team of scientists provided for the first time experimental evidence of the structural sensitivity and accuracy of the standing wave technique at a high repetition rate free-electron laser, FLASH at DESY, by measuring the photoelectron yield from the SiO_2 surface of Mo/Si multilayers [1]. The combination of the high chemical specificity and surface sensitivity of photoemission spectroscopy, together with the X-ray standing wave structural sensitivity and the femtosecond duration of the FLASH pulses opens up the possibility of obtaining atomic positions with unprecedented picometre spatial accuracy and femtosecond temporal resolution. This work results from the collaboration between the Advanced Study Group of Universität Hamburg at CFEL formerly led by Wilfried Wurth, the group of Ivan Vartanyants from DESY and the University of Twente. More information can be found in the highlight section of this report.

A team of CFEL scientists headed by Andreas Maier from Universität Hamburg and by Franz Kärtner from DESY has achieved an important milestone in the quest for a new type of compact particle accelerator [2]. Using ultra-powerful pulses of laser light, they were able to produce particularly high-energy flashes of radiation in the terahertz range (Fig. 1) having a sharply defined wavelength. Terahertz radiation is one possibility to open the way for a new generation of compact particle accelerators that will find room on a lab bench. The wavelength of terahertz radiation is about a thousand times shorter than the radio waves that are currently used to accelerate particles. This gives great hopes to that the components of the accelerator can also be built to be around a thousand times smaller. The generation of high-energy terahertz pulses is therefore also an important step for the AXSIS (Frontiers in Attosecond X-ray Science, Imaging and Spectroscopy) project at CFEL, funded by the European Research Council (ERC), which aims to open up completely new applications with compact terahertz particle accelerators.

CFEL scientists from the MPSD led by Andrea Cavalleri used terahertz frequency light pulses to transform a non-ferroelectric material into a ferroelectric one [3]. Light can be used not only to measure materials' properties, but also to change them. Especially interesting are those cases in which the function of a material can be modified, such as the ability to conduct electricity or to store information in its magnetic state. Ferroelectricity is a state in which the constituent lattice 'points' in one specific direction, forming a macroscopic electrical polarisation (Fig. 2). The ability to reverse such a polarisation makes ferroelectric materials particularly suitable for digital information encoding and processing.

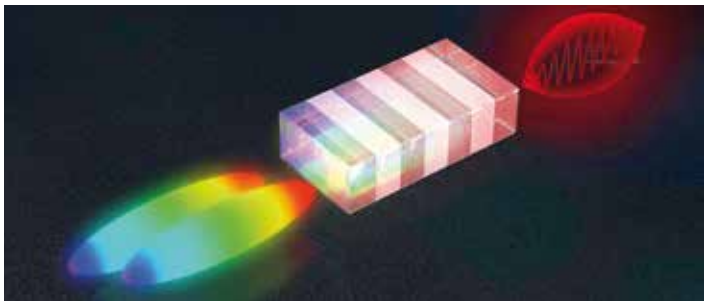

Figure 1

From the colour difference of two slightly delayed laser flashes (left) a non-linear crystal generates an energetic terahertz pulse (right). Credit: DESY, Lucid Berlin

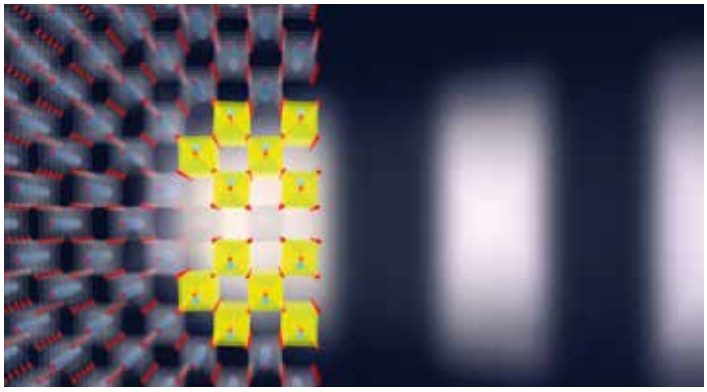

Figure 2

Ultrashort terahertz pulses create a ferroelectric phase in the paraelectric strontium titanate. An optically-induced deformation of the sample results in pairs of flexoelectric domains with opposing polarisations. Credit: MPSD, Jörg Harms

Contact: Ralf Köhn, ralf.koehn@cfel.de

References

1. G. Mercurio et al., New J. Phys. 21, 033031 (2019).
2. S. W. Jolly and N. H. Matlis et al., Nat. Commun. 10, 2591 (2019).
3. T. F. Nova et al., Science 364, 1075-1079 (2019).

DESY NanoLab at the Center for X-ray and Nanoscience

Shaping up for the nano future

Figure 1
Picture of the CXNS construction site (December 2019).

The DESY NanoLab provides nano-imaging, nano-structuring, spectroscopy as well as X-ray diffraction methods, which are complementary to the photon based techniques available for users at the DESY X-ray facilities PETRA III and FLASH. Access to the DESY NanoLab is granted for external users via regular PETRA III or FLASH proposals. Furthermore, the DESY NanoLab is involved in cooperative projects with various German universities: Universität Hamburg (UHH), Technische Universität Hamburg (TUHH), Christian-Albrechts-Universität zu Kiel (CAU), Friedrich-Alexander Universität Erlangen-Nürnberg (FAU) and Justus-Liebig-Universität Gießen (JLU). In addition, it supports DESY Photon Science in nano and materials science as well as DESY-wide projects in the fields of nano-materials and interface related research projects. Industrial users can access via DESY ITT (Innovation and Technology Transfer).

As of 2021, the DESY NanoLab will be located at the Center for X-ray and Nanoscience (CXNS, building 94). It is currently under construction in close vicinity to the PETRA III experimental hall 'Max von Laue' (Fig. 1). In December 2019 the topping-out ceremony took place following which the interior work for the technical infrastructure commenced. On the ground floor with 730 m² there will be space for 20 high-tech laboratories for several DESY Photon Science teams as well as for the German Engineering Materials Science Centre (GEMS) of the Helmholtz-Zentrum Geesthacht. Furthermore, the CXNS will host offices for research groups of CAU in the frame of the cooperative Ruprecht-Haensel Laboratory.

Interdisciplinary nanoscience research, cooperation within the research groups residing in the new CXNS, and its close connection to DESY's photon sources as well as to university institutes from the UHH physics department will provide best possible research opportunities combining photons with nano as well as materials science.

Some of the labs will not be located in the CXNS building, such as the DESY NanoLab X-ray diffraction lab. This was planned in 2019, with construction work in the former DORIS hall (building 25) on track to be completed by the end of 2019. The move is expected to be in spring 2020. The new X-ray lab will consist of three independent hutches fully equipped with gas and laser interlocks. It will host a grazing incidence six-circle diffractometer, a reflectometer and as a new instrument a horizontal six-circle instrument with a 2D detector, which allows for grazing incidence small angle X-ray scattering. Furthermore, a dedicated electrochemistry lab is planned together with the CAU to serve future needs for the preparation of X-ray experiments in the field of electrochemistry, -catalysis and corrosion in relation to the Centre for Molecular Water Science (CMWS). To complement instruments for magnetic investigations, a Kerr microscope was purchased and installed, which is available for users since the middle of 2019. Future expansion of the instrumentation is planned in agreement with the tentative users requirements.

Contact: Andreas Stierle, andreas.stierle@desy.de

Centre for Structural Systems Biology CSSB

We investigate how pathogens infect humans

Figure 1

Multi-user cryo-EM facility. Image: Jörg Müller

The year 2019 has been dedicated to bringing our four core facilities and electron cryo-microscopy (cryo-EM, see Fig. 1) multi-user facility into operation for users. The facilities listed below offer a wide range of scientific services.

Core facilities:

- Advanced Light and Fluorescence Microscopy (ALFM, see Fig. 2)
- High-Throughput Crystallisation (HTXX)
- Protein Characterisation (PC)
- Protein Production (PP)

Multi-user facility:

- Cryo-EM Facility

Collaborative research highlights

CSSB's interdisciplinary and collaborative nature is illustrated below with a few examples of research highlights from the last year.

• *New protocol for screening membrane protein stability*

Six research groups, among them three from CSSB, have developed a protocol that will simplify the process of solubilising integral membrane proteins (IMPs), as they reported in Scientific Reports. The development of the protocol is the first result of a collaboration between various research groups using the Protein Characterisation (PC) facility at CSSB [1].

• *A tRNA modifier at work*

CSSB scientist Jan Kosinski (EMBL) in collaboration with international researchers managed to catch a crucial component of cellular modification machinery directly at work. Using cryo-EM, they have determined the structures of a large protein complex called Elongator, in the presence and absence of its natural substrate tRNA. For the Kosinski group, the cryo-EM structure of Elongator marks another success. Two years ago, they published a model of Elongator built using a computational modelling method developed by Jan Kosinski. Comparing this model with the high-resolution cryo-EM structure shows a remarkable similarity between them – a clear demonstration of the power of so-called integrative modelling methods, which model structures based on data from various experiments [2].

• *Cryo-SOFI: a new super-resolution cryo-FM concept*

Correlative light and electron cryo-microscopy (cryo-CLEM) combines the powers of fluorescence cryo-microscopy (cryo-FM) with those of cryo-EM to answer important biological questions. The CSSB research groups of Rainer Kaufmann (UHH) and Kay Grünewald (HPI, UHH), together with coworkers from the University of Oxford, have developed a new cryo-FM concept which enables cryo-CLEM imaging that not only preserves the structural integrity of the biological sample but also significantly reduces the resolution gap. This new concept is called cryo-SOFI (Fig. 3) [3].

• *First structure of peptide transporter in complex with pro-drug revealed*

Certain drugs and pro-drugs can hijack the human nutrient transporters PepT1 or PepT2 and hitch a ride directly into the cell, thus accelerating the drug's absorption into the blood stream. Pro-drugs are inactive medications that are metabolised into an active, functional form within the body. While the pro-drug concept is very effective, little is known at the molecular level about the peptide transporters' structure and how they recognise, bind and transport pro-drugs. The groups of CSSB scientists Christian Löw (EMBL) and Jan Kosinski (EMBL) are now a step closer to understanding this as they recently determined a high resolution crystal structure of a peptide transporter in complex with the pharmacological relevant pro-drug valganciclovir; a medication that combats certain viral infections [4].

Figure 2
Advanced Light and Fluorescence Microscopy Facility. Image: Jörg Müller

• *Protein assemblies ejected from native membranes*
An international team of scientists including CSSB's Kay Grünewald (HPI, UHH) have developed an approach to eject protein assemblies directly from native membranes for mass spectrometry. This detergent-free, chemical free method not only enables the oligomerisation state determination of individual membrane proteins but also reveals further functional information such as subunit composition in larger complexes and small-molecule binding [5].

CSSB research strategy activities
CSSB kicked off our external seminar series which has brought renowned scientific speakers and guest to our lecture hall. Additionally, this year has been dedicated to not only fostering communication between research groups but also establishing a greater presence for CSSB in the local and international scientific community. A sense of common purpose and collaboration has been established at CSSB through the bi-weekly internal seminar series as well as other social and networking events. The launch of the new website presents CSSB in a modern and innovative light while highlighting the available facilities as well as the Research Hotel.

New recruitments
In January 2019 Michael Filarsky joined us at CSSB as a Junior Professor recruited by Universität Hamburg. His expertise is in 'Systems Biology of human-pathogenic Parasites'.

Infrastructure Investments
Scientists from CSSB and partner institutions were successful in securing funding via the German Research Foundation's (DFG) major instrumentation initiative entitled 'Innovative, Experimental Optical Microscopes for Research', which will finance a lattice light-sheet microscope (LLS). This microscope will help scientists investigate important bio-medical questions such as which cellular processes are involved in viral infections.

In October, CSSB was awarded funding from the BMBF for the purchase of two light microscopes and a vitrification unit.

Contact: Chris Meier, chris.meier@cssb-hamburg.de

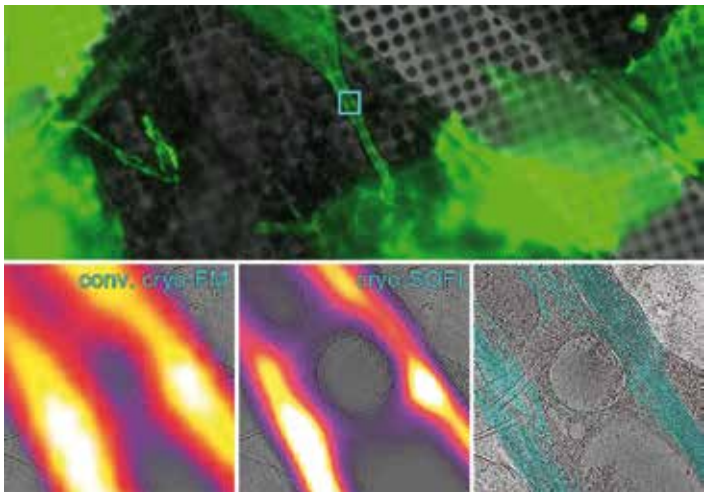

Figure 3
Super-resolution cryo-CLEM of actin in vitrified cells. Top: Overview of mammalian cells with fluorescently labelled actin (green) grown on standard holey carbon mesh of EM grids (grey). Bottom: Cryo-EM image acquired in the area indicated by the cyan square in the overview overlaid with the conventional cryo-FM image (left), the cryo-SOFI image (centre) and manually segmented actin (right). Image from [3]

References

1. V. Kotov et al., Scientific Reports, 9(1): 10379 (2019)
2. M. I. Dauden et al., Sci Adv, 10;5(7): eaaw2326 (2019)
3. F. Moser et al., PNAS, 116(11): 4804-4809 (2019)
4. Y. Ural-Blimke et al., J Am Chem Soc, 141(6): 2404-2412 (2019)
5. D. S. Chorev et al., Science, 16;362(6416): 829-834 (2019)

CSSB Partner Institutions

- Bernhard Nocht Institute for Tropical Medicine (BNITM)
- Deutsches Elektronen-Synchrotron (DESY)
- European Molecular Biology Laboratory (EMBL)
- Forschungszentrum Jülich (FZJ)
- Hannover Medical School (MHH)
- Heinrich Pette Institute (HPI)
- Helmholtz Centre for Infection Research (HZI)
- Universität Hamburg (UHH)
- University Medical Center Hamburg-Eppendorf (UKE)
- Research Center Borstel (FZB) (associated partner)

CSSB Investors

- Federal Republic of Germany
- Free and Hanseatic City of Hamburg
- Federal State of Lower Saxony
- Federal State of Schleswig-Holstein

European Molecular Biology Laboratory Hamburg Unit

Structural biology research and service provision

The Hamburg Unit of the European Molecular Biology Laboratory (EMBL) provides state-of-the art research services for applications in structural biology, complemented by in-house research activities focused on the development of new approaches in structural biology and infection biology.

Since the beginning of 2019, Edith Heard commenced her new position of EMBL Director General. Under her leadership, a new research theme provisionally entitled 'From Atoms to Ecosystems' is emerging. It aims at the expansion of the institute's research by taking the environment in its various facets as an additional variable into account. Future research opportunities for the EMBL Hamburg Unit have been recommended during its regular scientific review in February 2019, to reach out in new approaches that will make it possible to close the remaining gap between molecular structural biology and cell biology.

Research services in structural biology

EMBL operates three beamlines for structural biology applications at the PETRA III storage ring: one for Small Angle X-ray Scattering (SAXS) experiments (P12) and two for Macromolecular Crystallography (P13, shown in Fig. 1, and P14). The local dedicated IT infrastructure was upgraded to 1100 compute cores with high-speed access to a 1 PByte high-performance storage system enabling near real-time processing of experimental data.

At beamline P12, in-line size-exclusion chromatography (SEC-SAXS) operations allow extended studies of solubilised membrane proteins. A dedicated setup was developed for studies of Terahertz excitations of macromolecular solutions. The program CRYSOL, which allows for computation of scattering from macromolecules in solution, was extended to account for anomalous scattering effects. The Small Angle Scattering Biological Data Bank (SASBDB) counted its 1000th data set in 2019. One of the research highlights using data from P12 was on the structure and molecular mechanism of ATP citrate lyase (ACLY), allowing to target the enyzme in cancer and metabolic diseases such as atherosclerosis [1]).

At beamline P14, time-resolved pump-probe experiments previously performed on the first end station of the beamline have been moved to the new second end station named 'T-REXX' (Time-resolved experiments in crystallography) that was taken into operation in October 2018. During the first year of operation, users from more than ten laboratories have worked on a wide range of projects, leading to first high-impact publications. A new *in situ* mixing approach allows introducing substrates into micro-crystals to observe enzymatic reactions as they proceed inside the crystal [2]. In a first successful multiple-time-point serial synchrotron crystallography experiment, 18 consecutive structures for time-points in the millisecond to second regime allowed for the generation of a structural 'movie' of the catalysed reaction [3]. Pointing to a different research direction, X-ray imaging was applied for localising small biomolecular crystals in optically opaque matrices, such as cryogenically cooled lipidic cubic phase [4].

The services of the EMBL sample preparation and characterisation (SPC) facility were accessible to internal (EMBL, CSSB) and external users (in total 155). A first collaborative paper with several groups of the Centre for Structural Systems Biology (CSSB) was published [5]. Translational scientific discoveries with hospitals and industry partners led to two publications in Science Immunology [6, 7].

Figure 1

Top view on the sample of P13 in low-energy configuration: The crystal is mounted on a high-precision diffractometer axis including a mini-kappa goniostat entering from the right. X-rays arrive to the sample from the bottom of the picture; an open flow cryostat (from the left) is used to cool the sample. A large fraction of the path that the X-rays take from the sample to detector (top) is located in a Helium atmosphere ('tent'-like structure towards the top) minimising the effects of air absorption on the quality of anomalous measurements. Foto: EMBL/Kinga Lubowiecka.

Figure 2

Plenum discussions during the conference 'Tools for Structural Biology of Membrane Proteins' at the CSSB lecture hall.

Research in structural and infection biology

In an increasingly dense network with internal EMBL collaborators and external on-site collaborators from CSSB, Center for Free-Electron Laser Science (CFEL) and Hamburg Advanced Research Centre for Bioorganic Chemistry (HARBOR), group leaders from the Hamburg Unit continued to increase their methods portfolio for most challenging protein complexes and by focusing on themes in the field of infection biology.

The EMBL/CSSB research group of Christian Löw, in collaboration with another EMBL/CSSB group leader Jan Kosinski, published a highlight paper on the structure of a prototypic peptide transporter DtpA in the presence of the anti-Herpes pro-drug Valganciclovir [8]. The structure revealed that the drug is coordinated differently than originally anticipated and opens news ways to modify drugs for more efficient uptake.

The EMBL group of Annabel Parret and Matthias Wilmanns, in collaboration with the EMBL colleagues Thomas R. Schneider and Dmitri Svergun, published a highlight paper on the discovery and characterisation of a novel toxin/antitoxin system called MbcAT in Mycobacterium tuberculosis [9]. When released from the antidote antitoxin MbcA, the toxin MbcT shows a strong cidal activity by removing nicotinamide through phosphorylation from the pathogen's metabolism.

News and Events

With the new CSSB building been completed, the EMBL Hamburg Unit could make full use of the conference opportunities there the first time. The EMBO conference entitled 'Tools for Structural Biology of Membrane Proteins', coordinated by Christian Löw from EMBL as main organiser, featured various world-leading speakers of the field (Fig. 2). An EMBL Practical Course entitled 'Practical integrative structural biology' took place in November 2019 and was coordinated by Jan Kosinski as main organiser.

The EMBL Hamburg Unit is a key partner of the Stanford/EMBL Life Science Alliance. Leading researchers from Stanford and Hamburg working in the field of structural biology joined for a first workshop in Hamburg in May 2019. A call for joint Stanford/EMBL postdoctoral fellowships under the umbrella of the Life Science Alliance opened towards the end of 2019.

The EMBL Unit was also very much honoured by a dedicated visit of the First Major of the City of Hamburg Peter Tschentscher in December 2018. EMBL has an intensive ongoing cooperation with the French TARA Ocean Foundation, which already has led to various joint publications in leading research journals. As part of a European coastal campaign analysing micro-plastic pollution in main rivers across Europe, the TARA research boat visited the City of Hamburg (Fig. 3). Apart from several joint EMBL/TARA events at the centre of the Hamburg harbor, the city of Hamburg used the occasion to invite for a reception at the historical town of Hamburg, which was attended by the Senator for Science, Research and Equality Katharina Fegebank, the French ambassador in Germany Anne-Marie Descôtes, and the EMBL Director General Edith Heard.

Rob Meijers, who had been group leader at the EMBL Hamburg Unit since 2009, has accepted a new faculty position at Harvard University and left EMBL by the end of 2019.

Contact: Matthias Wilmanns, matthias.wilmanns@embl-hamburg.de

Figure 3

On board the TARA research vessel visiting Hamburg, from left to right: Matthias Wilmanns (EMBL Hamburg), Anne-Marie Descôtes (Ambassador of France to Germany), Romain Troublé (CEO TARA Foundation), Edith Heard (EMBL Director General), Eric Karsenti (EMBL), Laurent Toulouse (French Consul General in Hamburg).

References

1. K. H. G. Verschueren et al., Nature 568: 571-575 (2019).
2. P. Mehrabi et al., Nat Methods 16: 979-982 (2019).
3. P. Mehrabi et al., Science 365: 1167-1170. (2019).
4. M. Polikarpov et al., Acta Cryst. D, in press.
5. V. Kotov et al., Scientific Reports 9(1): 10379. (2019).
6. A. Moritz et al., Science Immunology 4: eaav0860 (2019).
7. S. K. Saini et al., Science Immunology 4: eaau9039 (2019).
8. Y. Ural-Blimke et al., J Am Chem Soc. 141: 2404-241 (2019).
9. D. M. Freire et al., Mol Cell. 73(6): 1282-1291 (2019).

The GEMS branch at DESY

Helmholtz-Zentrum Geesthacht operates the German Engineering Materials Science Centre

The experimental stations of GEMS have been continuously developed and upgraded for engineering materials science and general imaging users from institutions in Germany and all over Europe. The number of publications remains on a high level; a selection is presented below. New *in situ* techniques focussing on additive manufacturing (AM) as well as phase contrast and other imaging techniques are in the focus of interest.

Diffraction

P61, the only white-beam beamline at PETRA III, is shared between HZG (P61A) and DESY (P61B). The first diffractometer and energy-dispersive detectors at P61A will be ready for first experiments in spring 2020. HZG will focus on materials research with, e.g., depth-resolved residual stress analysis.

The experiments with an *in situ* selective laser melting (SLM) chamber of the TU Berlin groups of W. Reimers and E. Uhlmann at P07 have continued successfully in 2019. The large melting zone furnace for directional solidification experiments ('FlexiDS') has been used at P07 for a follow-up beamtime in 2019, and another one is planned. The BMBF-funded collaborative research project of KIT (M. Heilmeier) and University of Magdeburg (M. Krüger, now at FZ Jülich) ended in July; other groups will be welcome for cooperation.

At P07, an investigation related to additive manufacturing of Ni-based superalloys has been carried out [1]. The large thermal gradients and high solidification rates of selective electron beam melting (SEBM) give rise to microstructures that are very fine and far from equilibrium. CMSX-4 as a Ni-based superalloy is hardened by precipitates that can grow under a heat treatment. This reduces the ductility of the material, which can result in cracking. Laser scanning patterns used during the build-up of one layer and from subsequent layers result in multiple heat treatments. These can lead to different precipitation states in dependence of the temperature history. Therefore, the thermal history experienced by a volume element through cyclic heating and quenching of SEBM-built superalloy CMSX-4 was investigated using small-angle X-ray scattering (SAXS). Thereby, a fundamental understanding of phase transformations and particle coarsening processes that take place during additive manufacturing was gained. Although the dilatometer furnace used does not offer the high heating and cooling rates that occur in SEBM, a very precise control of heating and cooling sequences up to reasonably high gradients of 300 K/s can be realised for simulating the process heating cycles. The results show that the precipitation reaction is fast and that the volume fraction follows the temperature very closely (Fig. 1). However, the equilibrium volume fraction is not even reached after 20 min showing that SEBM is a non-equilibrium process. Significant coarsening is only observed when the temperature stays below the solvus temperature.

Such experiments are a perfect addition to *in situ* AM experiments, because temperatures cycles can be defined precisely, leading to perfect input for process simulations.

Imaging

Multiple technical improvements of the imaging facilites at beamlines P03, P05 and P07 have led to a continuous performance increase of these instruments over the past year. Improvements in monochromator stability and detector control led to yet another speed-up of tomography data acquisition in absorption and phase contrast modes. Usable, full tomography datasets can now be obtained in one second for microtomography and in one minute for nanotomography. A spatial resolution of below 40 nm for absorption and

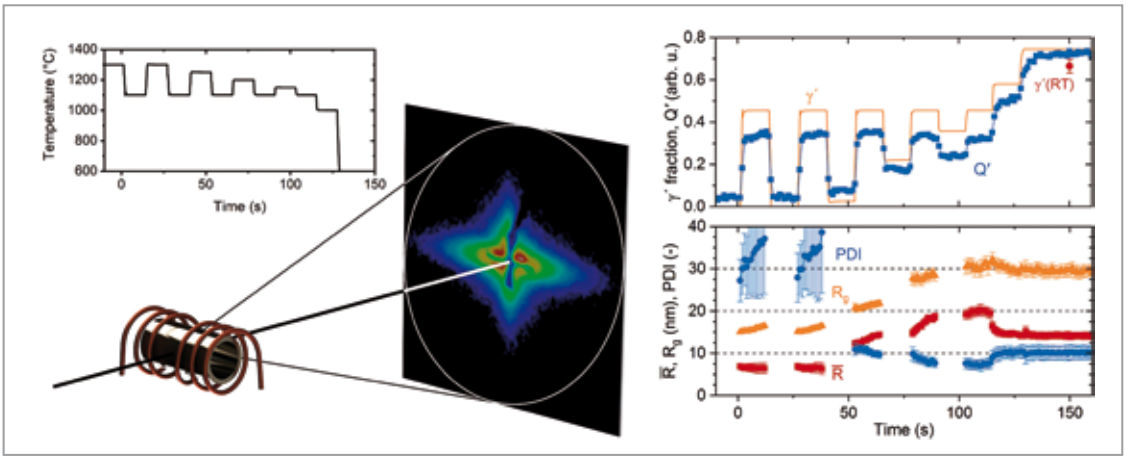

Figure 1

Temperature cycles (top left), volume fraction (top right) and mean radius (bottom right) of γ' precipitates in CSMX-4 as obtained from a high-energy SAXS experiment with a dilatometer for heating and quenching [1].

Zernike phase contrast imaging has been achieved, using specifically tailored optics. In addition, a fast scan mode was established, where a high-quality, full nano tomography scan (absorption as well as Zernike phase contrast), can be performed in less than three minutes.

The microtomography station of beamline P05 was used in a study of self-healing protective sealings. Plasma electrolytic oxidation (PEO) is a green anodising process using micro-discharges to produce hard and dense ceramic-like coatings with a good wear and corrosion resistance. However, the discharges introduce defects and pores, which can lead to a failure in long-term corrosion protection. A top coating of layered double hydroxide (LDH) can act as a 'smart' delivery system with reservoirs for corrosion inhibitors that are released in presence of corrosive species, changes in pH or even mechanical damage. This study investigated the growth of LDH on PEO coated aluminum alloys, aiming at an economically friendly corrosion protection method. Microtomography was essential to provide three-dimensional information about the pore size distribution along the different layers in a non-destructive manner, as shown in Fig. 2a [2].

Many biomaterials, such as nacre or bone, exhibit simultaneously high toughness and strength, owing to their hierarchical supercrystalline nanocomposite structure. Key to these properties is the structural organisation of multiple phases across multiple length scales. However, this structure requires fabrication through processes of self-assembly and is very challenging. Microtomography and diffraction data from beamline P07 were used to analyse the synthesis of a synthetic hierarchical nanocomposite material via the self-assembly of oleyl phosphate (OPh)-stabilised iron oxide (Fe_3O_4) nanoparticles (NPs). Beyond a critical concentration of the organic phase, a hierarchical material is consistently formed with ceramic nanoparticles self-assembling into supercrystals in face-centred cubic superlattices, which in turn form granules of up to hundreds of micrometres. These micrometric granules are the constituents of the final mm-sized material, as shown in Fig. 2b. This approach demonstrates a way towards the design of novel high-performance structural materials [3].

At the Nanofocus end station of P03 beamline, spatially resolved wide-angle X-ray scattering (WAXS) data provided the diffraction contrast to visualise strain and stress distributions in thermally annealed Ti-Al-N/Mo-Si-B multilayer coatings. Owing to its outstanding thermomechanical properties, physical vapor deposited (PVD) $Ti_{1-x}Al_xN$ is a prominent and versatile protective coating used in various industrial applications. However, if exposed to both thermal stresses and an oxidising atmosphere, Al_2O_3 and TiO_2 based oxides are formed and due to their differing specific volume, thermal expansion and elastic constants induce surface crack formation. Scanning X-ray nanodiffraction data, recorded at P03 with a nanofocused X-ray beam, was used to visualise the stress and strain evolution across different Ti-Al-N/Mo-Si-B multilayer systems with varying bilayer periods (ranging from

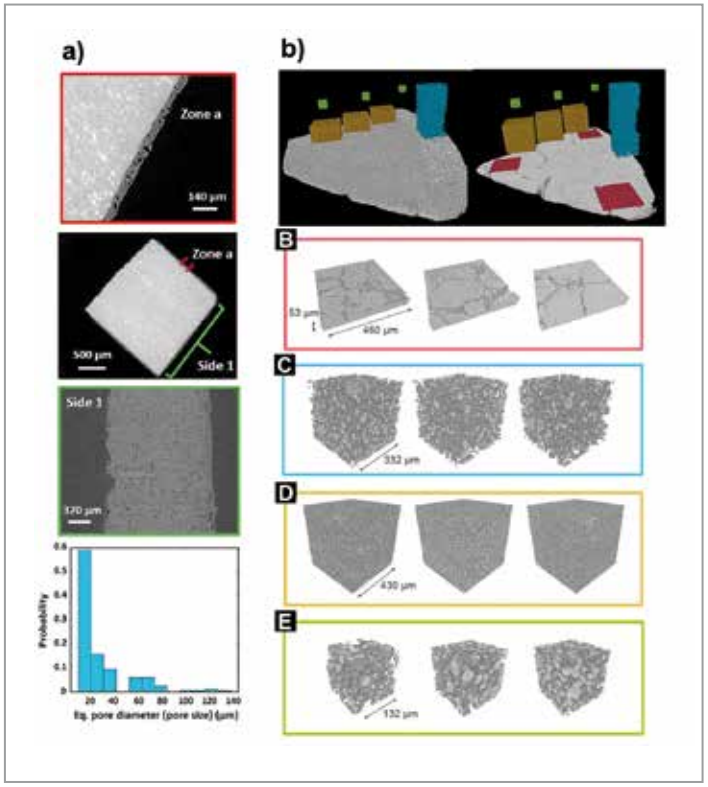

Figure 2

a) Slices through the tomographic reconstruction of a PEO/LDH hybrid in an orthogonal direction, magnification of a small area ('zone a') and along the PEO coating ('side 1') and a histogram of the pore size distribution of the PEO coating (image from [2]). b) Microtomography data of oleyl phosphate stabilised iron oxide nanoparticles where (B) is the flat super-crystalline bottom layer, (C) is the outer edge of the sample at an increasing distance from the bottom of the sample, (D) is the outer edge of the sample at an increasing distance from the edge of the sample and (E) is the upper part of the sample at an increasing distance from the edge of the sample (image from [3]).

1085 to 26 nm) under different states of thermal and oxidising wear. The study highlights the possibilities to influence the stress/strain state as well as the material's hardness by using well-defined designs in industrial manufacturing processes [4].

The coming year will bring further improvements and developments: Examples are the new EIGER 6M detector at the Nanofocus end station of beamline P03, the new lens tank at beamline P07 that will bring an additional increase in intensity, and the first friendly users at the new white-beam beamline P61A. Furthermore, the completion of the CXNS building with the GEMS wing is planned for 2020.

Contact: Christina Krywka, christina.krywka@hzg.de
Peter Staron, peter.staron@hzg.de
Martin Müller, martin.mueller@hzg.de

References

1. B. Wahlmann et al., Acta Mater. 180 (2019) 84–96.
2. A. C. Bouali et al., Appl. Surf. Sci. 494 (2019) 829-840.
3. B. Domenech et al., Sci. Rep. 9 (2019) 3435.
4. E. Aschauer et al., Surf. & Coat. Tech. 361 (2019) 364-370.

DESY Photon Science at the European XFEL

Status of the user consortia

SFX

The international SFX Consortium, led by DESY, provides methodologies and instrumentation for serial femtosecond crystallography experiments at the “Single Particles, Clusters, and Biomolecules and Serial Femtosecond Crystallography’ (SPB/SFX) instrument of the European XFEL (EuXFEL).

The method is becoming routinely applied at the instrument for structure determination of macromolecules at ambient pressures and temperatures, with several published accounts of the feasibility of the approach using the megahertz pulse trains, which are a unique feature of the European XFEL [1]. Using the Adaptive Gain Integrating Pixel Detector (AGIPD) available at the instrument it is now possible to record many thousands of diffraction frames per second, each potentially providing diffraction from a fresh new crystal. This represents a significant increase in the speed that experiments can be carried out, enabling high-resolution structures to be determined over an extensive range of environmental or chemical conditions, time points, or reacting species. Indeed, full datasets for structure determination have been collected in only a few minutes. Currently, the downstream interaction region of the instrument is being commissioned, to eventually allow two experiments to be conducted concurrently.

HIBEF

The HIBEF User Consortium contributes different drivers for experiments at high energy density like optical lasers and a diamond-anvil cell (DAC) setup to the High Energy Density (HED) instrument of EuXFEL. The consortium is led by the Helmholtz-Zentrum Dresden-Rossendorf, with DESY and the Central Laser Facility (CLF) from Oxford as the biggest consortium partners.

In 2019, the installation of the high-intensity laser was completed, and first commissioning experiments on the temporal correlation of laser and EuXFEL beam were successful. This laser is open for community commission proposals for the next run in 2020. The high-energy laser contributed by CLF passed the factory acceptance test and is currently being shipped to EuXFEL for installation in 2020. This system will enable high-pressure science like ramped and shock compression reaching multi-Mbar pressures and multi-MeV temperatures.

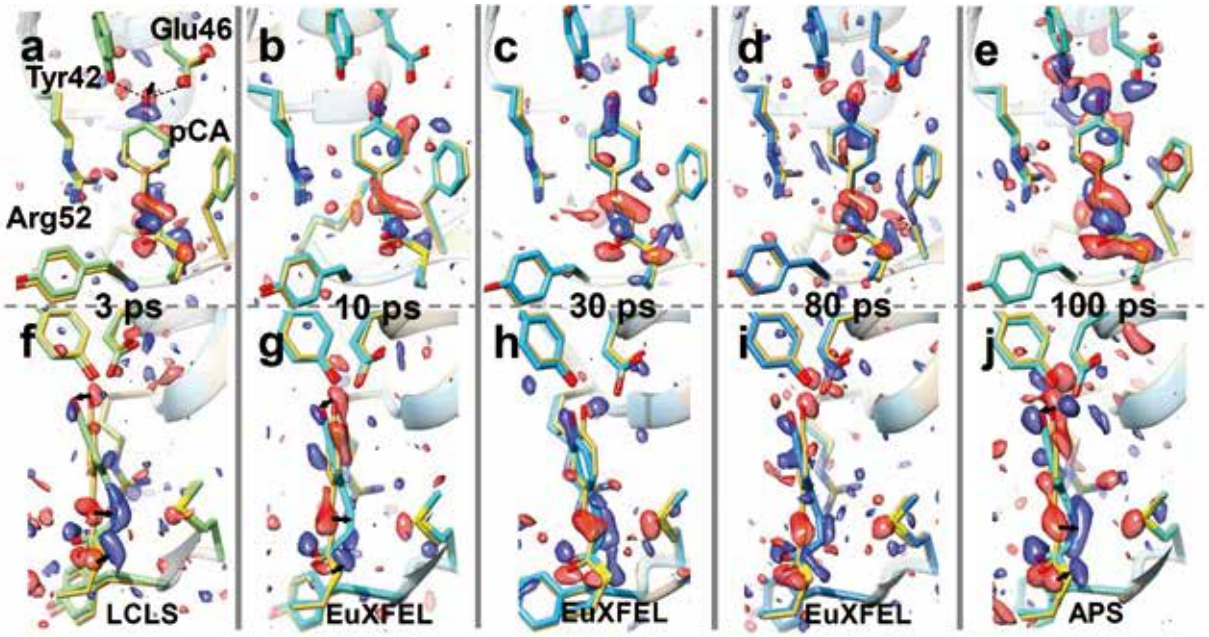

Figure 1

A series of structures of photoactive yellow protein at times after activation, collected at the LCLS, European XFEL, and the Advanced Photon Source [1].

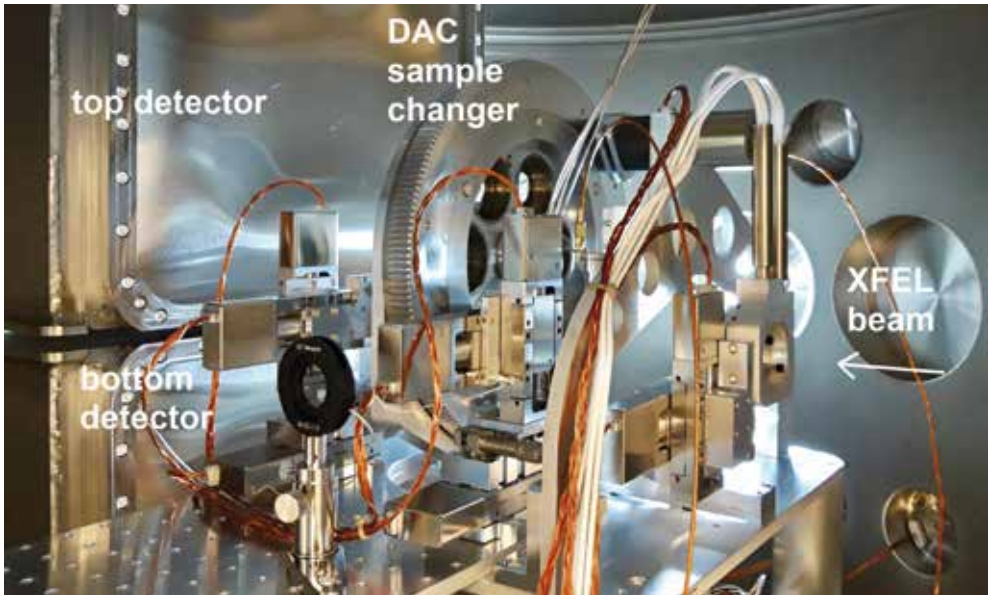

Figure 2
Setup in interaction chamber 2 changer that was successfully used in the first DAC community proposal with over 40 participants on-site from ten different countries.

DESY has completed the installation of interaction chamber 2, the DAC setup, and integrated two Varex flat panel detectors at HED (see Fig. 2). In October, the setup was commissioned in a very successful experimental campaign, with over 40 participants from the DAC community from ten different countries, exploiting both, single pulse and the bunch train structure. The DAC setup is available for users in the upcoming runs.

hRIXS

The Heisenberg RIXS consortium will bring resonant inelastic soft X-ray scattering (RIXS) to the transform limit in energy and time at the EuXFEL. Unique insights to chemical dynamics, driven phases as well as fundamental X-ray matter interaction open up new science directions. The optical design of the spectrometer is based on spherical variable linespacing gratings with the ability to achieve resolving powers ≥ 20 000 over an energy range of 250-1600 eV. hRIXS will be the world leading instrument to detect static properties and transient excitations in structure, charge, spin and orbital polarisation for chemical processes as well as a wide range of energy- and bio-relevant materials. To enable this vast range of experiments, the hRIXS spectrometer will be operated with two complementary, exchangeable end stations optimised for measurements on solid-state and liquid/gas phase targets.

The spectrometer and associated end stations are currently under construction at the Company Bestec (Fig. 3). The installation and commissioning at the Spectroscopy and Coherent Scattering (SCS) instrument at EuXFEL is scheduled for 2020.

Funding is provided by the Helmholtz Association via strategic investment in the Helmholtz-International Users consortium hRIXS. The project is partially supported by the ERC Advanced Grant ‘EDAX’ at Potsdam University. The hRIXS consortium includes partners from Germany, Switzerland, Finland, France, Sweden, Italy, and the UK. The project is coordinated by Potsdam University in close collaboration with DESY and European XFEL.

Contact:
SFX: Henry Chapman, CFEL/DESY and Universität Hamburg, henry.chapman@desy.de
HIBEF: Thomas Cowan, HZDR, t.cowan@hzdr.de
hRIXS: Alexander Föhlisch, Potsdam University and HZB, alexander.foehlisch@helmholtz-berlin.de

References

1. S. Pandey, et al., Nature Methods (2019). DOI: 10.1038/s41592-019-0628-z.

Figure 3
The photograph shows the hRIXS system in the Bestec assembly hall. The spectrometer is still under construction and in the test phase. Image: Bestec

DESY Innovation and Technology Transfer

Optimising steel for components in the automotive industry

Measurements at DESY's synchrotron radiation sources PETRA III and FLASH provide research-based companies with crucial information and data to better understand their materials and optimise manufacturing processes. An example for industrial beamtime at PETRA III is described here.

The joint research initiative of the company SSAB and the metals research institute Swerim, supported by the Swedish Innovation Agency Vinnova, had the aim to optimise materials and internal stresses introduced during the cutting processes of steel sheets for the automotive industry.

Using synchrotron radiation at PETRA III the measurements provided new insights in residual stress at cut edges of steel sheets after shearing. Alternative methods, namely milling after shearing and laser cutting that are believed to relieve or to lessen the effect stress has on the materials, were also investigated. The measurements were carried out by scientists of Swerim AB, SSAB and DESY.

Challenge: low endurance of steel sheets for the designated use

Shearing works are one step in the process from a steel sheet towards a finished product that may introduce stress, which can be detrimental at later stages of the product's life. One reason is fracture induced by hydrogen embrittlement (HE).

For the automotive industry, the use of ultra-high strength steel (UHSS) in structural components helps to reduce vehicle weight, which improves fuel efficiency and lowers greenhouse gas emissions.

Sensitivity towards HE, which is caused by high edge stress may limit the use of UHSS in this field. The residual stress can by analysed on a microscopic scale at high energy X-ray sources as they allow for deep penetration and a small probing focus.

Microscale analysis at the diffraction and imaging part of the Swedish Materials Beamline P21

In this work, high energy synchrotron radiation of beamline P21 at PETRA III was used to map stress in cut edges in an UHSS material. The examined material was a commercial steel from the project's industrial partner SSAB, which is used in the automotive industry and is fully martensitic with a minimum tensile strength of 1200 MPa. The material was cut with a power shearing device using recommended cutting parameters. Residual stress after alternative treatments used for stress relieve, namely milling after shearing and laser cutting, were also studied. Thin cross sections perpendicular to the cut edges were prepared, and the measurements were made in transmission mode.

Synchrotron radiation was used to map residual stress with resolution on the microscale. Thereby it became possible to localise regions of stress concentration that have been introduced during cutting of the ultra-high strength steel. The measured stress maps show that shearing will introduce concentrations of tensile stress leading to an enhanced hydrogen diffusion to critical areas in the material. As a result this study provides a method to map mechanically and thermally induced stress states with high resolution and to refine the cutting processes in industrial production processes. The results are an important basis to develop optimised steel components for the use in automotives and further fields of application.

This is an example showing how R&D-focused companies can benefit from the commercial use of large-scale facilities and foster product development and innovation. As part of its strategy with regard to innovation and technology transfer, DESY increasingly provides commercial access to large-scale facilities for industrial users by offering a broad portfolio of measurements at DESY's photon sources during beamtimes including the scientific support and consulting.

Contact: Arik Willner, arik.willner@desy.de

DESY Photon Science facilities on the research campus Hamburg-Bahrenfeld (July 2019).

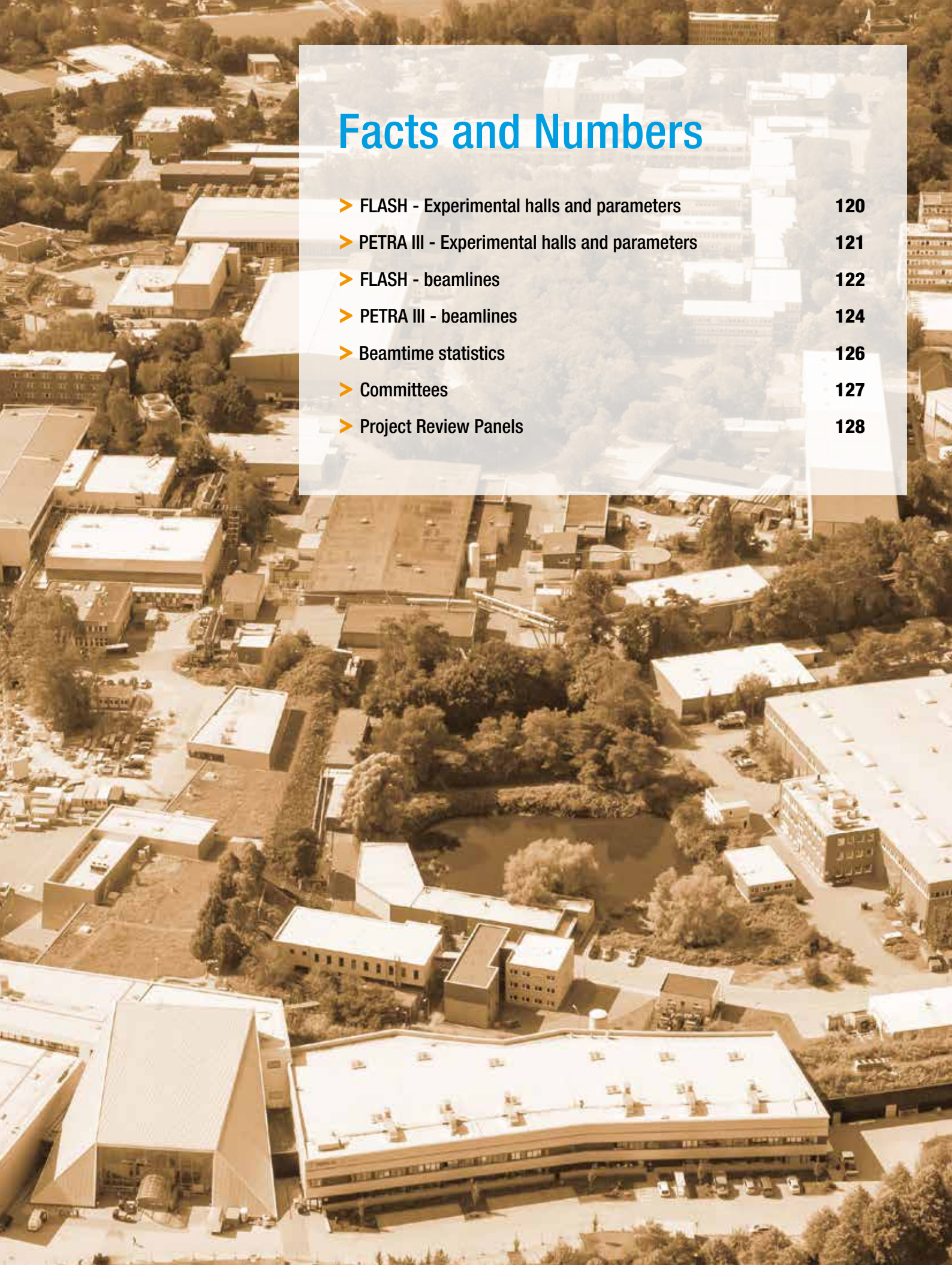

Facts and Numbers

FLASH

Experimental halls and parameters

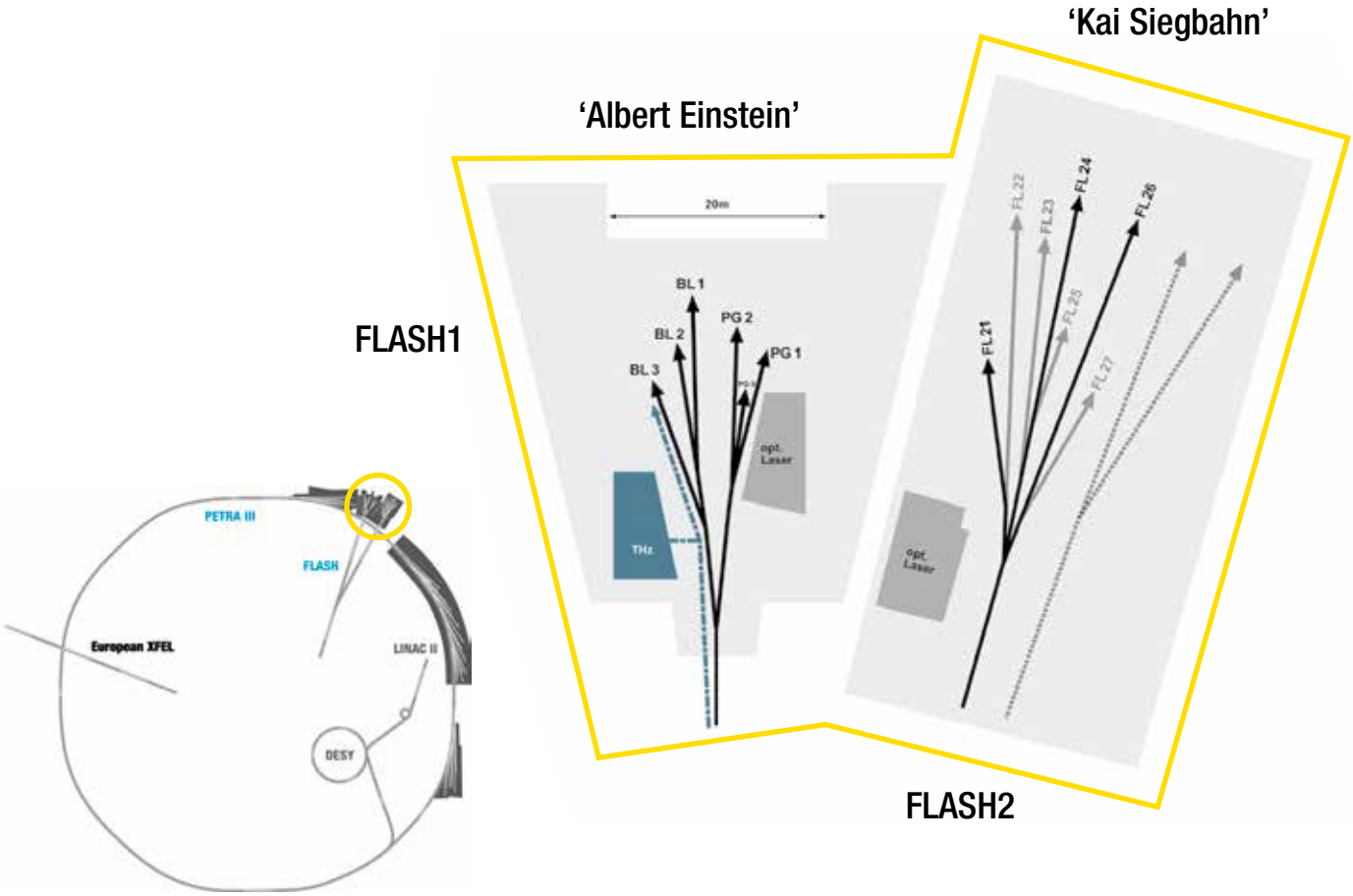

FLASH - machine parameters

	FLASH1	FLASH2
Electron energy range	0.35 – 1.25 GeV	0.4 – 1.25 GeV
Normalised emittance at 1 nC (rms)	1.4 mm mrad	1.4 mm mrad
Energy spread	200 keV	500 keV
Electron bunch charge	0.02 – 1.2 nC	0.02 – 1 nC
Peak current	1 – 2.5 kA	1 – 2.5 kA
Electron bunches per second (to be shared between FL1 and FL2)	5000	5000

FLASH - lasing parameters

	FLASH1	FLASH2
Photon energy fundamental	24 – 295 eV	14 – 310 eV
Wavelength fundamental	51 – 4.2 nm	90 – 4 nm
Photon pulse duration (FWHM)	30 – 200 fs	10 – 200 fs (estimated)
Peak power	1 – 5 GW	1 – 5 GW
Single photon pulse energy (average)	1 – 500 µJ	1 – 1000 µJ
Spectral width (FWHM)	0.7 – 2 %	0.5 – 2 %
Photons per bunch	10^{11} – 10^{14}	10^{11} – 10^{14}
Peak brilliance photons/sec/mm^2/mrad^2/0.1%	10^{28} – 10^{31}	10^{28} – 10^{31}

PETRA III

Experimental halls and parameters

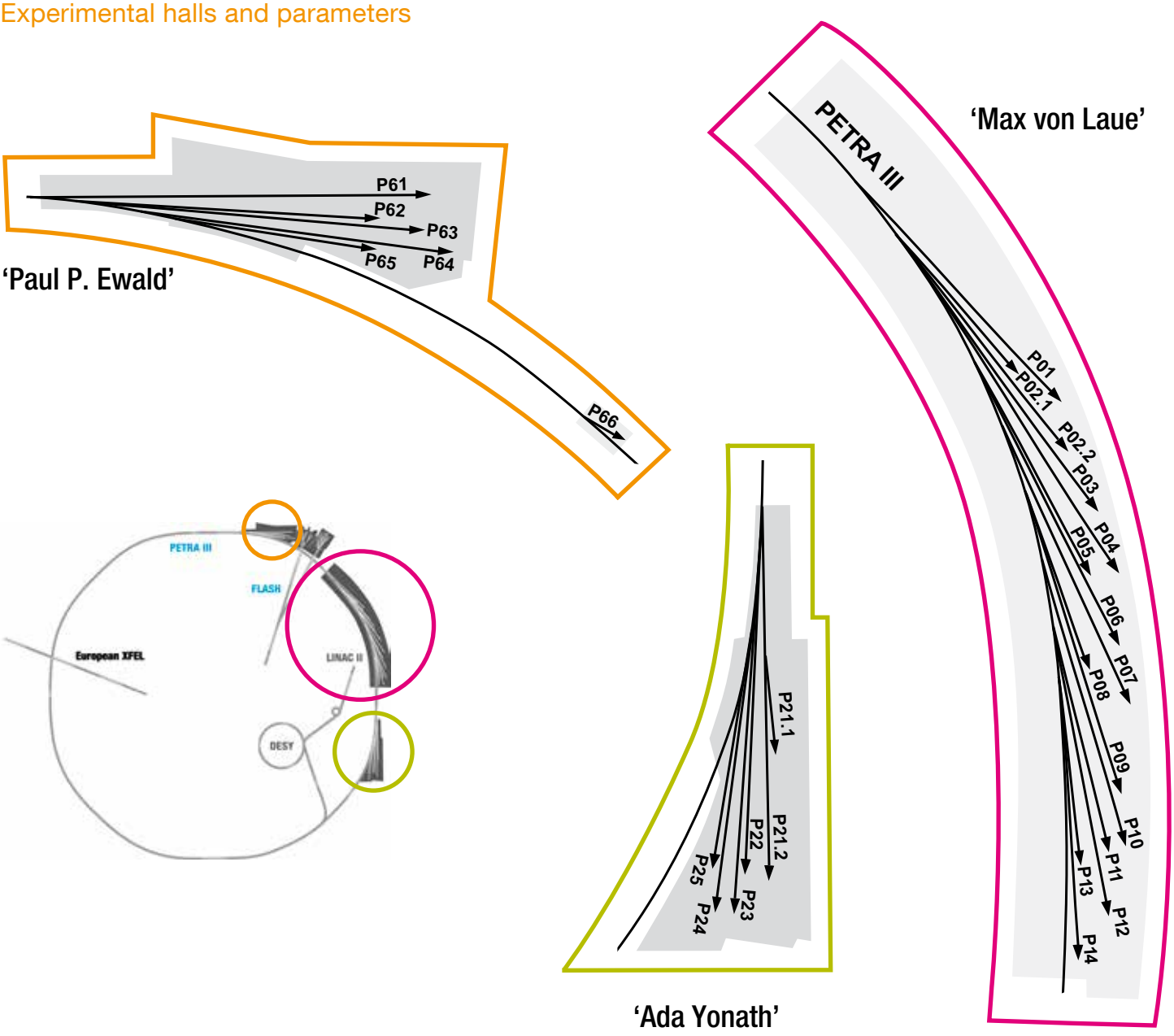

PETRA III - machine parameters

Electron energy	6.08 GeV
Circumference of the storage ring	2304 m
Number of bunches	960 or 480 (brightness mode) 60 or 40 (timing mode)
Bunch separation	8 ns, 16 ns, 128 ns, 192 ns
Electron beam current	100 mA (timing mode) 120mA (brightness mode)
Horizontal electron beam emittance	1.3 nmrad
Vertical electron beam emittance	0.01 nmrad
Electron beam energy spread (rms)	0.1%
Horizontal x vertical beam size (rms) at 5 m undulator (high β section) and 10 keV photon energy	141 µm x 5.2 µm
Horizontal x vertical beam size (rms) at 5 m undulator (low β section) and 10 keV photon energy	36 µm x 5.7 µm

FLASH

Beamlines

FLASH1 experimental hall 'Albert Einstein'

BL1	non-monochromatic FEL photons Kirkpatrick-Baez (KB) focusing optics, FEL focal spot of ~7 µm × 8 µm (FWHM)	
	split-and-delay unit for XUV pump – XUV probe experiments (mirrors for 13.57 nm, - 30 ps to + 650 ps delay)	*TU Berlin*
	optional pump – probe experiments using FLASH1 optical laser system	
	4-mirror polariser for variable FEL polarisation from 30 – 70 eV	*TU Berlin*
	permanent end station: multipurpose CAMP chamber with pnCCD detectors, electron and ion spectrometers and collinear incoupling optics for optical laser	
BL2	non-monochromatic FEL photons focused to ~20 µm (>4.5 nm) / unfocussed beam size ~5 – 10 mm (FWHM, depending on wavelength)	
	XUV beam splitter with variable time delay (-3 ps to 15 ps) for photon diagnostics and XUV pump – XUV probe experiments	
	optional pump – probe experiments using FLASH1 optical laser system	
	4-mirror polariser for variable FEL polarization from 30 – 70 eV	*TU Berlin*
	about 3 × 4 m platform for user-provided end station	
BL3	non-monochromatic FEL photons, spectral range: >4.5 nm (carbon coated optics) focused to ~20 µm / unfocussed beam size ~5 – 10 mm (FWHM, depending on wavelength)	
	optional pump – probe experiments using FLASH1 optical laser system	
	4-mirror polariser for variable FEL polarization from 30 – 70 eV	*TU Berlin*
	optional pump – probe experiments using **THz radiation**: - tunable: 10 – 230 µm; up to 150 µJ/pulse; ~ 10% bandwidth - broadband at 200 µm; up to 10 µJ/pulse; ~ 100% bandwidth - synchronised and phase stable to X-ray pulses (down to 5 fs) - delivered to the experiment via vacuum beamline as: (i) ultra-high vacuum (~10^{-8} mbar), shorter delay between THz and X-ray (~4 m path difference); can accommodate up to 0.3 m wide setup (ii) high vacuum (~10^{-6} mbar), longer delay between THz and X-ray (~7 m path difference); can accommodate up to 2 m wide setup - UHV chamber with mounts for refocusing XUV optics to compensate for XUV/THz path delay	
	about 3 × 4 m platform for user-provided end station	
PG1	high resolution plane grating XUV monochromator (SX 700 type, < 10^{-4} bandwidth, carbon coated optics): - variable combination of photon flux and resolution (from high flux to high resolution) - controlled temporal-spectral properties at moderate resolution for pump – probe experiments - high photon flux with harmonic filtering Kirkpatrick-Baez (KB) refocusing optics, FEL focal spot down to 5 µm FWHM (vertically)	
	permanent end station: - XUV-Raman spectrometer for high-resolution and time-resolved RIXS measurements on solid samples (60 - 600 K, resolving power ~1500) - optional pump - probe experiments using FLASH1 optical laser system (time resolution ~300 fs, wavelengths of 800 nm, 400 nm and 267 nm are available)	
PG2	uses the same monochromator as PG1 50 µm focus	
	XUV beam splitter with variable time delay (±6 ps) for time resolved studies	
	optional pump – probe experiments using FLASH1 optical laser system	
	about 3 × 4 m platform for user-provided end station	

FLASH1 optical / NIR laser system for pump – probe experiments

10 Hz single pulse	a)	compressed pulse transported over beamline 810 nm, 1.5 mJ, 60 fs FWHM pulse duration, 25 nm FWHM spectral bandwidth synchronization to FEL better than 60 fs rms
	b)	stretched pulse (chirped) transported over beamline pulse compressor must be included in experimental set-up 810 nm, 15 mJ, 200 ps FWHM uncompressed, 25 nm FWHM bandwidth 810 nm, 10 mJ, 60 fs FWHM with external pulse compressor, 25 nm FWHM bandwidth SHG 407 nm, 600 µJ, 5 nm FWHM spectral bandwidth THG 270 nm, 200 µJ, 2.5 nm FWHM spectral bandwidth synchronization to FEL better than 60 fs rms, corrected for drifts
burst-mode		up to 400 pulses / burst 805 nm, 20 µJ per single pulse, 120 fs FWHM pulse duration synchronization to FEL better than 60 fs rms
All laser options are available at Beamlines BL1-3, 10 Hz single pulse laser options are not available at PG1-2.		

FLASH2 experimental hall 'Kai Siegbahn'

FL24	non-monochromatic FEL photons wavelength range: 4 – 90 nm fundamental Kirkpatrick-Baez (KB) focusing optics with variable foci down to < 10 µm (FWHM) / unfocussed beam size ~5 – 10 mm (FWHM, depending on wavelength)	
	optional pump – probe experiments using FLASH2 optical laser system	
	grazing incidence split-and-delay unit with ±12 ps time delay	*Univ. Münster*
	about 3 × 4 m platform for user-provided end station	
FL26	non-monochromatic FEL photons wavelength range: 6 – 90 nm fundamental	
	optional pump – probe experiments using FLASH2 optical laser system	
	permanent end station: - reaction microscope (REMI) for time-resolved AMO spectroscopy - grazing incidence delay-line and refocusing optics: FEL focal spot < 10 µm × 10 µm (FWHM, depending on wavelength) - ±2.7 ps time delay range, 1 fs precision	*MPI-K Heidelberg*

FLASH2 optical / NIR laser system for pump – probe experiments
Available for the FLASH2 beamlines FL24 and FL26

central wavelength	700 to 900 nm (fast tuneable)
spectral bandwidth	30 to 100 nm (pre-set for experiment)
intra-burst-repetition rate	100 kHz
number of pulses per burst	1 – 80
pulse duration	15 – 35 fs FWHM (compressed to 1.1 × bandwidth limit), <500 fs FWHM (uncompressed)
timing jitter to FEL	< 75 fs rms
pulse energy	0 – 250 µJ (before coupling to chamber), 0 – 150 µJ (at interaction region)
polarization	flexible
focus size ($1/e^2$ diameter)	FL24: < 100 µm, FL26: < 50 µm
peak intensity	> 10^{14} W/cm^2
time delay to FEL	- 4 ns to + 4 ns, 10 fs resolution, larger delays optional
energy stability	< 10% pulse-to-pulse peak (3% rms)

Harmonic generation conversion to 400 nm and 266 nm central wavelength are available with conversion efficiencies of > 30% SHG, > 5% THG

All FLASH beamlines provide online photon diagnostics for intensity, wavelength and beam position, fast shutter, aperture and filter sets.

Acknowledgement
We would like to acknowledge all contributions to the development and operation of FLASH and PETRA III beamlines and instruments provided within the framework of BMBF-Verbundforschung, and as part of collaborations with the Department of Science and Technology (Government of India) 'India@DESY', the Ruprecht-Haensel-Laboratory (Kiel University), the Max Planck Society and the Forschungszentrum Jülich.

PETRA III

Beamlines

PETRA III experimental hall 'Max von Laue'

Beamline and instruments		Operated by
P01	High Resolution Dynamics 10 m U35 | 2.5 – 80 keV	DESY
	Nuclear resonant scattering	DESY
	Resonant inelastic scattering	DESY / MPG
	X-ray Raman scattering	DESY / MPG
P02.1	Powder Diffraction and Total Scattering 2 m U23 | 60 keV	DESY
	Standard and *in situ* powder diffraction	DESY
	Standard and *in situ* total scattering	DESY
P02.2	Extreme Conditions 2 m U23 | 10 – 60 keV	DESY
	Laser heated experiment for diamond anvil cells	DESY
	General purpose experiment for high pressure applications	DESY
P03	Micro- and Nano-SAXS / WAXS 2 m U29 | 8 – 23 keV	DESY
	Micro-beam small and wide angle scattering	DESY
	Nano-beam scattering and diffraction	DESY
P04	Variable Polarization Soft X-rays 5 m UE65 | 250 – 2800 eV	DESY
	UHV diffractometer and soft x-ray spectrometer	DESY
	Photon-ion spectrometer (PIPE)	DESY / collaborators
	Ultra-high resolution photoelectron spectroscopy (ASPHERE)	DESY / collaborators
	Soft X-ray absorption holographic imaging instrument	DESY / collaborators
	Nano focus apparatus for spatially resolved spectroscopy	DESY / collaborators
P05	Micro- and Nano-Imaging 2 m U29 | 8 – 50 keV	HZG
	Micro-tomography	HZG
	Nano-tomography	HZG
P06	Hard X-ray Micro- / Nanoprobe 2 m U32 | 5 – 100 keV	DESY
	Microprobe	DESY
	Nanoprobe	DESY
P07	High Energy X-ray Materials Science 4 m IVU21 | 50 – 200 keV	HZG
	Multi-purpose triple-axis diffractometer	DESY
	Heavy load diffractometer	HZG
	Grain mapper	HZG
	High energy tomography	HZG
P08	High Resolution Diffraction 2 m U29 | 5.4 – 29.4 keV	DESY
	High resolution diffractometer	DESY
	Liquid surface diffractometer	DESY / collaborators
	Langmuir trough in-plane diffractometer	DESY
P09	Resonant Scattering and Diffraction 2 m U32 | 2.7 – 31 keV	DESY
	Single crystal resonant elastic X-ray scattering & diffraction (4 K < T < 750K)	DESY
	Single crystal REXS with magnetic fields (0.3 K < T < 300 K; B < 14 T)	DESY
	High pressure single crystal REXS (4 K < T < 300 K; p < 30 GPa)	DESY
	X-ray circular magnetic dichroism (> 4 K, < 6 T; < 2 T for linear dichroism)	DESY
	X-ray resonant magnetic reflectivity	DESY
P10	Coherence Applications 5 m U29 | 4 – 20 keV	DESY
	X-ray photon correlation spectroscopy (SAXS/WAXS geometry) (5 – 15 keV)	DESY
	Bragg coherent diffraction imaging (5 – 13 keV)	DESY
	GINIX - Nanofocusing setup (8 & 13.8 keV)	DESY / collaborators
P11	Bio-Imaging and Diffraction 2 m U32 | 2.4 – 30 keV	DESY
	Macromolecular crystallography (5.5 – 30 keV)	DESY / HZI / U Lübeck
	Serial crystallography (5.5 – 30 keV)	DESY

Beamline and instruments		Operated by
P12	Bio SAXS 2 m U29 | 4 – 20 keV	EMBL
	Small-angle X-ray scattering	EMBL
P13	Macromolecular Crystallography 2 m U29 | 4.5 – 17.5 keV	EMBL
	Macromolecular crystallography	EMBL
P14	Macromolecular Crystallography and Imaging 2 m U29 | 6 – 20 keV	EMBL
	Macromolecular crystallography (6 – 20 keV) High throughput micro-tomography (6 – 20 keV) Time-resolved serial crystallography (12.7 keV)	EMBL EMBL EMBL

PETRA III experimental hall 'Ada Yonath'

P21.1	Swedish Materials Science Beamline side branch: 2 m U29 | 50, 80, 100 keV	Center for X-rays in Swedish materials science (CeXS) / DESY
	Broad band diffraction	CeXS / DESY
P21.2	Swedish Materials Science Beamline 4 m IVU21 | 40 – 150 keV	Center for X-rays in Swedish materials science (CeXS) / DESY
	Multi-purpose triple-axis diffractometer Small angle scattering Grain mapper	CeXS / DESY CeXS / DESY (in commissioning) CeXS / DESY (in commissioning)
P22	Hard X-ray Photoelectron Spectroscopy 2 m U33 | 2.4 – 15 keV	DESY
	Hard X-ray photoelectron spectrometer (HAXPES) Ambient pressure XPS (POLARIS) Hard X-ray photoemission electron microscope (HAXPEEM)	DESY DESY / collaborators DESY / collaborators
P23	*In situ* Nano-Diffraction Beamline 2 m U32 | 5 – 35 keV	DESY
	XRD and secondary processes, *in situ* and complex environments	DESY
	Tomography	DESY/KIT (operation planned 2022)
P24	Chemical Crystallography 2 m U29 | 8, 15 – 44 keV	DESY
	Single crystal diffraction in complex sample environments	DESY
	Small molecule crystallography	DESY
P25	t.b.d.	not yet funded

PETRA III experimental hall 'Paul P. Ewald'

P61	High-Energy Wiggler Beamline 10 x 4 m damping wigglers | white beam btw. 30 – 250 keV	DESY (user operation II-2020)
	High-energy engineering materials science	HZG
	Large volume press - extreme conditions	DESY
P62	Anomalous Small-Angle X-ray Scattering 2 m U32 | 3.5 – 35 keV	DESY (user operation II-2020)
	Anomalous small-angle X-ray scattering SAXS tomography	DESY DESY
P63	t.b.d.	not yet funded
P64	Advanced X-ray Absorption Spectroscopy 2 m U32 | 4 – 44 keV	DESY
	Ex situ and *in situ* XAS High-resolution X-ray emission spectroscopy (non-resonant and resonant) QEXAFS	DESY DESY DESY
P65	Applied X-ray Absorption Spectroscopy 36 cm U32 | 4 – 44 keV	DESY
	Ex situ and *in situ* XAFS of bulk samples	DESY
P66	Superlumi *(hutch between PETRA III halls 'Paul P. Ewald' and 'Max v. Laue')* Bending magnet | 4 – 40 eV	DESY (operation planned 2021)
	Time-resolved luminescence spectroscopy	DESY

Beamtime statistics 2019

FLASH
Operation period 2019

	User beamtime	Machine studies and user experiment preparation	Maintenance	Shutdown and commissioning
FLASH (Linac)				
1 Jan – 28 Oct	3855 h	2396 h	46 h	934 h
planned for 29 Oct – 31 Dec	768 h	479 h	6 h	276 h
FLASH1				
1 Jan – 28 Oct	3060 h			
planned for 29 Oct – 31 Dec	624 h			
FLASH2				
1 Jan – 28 Oct	2210 h			
planned for 29 Oct – 31 Dec	540 h			

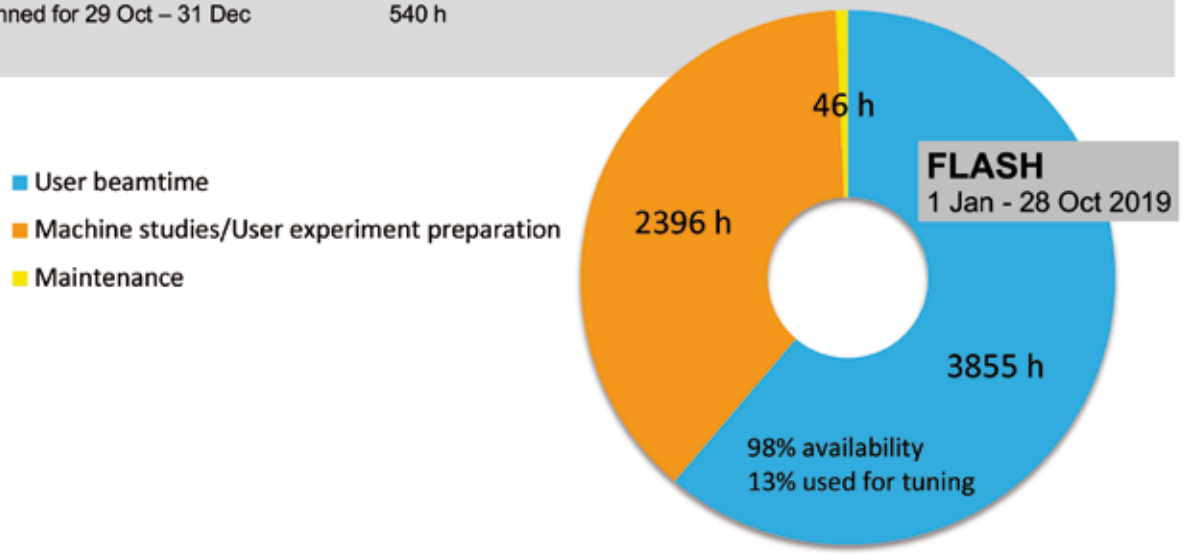

PETRA III
Operation period 2019

	User beamtime	Machine studies and test runs	Maintenance	Shutdown
1 Jan – 25 Nov	4217 h	1720 h	128 h	
planned for 26 Nov – 31 Dec	535 h	24 h	24 h	
				2112 h

run periods:
11 Mar – 15 Jul
5 Aug – 20 Dec

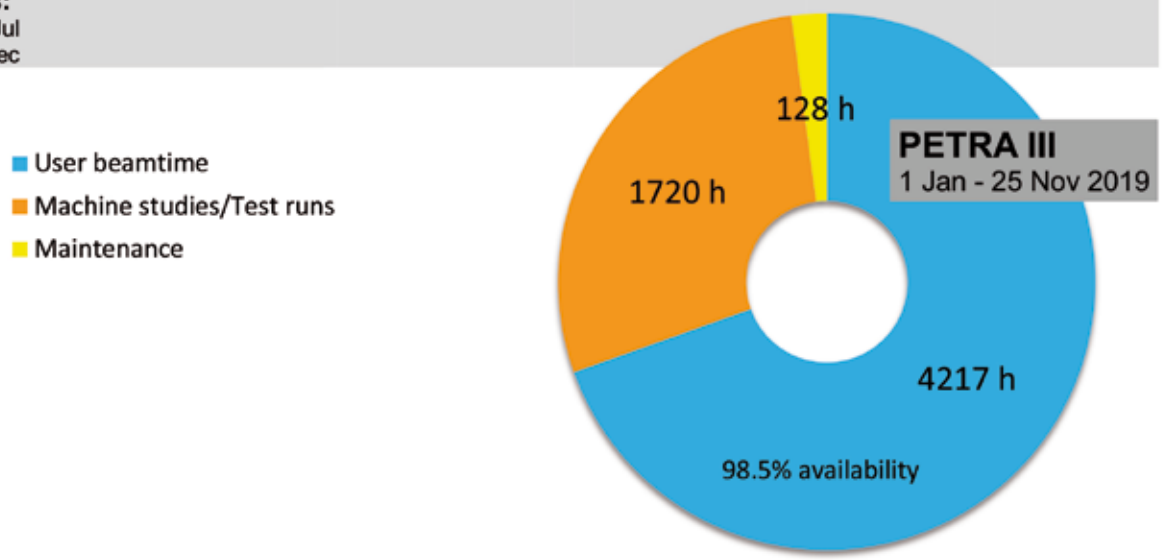

Committees 2019

Photon Science Committee PSC — advises the DESY Photon Science management

Christian David (chair)	PSI, Villigen, CH
Stefan Eisebitt (vice chair)	MBI and Technische Universität Berlin, DE
Gwyndaf Evans	Diamond Light Source Ltd., Didcot, UK
Jan-Dierk Grunwaldt	KIT, Karlsruhe, DE
Simo Huotari	University of Helsinki, FI
Sarah Köster	Georg-August-Universität Göttingen, DE
Edvin Lundgren	Lund University, SE
Arwen Pearson	CUI, Universität Hamburg, DE
Thomas Pfeifer	MPI for Nuclear Physics, Heidelberg, DE
Harald Reichert	ESRF, Grenoble, FR
Daniela Rupp	ETH, Zürich, CH
Bernd Schmitt	PSI, Villigen, CH
Thomas Schröder	HU Berlin and IKZ, Berlin, DE
Andrea Somogyi	Synchrotron SOLEIL, Saint-Aubin, FR
Stefan Vogt	Argonne National Laboratory, Lemont, US
Nele Müller (PSC secretary)	DESY, Hamburg, DE

Laser Advisory Committee LAC — advises DESY and European XFEL

Jonathan Zuegel (chair)	LLE, Rochester, US
Miltcho Danailov	Elettra-Sincrotrone, Trieste, IT
Thomas Dekorsy	DLR, Stuttgart, DE
Alan Fry	SLAC, US
Patrick Georges	CNRS, FR
Catherine Le Blanc	Ecole Polytechnique,Laboratoire LULI, FR
Emma Springate	STFC Rutherford Appleton Laboratory, US
William E. White	SLAC, Menlo Park, US
Andreas Galler (LAC secretary)	European XFEL, Schenefeld, DE
Nele Müller (LAC secretary)	DESY, Hamburg, DE

DESY Photon Science User Committee DPS-UC — represents the user community

Peter Müller-Buschbaum (chair)	Technische Universität München, DE
Markus Mezger	MPI für Polymerforschung, Mainz, DE
Daniela Rupp	Technische Universität Berlin, DE
Chrystèle Sanloup	Sorbonne Université, Paris, FR
Gregor Witte	Ludwig-Maximilians-Universität München, DE

Komitee Forschung mit Synchrotronstrahlung KFS

representative body of the German SR and FEL user community

Bridget Murphy (chair)	Christian-Albrechts-Universität zu Kiel, DE
Jan-Dierk Grunwaldt (vice chair)	KIT, Karlsruhe, DE
Peter Albers	Evonik Technology & Infrastructure GmbH, DE
Stefan Eisebitt	MBI and Technische Universität Berlin, DE
Ronald Frahm	Universität Wuppertal, DE
Christian Gutt	Universität Siegen, DE
Birgit Kanngießer	Technische Universität Berlin, DE
Sarah Köster	Georg-August-Universität Göttingen, DE
Kai Rossnagel	Christian-Albrechts-Universität zu Kiel, DE
Hermann Schindelin	Universität Würzburg, DE

Project Review Panels 2019

PRP VUV- and Soft X-ray	
Yves Acremann	ETH Zürich, CH
Arno Ehresmann	Universität Kassel, DE
Marc Golden	University of Amsterdam, NL
Jan-Erik Rubensson	Uppsala University, SE
Emma Sokell	University College Dublin, IE
Moritz Hoesch (PRP secretary)	DESY, Hamburg, DE

PRP X-ray Absorption Spectroscopy (XAFS)	
Iztok Arčon	University of Nova Gorica, SL
Matthias Bauer	Universität Paderborn, DE
Kajsa Sigfridsson Clauss	MAX IV Laboratory, Lund University, SE
Dmitry Doronkin	Karlsruher Institut für Technologie KIT, DE
Stephan Klemme	Universität Münster, DE
Alexei Kuzmin	University of Latvia, Riga, LV
Maarten Nachtegaal	PSI, Villigen, CH
Christina Roth	Universität Bayreuth, DE
Karel Saksl	Slovak Academy of Sciences, Košice, SK
Claudia Schnohr	Friedrich-Schiller-Universität Jena, DE
Wolfgang Caliebe, Edmund Welter (PRP secretaries)	DESY, Hamburg, DE

PRP Nuclear and Inelastic Scattering, X-ray Emission	
Catherine McCammon	Bayerisches Geoinstitut, Bayreuth, DE
Marco Moretti	ESRF, Grenoble, FR
Volker Schünemann	Technische Universität Kaiserslautern, DE
Svetoslav Stankov	Karlsruher Institut für Technologie KIT, DE
Hans-Christian Wille (PRP secretary)	DESY, Hamburg, DE

PRP Hard X-ray Photoelectron Spectroscopy (HAXPES)	
Maria Hahlin	Uppsala University, SE
Martina Müller	Forschungszentrum Jülich, DE
Christian Papp	FAU Erlangen-Nürnberg, DE
Anna Regoutz	Imperial College London, GB
Håkan Rensmo	Uppsala University, SE
Vladimir N. Strocov	PSI, Villigen, CH
Christoph Schlüter (PRP secretary)	DESY, Hamburg, DE

PRP High Pressure and Extreme Conditions	
Daniel Errandonea	Universidad de Valencia, ES
Ulrich Häussermann	Stockholm University, SE
Malcolm McMahon	University of Edinburgh, UK
Sébastien Merkel	Lille University, FR
Marco Merlini	Università degli Studi di Milano, IT
Guillaume Morard	Université Grenoble Alpes, FR
Carmen Sanchez-Valle	Universität Münster, DE
Chrystèle Sanloup	Sorbonne Université, Paris, FR
Andreas Zerr	Université Paris Nord, Villetaneuse, FR
Hanns-Peter Liermann (PRP secretary)	DESY, Hamburg, DE

PRP Engineering Materials Science	
Jens Gibmeier	Karlsruher Institut für Technologie KIT, DE
Astrid Haibel	Beuth Hochschule für Technik Berlin, DE
Patrick Huber	Technische Universität Hamburg-Harburg, DE
Rolf Kaufmann	Comet Group, Flamatt, CH
Jozef Keckes	Montanuniversität Leoben, AT
Ingo Manke	Helmholtz-Zentrum Berlin, DE
Svea Mayer	Montanuniversität Leoben, AT
Thomas Niendorf	Universität Kassel, DE
Wolfgang Pantleon	Technical University of Denmark, DK
Walter Reimers	Technische Universität Berlin, DE
Carsten Siemers	Technische Universität Braunschweig, DE
Dieter Lott (PRP secretary)	HZG, Geesthacht, DE
Ulrich Lienert (DESY representative)	DESY, Hamburg, DE

PRP Soft Condensed Matter – Bulk	
Christian Gutt	Universität Siegen, DE
Thomas Hellweg	Universität Bielefeld, DE
Fredrik Lundell	KTH, Stockholm, SE
Konrad Schneider	Leibniz-Institut für Polymerforschung, Dresden, DE
Beatrice Ruta	ESRF, Grenoble, FR
Rainer Gehrke (PRP secretary)	DESY, Hamburg, DE

PRP Soft Condensed Matter – Surfaces and Interfaces	
Alexander Gerlach	Universität Tübingen, DE
Christiane A. Helm	Universität Greifswald, DE
Beate Kloesgen	University of Southern Denmark, Odense, DK
Markus Mezger	MPI für Polymerforschung, Mainz, DE
Guiseppe Portale	University of Groningen, NL
Tobias Unruh	Technische Universität München, Garching, DE
Andreas Zumbühl	University of Fribourg, CH
Oliver Seeck (PRP secretary)	DESY, Hamburg, DE

PRP Imaging (full-field, scanning, coherent)	
Matthias Alfeld	Technische Universiteit Delft, NL
Martin Bech	Lund University, SE
Oliver Bunk	PSI, Villigen, CH
Manfred Burghammer	ESRF, Grenoble, FR
David Fenning	University of California San Diego, La Jolla, US
Frank Friedrich	Universität Hamburg, DE
Julia Herzen	Technische Universität München, DE
Florian Meirer	Utrecht University, NL
Bert Müller	University of Basel, CH
Stephan Peth	Universität Kassel, DE
Sebastian Schoeder	Synchrotron SOLEIL, Saint-Aubin, FR
Jürgen Thieme	Brookhaven National Laboratory, Upton NY, US
Katarina Vogel-Mikuš	University of Ljubljana, SL
Gerald Falkenberg (PRP secretary)	DESY, Hamburg, DE
Felix Beckmann (HZG representative)	HZG, Geesthacht, DE

PRP Methods and Instrumentation	
Yngve Cerenius	MAX IV Laboratory, Lund University, SE
Cameron Kewish	Australian Synchrotron, Melbourne, AU
Raymond Barrett	ESRF, Grenoble, FR
Horst Schulte-Schrepping (PRP secretary)	DESY, Hamburg, DE

PRP Hard Condensed Matter – Surface and Coherent Scattering	
Del Atkinson	Durham University, GB
Ralf Busch	Universität des Saarlandes, Saarbrücken, DE
Guido Meier	MPI MPSD, Hamburg, DE
Beatriz Noheda	University of Groningen, NL
Herbert Over	Justus Liebig Universität Giessen, DE
Ullrich Pietsch	Universität Siegen, DE
Jesper Wallentin	University Lund, SE
Peter Wochner	MPI für Festkörperforschung, Stuttgart, DE
Michael Sprung (PRP secretary)	DESY, Hamburg, DE

PRP Hard Condensed Matter – Bulk (diffraction and scattering)	
Manuel Angst	Forschungszentrum Jülich, DE
Emil Bozin	Brookhaven National Laboratory, Upton NY, US
Per-Anders Carlsson	Chalmers University of Technology, Gothenburg, SE
Robert Dinnebier	MPI für Festkörperforschung, Stuttgart, DE
Markus Huecker	Weizmann Institute of Science, Rehovot, IL
Kirsten Marie Ørnsbjerg Jensen	University of Copenhagen, DK
Mads Ry Vogel Jørgensen	Aarhus University, DK
Gregor Kieslich	TU München, DE
Simon Pauly	IFW Dresden, DE
Helen Walker	ISIS, Didcot, GB
Xiaodong Zou	Stockholm University, SE
Ann-Christin Dippel (PRP secretary)	DESY, Hamburg, DE

PRP Soft X-Ray – FEL Experiments (FLASH)	
Katharina Al-Shamery	Universität Oldenburg, DE
Michael Bonitz	Universität Kiel, DE
Christoph Bostedt	EPFL, Lausanne and PSI, Villigen, CH
Hermann Dürr	SLAC Nat. Accelerator Laboratory, Menlo Park, US
Marion Harmand	Sorbonne Université, Paris, FR
Chris Jacobsen	APS, Argonne, US
Claudio Masciovecchio	Elettra Sincrotrone Trieste, IT
Ronald Redmer	Universität Rostock, DE
Robert W. Schoenlein	SLAC Nat. Accelerator Laboratory, Menlo Park, US
Marc Simon	Sorbonne Université, Paris, FR
Kiyoshi Ueda	Tohoku University, Sendai, JP
Marc Vrakking	MBI, Berlin, DE
Martin Weinelt	FU Berlin, DE
Elke Plönjes-Palm, Rolf Treusch (PRP secretaries)	DESY, Hamburg, DE

PEC: EMBL Life Science beamlines P12-P14 / PRP Bio-crystallography at P11	
Savvas Savvides (chair)	Ghent University, BE
Pau Bernadó	CBS/CNRS, Montpellier, FR
Kristina Djinovic-Carugo	Universität Wien, AT
Gwyndaf Evans	Diamond Light Source, Didcot, GB
Robert Fischetti	Argonne National Laboratory, US
Mariusz Jaskolski	Adam Mickiewicz University of Poznan, PL
Gergely Katona	University of Gothenburg, SE
Annette E. Langkilde	University of Copenhagen, DK
Javier Pérez	Synchrotron SOLEIL, Saint-Aubin, FR
Teresa Santos-Silva	Universidade NOVA de Lisboa, PT
Zehra Sayers	Sabanci University, Istanbul, TR
Joel Sussman	Weizmann Institute of Sciences, Rehovot, IL
Maria Vanoni	University of Milan, IT
Mark J. van Raaij	CNB-CSIC, ES
Gregor Witte	Ludwig-Maximilians-Universität München, DE
Christian Schroer (DESY observer)	DESY, Hamburg, DE

Photographs and Graphics:

Bestec
Gesine Born
CAU
CSSB
DESY
EMBL
European XFEL
Jörg Harms, MPSD
Axel Heimken
HGF
HZB
HZG
C. Lemke, CAU
Kinga Lubowiecka, EMBL
Lucid Berlin
Marta Mayer, DESY
A. Mentz, Univ. Hamburg
MPG
Richard Ohme, Univ. Hamburg
Reimo Schaaf
Frank Scholz
M. Setzpfandt, HZB
Universität Hamburg
Meletios Verras
Jessica Wahl
Alena Zielinski

Figures of the Research Highlights were reproduced by permission from authors or journals.

Acknowledgement

We would like to thank all the authors and all those who have contributed to the realisation of this Annual Report.

Imprint

Publishing and Contact:
Deutsches Elektronen-Synchrotron DESY
A Research Centre of the Helmholtz Association

Hamburg location:
Notkestr. 85, 22607 Hamburg, Germany
Tel.: +49 40 8998-0, Fax: +49 40 8998-3282
desyinfo@desy.de

Zeuthen location:
Platanenallee 6, 15738 Zeuthen, Germany
Tel.: +49 33762 7-70, Fax: +49 33762 7-7413
desyinfo.zeuthen@desy.de

Photon Science at DESY
Tel.: +49 40 8998-2304, Fax: +49 40 8998-4475
photon-science@desy.de
photon-science.desy.de

www.desy.de

ISBN 978-3-945931-27-1

Online version:
photon-science.desy.de/annual_report

Realisation:
Wiebke Laasch, Daniela Unger

Editing:
Sadia Bari, Lars Bocklage, Günter Brenner, Rainer Gehrke, Wiebke Laasch, Britta Niemann, Wolfgang Morgenroth, Leonard Müller, Nele Müller, Christoph Schlueter, Sang-Kil Son, Daniela Unger, Thomas White

Layout: Sabine Kuhls-Dawideit, Büro für Grafik und Design, Halstenbek

Printing and image processing: EHS Druck GmbH, Schenefeld

Copy deadline: December 2019

HELMHOLTZ
RESEARCH FOR GRAND CHALLENGES

Deutsches Elektronen-Synchrotron DESY
A Research Centre of the Helmholtz Association

The Helmholtz Association is a community of 19 scientific-technical and biological-medical research centres. These centres have been commissioned with pursuing long-term research goals on behalf of the state and society. The Association strives to gain insights and knowledge so that it can help to preserve and improve the foundations of human life. It does this by identifying and working on the grand challenges faced by society, science and industry. Helmholtz Centres perform top-class research in strategic programmes in six core fields: Energy, Earth & Environment, Health, Aeronautics, Space and Transport, Matter, and Key Technologies.

www.helmholtz.de